Division of Materials, Mechanics and Structures

Faculty of Engineering

EXTENSION OF THE USE OF CELLULOSE NANOWHISKERS IN COMPOSITE MATERIALS

By

KAZI MD. ZAKIR HOSSAIN

BSc. (Hons.) and MS

Thesis submitted to the University of Nottingham for the degree of Doctor of Philosophy

December, 2013

This thesis is dedicated to my Mother,

Wife

&

My beloved Son (Zarif)

ABSTRACT

This thesis explores the use of cotton derived cellulose nanowhiskers (CNWs) in composite materials in the form of nanocomposite films, surface modified polymer fibres and also in self-reinforced (SR) composites.

Cellulose nanowhiskers (CNWs) were produced from cotton via sulphuric acid hydrolysis process and blended with polylactic acid (PLA) to produce CNW-PLA and was added to hydroxyethyl cellulose (HEC) to manufacture CNW-HEC nanocomposite films. The aggregated morphology and hydrophilicity of CNWs, hydrophobicity of PLA and the solvent used (Chloroform) played a major role in creation of voids within the CNW-PLA nanocomposites. In addition, the aggregated morphology of the CNWs also influenced the surface roughness and light transparency properties of the CNW-HEC films. Improvement in the mechanical, thermal and thermomechanical properties for both types of nanocomposites was achieved due to the reinforcing effect of the rod-like nanowhiskers. An increase in the crystallinity of the nanocomposites indicated that the CNWs induced crystallisation in the matrices. Incorporation of CNWs also had a significant influence on accelerating the degradation profile of the CNW-PLA nanocomposites and reducing the swelling capacity and initial swelling rate for the CNW-HEC films.

PLA fibres were also produced with varying diameters (11 µm to 38 µm) via a melt drawing process employing increasing take-up velocities. A higher degree of chain orientation as well as an increase in crystallinity for the thinner fibres was

achieved due to strain-induced crystallisation. The variation in PLA fibre diameter also revealed a noticeable influence in their mechanical and moisture absorption properties at various humidity levels. Further, the hydrophobic and smooth surface of the PLA fibres was coated with various blends of CNWs (65 to 95 wt%) and polyvinyl acetate (PVAc) to impart roughness, where PVAc acted as a binder. An increase in tensile modulus and moisture absorption properties were achieved for the CNW/PVAc coated PLA fibres. These surface modified PLA fibres were aligned to produce unidirectional (UD) fibre mats prior to hot compaction (at 95°C) to manufacture SR PLA composites. Incorporation of CNW/PVAc within the SR PLA composites revealed an increase in their flexural and ductile properties compared to the control composite.

LIST OF PUBLICATIONS

Book Chapters

1. M. Labet, <u>K.M.Z Hossain</u>, I. Ahmed, and W. Thielemans, *Biomass in Composite Materials*, in *Materials for a Sustainable Future*, T.M. Letcher and J.L. Scott, Editors. 2012, Royal Society of Chemistry. p. 698-739.

2. <u>K.M.Z Hossain</u>, R.M. Felfel, C.D. Rudd and I. Ahmed*, Biocomposites: Natural and Synthetic Fibers*, M.K. Mishra, Editor, Encyclopedia of Biomedical Polymers and Polymeric Biomaterials, Taylor and Francis, USA. Accepted, in press (Ms. No. 120050019, Publication date: February, 2014).

3. <u>K.M.Z Hossain</u>, M.S. Hassan, R.M. Felfel, and I. Ahmed, *Development of Phosphate-Based Glass Fibres for Biomedical Applications*, ebook chapter in "Hot Topics in Biomedical Materials", Future Science Group (Accepted, in press).

Peer Reviewed Journal Papers

1. <u>K.M.Z Hossain</u>, L. Jasmani, I. Ahmed, A.J. Parsons, C.A. Scotchford, W. Thielemans, and C.D. Rudd, *High cellulose nanowhisker content composites through cellosize bonding.* Soft Matter, 2012. 8(48): p. 12099-12110.

2. <u>K.M.Z Hossain</u>, I. Ahmed, A. Parsons, C. Scotchford, G. Walker, W. Thielemans, and C. Rudd, *Physico-chemical and mechanical properties of nanocomposites prepared using cellulose nanowhiskers and poly(lactic acid).* Journal of Materials Science, 2012. 47(6): p. 2675-2686.

3. <u>K.M.Z Hossain</u>, A.J. Parsons, C.D. Rudd, I. Ahmed and W. Thielemans, *Mechanical, crystallisation and moisture absorption properties of melt drawn polylactic acid fibres*. Submitted to the European Polymer Journal (Under review).

Conference Abstracts

1. <u>K.M.Z Hossain</u>, I. Ahmed, A. Parsons, W. Thielemans, and C. Rudd, *Cellulose based Thin Composite Films for Biomedical Applications*, UKSB 13th ANNUAL

CONFERENCE, p. 25 and 32, 24-25th June, 2013, Birmingham, UK (**Oral + Poster**).

2. K.M.Z Hossain, I. Ahmed, A. Parsons, W. Thielemans, and C. Rudd, *Cellulose Nanowhisker Content Flexible Thin Composite Films*, 1st International Conference on Natural Fibers, p. 29-30, 09-11th June, 2013, Guimaraes, Portugal (**Oral**).

3. K.M.Z Hossain, I. Ahmed, A. Parsons, W. Thielemans, and C. Rudd, SAMPE Student Conference, *High Cellulose Nanowhisker Content Flexible Thin Composite Films*, 09-10th March, 2013, Paris, France (**Oral**).

4. K.M.Z Hossain, I. Ahmed, A. Parsons, W. Thielemans, and C. Rudd, SEICO-13, *High Cellulose Nanowhisker Content Flexible Thin Composite Films*, 11-12th March, 2013, Paris, France (**Poster**).

5. K.M.Z Hossain, I. Ahmed, A. Parsons, W. Thielemans, and C. Rudd, NanoKTN Conference on Nanofibres to Nanocomposites II, *Cellulose Nanowhisker Reinforced Poly (lactic acid) Nanocomposites*, 17th October, 2012, Nottingham Trent University, UK (**Poster**).

6. K.M.Z Hossain, I. Ahmed, A. Parsons, W. Thielemans, and C. Rudd, UKSB 11th ANNUAL CONFERENCE, *Investigation of mechanical, crystallisation and degradation properties of bio-based nanocomposites,* 27-28th June 2012, University of Nottingham, UK (**Oral**).

ACKNOWLEDGEMENTS

CNWs	Cellulose nanowhiskers
PLA	Polylactic acid
HEC	Hydroxyethyl cellulose
PVAc	Polyvinyl acetate
SR	Self-reinforced/self-reinforcement
SRC	Self-reinforced composite
wt%	Weight fraction
BS	British standard
ASTM	American society for testing and materials
ISO	International standards organization
SEM	Scanning electron microscope
TEM	Transmission electron microscope
OM	Optical microscope
FTIR	Fourier transform infra-red
ATR	Attenuated total reflectance
XRD	X-ray diffraction
DSC	Differential scanning calorimetry
TGA	Thermogravimetric analyser
DMA	Dynamic mechanical analyser
^{o}C	Degree centigrade
T_g	Glass transition temperature
T_m	Melting temperature
T_{cc}	Cold crystallisation temperature

TABLE OF CONTENTS

CHAPTER 7. ROLE OF CELLULOSE NANOWHISKERS ON THE FLEXURAL PROPERTIES OF SELF-REINFORCED POLYLACTIC ACID (SR PLA) COMPOSITES

LIST OF FIGURES

LIST OF TABLES

CHAPTER 1.

INTRODUCTION

The demand for sustainable materials is growing significantly as sustainability has the potential to drive new growth for environmentally friendly products. As such, there has been huge interest in the use of natural fibres for use in fields as varied as automobile, construction, electronics, textile, packaging and biomedical including many others. The International Year of Natural Fibres was declared in 2009 and was intended to raise awareness of, and promote demand for, sustainably produced natural fibres. For thousands of years, people all over the world have used fibres from plants and animals to make cloth, string and paper, and strengthen building materials.

Global production of natural fibres amounts to around 32 million tonnes annually; amongst these, 24.6 million tonnes of cotton are produced which encompasses around 76% of the total market share (FAOSTAT, 2009) [1]. Plant based other natural fibres (jute, sisal, hemp, flax, ramie, etc.) make up around 20%, and wool approximately 4% (see Figure 1.1). China, India and United States are the major producers of cotton, where China dominates with production of ca. 32% of the global production followed by India (22%) and USA (12%). On the other hand, approximately 2.8 million tonnes of jute are produced each year, with India producing 60% of the world's jute and Bangladesh being the other major producer. Other fibres are produced in lower quantities such as flax (~1 million tonnes), hemp (~0.09 million tonnes), and sisal (~0.33 million tonnes). The recent

environmental awareness issues, together with the rising costs of oil are creating an increasing market for natural fibres which are finding their way into varying commercial applications in composite materials.
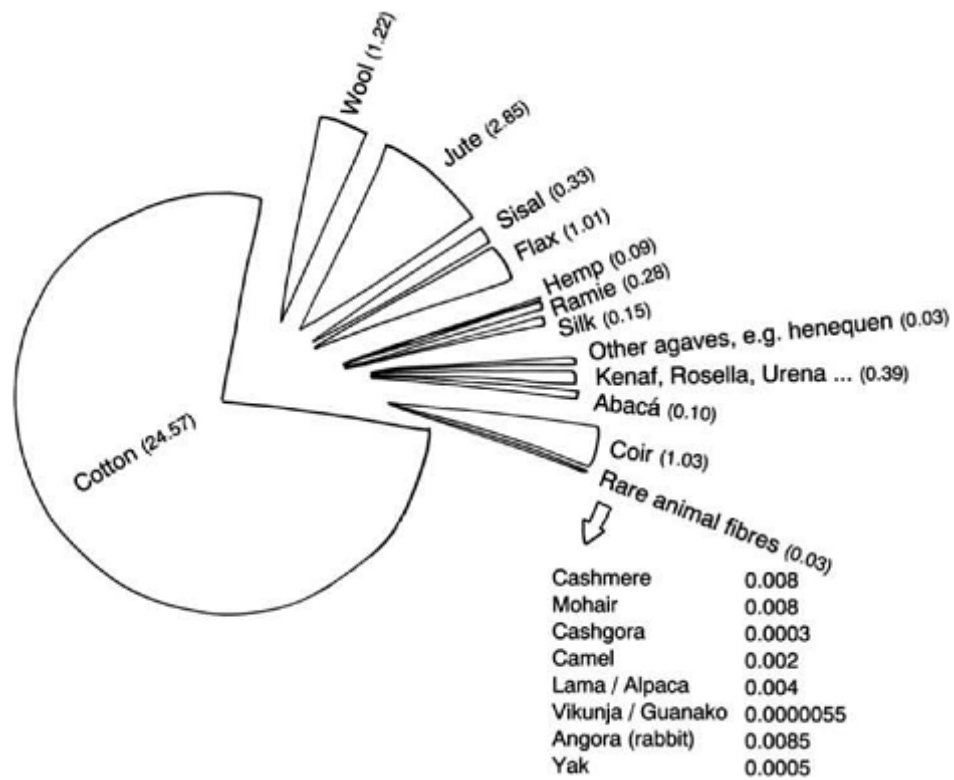
Figure 1.1: *Worldwide production of natural fibres, in million tonnes [1].*

1.1 COMPOSITES

Composites consists of two or more distinct materials or phases, which are mixed in a controlled way to achieve enhanced material properties [2]. Generally, one or more discontinuous phases (stiffer and stronger) embedded within the continuous phase (comparatively softer) to form composites. The discontinuous phase usually termed as reinforcing agents, while the continuous phase is called the matrix. Composites can be categorised on the basis of reinforcement, such as, fibre, flake, particle, laminar and filled composites. Composites have also been classified as

Metal Matrix Composites, Ceramic Matrix Composites and Polymer Matrix Composites.

Many materials in nature are found as composites, for example, wood is composed of fibrous chains of cellulose molecules in matrix of lignin [3]. In applications with polymer matrix materials, the discontinuous phase often consists of fibres of high strength and modulus, which can be used in different shapes such as, short fibres, long or continuous fibres, and three dimensional fibre structures. Figure 1.2 represents the classification of composites based on fibre shape and orientation within the matrix.
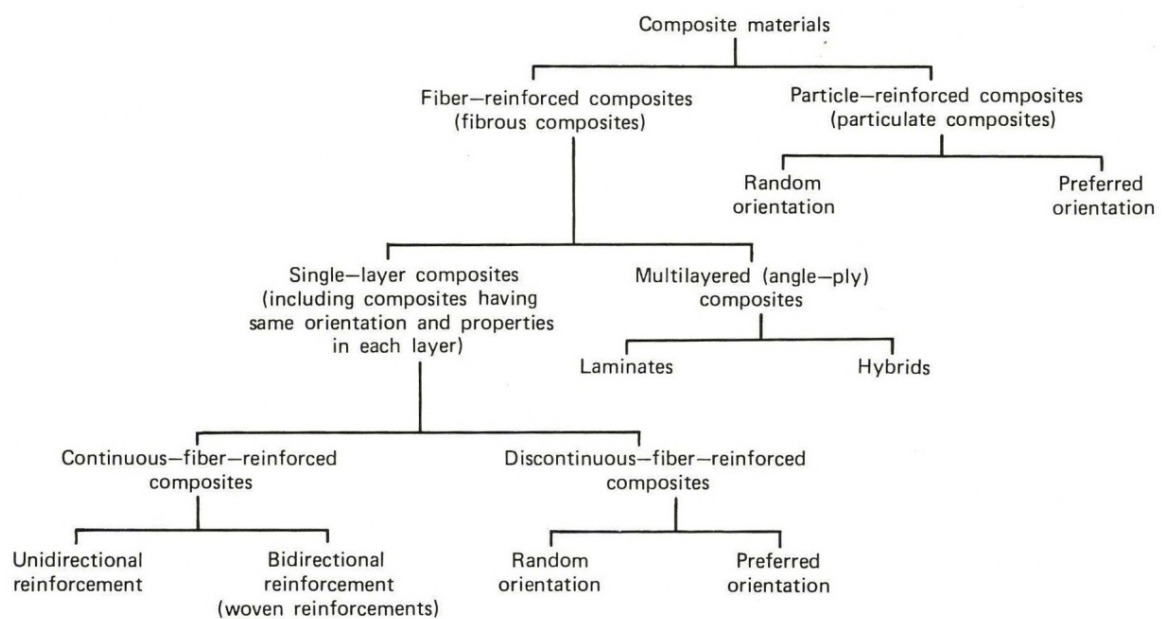
Figure 1.2: *Classification of composite materials based on the fibre shape and orientation within the matrix [4].*

1.2 FIBRE-REINFORCED COMPOSITES

Fibre reinforcement of polymeric matrices has been widely used to improve mechanical as well as thermomechanical properties of polymers due to their excellent load transfer capacity and the light-weight structures that can be

formed. The mechanical properties of the reinforcing fibres, which can be natural or synthetic, can have a significant influence on the overall properties of the composites produced. Table 1.1 highlights the density and mechanical properties for fibres used as reinforcement.

Table 1.1: *Mechanical properties of some natural and synthetic reinforcing fibres [5-8].*

Fibres	Density (g cm^{-3})	Tensile Strength (MPa)	Tensile Modulus (GPa)	Elongation (%)
Cotton	1.21	287-597	5.5-12.6	2.0-10
Jute	1.3	393-773	10-30	1.5-1.8
Flax	1.5	780-1,500	60-80	1.2-2.4
Hemp	1.35	580-1,110	30-70	1.6-4.5
Kenaf	1.2	295-930	53	2.7-6.9
Ramie	1.44	400-938	61.4-128	2.0-4.0
Sisal	1.5	511-635	9.4-22	2.0-2.5
Coir	1.2	593	4.6-6	15-25
E-glass	2.5	2,000-3,500	70-72	0.5
Carbon	1.4	4,000	230-240	1.4-1.8

Strong reinforcement is achieved through chemical and/or mechanical coupling between the fibres/fillers and matrix so that the load is shared between the fibres and the matrix [3, 9]. Natural reinforcements such as cellulose and starch have a strong tendency for self-association because of their strongly interacting surface

hydroxyl groups [10]. This poses problems during processing to attain individualisation, but can also aid in the formation of stabilising percolated networks. The properties of composites prepared by fibre reinforcing polymers are largely dependent on the fibre architecture, such as fibre mechanical properties, volume fraction and alignment of fibres within the matrix. The compounding processes are also an important factor controlling the properties of composite materials as they affect fibre orientation, individualisation in the case of short fibres. The orientation and distribution of short fibres in the matrix are more difficult to control, to measure and to characterise, while long fibres offer better control of the distribution of fibres into the matrix, resulting in improved composite properties. Despite this, industrial and large–scale production of composite materials have mainly focused on short fibre reinforced matrices using injection moulding and extrusion processes. These methods can easily be turned into continuous processing while long fibre composite manufacturing with natural fibres generally requires significant manual labour and longer batch processing times. The cost of manual labour and longer processing times is inhibitive for low cost applications where natural fibre reinforced composites are currently targeted. However, compression and injection moulding processes are still not properly optimised and variability in composite properties can easily occur.

Short natural fibres have attracted much attention as reinforcement in polymers in order to produce biodegradable composites [11-13]. Natural fibres, isolated from plants, animals and also some minerals sources, have been used aligned or randomly distributed in polymer matrices either in the same plane or in three

dimensions [14] (Figure 1.3). Aligned reinforcing fibres show strong reinforcement in the longitudinal direction of the fibre but low reinforcement capability in the transverse direction. Random three dimensional fibre orientation results in equal reinforcement in all directions. The mode of their reinforcement has also been studied extensively through experimental and theoretical studies [15, 16].
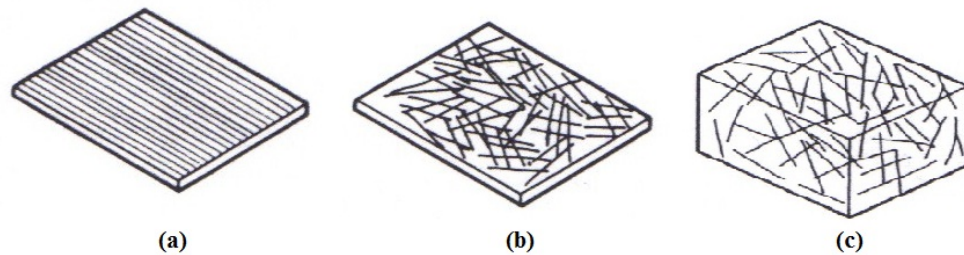
Figure 1.3: *Patterns of fibre reinforcement in polymer: **(a)** aligned fibre,*

***(b)** random-in-plane, and **(c)** random in three dimensions [14].*

1.2.1 Micro and nano reinforcement

Micro- and nanofibres derived from various natural sources have been paid much attention for composite production due to their high mechanical properties and high reinforcement capability at low loadings [17]. Polymers have been reinforced with macroscopic as well as micro- and nanofibres. Microfibres have diameters in the micrometre range while nanofibres have at least one dimension on the nanometre scale. Improved mechanical properties stem from the reduction of defects with reduction in size, while the improved reinforcement capability arises from a higher surface to volume ratio and smaller distance between reinforcing fibres with decreasing fibre size for the same fibre loading. The fibre diameter has

also been reported to have a great influential effect on the mechanical properties of the fibre itself (see Figure 1.4) [18].
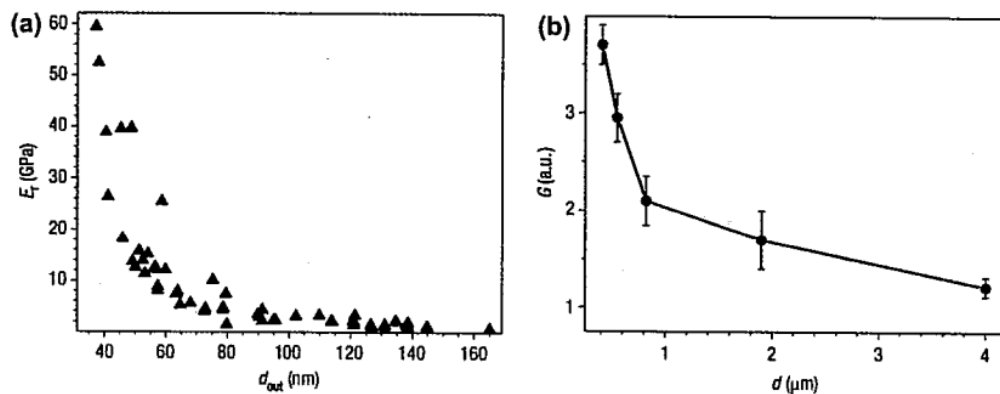
Figure 1.4: *Dependence of modulus on fibre diameter: **a)** elastic modulus versus diameter of polypyrrole nanofibre, and **b)** relative shear modulus versus diameter of electrospun polystyrene fibre [18].*

An added advantage of nanoscale reinforcement is that they tend to be more transparent than micro- and macro-reinforced composites as they are smaller than the wavelength of visible light.

However, when comparing nanowhiskers and microfibrillated cellulose (MFC) (Figure 1.5) derived from sisal in a polycaprolactone (PCL) matrix and using octadecyl isocyanate ($C_{18}HNCO$) as a fibre grafting agent to improve compatibilisation, MFC showed a significantly higher reinforcing capability (60% vs 15% increase in tensile modulus for the same amount of reinforcing fibres) [19]. The MFC allowed better inter-fibre entanglement when compared to the nanoscale reinforcements, resulting in better reinforcing performance. This clearly shows that fibre properties and interfacial compatibility alone are insufficient to predict composite performance.
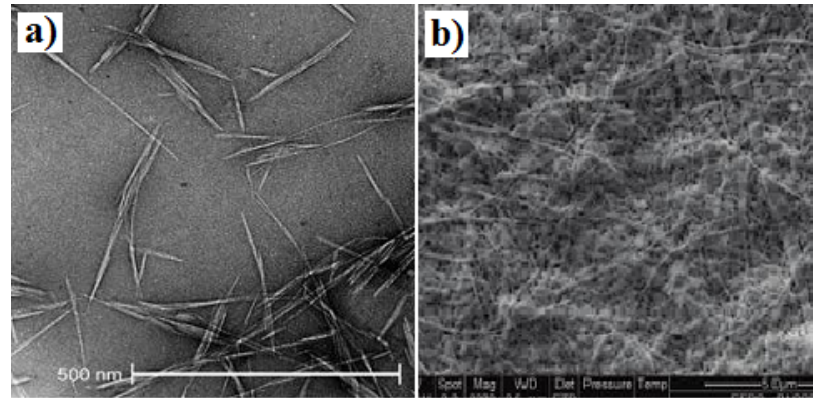
Figure 1.5: *a)* *TEM image of cellulose nanowhiskers from sisal, and* *b)* *SEM image of*

cellulose microfibre [19].

A vast amount of work has been done on natural fibre-reinforced composites, and some of the representative literature will be detailed in the following chapter (Chapter 2), which will aim to describe the potential for the use of natural and biopolymer fibres in composite materials.

1.3 AIMS AND OBJECTIVES

The main aim of this work was to manufacture cellulose nanowhiskers (CNWs) derived from cotton to incorporate them within polymer films, to use them as coatings for polymer fibre surface modification and in self-reinforced composites.

The objectives of the research conducted were:

1. To investigate the dispersion of cellulose nanowhiskers (CNWs) in solvent cast polylactic acid (PLA) nanocomposite films and to ascertain their effect on the mechanical, thermomechanical and water uptake properties.

2. To optimise the production of cellulose nanowhisker flexible thin composite films.

3. To investigate the mechanical, thermal, thermomechanical, crystallisation, chain orientation and moisture absorption properties of gravitationally induced melt drawn PLA fibres with varying diameters.

4. To modify the surface morphology of melt drawn PLA fibres coated with cellulose nanowhiskers and to investigate their mechanical and moisture absorption properties at different humidity conditions.

5. To develop a methodology for the production of cellulose nanowhisker (CNWs) incorporated self-reinforced PLA composite plates and to investigate the influence of the CNWs on their flexural and ductile properties.

1.4 STRUCTURE OF THIS THESIS

The thesis is sub-divided as follows:

Chapter 1: Introduction and background into fibre reinforcement in composite materials followed by the aims and objectives of this project.

Chapter 2: Properties of cellulose and biopolymer fibres and their role in composite materials including a brief literature review highlighting their use in packaging, electronics, construction and biomedical applications.

Chapter 3: The production of cellulose nanowhiskers (CNWs) from cotton and formulation of CNW reinforced polylactic acid (PLA) nanocomposite films. The dispersion of CNWs within the PLA matrix is also investigated to ascertain their effect on the mechanical, thermal,

thermomechanical, crystallisation and degradation properties of the nanocomposite films.

Chapter 4: Production of high CNW content flexible thin nanocomposite films using hydroxyethyl cellulose (HEC) matrix. The surface morphology, optical, mechanical, thermal, thermomechanical and swelling properties of these thin films are also characterised.

Chapter 5: Investigation of the thermal, crystallisation, chain orientation, and moisture absorption properties of melt drawn PLA fibres with diameters ranging from 11 to 38 microns. The mechanical properties of PLA fibres at room temperature, body temperature (37°C) and at varying humidity (0%, 35%, 75% and 98% RH) are also highlighted.

Chapter 6: Modification of the PLA fibre surface via attachment of CNWs to improve the surface roughness and hydrophilic properties of the PLA fibres. The tensile properties of the CNW coated PLA fibres are also presented.

Chapter 7: The use of the CNW coated PLA fibre mats for the manufacture of self-reinforced PLA (SR PLA) composites. The effect of CNWs on the flexural properties and ductile characteristics of SR-PLA composites are evaluated.

Chapter 8: Summary of the previous chapters and recommendations for future work to further explore the use of CNW-based composites.

CHAPTER 2.

LITERATURE REVIEW

2.1 BIO-BASED POLYMERS

Bio-based polymers, derived from renewable sources are widely used in various applications such as automotive, packaging, construction and biomedical sectors. Bio-based polymers can be reinforced with natural and synthetic materials to alter their properties and achieve wide ranging mechanical, physical and thermal conductivity properties. Due to their excellent dimensional stability bio-based polymer reinforced composites can easily be fabricated into plates, films, textiles, rods, fibres and gels [20, 21]. Biodegradability and biocompatibility, these two important properties of polymer must be considered when they are aimed for biomedical applications. Biodegradable polymers are able to breakdown gradually over time to lose their initial integrity in a physiological environment into biocompatible (not toxic and injurious to biological systems) degradation products [22]. These biodegradable polymers can be further split into natural and/or synthetic polymers. Natural polymers, including cellulose [23-25], chitosan [26, 27], alginate [28, 29], collagen [30-32], silk [33, 34], agarose [35] and fibrin [36] and synthetic polymers such as polycaprolactone (PCL), polyglycolic acid (PGA), polylactic acid (PLA) and polylactic-co-glycolic acid (PLGA), polyhydroxybutyrate (PHB) and polypropylene fumerate (PPF) have been considered for applications within food packaging [37], wound healing, soft tissue regeneration and as bone fixation devices [38, 39].

2.1.1 Polysaccharides

Polysaccharides such as cellulose, chitin, and alginate are one of the most abundant naturally occurring biomacromolecular carbohydrate materials, which encompass glycosidically linked saccharide units as well as covalently linked proteins, lipids, peptides and amino acids [40]. Cellulose is the most abundant renewable biomass in nature and is composed of long chain β-glycoside units in a linear orientation [41].
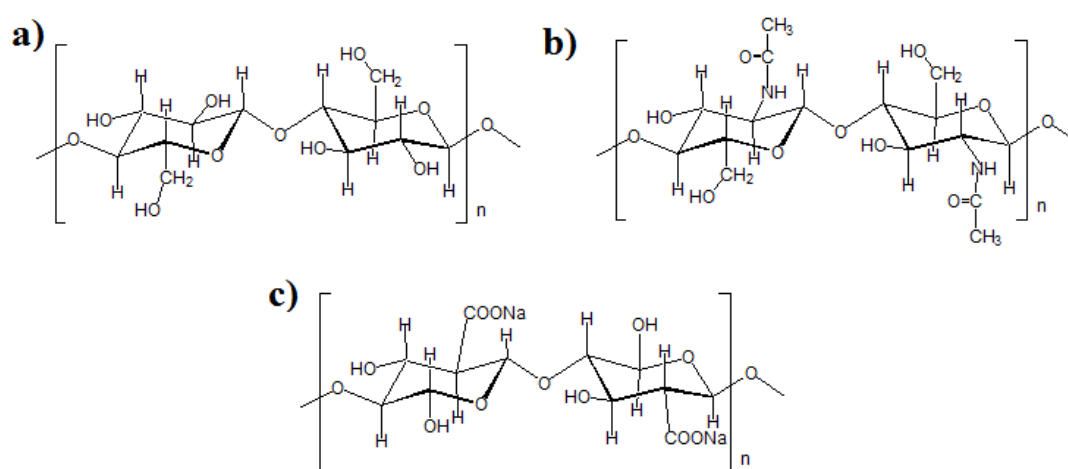
Figure 2.1: *Represents the chemical structures for the most common types of polysaccharides:* **a)** *cellulose,* **b)** *chitin, and* **c)** *sodium alginate.*

Chitin is widely distributed in marine invertebrates found in the exoskeleton of insects and arthropods such as crustaceans. It has been used as wound-dressing materials, drug carrier excipients and mucoadhesivity purposes [32, 42]. It has also been used as a raw material for chitosan production, which is widely employed in biomedical applications, such as tissue regeneration, bone filling materials and wound treatment [40] due to its gel forming, self-hardening, bioadhesive, bacteriostatic and fungistatic properties.

Alginates, derived from brown algae or soil bacteria are anionic polysaccharides consisting of (1-4)-linkages with alternating β-D-mannuronic acid and α-L-guluronic acid residues [43] and have been investigated as biomaterials for the treatment of esophageal reflux, dermatology, wound healing and dental impression materials [40, 44]. Alginates are usually regarded as non-toxic, biocompatible and biodegradable gel forming materials and have been widely used as pharmaceutical excipients (such as tablet binders, disintegrants and sustained release materials).

2.1.1.1 Cellulose

Cellulose is mainly obtained from wood, plants (cotton, ramie, flax, jute, sisal, wheat straw, etc.), animals (tunicate), algae, fungi and even in bacteria [45]. Cellulose is composed of linear chain of ringed glucose units, where the repeat unit is joined by two glucose rings through an oxygen covalently bonded to C1 of the glucose ring and C4 of the adjoining ring (β-1,4-glycosidic bond) [45]. The linear configuration of cellulose chain structure is maintained by the intra-chain hydrogen bonding between hydroxyl groups and oxygen of the adjoining ring (see Figure 2.2a). The inter-chain hydrogen bonds between the adjacent glucose rings promote parallel stacking of multiple cellulose chains forming elementary fibrils that further aggregate into larger micro fibrils. The intra- and inter-chain hydrogen bonds give the cellulose fibrils high axial stiffness that makes them suitable as reinforcing agent in composite materials. These cellulose fibrils are composed of highly ordered (crystalline) and disordered (amorphous) cellulose chains, as presented (see Figure 2.2b) [45].
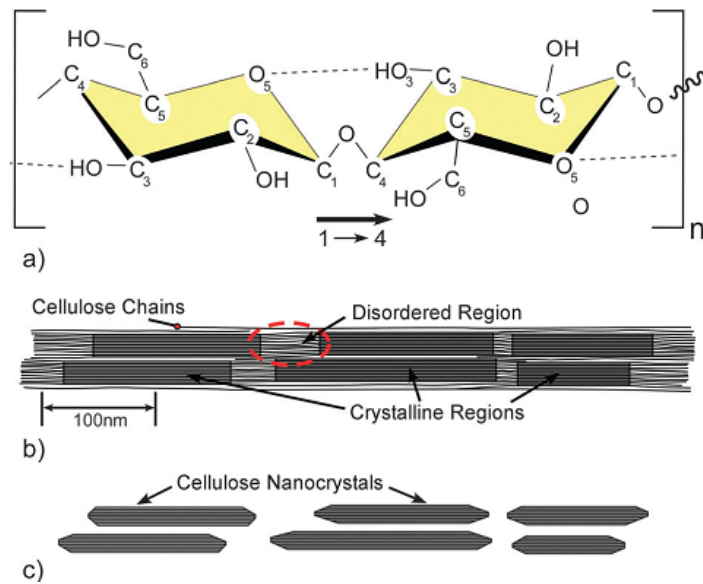
Figure 2.2: *a) Represents the repeat unit of the cellulose structure, b) crystalline and amorphous regions within cellulose microfibril, and c) cellulose nanocrystals after the acid hydrolysis process [45].*

The cell-wall morphology of cotton fibre is presented in Figure 2.3, where the cell-wall architecture of cellulose fibres composed of micro- and macro-fibrils units [46]. The density and texture of these fibres depends on the different layers of the fibrils and their position. The outer layer, called the primary wall (P) consists of fibrils measuring approximately 10 nm which are positioned crosswise in a layer of around 50 nm thickness. The secondary wall (S) has two layers: the winding layer (S1, thickness around 100 nm), where the fibrils are densely packed and the main body of the secondary wall (S2, thickness several µm) contains most of the cellulose mass. Lumen (L, inner layer) consists of fibrils aligned in a flat helix [46].
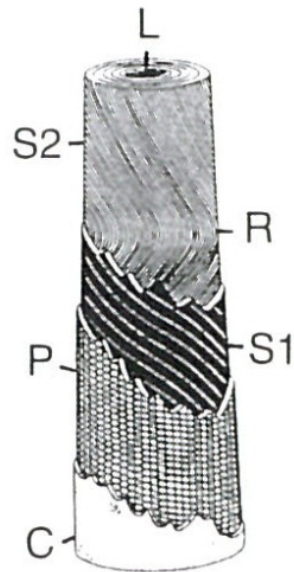
Figure 2.3: *Morphological architecture of cotton fibre: L-lumen, C-cuticle (pectins*

and waxes), P-primary cell-wall, S1-secondary wall (winding layer), S2-secondary

wall (main body) and R-reversal of the fibril spiral [46].

The commercial sources of cellulose are mainly from the cotton linters (shorter

fibres, which are obtained after removing the long fibres from cotton seeds), jute

and wood pulp. Cotton linters contain around 90-95% cellulose, whereas, in jute it

is approximately 45-63% and in wood pulp about 40-45% [8]. Therefore, cellulose

extracted from cotton linters with high purity required minimum treatment

(NaOH treatment) to remove hemicellulose, lignin and wax materials. On the

other hand, other fibres like jute, wood pulp, hemp and ramie require extensive

processing to dissolve the non-cellulosic components.

2.1.1.1.1 Cellulose nanowhiskers

Cellulose nanowhiskers (also known as nanocrystals) are the highly crystalline

portion of the cellulose components, which are the elongated crystalline rod-like

nanoparticle and can be produced by acid hydrolysis, and enzymatic hydrolysis

processes. On the other hand, flexible cellulose nanofibrils and/or microfibrils consist of alternating crystalline and amorphous portions of cellulose particles. Revol *et al.* [47] first reported the production of cellulose nanowhiskers via the acid hydrolysis process. During acid hydrolysis the amorphous portions of the cellulose chain are dissolved leaving the crystalline parts unaffected as whiskers form on the nanoscale dimension, usually the length ranges from 100 to 300 nm depending on the source of cellulose [48]. The morphology of acid hydrolysed cellulose nanowhiskers obtained from different sources is presented in Figure 2.4.
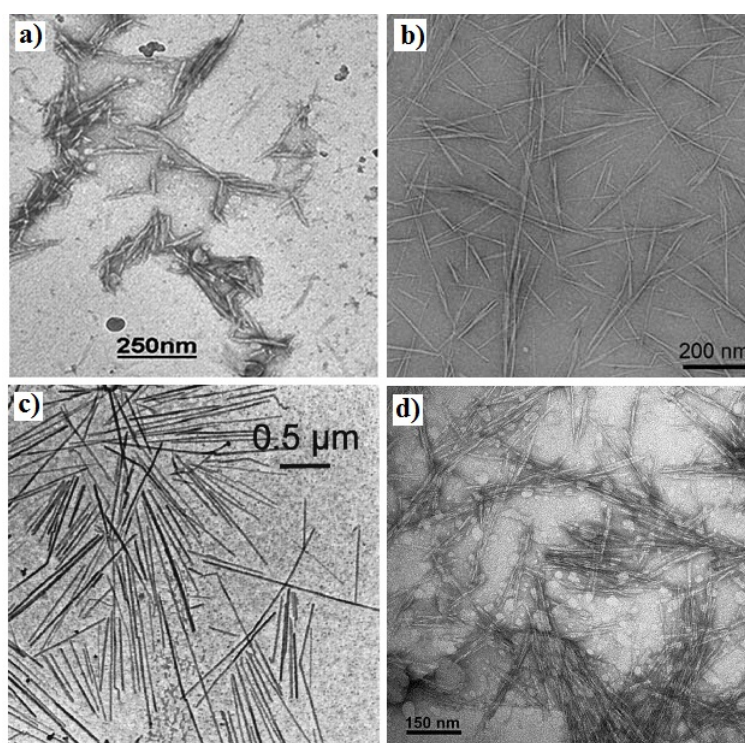
Figure 2.4: *Transmission electron microscope (TEM) images of cellulose nanowhiskers, obtained from acid hydrolysis of **(a)** cotton [49], **(b)** sisal [50], **(c)** tunicate [51], and **(d)** microcrystalline cellulose [52].*

In one study, the elastic modulus of crystalline cellulose along the chain axis was calculated to be around 167 GPa for native cellulose [53]. However, the Young's

modulus was seen to be significantly affected by the intra-molecular hydrogen bonding along their chain axis, resulting in the reduction of the tensile properties. The elastic modulus (in the axial direction) of the cotton based nanowhiskers was reported to be 57 GPa (for a 2D network) and 105 GPa (for a 3D network) in the literature [54].

2.1.2 Polylactic acid (PLA)

Polylactic acid (PLA) is one of the most popular bio-based polymers investigated and has many potential applications in the medical, textile, food and packaging industries [55-58]. The monomer lactic acid is obtained through fermentation of glucose with conversion reaching 90% [59] and PLA is usually produced by ring opening, polycondensation or chain extension polymerisation of lactide [60].

Though the large-scale use of PLA based packaging materials is still stayed behind the synthetic plastics, recently this PLA is using extensively in reinforcing composites to expand their applications [61-64].
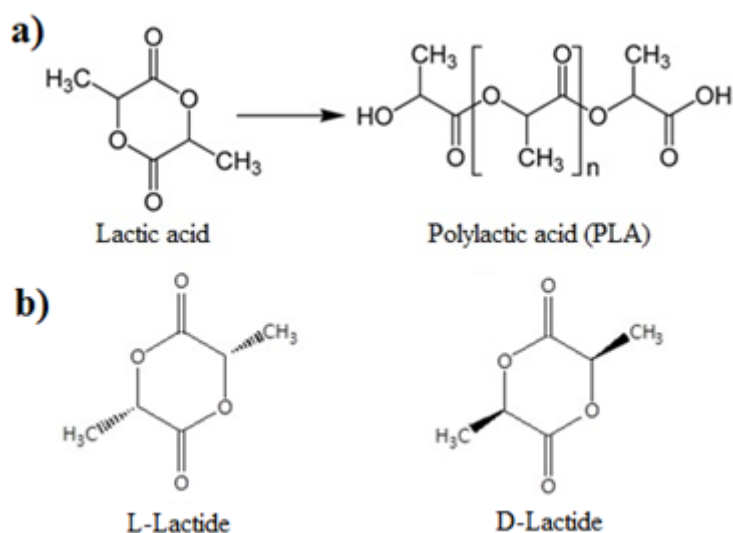
Figure 2.5: *a) Ring opening polymerisation of polylactic acid (PLA), and*

b) chemical structure of L-Lactide and D-Lactide isomers [60].

PLA is one of the most common bioresorbable polymers (polymers that break down by the physiological environment and the degraded materials are biocompatible that absorbed in the body once the purpose has been served) investigated widely for internal bone fixation implants due to its degradation rates, good mechanical properties and availability in different lactide content (i.e. L/D ratio). Lactic acid (2-hydroxy propionic acid) monomer exists in two optically active configurations; levo-(L-)lactide and dextro-(D-)lactide [58, 65]. Therefore, it is also possible to produce PLLA (100 % L-Lactide) and PDLLA as a copolymer with different L- to D-lactide ratios. The mechanical properties, crystallinity, resorption time and molecular weight of PDLLA depend on the L/D ratio [66-68]. PLLA possesses high percentage of crystallinity, whereas the crystallinity for PDLLA depends on the D-lactide content, for example, the crystallinity for PDLLA can be higher when the D-lactide content is less than 2 % [60]. PLA degraded into lactic

acid via hydrolysis process which converts to pyruvic acid and then carbon dioxide and water through the tricarboxylic acid cycle (TCA) [68, 69].

2.1.3 Polycaprolactone (PCL)

Polycaprolactone (PCL) was synthesised by the Carothers group in the 1930s and can be prepared by either ring opening polymerisation of ε–caprolactone or via free radical ring-opening polymerisation of 2-methylene-1-3-dioxepane. It is a semi-crystalline polymer and its crystallinity decreases with increasing molecular weight. PCL and its copolymers have been used for varying biomedical applications [70].
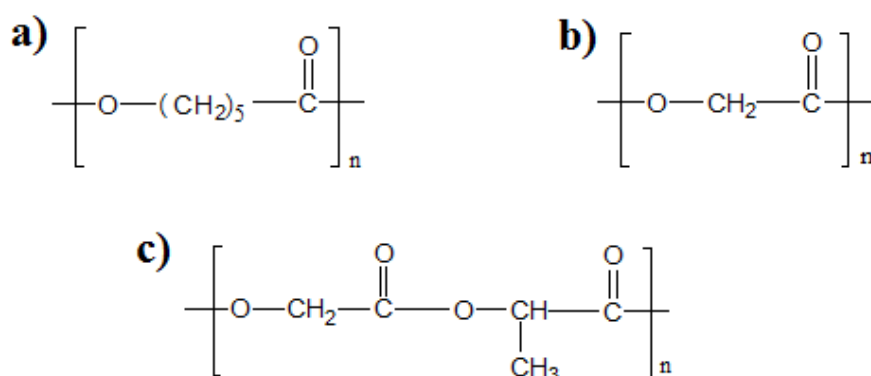
Figure 2.6: *Chemical Structures of some common types of biopolymer:*

a) polycaprolactone (PCL), b) polyglycolic acid (PGA), and c) polylactic-co-glycolic

acid (PLGA).

2.1.4 Polyglycolic acid (PGA)

Polyglycolic acid (PGA) belongs to the aliphatic polyester group usually obtained from glycolic acid by means of ring-opening or poly condensation polymerisation. PGA has been regarded as a tough fibre-forming biodegradable and biocompatible polymer. However, unlike PLA, PGA is readily soluble in water. Thermoplastic PGA and its copolymers (polylactic-co-glycolic acid - PLGA) with lactic acid have been

widely used in the biomedical field for the synthesis of resorbable sutures, drug delivery devices and rods [71-73].

The mechanical, thermal and degradation properties of the most commonly used aliphatic polyesters [67] are presented in Table 2.1.

Table 2.1: *Degradation rates, physical and mechanical properties of the most commonly used aliphatic polyesters [67].*

Property	PCL	PGA	PLLA	PLA	PLGA
Glass transition temperature T_g (°C)	-60 - -65	35-45	55 - 65	50 - 60	$40 - 50$
Melting temperature T_m (°C)	58 - 65	220 - 233	170 - 200	170	*Am.*
Elastic modulus (GPa) *	$0.2 - 0.4$	$6 - 7$	3 - 6	$1 - 3.5$	$1 - 3$
Flexural strength (MPa)	16 - 29	195 - 375	109 - 145	95 - 130	~ 65
Tensile strength (MPa)	20 - 35	60 - 80	50 - 80	20 - 60	$40 - 55$
Degradation time (month) **	24 - 48	6 - 12	24 - 72	12 - 16	1 -12

*Am. refers to amorphous, * Tensile or flexural modulus and ** represents the required time for complete degradation.*

2.2 PLA FIBRE

Thermoplastic PLA can be produced into fibrous structures via melt spinning and/or electrospinning with distinct fibre properties [74-77]. For example, melt

spinning is employed to produce microfibres whilst the electrospinning process has been used for nanofibre to submicron fibre production.

Properties of melt drawn PLA fibres produced using different processing conditions with varying L-lactide to D-lactide ratios have been reported in the literature [74, 78-83]. Kim *et al.* [83] produced melt spun PLA fibres with a 1 to 9 mol% D-lactide content and investigated the mechanical, thermal and crystallisation properties of uniaxial elongated PLA monofilaments at varying draw ratios (DR), from 1 to 8, in the temperature range between 25°C to 65°C. They reported that the tensile strength and modulus of control PLA monofilaments (4.2 mol% D-lactide content) decreased from 71 MPa to 18 MPa and 2.4 GPa to almost zero, respectively, with increasing temperature due to chain mobility of the polymer in the glass transition region. The glass transition (T_g) temperature of PLA fibre drawn at higher ratios (DR=8) was seen to shift to 68°C, which was approximately 12°C higher than the undrawn fibre, which suggested a higher degree of chain orientation due to strain induced crystallisation during the fibre drawing process. Chain orientation ascertained in terms of inverse dichroic ratio (measured using polarised Raman spectroscopy) within the PLA fibres was also reported to increase with an increase in the draw ratio of the spun fibres.

Okuzaki *et al.* [84] investigated melt spun PLLA fibres (processed at 185°C) with a 394 μm diameter and reported that further drawing (DR=10.5) of the as-spun fibre at 90°C increased the crystallinity of the PLLA fibre by 30% when compared to undrawn fibres (crystallinity 7.4%). In addition, drawing the fibres (DR=10.5) increased the tensile strength from 16 MPa to 275 MPa, whilst the modulus

increased from 1.8 GPa to 9.1 GPa. They further suggested that the improved properties were due to the increased orientation factor of the polymer chains within the fibre as a direct result of drawing at 90°C. PLLA fibres with diameters ranging from 11 to 14 μm obtained at 5000 m min^{-1} take up velocity and at 233°C [81] were shown to display a maximum crystallinity, tensile strength and modulus of 42%, 385 MPa and 6 GPa, respectively.

2.3 BIOPOLYMER FIBRE IN SELF-REINFORCED (SR) COMPOSITES

Self-reinforced composites (SRCs) have found widespread use for applications in the biomedical, construction and packaging industries [85, 86]. The concept of self-reinforced composites was first developed by Capiati and Porter [87] who demonstrated that the orientation of aligned chains within the same polymer significantly improved their initial mechanical and fracture failure properties. In this process, fibres derived from the same polymer were heated above the glass transition (T_g) temperature but below their melting temperature (T_m) and compressed to produce composite plates using high pressure where the ultimate mechanical properties of the composites formed depend on the molecular weight of the polymer and the fraction of aligned chains within the self-reinforced composites [88, 89]. The selection of temperature, pressure and time are very important in order to maintain optimum reinforcing effect of the fibres in SRC processing [90]. Various techniques, such as hot compaction, physical treatment, partial dissolution, cold drawing and chemical modification have been employed to manufacture SRCs [85]. Several studies have reported on successful production

of SRCs using a wide variety of polymer fibres, including polyethylene (PE) [91-94], polypropylene (PP) [95, 96], polyethylene terephthalate (PET) [97], polyamides [98, 99], polylactic acid (PLA) [88, 100, 101], polyglycolic acid (PGA) [102, 103] and polymethylmethacryalate (PMMA) [104, 105].

Fibres derived from biopolymers, such as polylactic acid (PLA), polyglycolic acid (PGA), their copolymer PLGA and polycaprolactone are the most widely investigated bioresorbable materials for use in medical applications [1, 2]. Biopolymer composites have also been manufactured as self-reinforced (SR) composites. The principal of self-reinforcement is consolidation of orientated fibres within the same matrix, where the aligned chain of that polymer acted as reinforcing agent to provide sufficient strong and stiff SR composites [85, 102, 106].
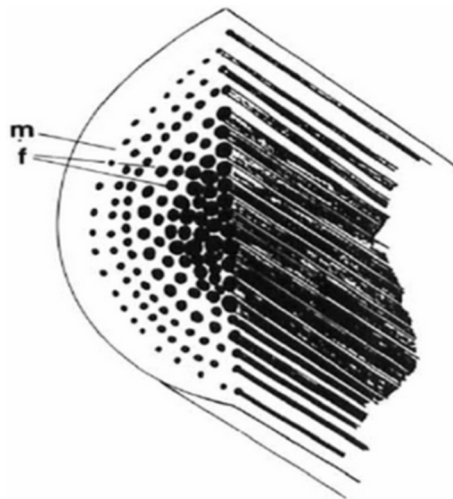
Figure 2.7: *A schematic diagram of self-reinforced composites consisting of matrix (m) and reinforcing fibre (f) derived from the same polymer [102].*

SR composites can be produced employing different methods, such as fibre sintering, mechanical deformation/drawing process and die extrusion [88, 102,

107, 108]. However, to maintain the integrity of the fibrous structures of the polymer chains the processing temperatures must be maintained above the glass transition temperature (T_g) and below the melt temperature (T_m) for the polymer. In case of the polymers whose T_g were lower than room temperature, the cold drawing (at room temperature) method could be applied for SR composite processing. In addition, during the mechanical deformation process, fractions of crystalline spherulites could also convert into oriented chains [102, 109].

Commonly, fibres or a mixture of fibres and resin derived from the same polymer are sintered/hot compacted using mould cavities maintaining the temperature adjusted for the partial melting of the fibres [106]. In order to produce highly compacted materials, high pressure should also be applied during the SR composite processing. However, some types of SR composites could also be produced by rapid solidification of the molten polymer flowing through an extrusion die [108].

The advantages of SR composites over other composites include the ability to achieve excellent interfaces between the components, pure chemical functionality, light weight, low cost, high initial mechanical strength and ductile failure mode. The improvement in the mechanical properties of SR composites depends on the molecular weight of the polymer and processing conditions (such as, temperature, pressure, compression time) so that optimum portion of aligned chains could be obtained within the composite [88, 89]. Wright-Charlesworth *et al.* [100] investigated the flexural properties of SR PLLA composite produced via a hot compaction process at 95°C and reported that SR-PLLA had an initial flexural

strength of 139.2 MPa and flexural modulus of 5.4 GPa compared to non-reinforced PLLA (strength~110.8 MPa and modulus~3.9 GPa) [100]. An example of mechanical properties for some SR PLA composites developed for biomedical applications are reported in Table 2.2.

Table 2.2: *Mechanical properties for self-reinforced PLA biocomposites [67].*

Composite	Sample Geometry	Flexural Modulus (GPa)	Flexural Strength (MPa)	References
Extruded SR-PDLLA[*]	Rod	3.6 - 8.8	125 - 237	[110-113]
Sintered SR-PLA	Rod	-	270	[101]
Drawn SR-PLLA (Draw ratio=12)	Plate	10	300	[107]

[*]*L- content within copolymer was varied from 70 to 96 %.*

For biomedical applications, fibres derived from biopolymers such as PLA, PGA, and their copolymer PLGA have been the most widely investigated for SRC processing [101-103]. Amongst them PLA is one of the most common bioresorbable polymers utilised for internal bone fixation implants due to its favourable degradation and mechanical properties and availability with different lactide contents (i.e. L/D ratio) [66, 67]. Waris *et al.* [114] investigated the SR-PLLA sheet for the treatment of bone defect in craniofacial surgery (see Figure 2.8) and reported the use of SR-PLLA would be favourable in growing skull. The mechanical properties of SR-PLLA also reported near to that of the cortical bone.
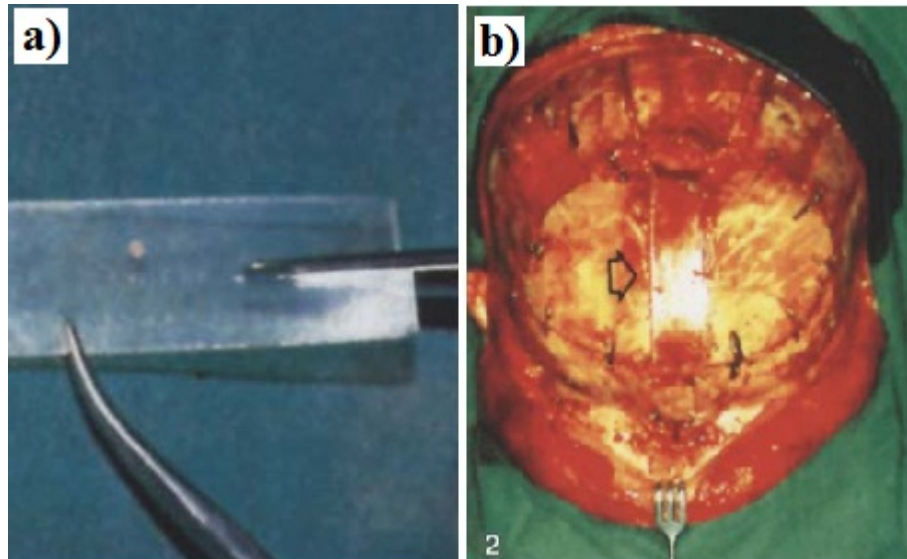
Figure 2.8: *a) 0.5 mm thick SR-PLLA sheet, and b) SR-PLLA sheet (arrow) used for*

the treatment of bone defect created between halves of frontal bone

[114].

2.4 NATURAL FIBRES IN COMPOSITE MATERIALS

Natural fibres, manufactured from renewable sources are being widely used with

biopolymers to produce biocomposite materials, which have already shown huge

potential as an alternative to conventional reinforcement fibres (such as, carbon,

glass, etc.) due to their low cost, availability, biodegradability, high strength and

toughness [115]. More recently, micro and nano reinforcements using natural

fibres in different polymers based on renewable resources have been investigated

[116].

2.4.1 Cellulosic fibre composites

Cellulose is the most abundant polymer obtained from renewable natural sources

(such as cotton, jute, flax, hemp, sisal, hardwoods, softwood, tunicates, bacteria,

etc.) as a fibrous structure and has been investigated as reinforcement in polymer

composites for numerous applications [6, 45, 117]. The composition of cellulose is

related to the natural source from which it was obtained like climate, maturity, fibre modification and processing (retting, scotching, bleaching, spinning). Several types of cellulosic fibres have also been investigated for reinforcement of polymers intended for use in several structural (roof systems, load bearing walls, and stairs) [118], constructional (furniture, windows, doors, and ceiling tiles) [119], electronics [120, 121], packaging [37], biomedical and tissue engineering applications [116, 122, 123]. Surface modifications of cellulose have also been widely explored due to its hydrophilicity and bonding between the polymer chains to improve their interfacial compatibility with polymers to enhance the material (mechanical, thermal and thermomechanical) properties of the composites.

Figure 2.9: *Roof panel prepared using biocomposite materials [118].*

For composite materials, the interface between the matrix and the natural fibre is critical in stress transfer between the polymer and the fibre. Therefore, a large amount of work has investigated improving the fibre/matrix interface by modifying the fibre surface. These surface modifications include etherification,

esterification, siloxane and urethane formation, click-chemistry, and adsorption of lignin or carboxylic waxes [124-132]. Additionally, fibre/matrix mechanical interlocking can be improved by roughening the fibre surface through mercerisation (alkali-treatment). It also decreases fibre shrinkage and lowers the microfibrillar angle which results in improved fibre mechanical properties [133, 134]. The fibres were usually treated before incorporation into the matrix to improve the compatibility with the polymer. The treatments investigated included impregnation [135] or encapsulation [136] with polymer, coating with latex [137], grafting with silanes [135] , with isocyanates [136, 138, 139], with carboxylic acids [137] and with acid anhydrides [137, 138], with grafting found to be more effective than coating. Among grafting agents, isocyanates [138] and linoleic acid [137] were found to perform the best. Composites reinforced with wood fibres presented quite comparable mechanical properties with glass fibres reinforced composites [135, 139].

The mechanical properties of flax fibres (modified with 5% maleic anhydride-polypropylene (MAPP) copolymer) reinforced polypropylene (PP) composites was investigated by Arbelaiz *et al*. [140]. The SEM images of untreated, MAPP treated flax/PP and E-glass/PP composites are represented in Figures 2.10. The untreated flax/PP composites exhibited a gap between the fibre and matrix suggesting poor fibre/matrix interaction. Whereas, MAPP treated flax/PP composites revealed much improved fibre/matrix interface. The E-glass fibre/PP matrix also displayed poor interfacial adhesion due to the polar surface of the glass fibre. Composites containing approximately 30 wt% fibres were reported to have tensile strengths of

27 MPa and 37 MPa for untreated and MAPP treated flax/PP composites respectively compared to 32.4 MPa for PP alone. The tensile modulus for flax and MAPP treated flax/PP composites revealed values of 1.6 GPa and 2.1 GPa respectively, compared with 2.2 GPa for the E-glass fibre/PP composites with a similar fibre content.
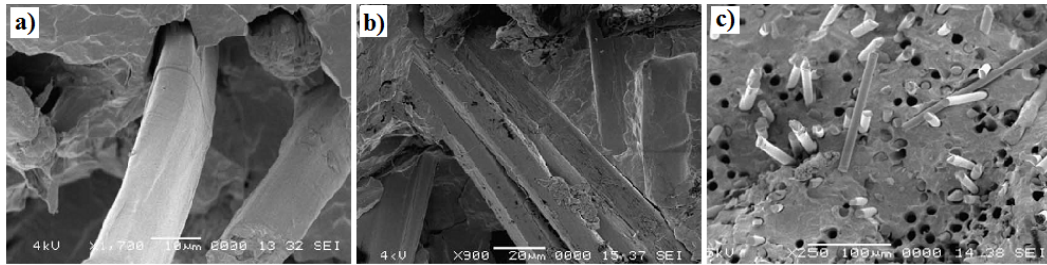
Figure 2.10: *SEM micrographs of fracture surface of composites: **a)** untreated flax/PP, **b)** MAPP modified flax/PP, and **c)** E-glass/PP composites [140].*

A vast amount of biomass-derived cellulosic fibre reinforced composites have also been investigated [141]. These composites have bio-based polymer matrices such as plant oil triglyceride based resins [142-146], PLA [147-149], soy-protein [133, 150], polyhydroxy alkanoates (PHA) [151-153], and wheat gluten [154]. Compared to petroleum-based polymer matrices, bio-based polymers are not a magical solution for good composite properties. While it has been predicted that good adhesion could occur between natural fibres and more hydrophilic polymers which display groups capable of hydrogen bonding, this is not obvious from work using bio-based polymer such as PLA [63, 155, 156]. For example, Bax and Müssig [155] investigated flax-PLA composites and compared their properties to rayon fibre/PLA composites. Flax reinforced composites were comparable to their rayon reinforced counterparts for modulus and strength, however, performed poorly for

impact properties, similar to other work using flax and jute fibres. Despite relatively poor interaction between the matrix and the fibres, which usually is beneficial for impact, a decrease in impact strength was noticed upon fibre reinforcement. In general, bio-based polymer composites encounter the same issues and control over the fibre/matrix interface and improvement of the inherent fibre properties remain important fields of research [124-132].

2.4.2 Nanocellulose in composite materials

Cellulose reinforcements have also arrived in the nano reinforcement area. Treatment of pure cellulose fibres by enzymatic, mechanical and/or concentrated acid results in a reduction of the cellulosic fibre length. There are two main methods in obtaining submicron/nanosized cellulose from macroscopic cellulose fibres. A method described first by Turbak *et al*. [157] uses mechanical disintegration as the main driver, resulting in long somewhat flexible nanofibrils. A second method relies on acid hydrolysis using inorganic acids first reported by Nickerson and Habrle [158], results in highly crystalline ribbon-like nanowhiskers. In 1995, Favier *et al.* [15] were the first ones to mention the use of cellulose whiskers as reinforcements in composites. Since then an enormous amount of work has appeared on nanocellulose-reinforced composites.

Cellulose nanowhiskers have been used as reinforcements in polymer matrices such as poly(styrene-co-butyl acetate) [159], plasticised starch [160], pectin [161], epoxy resin [162], polyvinyl acetate) (PVAc) [163], polyethylene oxide (PEO) [164], PVA [165], and PLA [166]. Layer-by-layer assembly processes have also been used

to make layered composites for mechanical applications [167], but which have also been explored in sensor development [168-170].

Garcia de Rodriguez *et al.* [50] investigated cellulose nanowhiskers (obtained from sisal) reinforced PVAc nanocomposite films and found that the high aspect ratio of the whiskers (length 250 nm and diameter 4 nm) ensured that a percolation network would improve the mechanical and thermal properties of nanocomposite at lower whisker loading. Furthermore, water uptake properties of PVAc/whisker nanocomposites were reported to increase with the addition of nanowhiskers into the matrix and water diffusion into films was found to be hindered by a percolated network of cellulose nanowhiskers above the percolation threshold. Biomimetic, stimuli responsive cotton based nanocomposites were produced by Shanmuganathan *et al.* [49], who introduced the percolated network of cellulose whiskers into a PVAc matrix. Addition of nanowhiskers isolated from tunicin within the PVAc matrix were reported to play an important role to increase their storage modulus ($E^{'}$) from 2 GPa to 4 GPa for nanocomposites comprising 16.5% v/v whiskers. The tan delta curves were also seen to shift to the higher temperature regions by 5-7°C in case of nanocomposites when compared to neat PVAc (Figure 2.11b). They also reported that immersion into artificial cerebrospinal fluid (ACSF) at 37°C the nanocomposites showed a noticeable decrease in storage modulus (from 4 GPa to 5 MPa for 16.5% whisker content) with around 28% swelling.
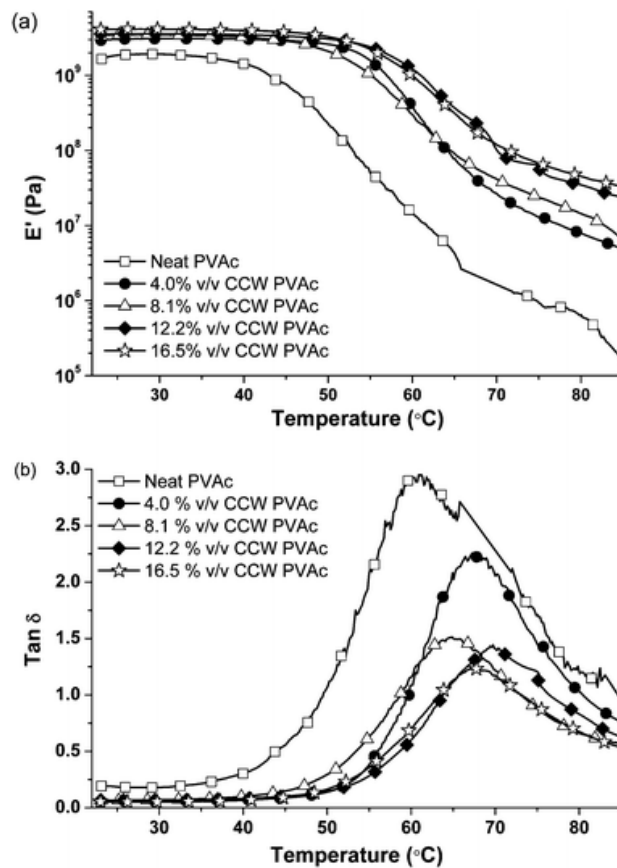
Figure 2.11: *(a) Tensile storage moduli (E') of PVAc/cotton cellulose whisker (CCW)*

nanocomposite films as a function of temperature obtained by dynamic

mechanical analysis (DMA)and (b) Tan delta curves (ratio of loss modulus and

storage modulus) for the nanocomposite films [49].

Petersson *et al.* [52] investigated the structural and thermo-mechanical properties

of composites made using solution cast PLA/cellulose whiskers (obtained from

microcrystalline cellulose) materials using *tert*-butanol with reasonably good

dispersion of the whiskers (5 wt%) within the polymer matrix. Enhanced thermal

stability in the region between $25^{o}C$ and $220^{o}C$ and improved storage modulus at

higher temperature (64% increased at $60^{o}C$) was also reported (see Figure 2.12).

In addition the tan peak was seen to shift by $20^{o}C$ compared to the control PLA.
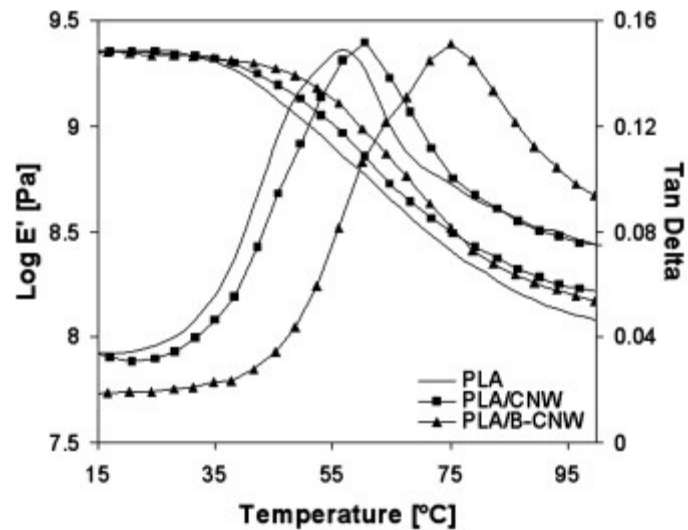
Figure 2.12: *Storage modulus curves and tan delta peaks obtained from DMA*

analysis. Here CNW and B-CNW represent the untreated and tert-butanol treated

CNW [52].

Water and oxygen permeability of nanocomposite films prepared using CNWs

(obtained from microcrystalline cellulose) and PLA was investigated by Sanchez-

Garcia and Lagaron [171]. The water permeability of nanocomposite containing 3

wt% nanowhiskers were reported to decrease by 82% and the oxygen

permeability by up to 90% compared to control PLA film. The mechanical

properties of microcrystalline cellulose based CNWs reinforced PLA

nanocomposite films was investigated by Oksman *et al.* [172]; they reported

improvement of tensile modulus and strength by 35% and 90% was achieved for

CNWs reinforced PLA composites produced using an extrusion moulding process

compared to the control PLA (tensile modulus~2.9 GPa and strength~40.9 MPa).

Jonoobi *et al.* [173] studied cellulose nanofibres (isolated from Kenaf pulp)

reinforced PLA composites produced using melt extrusion process and found a

significant increase in tensile strength from 58 MPa to 71 MPa with a slight

increase in tensile modulus from 2.9 GPa to 3.2 GPa for the nanocomposite containing 5 wt% cellulose nanofibres.

Bio-based nanocomposites have also been produced using CNWs (obtained from cotton linter pulp) and chitosan [174]. It was reported that the nanocomposite films exhibited good miscibility as well as strong interactions between the CNWs and the matrix with increasing tensile strength from 85 MPa to 120 MPa for 20 wt% CNWs loading within the films. In addition, CNW/chitosan based nanocomposite displayed excellent thermal stability and water resistance properties.

Zhou *et al.* [175] investigated rod-shaped cellulose nanocrystals obtained from microcrystalline cellulose to reinforce polyacrylamide hydrogels (Figure 2.13). They suggested that the cellulose nanocrystals acted not only as a reinforcing agent for hydrogel formation, but also as a multifunctional cross-linker for gelation and that they could be used for bone defect repairs and bone tissue engineering.
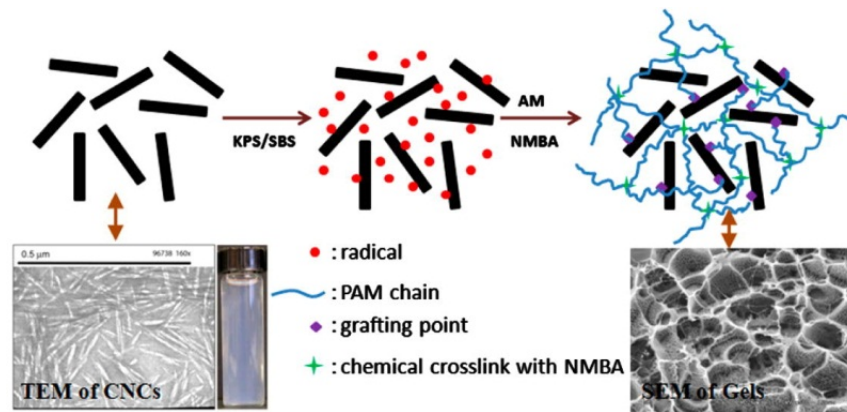
Figure 2.13: *Represents the scheme of the gelation mechanism of polyacrylamide-cellulose nanocrystals hydrogels* [175].

Heath and Thielemans [176] successfully produced highly porous cellulose aerogels (porosity ranges from 95 to 91%) using cotton extracted cellulose nanowhisker with high specific surface areas (up to 605 m^2 g^{-1}) and also suggested that the density and porosity of the aerogel could be easily altered by varying the cellulose nanowhisker concentration.
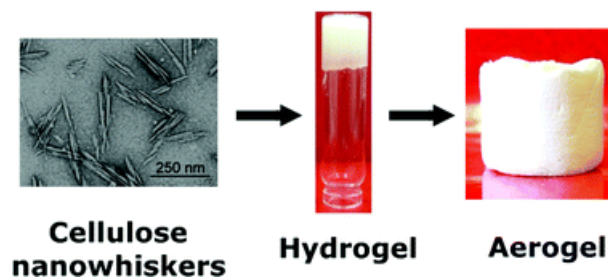
Figure 2.14: *Cellulose aerogel produced by self-assembly of cellulose nanowhiskers isolated from cotton [176].*

Recently, applications of nanocellulose have been widely extended from paper and packaging sectors to construction, automotive, furniture, electronics, cosmetics, pharmaceuticals and biomedical fields. For example, cellulose derivatives such as cellophane, cellulose acetate (CA), cellulose acetate

propionate (CAP) and cellulose acetate butyrate (CAB) are being used to produce hybrid plasticised nanocomposites for food packaging applications (baked goods, fresh product, processed meat and cheese) [37]. In electronic sectors, nanocellulose diaphragms have been used in SONY headphones (see Figure 2.15) [116]. The diaphragms were produced by dehydration and compression of nanocellulose into ultrathin film (20 microns thickness) which had a high sound velocity and low dynamic loss that were comparable with aluminium or titanium diaphragm.

Figure 2.15: *Nanocellulose diaphragm used in SONY headphones [116].*

Highly optically transparent and flexible nanocellulose films with high cellulose content were reported to have potential to be used in flexible display devices (Figure 2.16a) [177]. Shah and Brown [120] have shown the use of nanocellulose in flexible electronic display devices, which was fabricated by integrating an electronic dye into the nanostructure of cellulose (Figure 2.16 b &c).
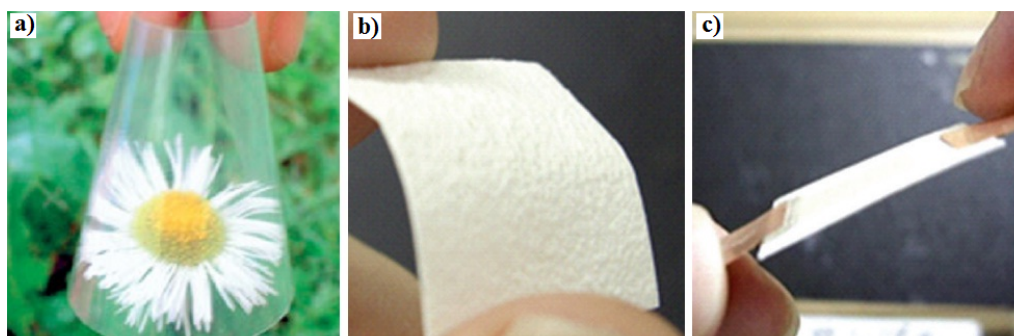
Figure 2.16: *a) Flexible optically transparent nanocellulose sheet [177],*

b) nanocellulose paper, and c) nanocellulose paper used in bendable display device

[120].

Cellulose nanocrystals have also been investigated as sustain released drug delivery excipients in the pharmaceuticals industries [116, 178]. Watanabe *et al.* [178] investigated press-coated tablets coated with a blend of crystalline cellulose and polyethylene glycol (PEG) (ratio 8:2) and reported the timed-release characteristics of the coated tablets in the gastrointestinal tract of rabbits. Ni *et al.* [179] evaluated the cytotoxicity of cotton based CNWs and suggested that CNW as a nanobiomaterial had potential applications in drug delivery devices and implants; results from their MTT assay and cell cytotoxicity showed that CNWs at low concentrations (0.2 wt%) had low toxicity to L929 cells. In addition, cotton extracted cellulose nanofibres were studied with a sophisticated 3D human lung cell by Clift *et al.* [180] and they suggested that the cellulose nanofibres elicited a significantly lower cytotoxicity and inflammatory response than multi-walled carbon nanotubes and asbestos fibres.

Mahmoud *et al.* [181] suggested the surface charge of cellulose nanocrystals (CNCs) (isolated from flax) played an important role in cellular uptake and

cytotoxicity properties with human embryonic kidney 293 (HEK 293) cells. CNCs were positively charged with Rhodamine-B isothiocyanate (RBITC) and were observed to be well conjugated with HEK 293 cells with no noticeable cytotoxic effect.

Recently highly crystalline CNWs have been investigated as novel biomaterials in pharmaceutical and biomedical applications such as, surface coatings, regenerative medicine and drug delivery devices. The high surface area, abundant surface hydroxyl groups and the negative charge of the nanocellulose has enabled them to provide a wide range of chemical modifications to bind with other drugs for varying clinical applications.

2.5 CONCLUSIONS

From the literature surveyed for the purpose of this project, it can be concluded that cellulose nanowhisker and biopolymer fibre reinforced composites (in the form of biocomposites/nanocomposites/self-reinforced composites) have been shown to have huge potential in a wide range of applications within the packaging, electronics and biomedical fields. However, improvements in biocompatibility, fibre/matrix interaction, fibre size and shape, fibre orientation within matrix and consistency in properties still requires further attention in order to extend their application. The main problem associated with the use of CNWs in composite materials is related to their homogeneous dispersion within hydrophobic polymer matrix, such as PLA. Composites based on PLA also exhibited

brittle characteristics, which is regarded as one of the limitations of PLA. In addition, the surface of PLA possesses too poor a hydrophilicity to support degradation due to environmental moisture.

This research aimed to investigate the dispersion of cotton based CNWs in hydrophobic PLA and in hydrosoluble hydroxyethyl cellulose (HEC) matrices to produce flexible composite films. In addition, cellulose nanowhisker was chosen in this research to treat the surface of melt drawn PLA fibre in order to improve their mechanical, surface roughness and hydrophilic properties. Furthermore, cellulose nanowhisker coated PLA fibres were aimed to manufacture self-reinforced composites with improved mechanical properties.

CHAPTER 3.

PHYSICO-CHEMICAL AND MECHANICAL PROPERTIES OF NANOCOMPOSITES PREPARED USING CELLULOSE NANOWHISKERS AND POLYLACTIC ACID

3.1 SUMMARY

In this chapter, a range of nanocomposite films were prepared using cellulose nanowhiskers (CNWs) and polylactic acid (PLA) via a solvent casting process. Acid hydrolysis process was used to produce CNWs from bleached cotton. Transmission electron microscopy (TEM) image revealed rod-like whiskers in the nano-scale region which were dispersed within the PLA matrix. The presence of the functional groups of CNWs and PLA were confirmed via FTIR analysis. Tensile tests were conducted on thin films and the nanocomposites containing 1 wt% CNWs showed a 34% and 39% increase in tensile strength and modulus, respectively, compared to pure PLA. However, voids identified within the nanocomposite films believed to have played an important role on the mechanical and degradation properties of the films containing higher percent of CNW. Dynamic mechanical analysis (DMA) revealed that the tensile storage modulus also increased in the visco-elastic temperature region with increasing CNWs content in nanocomposites. Thermogravimetric analysis showed that all the materials investigated were thermally stable from room temperature to 210°C. A positive effect of CNWs on the crystal nucleation of PLA polymer in the

nanocomposites was observed using differential scanning calorimetry (DSC) and X-ray diffraction (XRD) analyses. The degradation profiles of the nanocomposites in deionised water over one week period revealed a mass loss of 1.5 to 5.6% at alternate temperatures (25°C, 37°C and 50°C) with increasing CNWs content in the nanocomposites, which was strongly influenced by the presence of crystalline CNWs.

3.2 INTRODUCTION

Materials, derived from biological origin, having at least one dimension in the nano-scale region can be incorporated into a natural polymer matrix [174, 182] to produce bio-based nanocomposites. These types of composites have shown potential applications in the field of food packaging, biomedical and tissue engineering with improved thermal and mechanical properties [183-185]. High strength cellulose nanowhiskers (CNWs) embedded within a biopolymer matrix has huge scope as bone implants, in soft tissue repair and as resorbable sutures. Cellulosic fibre, a polysaccharide composed of several hundred to tens of thousands of β-glycoside units in a linear orientation [41], is a natural polymer obtained from vegetable origin and is both biodegradable [11, 12, 186] and biocompatible [187, 188]. Cellulose nanocrystals are generally produced via acid hydrolysis using either sulphuric acid [15, 189], hydrochloric acid [190, 191] or nitric acid [192]. Recently CNWs have been used to reinforce biopolymeric matrices and several studies have investigated the mode of their reinforcement

[48, 159]. CNWs have high mechanical properties; for instance they have a tensile modulus of approximately 105 GPa [54].

Polymeric biomaterials are compatible with biological systems and have been used to treat, augment, or replace tissues, organs and/or functions of the biological systems. PLA has many potential applications in the medical, textile, food and packaging industries [55-58]. Within the medical field PLA has been investigated for use in drug delivery systems, drug encapsulation, surgical implants, sutures, soft tissue and bone fixative materials [62, 193, 194].

For composite preparation, PLA has been blended with reinforcing fibres [61, 63, 64], polymers including starch [195, 196], chitosan [167, 174, 197] and inorganic fillers [198]. Bondeson and Oksman [199] showed that nanocomposites prepared via extrusion moulding of PLA/CNWs modified using polyvinyl alcohol followed by compression moulding showed improved mechanical properties, for example, tensile modulus increased from 3.31 GPa to 3.71 GPa for the composite containing 65% PLA, 30% PVA and 5% CNWs compared with pure PLA. Cellulose nanofibre (produced from kenaf pulp) reinforced PLA composites produced via melt compounding and extrusion also showed a tensile modulus and strength increase from 2.9 GPa to 3.2 GPa and from 58 MPa to 71 MPa, respectively, for nanocomposites containing 5% cellulose nanofibre. The dynamic mechanical analysis results also reported that the storage modulus increased for all nanocomposites that were investigated, compared to PLA in the higher temperature region (70°C) [173]. Liu *et al.* [200] also investigated composite films prepared using PLA and flax cellulose obtained via acid hydrolysis of flax yarns and

reported that composites containing 5% flax cellulose showed the tensile strength and modulus increased by 59% and 47%, respectively. In contrast with the studies above [52, 173, 199], it has also been reported that the tensile modulus of nanocomposites containing 1, 2, 3 and 5% freeze dried CNWs isolated from highly purified alpha microcrystalline cellulose reduced by 37, 47, 43 and 35% respectively, compared to pure PLA [171]. However, the dispersion of CNWs in chloroform was performed in that study using a homogeniser and then stirred with PLA solution at 40°C for 30 minutes. A significant decrease in tensile strength (up to 54%) was also reported in these nanocomposites.

The chapter aimed to investigate the effect of the addition of CNWs in PLA on the thermomechanical, crystallisation and degradation properties of the biodegradable nanocomposites. To achieve this goal the nanocomposites (comprising of PLA reinforced with 1, 3 and 5 wt% CNWs) produced have been manufactured using cotton based CNWs and Natureworks PLA via a solvent casting process. The morphological, mechanical and thermal properties of these bio-based nanocomposite films are also reported in this chapter. Melt compounding process for the manufacture of PLA/CNWs composite films were also attempted at 190~200°C. However, the composite samples obtained were found to be quite brittle and the colour of the films was seen to turn into a dark brownish colour which was suggested to be due to thermal decomposition of CNWs. Therefore, the solvent casting process was considered to further progress the work conducted on PLA/CNWs based composite films.

3.3 MATERIALS AND METHODOLOGY

3.3.1 Materials

Sulphuric acid (purity 95%, specific gravity 1.83), cotton wool (Bleached), chloroform and amberlite MB 6113 resin were obtained from Fisher Scientific (UK). Uranyl acetate was supplied by Sigma-Aldrich (UK). Polylactic acid (PLA) beads purchased from NatureWorks LLC (Ingeo[TM] Grade 3251D average M_w~90,000-120,000 g mol^{-1}, Density=1.24 g cm^{-3}) were used as the matrix for the nanocomposites.

3.3.2 Cellulose nanowhiskers (CNWs) preparation

CNWs were prepared via hydrolysis of cotton wool (see Figure 3.1) for 45 min at 45°C in 64 wt % aqueous H_2SO_4 with constant stirring [201]. The resulting suspension was then treated as described in the literature to obtain the cellulose nanocrystals [202]. Briefly, the acid hydrolysed suspension was washed with deionised water utilising three successive centrifugations at 10,000 rpm and 10°C for 15 min. For the removal of residual free acid from the suspension a dialysis under running tap water was conducted for 48 hours after which the pH of the eluent was measured (as it was required to be neutral). The dispersion of CNWs in water was homogenised using a Branson sonicator for 4 min and then filtered over a n°2 fritted glass filter. The filtrate was stirred overnight with amberlite resin to remove non H_3O^+ cations from the CNWs suspension and then filtered again to obtain the final CNWs in deionised water. Finally, crystalline CNWs were obtained by freezing the suspension in liquid nitrogen and freeze drying. Prior to producing

the nanocomposites, a homogeneous suspension of CNWs in chloroform was prepared by stirring and sonication.
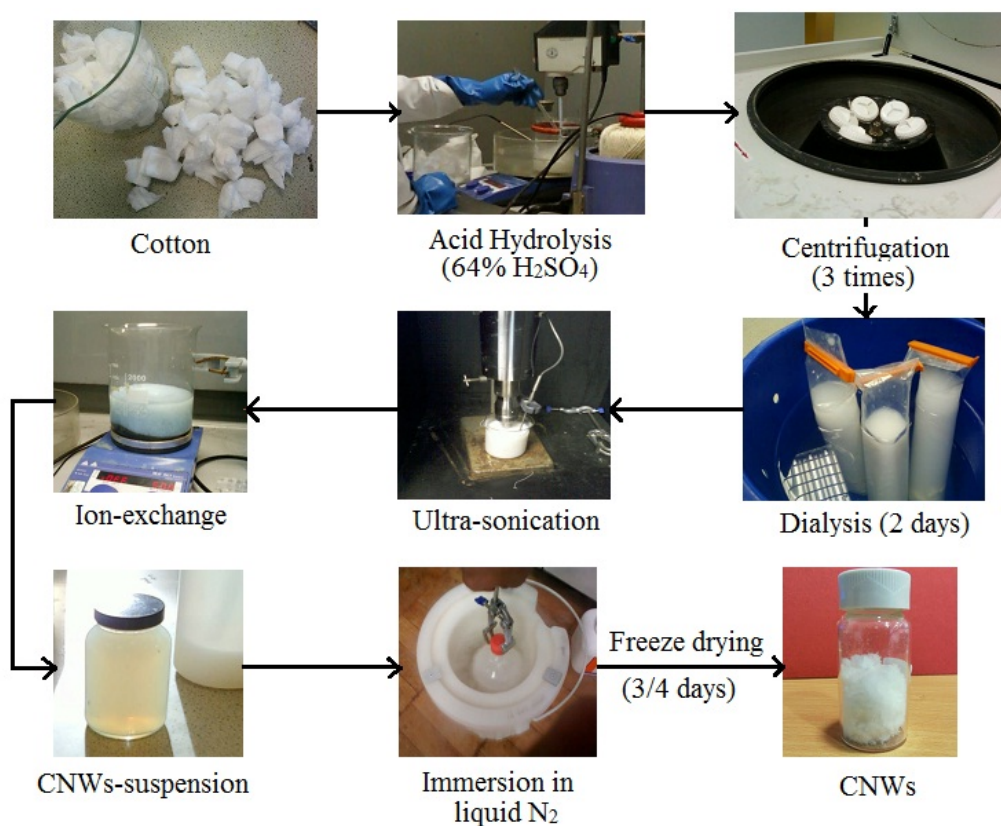
Figure 3.1: *Scheme of CNWs production from cotton via acid hydrolysis process.*

3.3.3 Nanocomposites preparation

The solvent cast nanocomposites were prepared by dissolving PLA pellets in Chloroform (10% w/v), which was stirred constantly using a magnetic stirrer at 40°C until the pellets were fully dissolved before adding the CNWs suspension in chloroform and mixing thoroughly for 2 hours. The formulations (Table 3.1) were poured into glass petri dishes placed on a horizontal surface and previously greased with silicon. The mixture was allowed to evaporate at room temperature (25°C) and after 24 hours the resulting films (approximate thickness 0.25 mm) were dried in a vacuum oven at 50°C for 48 hours to remove residual solvent.

Table 3.1: *Formulations and sample codes for the nanocomposites investigated in*

this study.

Sample **Codes** used in this study	PLA (wt %)	CNWs (wt %)
PLA	100	-
PLA-1	99	1
PLA-3	97	3
PLA-5	95	5

3.3.4 Characterisation

3.3.4.1 Electron microscopic analysis

The shape of the CNWs produced in this study were examined using transmission

electron microscopy (TEM) on a JEOL (JEM-2000FXII, UK) at an accelerating

voltage of 80 kV. CNWs were deposited from dilute aqueous dispersions onto

carbon coated copper grids (mesh size 300) hydrophilysed by plasma treatment in

an oxygen/argon 25/75% atmosphere for 5s. For the characterisation of

nanocomposites, a small sample was embedded in epoxy resin and cured for 1

day at room temperature (25^oC). The epoxy embedded films were cut into thin

slices (~100 nm) using an ultra-microtome cutter equipped with a sharp glass

edge. To obtain better contrast in TEM the Cu-grid containing the samples was

stained negatively using uranyl acetate (Sigma-Aldrich, UK) (2 wt%) for 3 min.

The surface topography of the nanocomposites was characterised using a

scanning electron microscopy (Philips XL30, FEI, USA) at an accelerating voltage of

12 kV and a working distance of 10 mm. A sputtered coating of platinum was used to avoid image distortion due to charging.

3.3.4.2 Void content of nanocomposites

The void content of solvent cast pure PLA and the nanocomposites were determined according to ASTM D 2734-94 method [203] using the theoretical ($\rho_{Theoretical}$) and experimental ($\rho_{Experimental}$) density of the nanocomposites:

$$\text{Void content=}\frac{\rho_{Theoretical}-\rho_{Experimental}}{\rho_{Theoretical}}\dots\dots\dots\dots\dots(3.1)$$

$$\rho_{Theoretical}=\frac{1}{\left[\frac{W_{CNWs}}{\rho_{CNWs}}+\frac{W_{PLA}}{\rho_{PLA}}\right]}\dots\dots\dots\dots(3.2)$$

Where, W_{CNWs} and W_{PLA} are the weight fraction of CNWs and PLA, respectively and ρ_{CNWs} and ρ_{PLA} are the density of CNWs and PLA, respectively.

3.3.4.3 Fourier transform infrared (FTIR) spectroscopic analysis

Identification of functional groups of the CNWs produced was confirmed after acid hydrolysis of cotton using FTIR (Tensor-27, Bruker, Germany). All spectra were analysed with Opus™ software version 5.5. The nanocrystals and the thin films were scanned in transmittance mode in the region of 4000 and 550 cm^{-1} (wave numbers) using standard pike attenuated total reflectance (ATR) cell (Pike Technology, UK).

3.3.4.4 Tensile tests

The nanocomposite films produced were cut into dog bone shapes using a 10 mm× 64 mm dog bone cutter and the tensile properties were characterised using a Hounsfield Series-S tensile test machine (Software-QMAT) with a cross head

speed of 1 mm min^{-1}, gauge length 25 mm and a 1 kN load cell. The tensile strength and modulus were calculated from experimental data according to the European standard (ISO/DIS 527-1:2010).

3.3.4.5 Dynamic mechanical analysis (DMA)

Thermomechanical properties of the PLA films and the nanocomposites were measured using a DMA (Q-800 from TA Instruments, USA) in mutifrequency strain mode using the tension film clamp. The characterisation was conducted using Q series (Q-800) software and parameters maintained during the analysis were: 0.05% strain, 0.01N preload force, 125% force track, 1 Hz constant frequency. The temperature was ramped from room temperature (25°C) to 80°C with a heating rate of 5°C min^{-1} and a gap distance of around 20 mm was maintained. Three repeat samples were used to characterise each material. The samples were prepared by cutting strips from the films with a width of 5 mm and length of 30 mm. The storage modulus (*E'*) and tan delta of the nanocomposites were recorded with respect to increasing temperature.

3.3.4.6 Thermogravimetric analysis (TGA)

The TG analysis was conducted from room temperature (25°C) to 480°C using a SDT Q600 thermogravimetric analyser from TA instruments (USA) with a heating rate of 10°C min^{-1} under 100 mL min^{-1} nitrogen gas flow. For background correction a blank analysis was conducted. The weight loss (%) with temperature of freeze dried CNWs and the nanocomposite films (6~10 mg) were determined. Data acquisition and processing was performed using TA Universal analysis 2000 software.

3.3.4.7 Differential scanning calorimetric (DSC) analysis

The percentage crystallinity of PLA in the nanocomposite films was investigated using a DSC (Q2000, TA instruments, UK). A sample size of approximately 6 mg was used in a Tzero aluminium pan and heated from 20 to 200°C at a heating rate of 10°C min^{-1} under nitrogen gas flow (50 mL min^{-1}). The samples were isothermally held at 200°C for 5 minutes and then subsequently cooled down to 20°C at -5°C min^{-1} and for the second time held isothermally at 20°C for 5 minutes before heating once again to 200°C at the same heating rate. Data acquisition and processing was performed using TA Universal analysis 2000 software. A blank pan measurement was conducted for background and at least three tests were done for each material to ensure repeatability. All the data were taken from both the first and second heating cycle (to eliminate thermal history effects) of DSC scan. The percentage crystallinity (X_c) of PLA in the nanocomposites was calculated according to Equation 3.3 [204]:

$$X_c[\%] = \frac{(\Delta H_m - \Delta H_{cc} - \Delta H_{mc})/\Phi_{PLA}}{\Delta H^o{}_m} \times 100\% ....(3.3)$$

Where, ΔH_m, ΔH_{cc} and ΔH_{mc} are the enthalpy of melting, cold crystallisation and melt crystallisation (J g^{-1}), respectively, of the polymer nanocomposites, $\Delta H^o{}_m$ is the enthalpy of fusion for a PLA crystal of infinite size (taken to be 93.6 J g^{-1}) [205] and Φ_{PLA} is the fraction of PLA in the nanocomposites.

3.3.4.8 X-ray diffraction (XRD) analysis

The X-ray diffraction patterns of freeze dried CNWs and the nanocomposites films were obtained using a D500 diffractometer (SIEMENS) operated at 30 kV and 15

mA, utilising a Cu-Kα radiation source (λ= 0.154) . The diffraction patterns were recorded for 2θ values between 2° and 50° , using a step size of 0.04° , providing 1200 steps, and a scan step time of 2 sec. The scans were controlled by the Diffrac-AC software program. The degree of crystallinity of cellulose nanowhiskers was calculated according to Equation 3.4 [206, 207]:

$$I_c[\%] = \frac{I_{(Crys+am)} - I_{(am)}}{I_{(Crys+am)}} \times 100 ....(3.4)$$

Where, $I_{(Crys+am))}$ represent the peak intensity (count per second) around 22.8° for the crystalline and amorphous part $I_{(am)}$ is the peak intensity around 18° and represents the amorphous part of the cellulose whiskers.

3.3.4.9 Degradation properties

The degradation of the nanocomposite films was evaluated by means of mass loss measurements. The initial weight of four repeat specimens of each material (30mm × 5mm × 0.2mm) was measured before being immersed in glass vials containing 20 mL deionised water at different temperatures (25°C, 37°C and 50°C). After one week, specimens were recovered from the media and dried in a vacuum oven at 50°C until constant weight. After that, the weight of the dried specimens and the pH of the media containing the degraded materials were recorded. The percentage mass loss was determined using Equation 3.5:

$$\text{Mass loss} \ (\%) = \frac{(M_o - M_{ds})}{M_o} \times 100 ....(3.5)$$

Where, M_o is the mass of the dry sample and M_{ds} is the mass of the dry sample after degradation.

3.3.4.10 Statistical analysis

Unpaired *t*-tests were conducted to investigate any statistically significant differences between the means of the data sets that were obtained. To interpret the t-test results, a two tailed *P*-value (*P*) was considered with a 95% confidence interval and a significance level of 0.05. The difference was accepted as significant when the value of *P* obtained was less than 0.05.

3.4 RESULTS AND DISCUSSION

3.4.1 Morphological properties

The TEM image of the CNWs (before freeze drying) presented in Figure 3.2a revealed a rod-like structure for the nanowhiskers and addition of 2 wt% uranyl acetate solution provided some contrast for this image. Due to acid hydrolysis, the amorphous portions of the long chain cellulose were hydrolysed, and the crystalline portion remained unaffected to produce rod-like whiskers in the nano-scale region which was confirmed via TEM. The average length and width of the CNWs were approximately 200 ± 100 nm and 10 ± 2 nm respectively obtained from several TEM images, which was found to be very similar to the analysis conducted by Elazzouzi-Hafraoui *et al.* [208], who also obtained cotton nanocrystals of dimensions ranging from 25 to 320 nm in length and 6 to 70 nm in width. CNWs were observed to be aggregated into small bundles in the PLA matrix as can be seen in Figure 3.2b. This was suggested to be due to strong self-association tendency of CNWs via hydrogen bonding of their hydroxyl groups and their high surface area [176, 209, 210]. The freeze drying process employed

during the nanowhisker production may also have influenced their self-association nature. It has been suggested that higher concentrations of CNW suspensions (~1.0 wt% and more) used in the freeze drying process had a lower surface charge (zeta potential less than -32.61 mV) which may have promoted the self-assembling of CNWs into lamellar structure rather than rod like shapes [211]. However, the concentration of CNW suspensions used in this study to isolate the freeze dried CNW was 1.4 (±0.4) wt%. In addition, the surface charge (zeta potential) of similar cotton extracted CNW was reported to be around -9.49 mV [212]. Therefore, the freeze drying process may have contributed to the aggregation of freeze dried CNWs within the matrix (as can be seen by the TEM image, Figure 3.2b).

The surface topography of the pure PLA and nanocomposites was also analysed via SEM, as presented in Figure 3.2c and Figure 3.2d, where the presence of voids were identified in both PLA and nanocomposite films, which was suggested to be due to the highly volatile chloroform escaping during the film drying process. The shape and size of the voids was seen to vary throughout the nanocomposites.
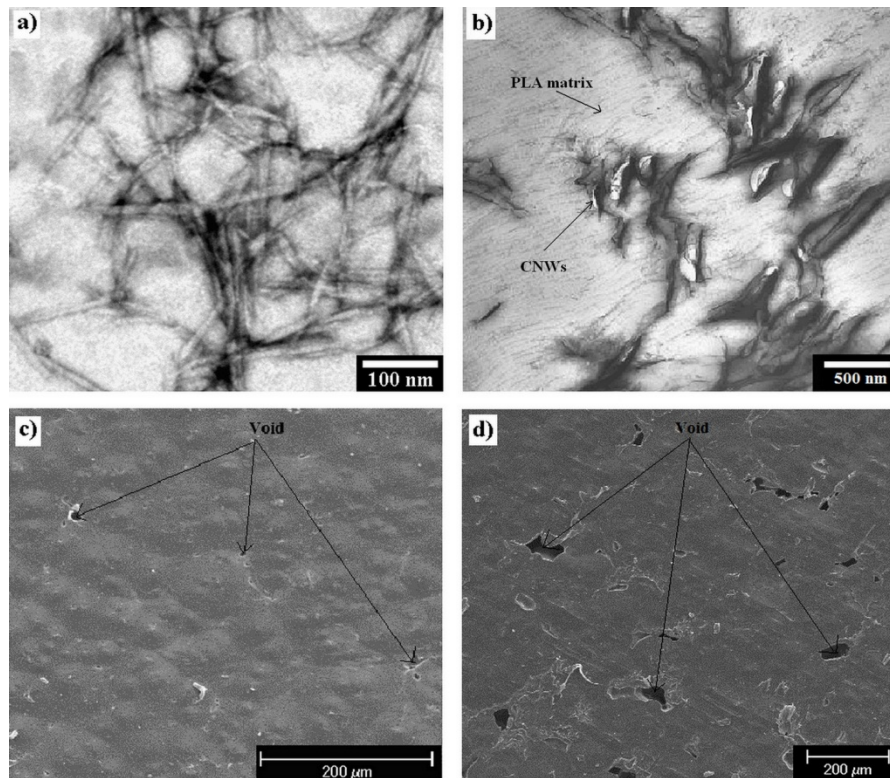
Figure 3.2: *Electron microscopy images: **a)** TEM image of CNWs (before freeze drying), **b)** TEM image of nanocomposite (PLA-1) prepared using 1 wt% freeze dried CNWs, **c)** SEM image of the surface topography of pure PLA film, and **d)** SEM image of the surface topography of the nanocomposite (PLA-1) film.*

A representative image of the solvent cast nanocomposites (approximate dimensions 15mm × 7mm × 0.25mm) prepared using different percentages of CNWs are shown in Figure 3.3. Images obtained showed that the PLA film was fairly transparent, whilst the PLA-1, PLA-3 and PLA-5 became increasingly opaque with increasing additions of CNWs in the nanocomposites. This was suggested to be due to the flocculation effect of CNW aggregates, where discrete CNW aggregates were randomly distributed within the transparent PLA matrix.
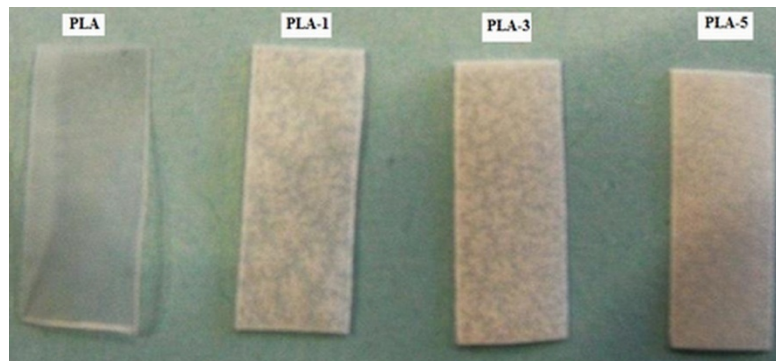
Figure 3.3: *Representative image of the solvent cast pure PLA and nanocomposites*

films.

3.4.2 Void content

The presence of void content in nanocomposites can have a significant influence on the mechanical properties of nanocomposite films. The void content (%) of nanocomposite films was seen to increase with increasing content of CNWs in the nanocomposites. In PLA-1, PLA-3 and PLA-5 nanocomposites, approximately 8.7, 11.2 and 13.9% voids were calculated, whereas around 1.2% voids were found in the solvent cast pure PLA film. This was suggested to be due to entrapped moisture within the CNWs and use of volatile solvents during the film processing stage, which was also reported in the literature [213-215]. In addition, the shape of the voids were observed to have sharp edges, which was believed to have a strong influence on reducing the mechanical properties during the testing.

3.4.3 FTIR analysis

The functional groups of acid hydrolysed CNWs, PLA and nanocomposites were identified using FTIR-ATR spectroscopy (see Figure 3.4).
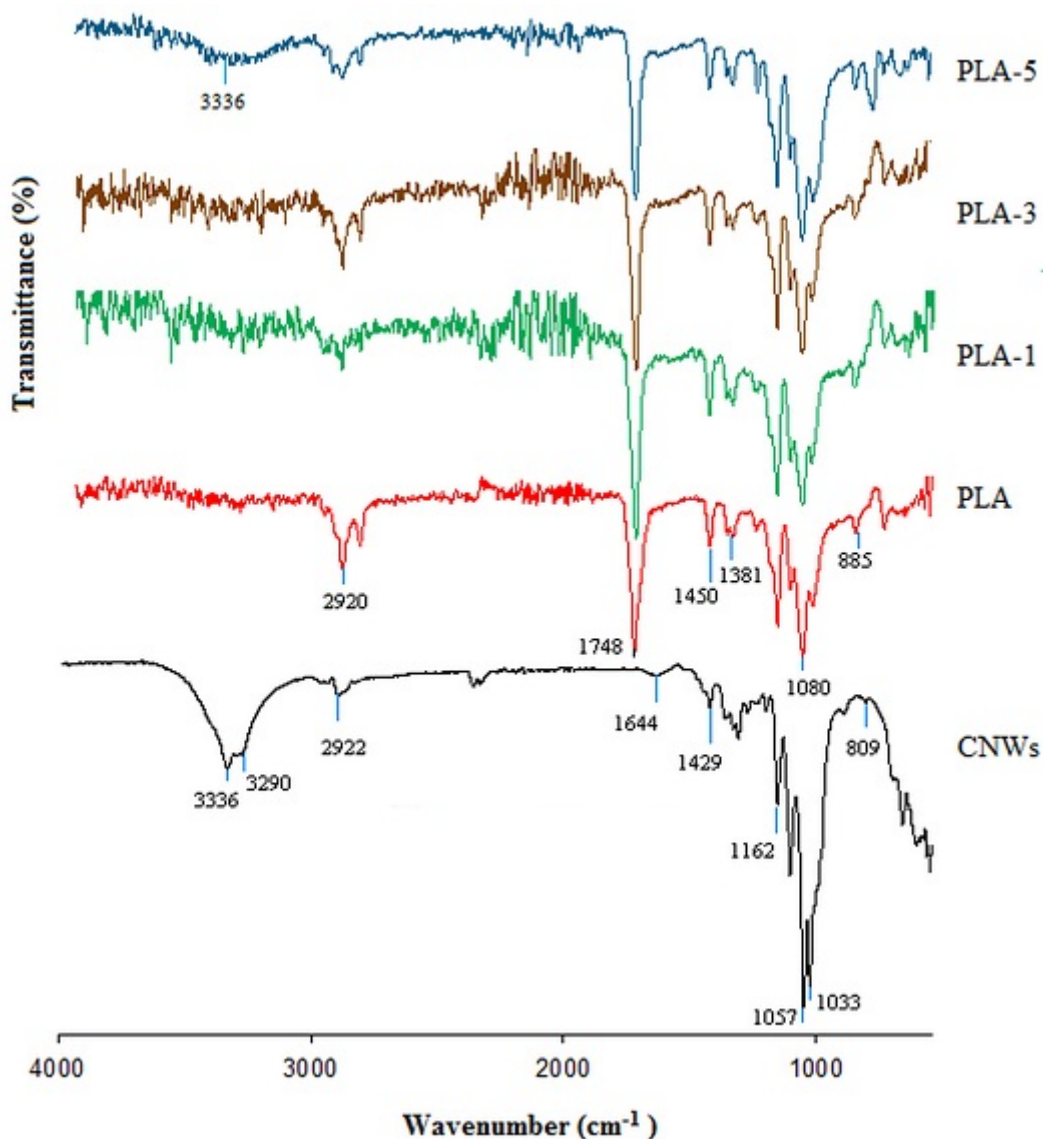
Figure 3.4: *FTIR-ATR spectrum for the CNWs, pure PLA and nanocomposites*

investigated in this study.

For the CNWs alone, the bands at 3336 cm^{-1} and 3290 cm^{-1} were attributed to free O-H stretching vibration and H-bond, respectively. The bands at 2900 cm^{-1} and 1429 cm^{-1} indicated the C-H stretching and bending of –CH_2 groups, respectively. The peak at 1162cm^{-1} was attributed to the C-O-C stretching bridge of glucose ring structure of cellulose. The bands at 1057 cm^{-1} and 1033cm^{-1} represented the C-O stretching at position C-6 and C-3 in the saccharide structure, respectively [174].

The absorbance band at 809 cm^{-1} representing the C-O-S vibration associated with the C-O-SO$_3$ group present on the surface of the CNWs [211] was expected, due to the esterification of hydroxyl groups by sulphate ions formed during the suphuric acid hydrolysis process employed to isolate the CNW from cotton. For pure PLA, the peak at 1748 cm^{-1} and 1080 cm^{-1} represented the symmetrical stretching of C=O and -C-O- groups of ester bonds, respectively and the bands at 1450 cm^{-1}, 1381 cm^{-1} and 885 cm^{-1} were assigned to asymmetrical stretching of –CH$_3$ group, symmetrical deformation of –CH$_3$ and C-H group in the polymer, respectively [216]. It was seen that the peak for free hydroxyl groups at 3336 cm^{-1} in PLA-1 and PLA-3 disappeared, which was suggested to be due to presence of small amount of CNWs in the nanocomposites, however, this peak was observed in PLA-5 for containing higher percentage of CNWs. The intensity of the peak at 1033-1057 cm^{-1} for the C-O group of the saccharide structure in the nanowhiskers increased with an increasing loading of the nanowhiskers, as expected.

3.4.4 Mechanical properties

The mechanical properties of the nanocomposites compared to the pure PLA are depicted in Figure 3.5. PLA-1 showed a significant percentage increase (34%) in tensile strength, whilst PLA-3 and PLA-5 showed little increase (8%) in comparison with the pure PLA (tensile strength ~21.2 MPa). This was suggested to be due to better dispersion of the CNWs within the polymer matrix for PLA-1 compared to PLA-3 and PLA-5. At higher concentrations of CNWs in the nanocomposites, poor dispersion was observed due to the strong self-aggregating nature of CNWs leading to a less pronounced increase in tensile strength. The tensile modulus of

PLA-1, PLA-3 and PLA-5 also showed an improvement of 39%, 34% and 51%, respectively as compared to PLA alone. This significant increase in tensile modulus for all the nanocomposites investigated was expected due to the higher modulus (57 GPa) of the CNWs [54].

However, the tensile properties of pure PLA investigated in this study found lower in comparison to expectation and this was due to the presence of lots of voids created within the film during the processing into thin film. Similar mechanical properties for pure PLA film was also reported by Liu *et al.* [200] who investigated solvent cast PLA film (Natureworks, 2002D) and found the tensile strength ~ 19.4 MPa and modulus ~1.4 GPa. The tensile test data calculated in this study was found to be statistically significant comparing PLA alone against PLA-1 ($P<0.05$), PLA-3 ($P<0.05$) and PLA-5 ($P<0.05$). Comparing PLA-3 and PLA-5 against PLA-1 the tensile strength data was also found to be statistically significant ($P<0.05$). However, comparing PLA-3 and PLA-5 the tensile strength data was considered not to be statistically significant ($P>0.05$).
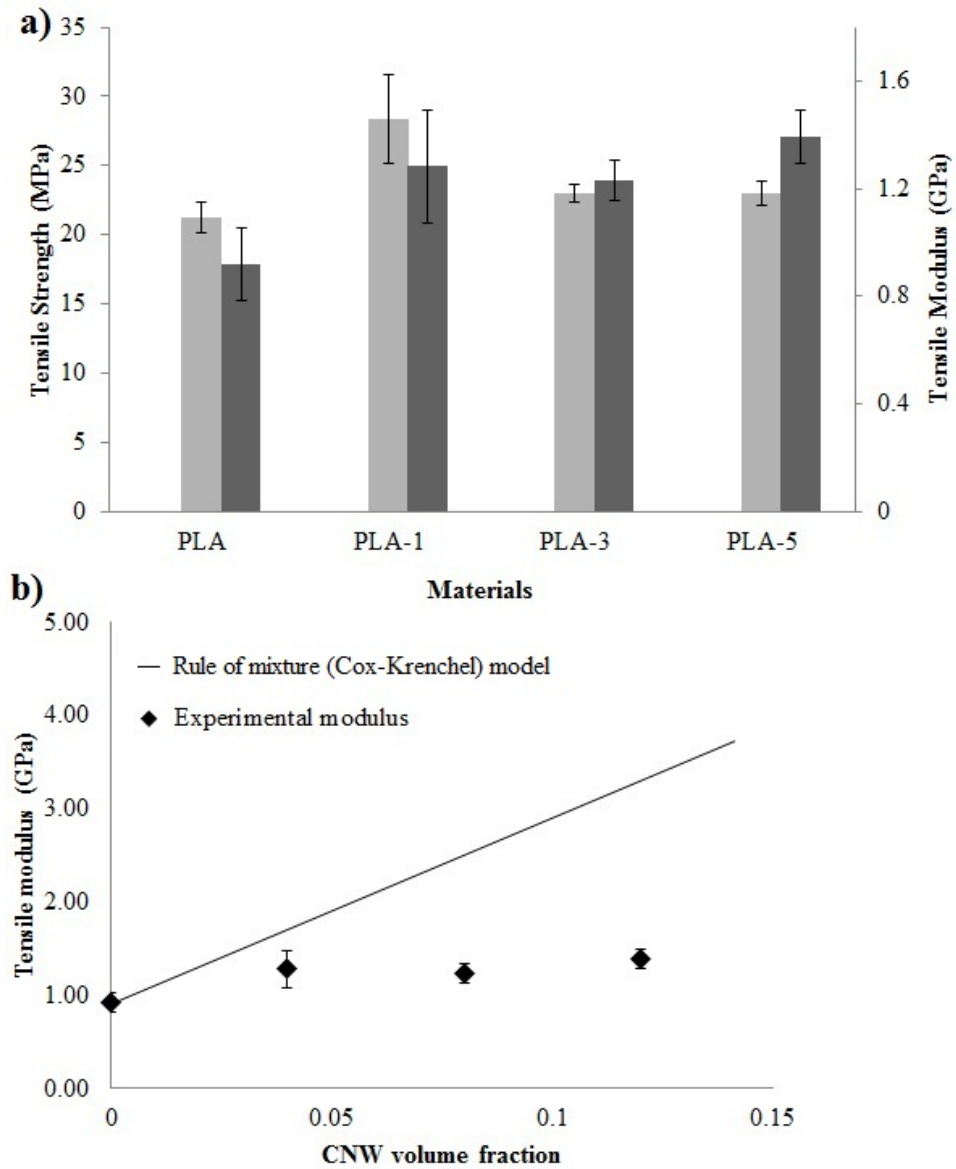
Figure 3.5: a) *Tensile strength and modulus properties for the PLA and nanocomposite films, and* **b)** *comparison between the experimental and predicted modulus calculated using the 'Rule of mixture' (Cox-Krenchel) model.*

The tensile modulus of short fibre reinforced composite materials could be predicted using the well-known 'Rule of mixture' equation (see Equation 3.6) [3], which was later modified by Cox and Krenchel by introducing efficiency factors in the 'Rule of mixture' equation as presented in Equation 3.7:

$$E_c = E_f V_f + E_m(1 - V_f) \ldots \ldots \ldots \ldots \ldots \ldots (3.6)$$

$$E_c = \eta_1\,\eta_0 E_f V_f + E_m(1 - V_f) \ldots\ldots\ldots\ldots\ldots (3.7)$$

Where, η_1 and η_0 represent the efficiency factors of fibre length and fibre orientation. For a random fibre composite, η_1 is regarded as 1 and η_0 is taken to be 3/8 [217, 218]. Therefore, the Equations 3.7 can be presented as follows:

$$E_c = {}^3\!/_8\; E_f V_f + E_m(1 - V_f) \ldots\ldots\ldots\ldots (3.8)$$

The predicted modulus calculated using Equation 3.8 is plotted in Figure 3.5b and compared with the experimental modulus. The following assumptions were considered: tensile modulus of filler (CNW), E_f = 57 GPa [54], tensile modulus of matrix (PLA), E_m = 0.92 GPa (experimental), density of filler (CNW), ρ_f = 1.59 g cm^{-3} [176] and density of matrix (PLA), ρ_m = 1.24 g cm^{-3}. The volume fraction (V_f) was calculated using the following Equation 3.9 [219]:

$$V_f = \frac{W_f/\rho_f}{W_f/\rho_f + (1 - W_f)/\rho_m} \ldots\ldots\ldots\ldots\ldots\ldots (3.9)$$

The tensile modulus of the nanocomposite films investigated in this study was found to be lower in comparison to predicted values (see Figure 3.5b). In addition, the deviation between the experimental values and the predicted line was observed to increase with CNW content. This may have been due to higher volume fraction of nanowhiskers resulting in poor dispersion and increasing void contents within the nanocomposite films, which has been reported in Section 3.4.2. The size and shape of the voids as well as their distribution within the composite were also suggested as having a significant influence in decreasing the mechanical properties [220, 221]. It has been reported that voids within the

composite can cause premature failure initiated from the sharp edge of the longer voids.

In comparison with pure PLA film, a dramatic reduction in elongation at break was seen for all the nanocomposites (see Figure 3.6). In case of PLA-1, PLA-3 and PLA-5 the reduction in elongation property of approximately 85, 88 and 90% was observed compared to PLA alone, suggesting the stiffening and hardening effect in the nanocomposites with increasing content of CNWs [222].
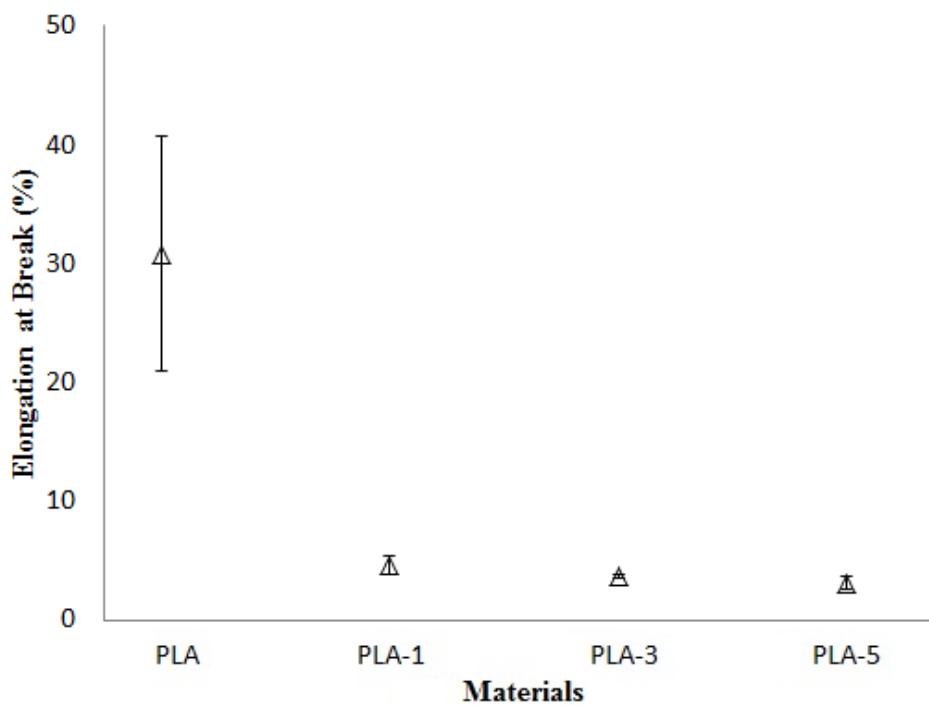
Figure 3.6: *Elongation at break properties for the PLA and nanocomposite films.*

3.4.5 Thermo-mechanical properties

The thermo-mechanical properties of the nanocomposite films were investigated via DMA to explain the mechanical behaviour of materials with change in temperature, as the modulus is dependent on the temperature and applied stress. In a DMA deformation (as a sinusoidal wave) is applied to measure the response

of the sample. The frequency or the temperature can be varied during testing to probe effects on the mechanical properties of these changes. The mechanical properties (i.e. modulus) are then obtained from measuring force and deformation during cycling. The difference between pure viscous behaviour (i.e. liquid) and pure solid behaviour can be obtained from the change in phase angle between the input and the material response.

In this experiment, the frequency was fixed at 1 Hz (1 cycle second^{-1} to record the modulus every second) and the temperature was ramped from 25 to 80°C at a rate of 5°C min^{-1} (Please see section 3.3.4.5 for detail parameters) to measure the storage modulus. However, the storage modulus obtained using DMA should not be exactly same as the Young's modulus, as the Young's modulus was calculated from the slope of initial linear portion of stress-strain curve. Whereas, in DMA, a complex modulus (E^{*}), storage modulus ($E^{'}$) and loss modulus ($E^{''}$) were obtained from the material response to the sine wave ($E^{*} = E^{'} + iE^{''}$) [223].

The DMA results revealed the storage modulus of the nanocomposite films as a function of temperature as seen in Figure 3.7a. The incorporation of CNWs in the PLA matrix showed an improvement in storage modulus for all the nanocomposites in the visco-elastic temperature region of polymer. The amount of CNWs incorporated in the PLA matrix played a significant role in the improvement of storage modulus of the nanocomposites at all the temperature regions investigated in this study.
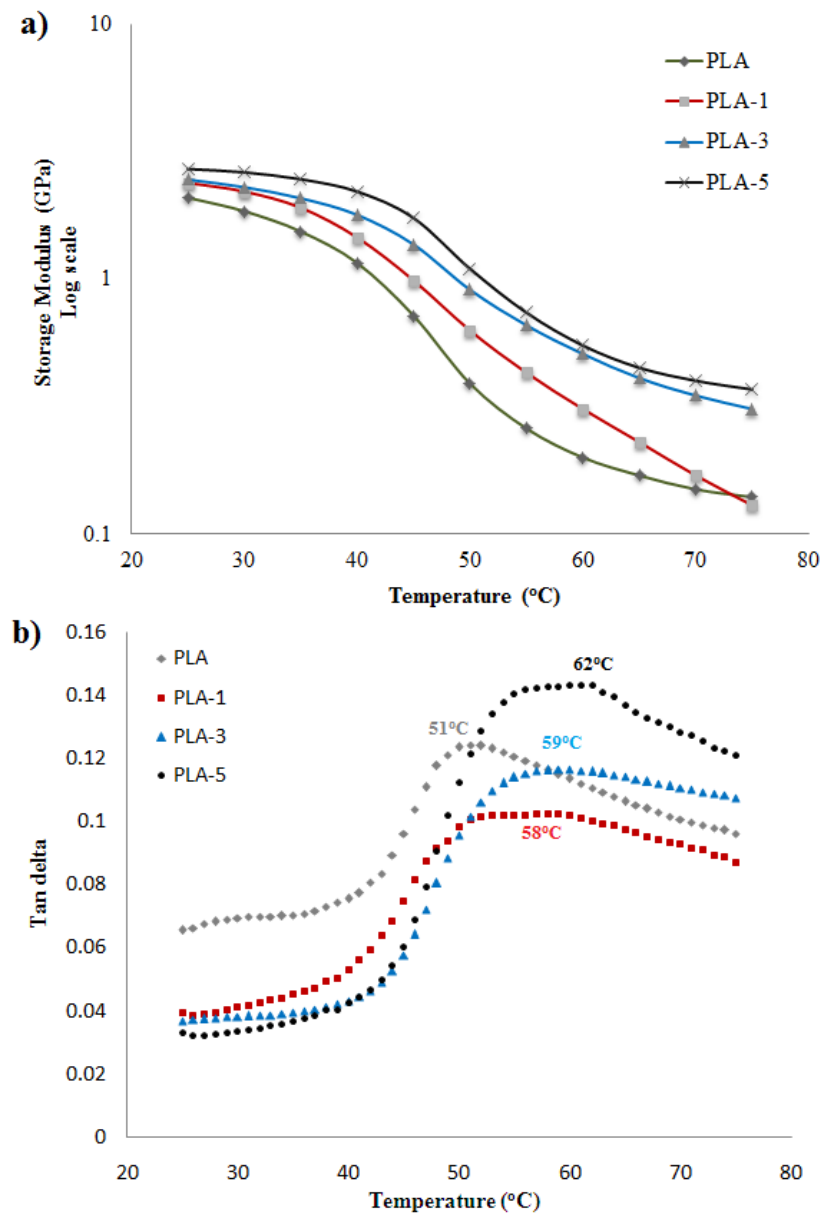
Figure 3.7: *a) Tensile storage modulus curves from DMA data for pure PLA and nanocomposites, and b) tan delta curves from DMA data for pure PLA and nanocomposites.*

Tan delta (also called damping) measured using DMA indicated the efficiency of a material losing energy due to the molecular rearrangement and internal friction and is calculated from the ratio of the loss to the storage modulus [223]. The tan delta peaks obtained for the nanocomposites investigated have been shifted to

the higher temperature regions compared to the tan delta peak for PLA alone (see Figure 3.7b). The tan delta peaks for PLA-1, PLA-3 and PLA-5 were seen at 58°C, 59°C and 62°C compared to that for pure PLA at around 51°C, suggesting the addition of CNWs in nanocomposites remarkably improved the storage modulus in the plastic region of the polymer. The right shift of tan delta peaks also suggested that the reinforcement established in the nanocomposites had significant influential effect on the segmental motion of PLA matrix. It was also seen that the width of the tan delta peaks in the nanocomposites were wider as compared to pure PLA which indicated the increasing temperature span required for the transition, which was also reported by the Petersson *et al.* [182]. This was attributed to be due to higher reinforcement and surface induced crystallisation of the polymer matrix with an increase in CNWs concentration in the nanocomposites.

3.4.6 Thermal properties

The thermal stability of the CNWs and nanocomposites are shown in Figure 3.8, which plots residual weight vs. temperature. All the materials were found to be thermally stable in the temperature region between 20°C and 210°C as compared to a very similar literature value 25° to 220°C for nanocomposites produced using PLA and nanowhiskers isolated from microcrystalline cellulose [52]. The CNWs started to lose their weight after 210°C, whilst the nanocomposites showed decomposition above 320°C. Similar thermal behaviour of CNWs was also reported in the literature [224, 225] and this was due to the sulphuric acid hydrolysis of cotton and may be presence of some sulphate groups in the

nanowhiskers. At higher temperature (~400°C) the residual weight percent of the nanocomposites was seen to increase with increasing CNWs content.
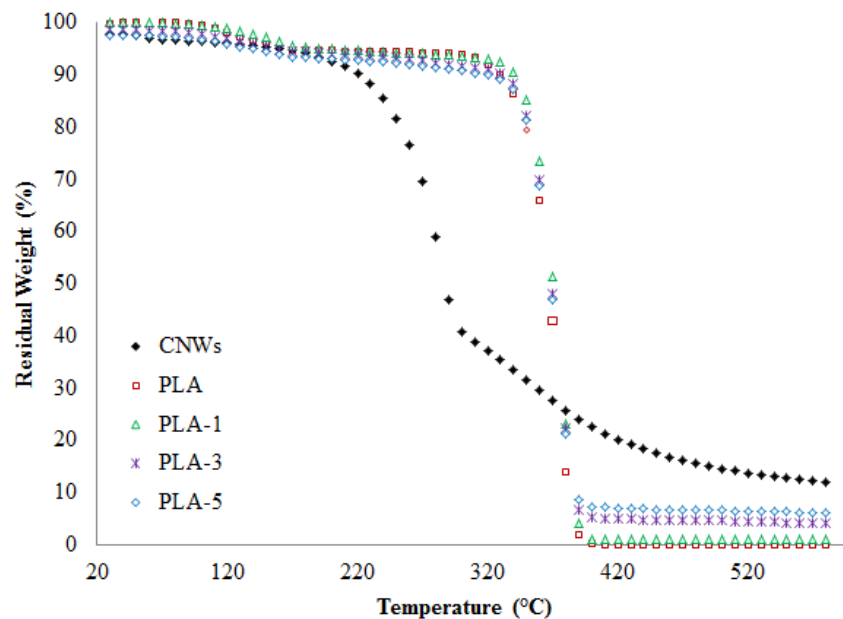
Figure 3.8: *TGA thermogram of the CNWs, pure PLA and nanocomposites investigated in this study.*

The melting thermogram of the pure PLA and nanocomposite films was depicted in Figure 3.9. The melting peak of pure PLA film appeared around 170°C, while a slight shift of melting peaks to the right at around 172°C was observed in all the nanocomposites and this was suggested a little effect of CNWs in increasing the melting temperature of the nanocomposites.

3.4.7 Crystallisation properties

The crystallisation behavior of PLA in the nanocomposites was investigated using DSC analysis. The enthalpy of fusion of pure PLA and nanocomposites was obtained from the first and second heating run of DSC data (see Figure 3.9).
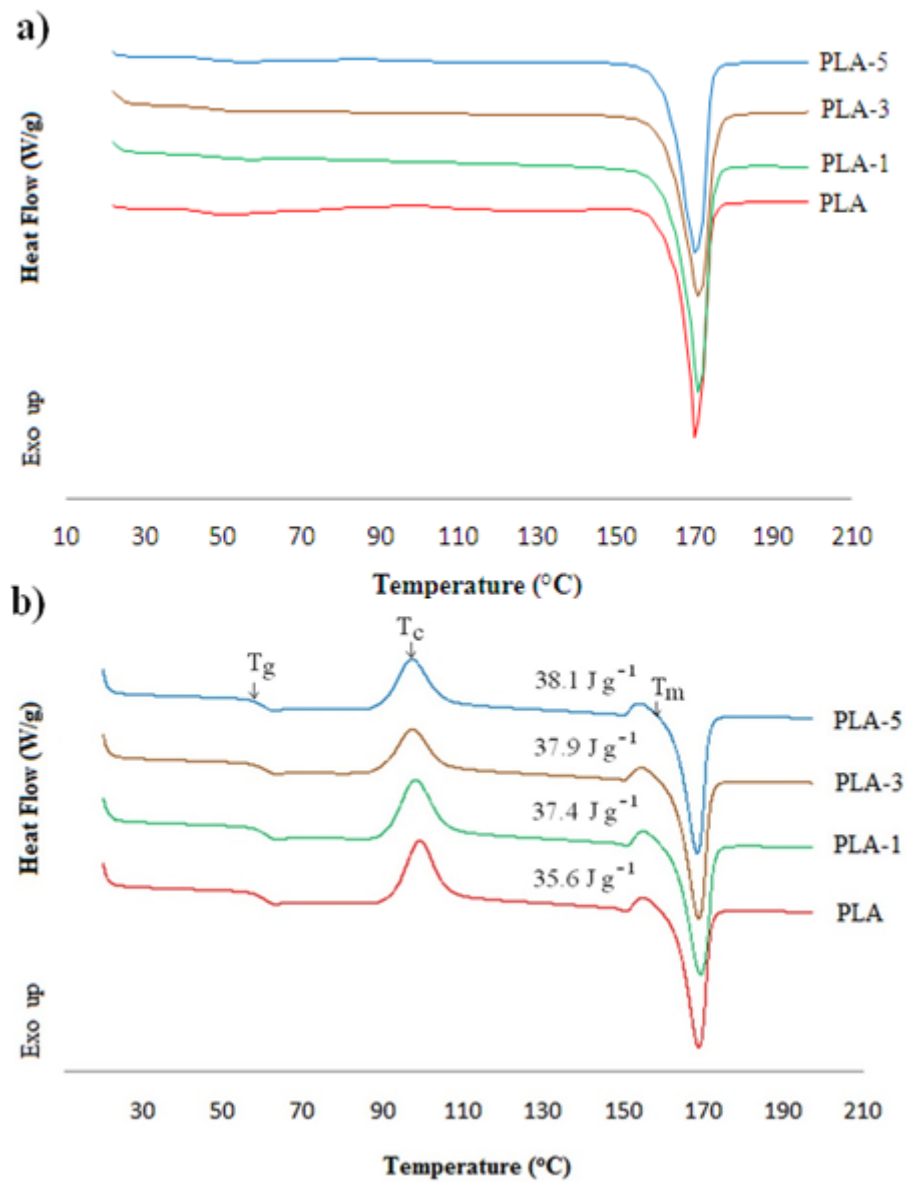
Figure 3.9: *DSC thermogram of the pure PLA and nanocomposites obtained from*

a) the first, and b) the second heating run.

Table 3.2: *Crystallinity Index of pure PLA and nanocomposite films investigated using DSC data.*

Materials	1st heating cycle		2nd heating cycle			
	ΔH_m (J g^{-1})	Crystallinity (%)	ΔH_m (J g^{-1})	ΔH_{cc} (J g^{-1})	ΔH_{mc} (J g^{-1})	Crystallinity (%)
PLA	36.9	**39.4**	35.6	24.6	3.0	**8.6**
PLA-1	39.7	**42.8**	37.4	25.1	2.5	**10.6**
PLA-3	40.8	**44.9**	37.9	20.6	2.7	**16.1**
PLA-5	41.5	**44.6**	38.1	20.0	2.8	**17.3**

[a] *Instrument's cell constant 0.9965*

The percentage crystallisation of PLA and the nanocomposites (Table 3.2) showed that the crystallinity of solvent cast PLA (around 39.4% calculated from the 1st heating cycle) was comparable to the literature values of 40.7% [205]. Though the crystallinity of the pure PLA found lower (8.6% crystalline) obtained from the 2nd heating cycle due to the elimination of thermal history effect, an increase in enthalpy of fusion was seen in the nanocomposites, which was due to the incorporation of crystalline CNWs in the nanocomposites. As a result, the crystallisation of PLA in the nanocomposites found increasing as expected probably due to the crystal nucleation of PLA polymer influenced by the presence of CNWs crystallites [200]. Since tensile properties are a function of crystallinity

[81], the increase in mechanical properties of the nanocomposite films achieved in this study (Section 3.4.4) also believed to be due to their increasing crystallinity. Furthermore, the crystallisation property of CNWs produced and their effect on the crystallisation of PLA in the nanocomposites were investigated further using XRD. Figure 3.10 shows the XRD traces of the CNWs and the nanocomposites. From the diffraction pattern of CNWs the highest peak was observed at $2\theta = 22.8^{o}$ and the double peak signal at $2\theta = 14.9^{o}$ and 16.5^{o} was consistent with the diffraction pattern of reference cotton based cellulose [226] identified from the ICDD patent PDF-2 database (File no. 00-050-2241).
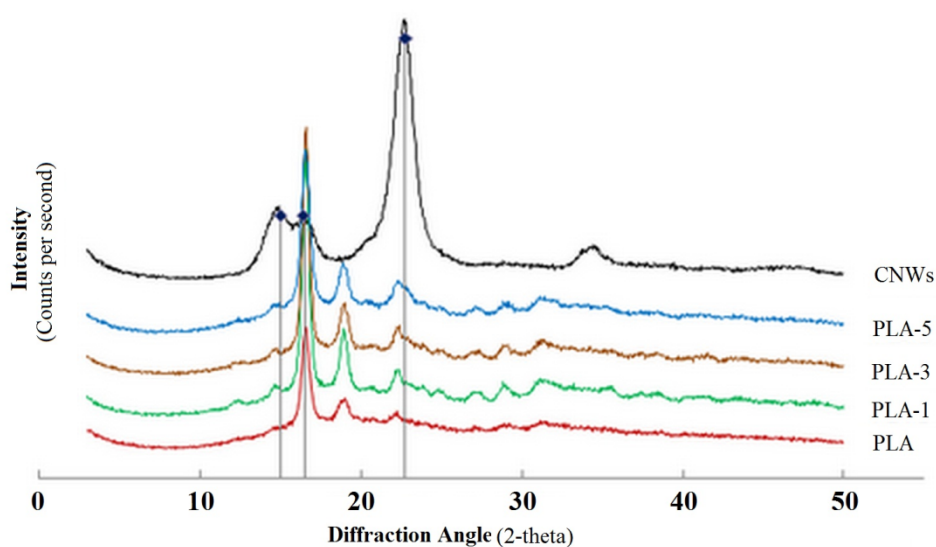
Figure 3.10: *X-Ray diffraction patterns of the CNWs, pure PLA and nanocomposites investigated in this study. Closed diamond (♦) = Reference cellulose peaks identified from the ICDD patent PDF-2 database (File no. 00-050-2241).*

An approximate crystallinity of 89.1% was calculated for the freeze dried CNWs, which was very close to the result stated by other studies [176, 208]. The main diffraction peaks for PLA alone were seen at $2\theta = 16.5^{o}$ and 18.9^{o} and a weaker peak at around 22.5^{o} which was also consistent with the literature values [227].

The XRD traces for the nanocomposites showed clear retention of the cellulose crystallites with increasing peak intensity at 2θ = 14.9 ^{o}, 16.5^{o} and 22.5^{o}, and this was again suggested to be due to an increase in the crystallinity of the nanocomposites, which was also well consistent with the aforementioned DSC results.

3.4.8 Degradation properties

The degradation behaviour of the nanocomposites after a week in deionised water at varying temperatures (25°C, 37°C and 50°C) can be seen in Figure 3.11a.
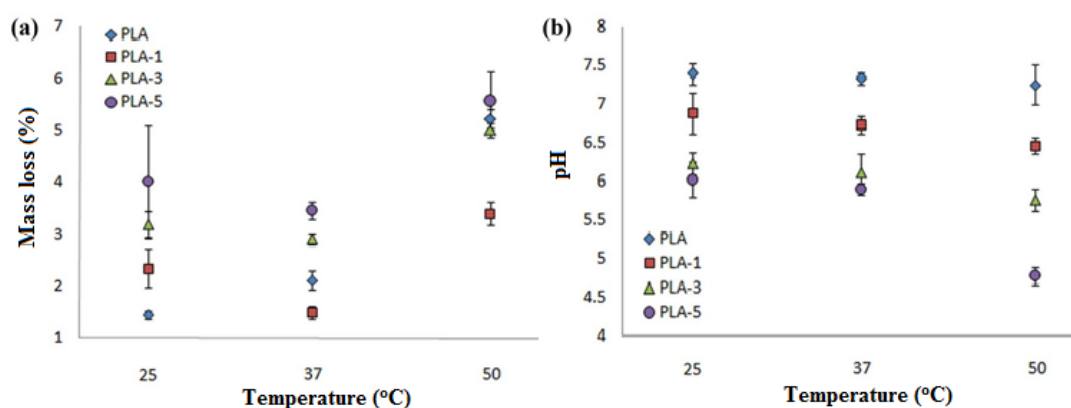
Figure 3.11: *a) Mass loss of nanocomposite films in deionised water at different temperatures for 1 week, and b) pH of deionised water containing degraded sample of nanocomposites at different temperatures.*

The percentage mass loss of PLA alone increased significantly with increasing temperature (up to ~5.2% at 50°C) and this loss was attributed to hydrolysis of the polymer influenced by higher temperature. At room temperature the mass loss of the nanocomposites was seen to increase with increasing CNWs content compared to PLA alone. However, at 37°C for all nanocomposites the percentage mass loss was slightly lower compared with room temperature studies and this

was suggested to be due to hydrolysis of the amorphous domain of the polymer at higher temperature and subsequent interfacial reinforcement of polymer by nanocrystals hindering the rapid degradation of these nanocomposites [216]. A significant percentage mass loss was observed at 50°C for all the nanocomposites and it was suggested that this increase was due to the leaching of CNWs and a continuous breakdown of the interface between the CNWs and the polymer matrix [228].

The pH of the degradation media for PLA alone remained relatively neutral for the duration of the study along with PLA-1 as seen in Figure 3.11b. However, a decrease in pH was observed for PLA-3 and PLA-5 with increasing temperature (from 37°C to 50°C) and this was suggested to be due to the leaching of acid hydrolysed CNWs in the deionised water.

3.5 CONCLUSIONS

The influence of the CNWs on the improvement of the mechanical, thermomechanical, crystallisation and hydrolytic degradation properties of nanocomposites based on PLA was investigated in this chapter. The morphology of CNWs was observed likely to be aggregates of rod-like structure. Dispersion of the nanowhiskers within the PLA matrix was limited and also observed as largely aggregated. However, despite this aggregation, significant differences were observed between the properties of the nanocomposites as compared to PLA alone. Presence of voids identified in the nanocomposites played an important role on the mechanical and degradation properties of the nanocomposites. The

nanocomposites containing 1 wt% CNWs showed 34% and 39% increase in tensile strength and modulus, respectively compared to PLA alone and this improved properties proved the mechanical reinforcement of PLA with CNWs. The DMA results revealed the incorporation of CNWs in the PLA matrix showed the significant improvement in the storage modulus properties of the nanocomposites, especially in the plastic temperature region of PLA and the tan delta peaks showed the significant reinforcement and surface induced crystallisation was established in the nanocomposites due to the addition of CNWs. TGA revealed that all the materials were thermally stable in the temperature region between $25^{o}C$ and $210^{o}C$. The mass loss of all the nanocomposites produced showed that the presence of cotton based CNWs had a significant influence on controlling the degradation properties at varying temperatures.

CHAPTER 4.

HIGH CELLULOSE NANOWHISKER CONTENT FLEXIBLE THIN

COMPOSITE FILMS

4.1 SUMMARY

Flexible composite films with a high cellulose nanowhisker (CNW) content of up to 75 wt% by weight were produced by casting from aqueous solution with water soluble hydroxyethyl cellulose (HEC). The surface topography of the films displayed an aggregated morphology influencing the surface roughness and light transparency properties of the thin films. Using fluorescently labelled HEC, the extent of CNWs aggregation in the composites was determined, which indicated that up to 13 wt% of CNWs can be homogeneously blended with HEC, above which larger CNWs aggregates occur. However, even in a somewhat aggregated form, the CNWs still form a percolated network and appear to be homogeneously dispersed as larger aggregated entities. The composite CNW-HEC films further exhibited improved thermal stability compared to both the CNWs and HEC alone with decomposition temperatures shifting from $261^{o}C$ for CNWs and $313^{o}C$ for HEC to $361^{o}C$ for blends containing 75 wt% CNWs. Surface induced crystallisation of HEC by CNWs was also found with higher crystallinity for the composite films. Due to the reinforcing effect of CNWs within the matrix, an increase in tensile strength (294%) and modulus (2004%) was observed for the blend containing 75 wt% CNWs compared to the pure HEC film (tensile strength ~12.23 MPa and modulus ~0.39 GPa). The storage modulus of all the flexible films investigated also

revealed an increasing trend with CNW content across the temperature region explored. The swelling kinetics of the CNW-HEC blends in phosphate buffered saline (PBS) media at 37°C were also investigated and CNWs were shown to have a strong influence on reducing the equilibrium swelling capacity and initial swelling rate of the blends.

4.2 INTRODUCTION

Composites based on water soluble biopolymers are of significant interest due to their biodegradability, biocompatibility and good processability and have already shown their potential for application in the fields of biomedical materials [229, 230], tissue engineering [231, 232] and pharmaceuticals [233, 234]. Dispersion, interfacial properties and/or miscibility of the biopolymers in the blends significantly influences the mechanical and degradation properties of the composite materials, which can be explained by the presence or absence of interactions and bonding between the constituents and the surface characteristics of the polymers and the fillers. A number of positive interactions between various water-soluble polysaccharides and biopolymers have been reported in the literature [235-237]. For example, the physicochemical properties of hydrophilic polymeric films prepared from the blends of hydroxyethylcellulose (HEC) and poly [(methyl vinyl ether)-alt-(maleic acid)] (PMVEMAc) were investigated by Khutoryanskaya *et al.* [238], who suggested that cross-linking of water-soluble polymers was achieved through the formation of inter macromolecular hydrogen bonds via thermal treatment of the blends. The glass transition temperature, T_g

for HEC was reported to be 97°C and the blend containing 50 wt% PMVEMAc showed an increase in T_g to 143°C due to the cross-linking effect on the polymers. Wang *et al.* [239] investigated a composite hydrogel prepared via graft copolymerisation of HEC, sodium acrylate (NaA) and medicinal stone (MS) and showed that by incorporating 10 and 50 wt% MS in the blends, the swelling capacity increased by 400% (from 162 to 810 g g^{-1}) and 117% (from 162 to 352 g g^{-1}) respectively. A 7.5 fold improvement in the initial swelling rate constant was also reported for incorporating MS in the blends compared to MS-free samples. They also confirmed the grafting of NaA on the HEC backbone and improved dispersion of MS in the polymer matrix after preparing the composite hydrogels via a facile free-radical graft copolymerisation [239]. The thermal degradation behaviour of pure HEC was reported by Chen *et al.* [240] and they found 67% weight loss had occurred at 350°C with their initial (T_d) and maximum (T_{dm}) decomposition temperatures at 243°C and 269°C, respectively. Li *et al.* [241] also reported similar thermal degradation properties for pure HEC, showing a 35.5 wt% char yield at 400°C with T_d and T_{dm} values at 239°C and 280°C, respectively.

Cellulose is a polysaccharide composed of linearly orientated crystalline and amorphous phases [41]. Their amorphous portions can be selectively hydrolysed, generally via a sulphuric acid [15, 189, 202] or hydrochloric acid [190, 191] hydrolysis process, to obtain cellulose nanocrystals. Incorporation of nanofillers in the polymer blends can have a significant influence on the interactions with polymers, resulting in improved thermal and mechanical properties [45, 48, 123]. CNWs reinforced water soluble biopolymer matrices have great potential for use

in many applications, such as in soft tissue engineering, drug delivery and drug coating and encapsulation. Recently nanocellulose has been used with both water-soluble and insoluble polymers, such as PCL [19, 202, 242], PLA [52, 63, 132, 166, 172, 199, 200, 222], chitosan [167, 174], starch [48, 243], polyvinyl alcohol (PVA) [244-246] and polyvinyl acetate (PVAc) [50]. This is due to their availability, low cost, biodegradability [11, 12, 186], biocompatibility [188] and high mechanical properties (tensile modulus ~105 GPa for cotton based nanocellulose) [54]. For example, Liu *et al.* [200] investigated the incorporation of 5% flax nanocellulose within a bioresorbable PLA matrix and found that the tensile strength and modulus of the nanocomposites increased by 59% and 47% respectively, compared to PLA alone. The enhanced tensile storage modulus in the rubbery plateau region (64% improvement at 60°C) and a shift to the right of the tan delta peak by 20°C suggested a reduction in the segmental motion of the matrix, which was also reported for composites containing 5 wt% surface modified nanocellulose by *tert*-Butanol [52]. Ma *et al.* [247] prepared 'green composites' using pre-treated (with NaOH) microcrystalline cellulose (PMCC) and nanocrystalline cellulose (NCC) and showed that the tensile strength and modulus increased to 49 MPa from 35 MPa and 3.6 GPa from 1.1 GPa, respectively, for composites containing 25 wt% NCC compared to NCC-free composites. The elongation to break of the composites containing 10 wt% NCC was reported to be 9.63% compared to 13.39% for the 10 wt% PMCC composites. The high strength all-cellulose based nanocomposite films with different ratios of cellulose I and II were reported in the literature [248] to have a tensile modulus and strength of

13.1 GPa and 242.8 MPa, respectively for nanocomposites containing cellulose I and II ratios of 43/57. Cellulose based nanofibre paper without any binder was investigated by Nogi *et al.* [249] for their light transparency, high modulus (13 GPa) and strength (223 MPa), indicated strong H-bonding of nanocellulose. This type of H-bonded networks in CNWs has also been used to prepare CNW-based porous membranes [209], aerogels [176] and composites with variable mechanical properties controlled by water ingress [250].

The composite materials investigated in this chapter were manufactured using cotton based CNWs and hydroxyethyl cellulose (HEC) matrix. HEC is a non-ionic water-soluble material used for thickening, colloid stabilisation, improvement of water retention, emulsification, and film formation. This study was aimed at using HEC as a binder for the CNWs to create high CNW content composites, with the intention to create strong yet flexible composite films. The molecular similarity of both compounds should provide strong interactions. However, higher HEC content in the composite films would lead to rapid dissolution of the film upon immersion in PBS or deionised water, which limited the use of lower CNW fraction in the composites. The structural, thermomechanical and crystalline properties of these composites have been evaluated.

4.3 MATERIALS AND METHODOLOGY

4.3.1 Preparation of cellulose nanowhiskers (CNWs)

CNWs were extracted from cotton via an acid hydrolysis process as described in Section 3.3.2.

4.3.2 Preparation of CNWs reinforced flexible films

The cellulose nanowhisker reinforced hydroxyethyl cellulose (CNW-HEC) flexible

films were prepared via a solvent casting process. HEC powder was purchased

from Dow Chemicals, Switzerland (Cellosize, HEC WP-52000HP, bulk density 0.4-

0.6 g cm^{-3}, molecular weight 10,000~1000,000, melting point 200°C) containing

hydroxyethyl cellulose (83-95%), sodium acetate (7.5%), water (5%), isopropanol

(3%) and cellulose (0.5%).

Table 4.1: *Formulations of flexible films prepared using CNWs and HEC.*

Sample **codes** used in this study	CNWs (wt%)	HEC (wt%)
HEC	-	100
CNW:HEC(50:50)	50	50
CNW:HEC(65:35)	65	35
CNW:HEC(75:25)	75	25

The HEC powder was dissolved in deionised water (1% w/v), which was stirred

using a magnetic stirrer at room temperature for 4 hours. To ensure complete

solubilisation of HEC in the deionised water, the mixture was subjected to heat at

90°C until the HEC powder had fully dissolved. A CNWs suspension in deionised

water was also prepared (1% w/v) by utilising constant stirring for 2 hours at room

temperature and then sonication for 5 minutes. The obtained suspension did not

show sedimentation. The two suspensions were then combined together in

different ratios (see Table 4.1) and mixed thoroughly for a further 2 hours at room

temperature. These were then poured into polystyrene petri dishes and allowed to evaporate at 50°C in an oven for 48 hours to obtain flexible films of approximately 0.06 mm thickness. The films were further dried in a vacuum oven at 50°C for 48 hours prior to testing.

4.3.3 Rhodamine isothiocyanate (RITC) labelling of HEC

HEC was labelled with rhodamine isothiocyanate (RITC) (Sigma Aldrich, U.K.) for fluorescence studies following the method proposed by Goff *et al.* [251]. Briefly, HEC (5.02 g) was suspended in 160 ml of dimethyl sulfoxide (Acros Organic, U.K.) containing 1 ml of pyridine (Acros Organic, U.K.), 0.25g of RITC and 100 mg of dibutylin dilaurate (Alfa Aesar, U.K.) were heated for 4 h at 95°C with continuous stirring. The resulting mixture was washed several times with ethanol (Fischer Scientific, U.K.) until no further free dye was visible. The RITC–HEC was then vacuum dried. Flexible films with similar formulations to those presented in Table 4.1 were also produced via solvent casting process using RITC–HEC and CNWs.

4.3.4 Characterisation

4.3.4.1 Electron microscopic analysis

The structural morphology of the acid hydrolysed CNWs was examined using transmission electron microscopy (TEM) as mentioned previously in Section 3.3.4.1. The surface topography of pure HEC and CNW-HEC films was characterised using SEM according to the procedure described previously in Section 3.3.4.1.

4.3.4.2 Fluorescence microscopic and image analysis

Brightfield and fluorescence images of the flexible films containing RITC-HEC and CNWs were obtained at room temperature using a Fluorescence Microscope (Leica DMLB) by placing the films on a flat glass slide. Fluorescence images were further analysed using ImageJ software (National Institutes of Health, USA) to calculate the area fraction of the CNWs on the surface of the composite films.

4.3.4.3 Surface roughness analysis

The surface roughness of the flexible thin films produced was conducted on a Surftest (SV-600, Mitutoyo) system using a diamond stylus tip (5 µm tip radius) with 0.5 mm s^{-1} travel speed. The measurement length was taken from 4.8 mm distance of at least six different positions of the film.

4.3.4.4 Light transmittance

Light transmittance of the flexible thin films was measured using a UV/visible spectrometer (PerkinElmer, Lambda-25) by scanning over the wavelength range of 200 to 800 nm.

4.3.4.5 Differential scanning calorimetric (DSC) analysis

As described in Section 3.3.4.7 (temperature range from 20 to $250^{o}C$).

4.3.4.6 Thermogravimetric analysis (TGA)

As described in Section 3.3.4.6 (temperature range from $25^{o}C$ to $1000^{o}C$).

 TA Universal Analysis 2000 software was used to calculate the weight loss (%) and the derivative weight loss with temperature from the TGA scans.

4.3.4.7 Tensile tests

As described in Section 3.3.4.4. The test specimens were cut into strips (55mm × 5mm) from the films and the European standard (ISO/DIS 527-1:2010) was

followed to calculate the tensile strength, modulus and elongation at break from experimental data. A minimum of five repeat specimens were tested for each formulation.

4.3.4.8 Dynamic mechanical analysis (DMA)

As described in Section 3.3.4.5. The specimens were prepared by cutting strips from the films with a width of 4 mm and length of 25 mm and heated from $-40^{o}C$ to $430^{o}C$ at rate of $10^{o}C$ min^{-1}, 15 mm gap distance, 0.05% strain, 0.01N preload force, 125% force track and 1 Hz frequency.

4.3.4.9 X-ray diffraction (XRD) analysis

The crystallinity index of the samples was measured according to the procedure described previously in Section 3.3.4.8. The degree of crystallinity of the samples was calculated according to the Equation 3.4 (please see Section 3.3.4.8, chapter 3).

4.3.4.10 Swelling kinetics

The swelling capacity of the CNW-HEC flexible films were calculated gravimetrically by measuring the mass of the sample before and after swelling in PBS media at $37^{o}C$ for 2 hours using Equation 4.1. The swelled films were placed onto tissue paper to blot dry and weighed immediately.

$$\text{Swelling capacity} \left(\%\right) = \frac{(M_W - M_o)}{M_o} \times 100 \dots\dots\dots\dots\dots(4.1)$$

Where, M_w is the mass of wet sample after swelling and M_o is the mass of dry sample before swelling.

4.4 RESULTS AND DISCUSSION

The high surface area, nano-scale dimensions and high mechanical properties of CNWs make them promising candidates to improve the thermal and mechanical properties of biopolymer based composites. Here we investigated whether hydroxyethyl cellulose, a cellulose sizing agent can be used to bind the nanowhiskers together to create high fibre content composites.

4.4.1 Morphological properties

A representative TEM image of CNWs obtained via acid hydrolysis of bleached cotton is provided in Figure 4.1. The rod-like morphology of the whiskers in the nanoscale region was clearly observed. The CNWs in the TEM micrograph were aggregated, which was expected due to drying as a result of to the presence of hydroxyl groups on the surface of CNW promoting association via hydrogen bonding [176, 209, 210].
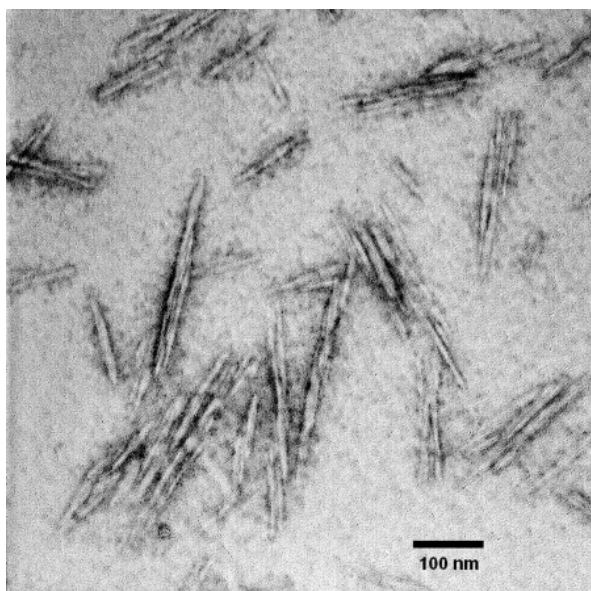
Figure 4.1: *TEM image of cellulose nanowhiskers (CNWs).*

The surface topography of the HEC films and the dispersion of CNWs in the CNW-HEC flexible films was also analysed via SEM and is presented in Figure 4.2 which suggests the Hydroxyethyl cellulose binder forms around the cellulose nanowhisker percolated network. Images obtained revealed that the surfaces of the HEC films were very smooth and homogeneous (see Figure 4.2a), whereas Figures 4.2b-d showed the nanowhiskers inducing surface roughness within the CNW-HEC blends and appearing to template the polymer onto the CNWs percolated network.
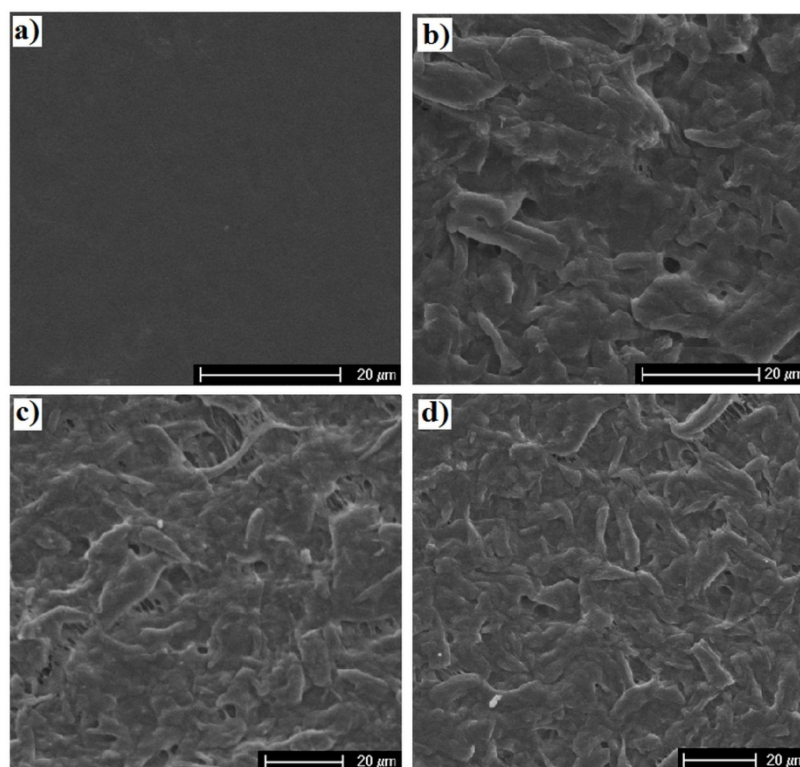
Figure 4.2: *SEM images of flexible films: a) HEC film, b) CNW:HEC (50:50), c) CNW:HEC (65:35), and d) CNW:HEC (75:25).*

However, brightfield and fluorescence images revealed clear morphological differences between the RITC labelled HEC containing varying amount of CNWs and the pure RITC-HEC. Absence of black spots in the control sample of pure RITC-

labelled HEC (Figure 4.3a) indicated that labelling of the HEC with RITC had been successful and was completely random with respect to the microscopy resolution. The composite films (Figure 4.3b-d) on the other hand revealed distribution of black spots due to the presence of un-labelled CNW particles. Whereas the darker regions are clear signs of CNWs aggregation, the CNWs structure formed still shows a homogeneous dispersion and a percolated network of these larger domains.
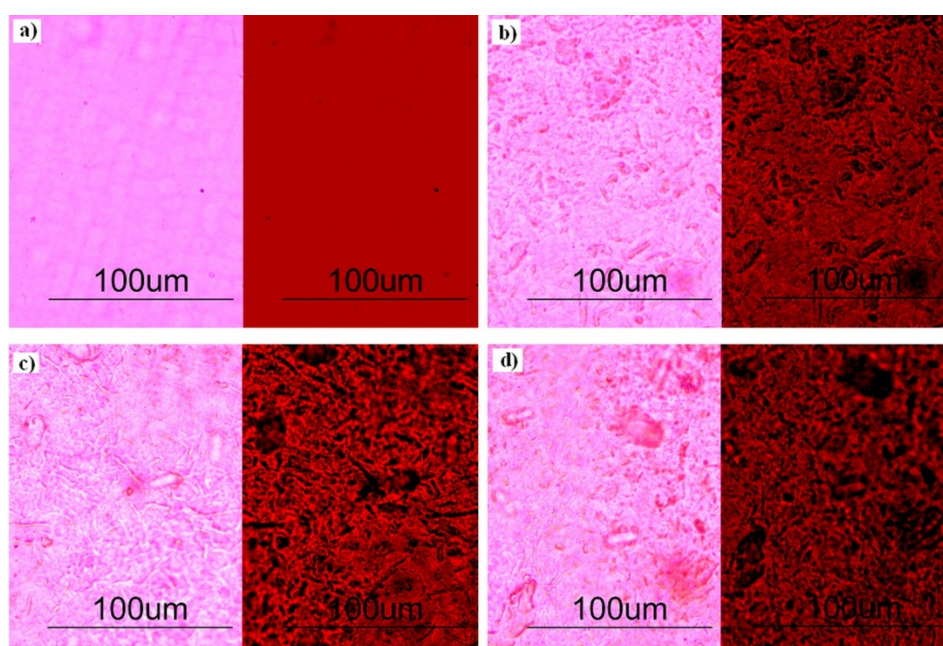
Figure 4.3: *Brightfield (left image of each set) and fluorescence (right image of each set) images of flexible films obtained from RITC labelled HEC with various CNW content: **a)** RITC-HEC, **b)** CNW:RITC-HEC(50:50), **c)** CNW:RITC-HEC(65:35), and **d)** CNW:RITC-HEC(75:25).*

An increase in the undyed CNW particles (black spots) in the composite films indicated the dispersion of CNWs increased with an increase in their content within the matrix. From the image analysis conducted approximately 37, 51 and

63% CNWs were calculated in CNW:RITC-HEC(50:50), CNW:RITC-HEC(65:35) and CNW:RITC-HEC(75:25) composite films, respectively. However, the calculated amount of undyed CNWs revealed lower CNW content in the composites compared to the formulation used in composites processing, which was also expected due to the presence of some CNW particles covered by the RITC labelled HEC matrix. This indicates that a consistent 13% of CNWs is well dispersed within the HEC matrix (and not visible due to resolution limitations of fluoresence microscopy). This may be the limit for the preparation of fully-dispersed CNWs in HEC composites. A variation of shapes of the nanofiller aggregates within the composite films is also evident from the fluorescence images, which was also expected due to the previously mentioned self-association nature of CNWs, use of a viscous matrix during composite processing, and the high CNW content in the composites. These aggregations in the composite material become more important with increasing cellulose content.
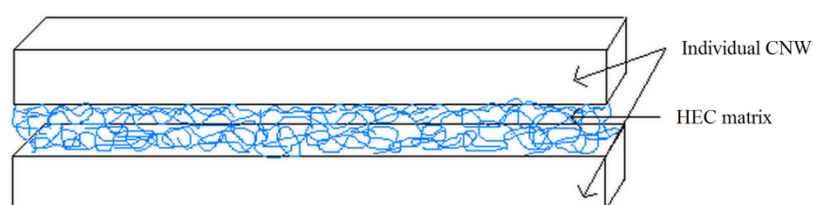
Figure 4.4: *A drawing showing the aggregated morphology of CNW-HEC blends.*

However, despite aggregation, the nanowhiskers still form a clearly visible percolated network and do not appear to accumulate into completely discrete regions. It can be expected that there is a competition between CNW-HEC interactions and CNW-CNW interactions and that under ideal conditions, an aggregated sandwiched structure as presented in Figure 4.4 can also be expected.

A similar aggregated morphology was also reported for composites prepared using cellulose nanowhiskers derived from eucalyptus wood and chitosan [167].

4.4.2 Surface roughness and light transparency

The average surface roughness (Ra) of the thin films was seen to increase with increasing CNW content in the blends as presented in Figure 4.5, which was attributed to the presence of higher amount of aggregated CNWs in the blends. The roughness increased from approximately 0.8 μm to 3.0 μm for the films containing 75% CNWs, in agreement with SEM results. Nogi *et al.* [249] investigated the influence of surface roughness on the light transparency of nanocellulose film and suggested that the rough surface of the film significantly reduced the light transmittance property due to light scattering effect, which was found to be consistent with the light transmittance properties (see Figure 4.6) of the CNW-HEC blends investigated in this study.
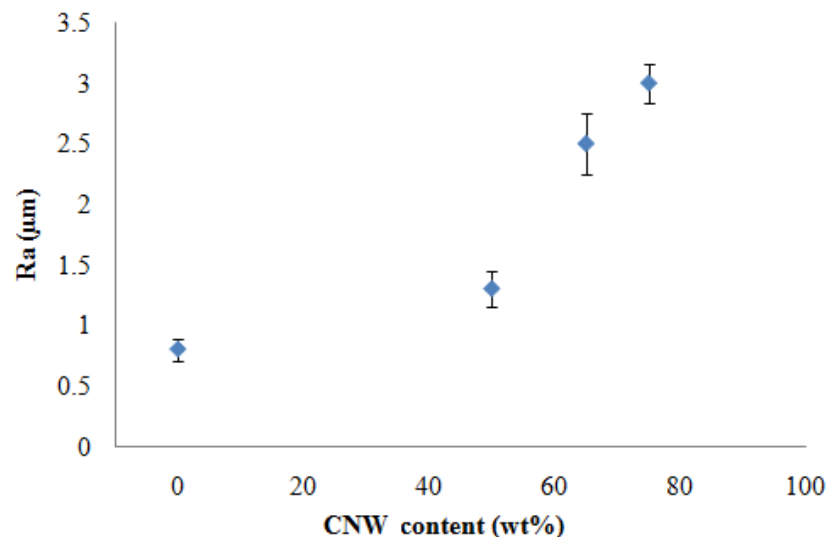
Figure 4.5: *Surface roughness of the pure HEC and CNW-HEC flexible thin films.*

The light transparency of thin films obtained by UV/Visible spectrometry shows pure HEC film revealed light transparency of around 86% in most of the visible

light region, whereas, the thin films based on CNW-HEC blends exhibited a significant decrease in light transmittance down to 5.2%, with increasing CNWs content in the blends. Representative images of the flexible thin films (see inset of Figure 4.6) also reveal that the optical transparency decreased with increasing CNW content.
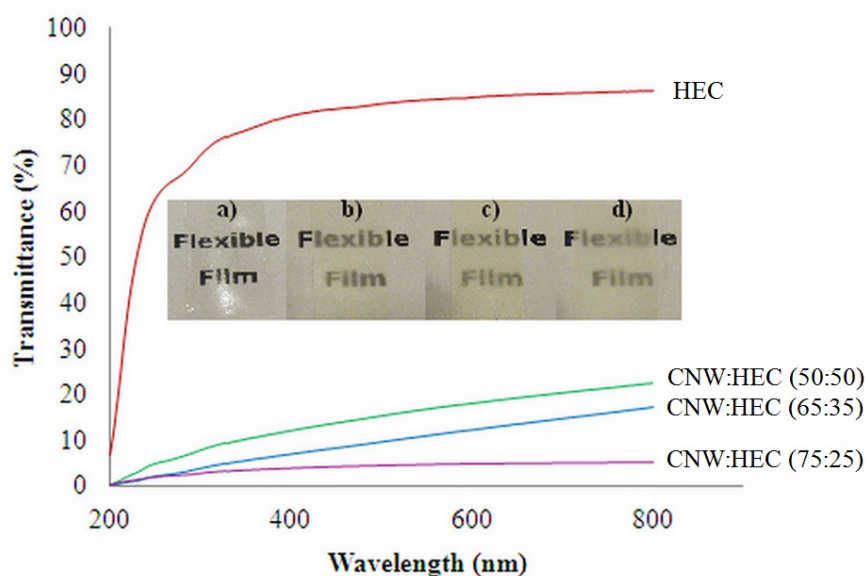
Figure 4.6: *Light transmittance of flexible thin films. Inset Figure shows the representative image of the flexible thin films: **a)** HEC, **b)** CNW:HEC(50:50), **c)** CNW:HEC(65:35), and **d)** CNW:HEC(75:25).*

4.4.3 Thermal properties

From DSC analysis of pure HEC and CNW-HEC flexible films (Figure 4.7) it can be seen that the glass transition temperature (T_g) of pure HEC film appeared at around 89°C which remained at this value with the addition of CNWs in the CNW-HEC blends for all CNW contents. The T_g value for pure hydroxyethylcellulose has been reported by Luo *et al.* [42] as 76±5°C and by Khutoryanskaya *et al.* [238] as 97°C. The variation in the T_g values of this material are suggested to be due to the

presence of moisture, the degree of sample deacetylation and the experimental protocols used to determine the T_g [42]. However, the deviation in T_g values of the pure HEC compared to the literature's pure hydroxyethylcellulose was also expected as the HEC used in this study contained additives as well as hydroxyethylcellulose. The DSC data presented in this study is taken from the second heating cycle of the thermogram in order to minimise the effect of thermal history and the influence of any residual moisture present within the samples.
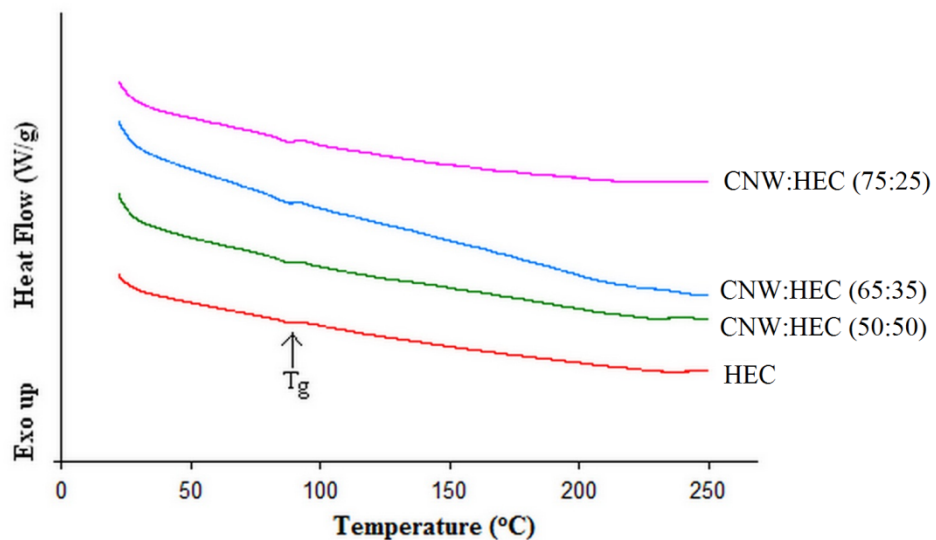
Figure 4.7: *DSC curves of pure HEC and CNW-HEC flexible films.*

Thermogravimetry (TG) and derivative thermogravimetry (DTG) curves of the CNWs, pure HEC and CNW-HEC blends are shown in Figure 4.8. The TG analysis revealed a weight loss of ~10% for each sample type below 150°C, which was attributed to the evaporation of loosely-bound water or other volatiles [238, 252]. It can be seen from Figure 4.8a that the composites and pure HEC matrix were stable up to 230°C (90% retention of residual weight) except for the CNWs alone

(stable upto only 192°C), indicating that the processing temperature for these blends should be kept below 192°C. The lower thermal decomposition of CNWs compared to HEC was attributed to residual sulphate groups on the surface of CNW created by the acid hydrolysis process used to produce them [225].
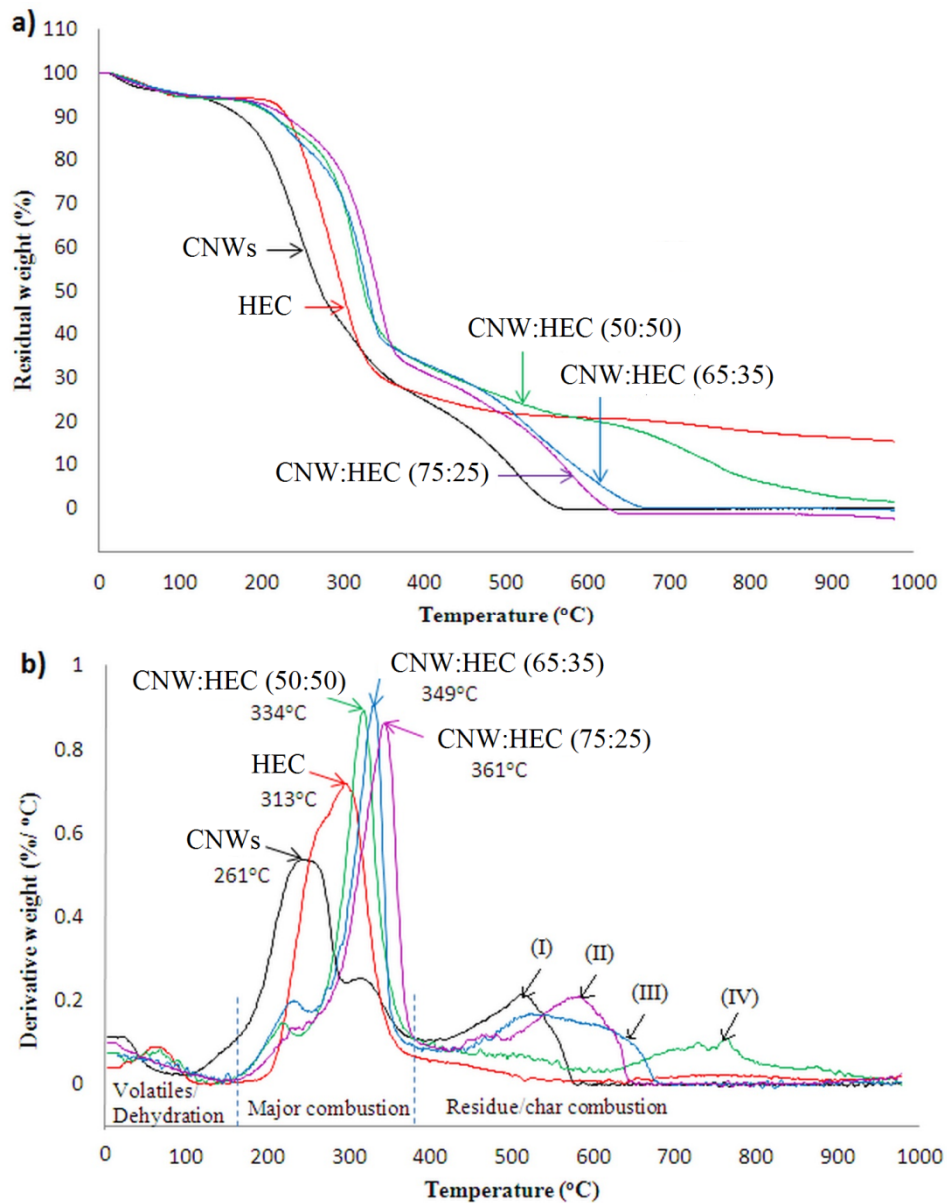
Figure 4.8: *a)* *TG curves of CNWs, HEC and CNW-HEC flexible films, and **b)** DTG curves of CNWs, HEC and CNW-HEC flexible films.*

The major thermal decomposition profiles of CNWs, HEC and their blends were evaluated from their derivative thermogravimetry (DTG) curves (see Figure 4.8b), which showed the maximum decomposition temperature (T_{max}) for acid hydrolysed CNWs and pure HEC film at 261°C and 313°C, respectively. The thermal degradation of all the major functional groups in the materials occurred in the range 190~380°C through solid state transformations and loss of low molecular mass fragments [238, 253]. The composite decomposition peaks in the range of 240~260°C indicated decomposition of some CNWs which may possibly have been loosely attached to the surface of the matrix. The char combustion peak (I), (II), (III) and (IV) for CNWs, CNW:HEC (75:25), (65:35) and (50:50), respectively, was further seen to shift to higher temperature region with increasing HEC content in the blends, probably due to interactions between HEC and CNWs resulting in closer packing and reduced oxygen ingress during combustion. The wider char combustion peaks also suggest that a larger temperature span was required to complete the char combustion reaction for blends with higher HEC content, further pointing towards a closer packed structure. The second derivative thermogravimetry (2DTG) data (see Table 4.2) were used to evaluate the onset (T_d) and the final (T_{df}) decomposition temperatures for the main degradation peak. Both the T_d and T_{df} for the blends of CNW-HEC were observed to increase with increasing CNW content in the blends compared to both CNWs and pure HEC film, indicating a synergistic effect. For all the blends investigated a shift to the higher temperature region for the major combustion reaction and the high char

content at 400°C compared to CNWs and HEC alone suggest that their interaction might have significant influence on improving their thermal properties.

A summary of the thermogravimetry analysis (TG, DTG and 2DTG) data is presented in Table 4.2 representing the comparison of T_d, T_{max}, T_{df}, weight loss at T_{max} and char content at 400°C of acid hydrolysed CNWs, pure HEC and CNW-HEC blends.

Table 4.2: *Summary of TGA data obtained for CNWs, HEC and CNW-HEC flexible films.*

Sample codes used in this study	Major decomposition profile				Char at 400°C (%) (from TGA curves)
	T_d (^{o}C) (from 2DTG curves)	T_{max} (^{o}C) (from DTG curves)	T_{df} (^{o}C) (from 2DTG curves)	Weight loss at T_{max} (%) (from TGA curves)	
CNWs	226	261	293	34.7	26.7
HEC	248	313	336	46.7	27.1
CNW:HEC (50:50)	317	334	346	41.8	34.9
CNW:HEC (65:35)	339	349	359	49.9	34.7
CNW:HEC (75:25)	354	361	375	50.8	32.9

4.4.4 Mechanical properties

The tensile strength and modulus properties of the CNW-HEC blended films compared to pure HEC film are shown in Figure 4.9. All the CNW-HEC blends displayed a statistically significant increase ($P<0.05$) in tensile strength and modulus when compared to the pure HEC film. For instance, 134%, 224% and 294% increase in tensile strength and 956%, 1243% and 2004% increase in tensile modulus was observed for CNW:HEC(50:50), (65:35) and (75:25) blends, respectively, compared to pure HEC film (tensile strength ~12.23 MPa and modulus ~0.39 GPa). A large increase was anticipated; since it has been reported in the literature that the tensile modulus of cotton based CNWs is around 57 GPa [54].

The experimental modulus obtained for the nanocomposite films was compared with the predicted upper (E_f=105 GPa for 3D orientation) and lower bounds (E_f=57 GPa for 2D orientation) [54] modulus calculated using the 'Rule of mixtures' (Cox-Krenchel) model (previously described in Section 3.4.4), as presented in Figure 4.9b. The experimental values were observed to follow a similar increasing trend as the lower bound predicted line. However, the nanocomposite containing lower volume fraction CNWs revealed comparatively higher values which followed the upper bounds of the 'Rule of mixtures' prediction line, which could have been due to the less aggregated particles as well as the creation of percolation network among the CNWs within the nanocomposite films containing comparatively lower concentration of CNWs.
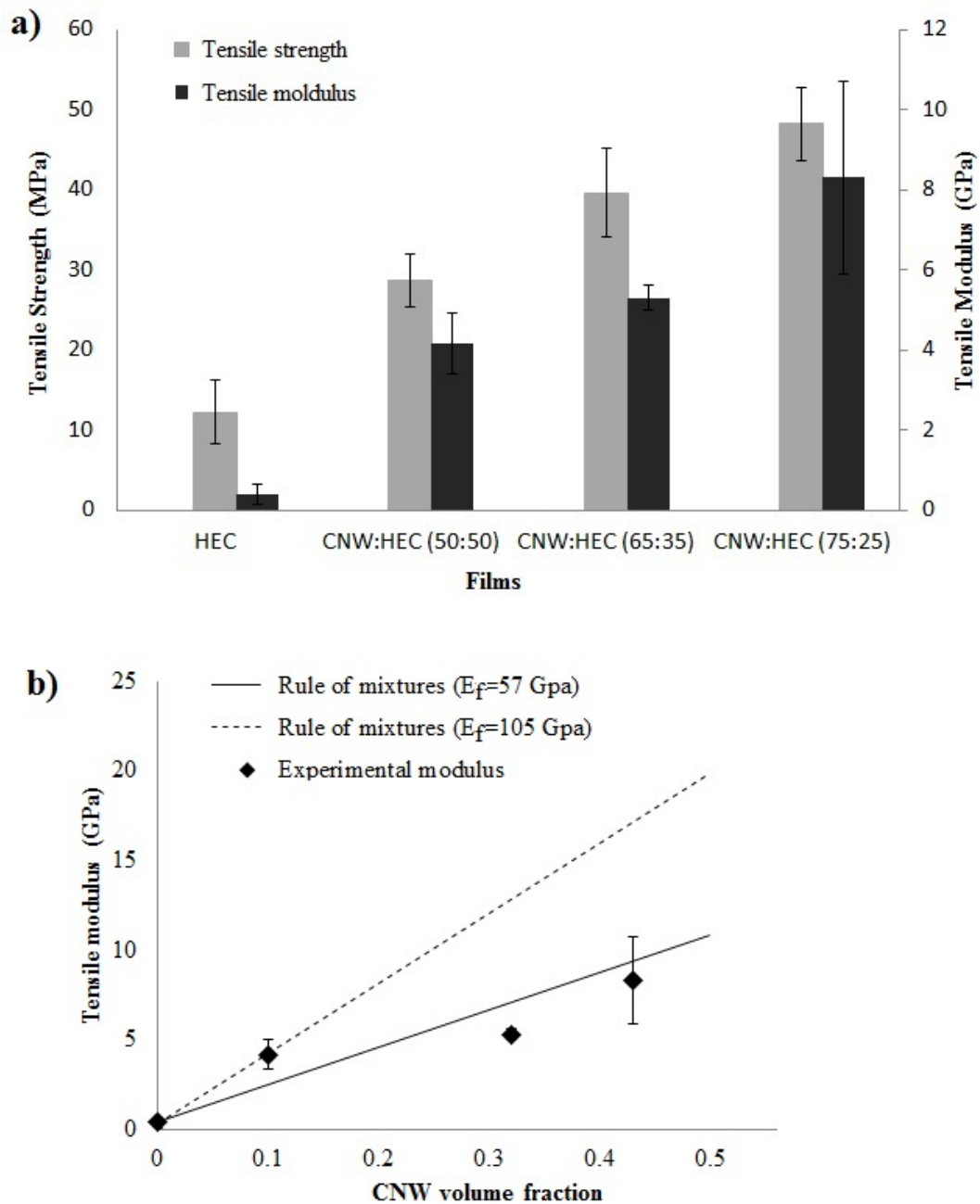
Figure 4.9: a) *Tensile strength and modulus curves of HEC and CNW-HEC flexible films, and **b)** comparison between the experimental and predicted modulus calculated using the 'Rule of mixtures' (Cox-Krenchel) model.*

The experimental results could be compared using the Percolation model, which predicts the tensile modulus of nanocomposites containing a percolating network of rigid fillers. The predicted tensile modulus, E'_c can be expressed by:

$$E'_c = \frac{(1 - 2\psi + \psi X_r)E'_s E'_r + (1 - X_r)\psi E'^2_r}{(1 - X_r)E'_r + (X_r - \psi)E'_s} \quad ....(4.2)$$

and

$$\psi = X_r \left(\frac{X_r - X_c}{1 - X_c} \right)^{0.4} \quad ....(4.3)$$

Where, ψ is the percolating volume fraction of nanofillers that participated in the load transfer, X_c is the critical filler percolation volume fraction (X_c= 0.7/A), A is the aspect ratio of the filler, X_r is the volume fraction of the rigid fillers (assuming $X_r \geq X_c$), E'_s and E'_r are the tensile modulus of the soft polymer and rigid filler. The density of CNWs is taken to be 1.59 g cm^{-3} from the literature [176].

The following assumptions were considered: tensile modulus of the neat matrix, $E'_s = 0.39$ GPa, tensile modulus of the filler, Poisson's ratio for both matrix and filler, v_s and v_r =0.3, aspect ratio for the filler (A=5, 20 and 60) [123, 254], longitudinal filler modulus, E'_{Lf}= 57 GPa (Lower value)- 105 GPa (Upper value) [54], transverse filler modulus, E'_{Tf} = 18 GPa [255], shear modulus of filler, G'_r = 0.250 GPa [256].
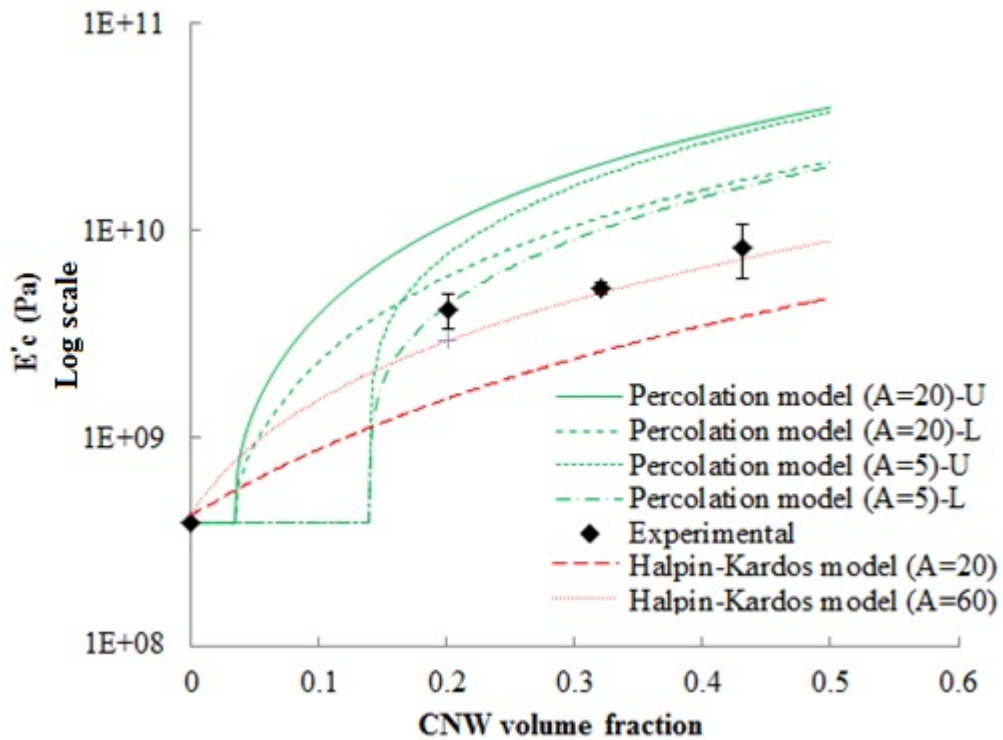
Figure 4.10: *Tensile modulus of CNW-HEC composite films as a function of filler*

volume fraction. Comparisons between the experimental results and predicted

modulus calculated using the Percolation and Halpin-Kardos model.

However, a mean-field approach developed by the Halpin-Kardos model which

predicts the modulus of the nanocomposites containing randomly oriented

nanofillers in a plane can be expressed as follows (see Equation 4.4): [257]

$$E^{'} = \frac{4U_5(U_1 - U_5)}{U_1} \quad \text{............................(4.4)}$$

with

$$U_1 = 1/8(3Q_{11} + 3Q_{22} + 2Q_{12} + 4Q_{66}$$

$$U_5 = 1/8(Q_{11} + Q_{22} - 2Q_{12} + 4Q_{66})$$

$$Q_{11} = E'_{Lf} /(1 - \nu_{12}\nu_{21})$$

$$Q_{22} = E'_{Tf} /(1 - \nu_{12}\nu_{21})$$

$$Q_{12} = \nu_{12}Q_{22} = \nu_{21}Q_{11}$$

$$Q_{66} = G'_{12}$$

$$\nu_{12} = X_r\nu_r + X_s\nu_s$$

$$\nu_{21} = \nu_{12}(E'_{Tf} / E'_{Lf})$$

$$G'_s = E'_s /2(1+\nu)$$

$$G'_{12} = G'_s(1 + \eta X_r)/(1 - \eta X_r)$$

$$\eta = (G'_r / G'_s - 1)/(G'_r / G'_s + 1)$$

Where, G'_r and G'_s are the shear modulus of the rigid filler and soft matrix.

To predict the tensile moduli using the Percolation model different aspect ratios (A=5 and 20) and upper and lower values for the longitudinal tensile modulus (57-105 GPa) [54] of the nanofiller were considered. The aspect ratio for the cotton based nanowhiskers was reported to be ~6 [123] and 19 [254]. For the upper value of longitudinal tensile modulus (105 GPa for a 3D orientation), the predicted tensile moduli (A=5 and 20) were seen to deviate from the experimental data with high volume fraction of the CNWs as compared to the predicted percolation tensile moduli calculated using lower longitudinal tensile modulus (i.e. 57 GPa for a 2D orientation). A similar deviation from the experimental modulus was also observed for the Halpin-Kardos predicted moduli (A=20). The experimental tensile moduli were found to be in between the predicted moduli calculated by the two models (A=20) described in this investigation which was attributed to the existence of aggregated CNWs (due to filler-filler interactions) randomly dispersed within the composite, as observed via fluorescence microscopy. However, E'_c

estimated by the Halpin-Kardos model for the higher aspect ratio (A=60) was in good agreement with the experimental measurements, which indicated that the random dispersion of the CNW bundle due to the use of HEC as a binder for the higher volume fraction composites limited the actual aspect ratio of the nanofiller.

4.4.5 Thermomechanical properties

DMA was used to obtain the storage modulus of the nanocomposites as a function of temperature (Figure 4.12a). The incorporation of CNWs in the HEC matrix showed a significant increase in storage modulus properties of all the blends with increasing CNW content in all temperature regions that was considered. Earlier studies also showed the ability of nanowhiskers blended with polymer to improve the storage modulus of the matrix at higher temperatures [52]. This was explained by the high interfacial surface area, higher cross-linking density and surface induced crystallisation within the blends.

The tan delta curves (Figure 4.12b) showing the α, β and γ-transitions of the CNW-HEC flexible films revealed that the tan delta peaks had shifted to a higher temperature region as compared to pure HEC film (131°C). These peaks were observed in the region of 130~140, 230~250 and 331~356°C, respectively. The α-transition in tan delta peaks for the blends was suggested to be due to the unbound CNWs and β-transition was attributed to the loosely bound CNWs in the blends. The more intense tan delta peaks due to the γ-transition for all the blends were seen to shift to higher temperatures (from 331 to 356°C) with increasing CNW content, which indicated that the incorporated CNWs governed a significant

reduction in the segmental motions of the HEC matrix in the blends through CNW-

HEC interactions [52].
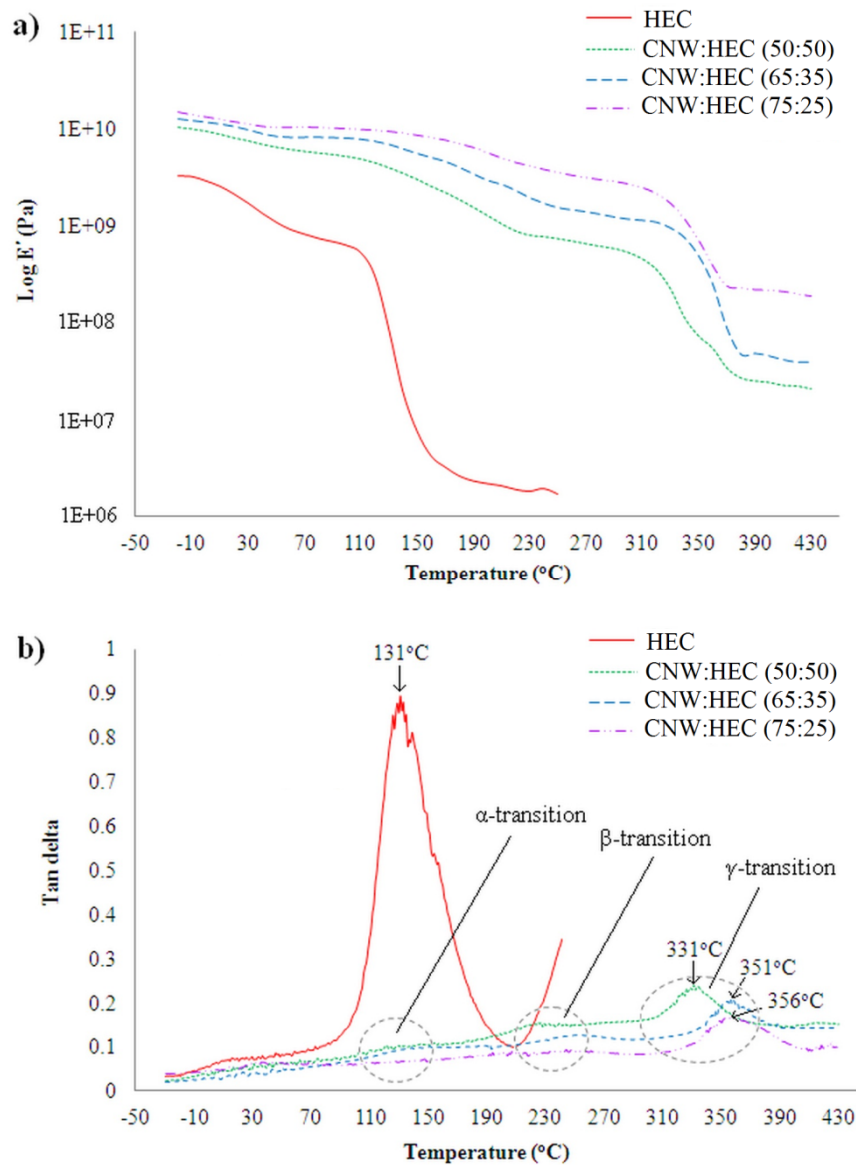
Figure 4.11: ***a)*** *Storage modulus curves of HEC and CNW-HEC flexible films from*

DMA data, and ***b)*** *Tan delta curves of HEC and CNW-HEC flexible films from DMA*

data.

The width of the tan delta peaks in the blends also broadened with increasing

CNW content, suggesting the higher temperature span required for the transition

[182] due to an increase in CNW-HEC interactions thereby reducing segmental freedom of movement.

4.4.6 Crystallisation properties

XRD analysis of the CNWs, pure HEC and CNW-HEC flexible films are presented in Figure 4.13. From the diffraction pattern of CNWs the most intense peak was observed at 22.8^o, with an additional double peak signal at 14.9^o and 16.5^o.
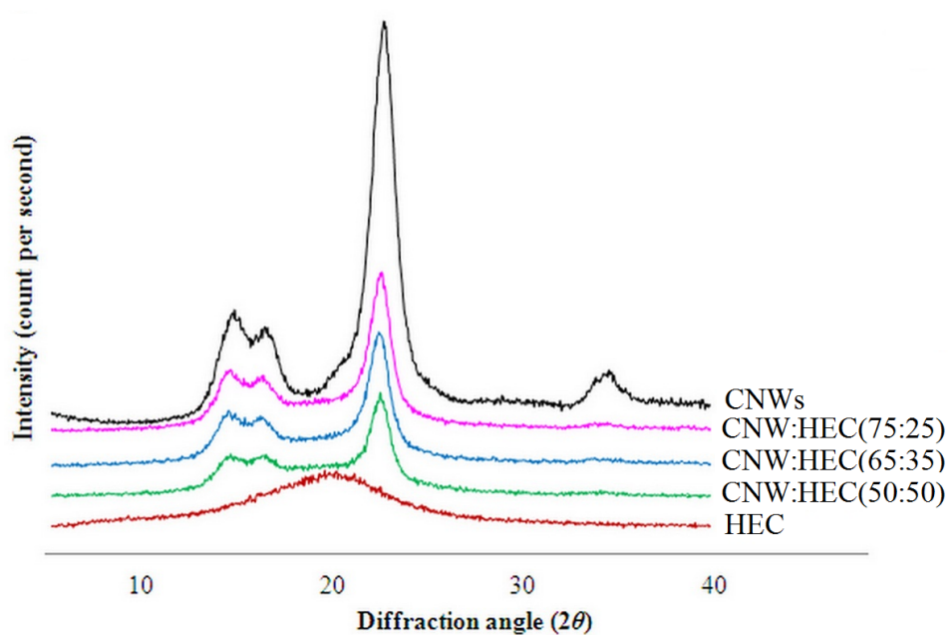
Figure 4.12: *X-ray Diffraction pattern of Hydroxyethyl cellulose and CNW-HEC flexible*

films.

The freeze dried CNWs were found to be ~89% crystalline, which was well consistent with other literature values [176, 258] and the XRD traces for the blends showed clear retention of the cellulose crystallites with increasing peak intensity at 2θ= 14.9 ^{o}, 16.5^o and 22.8^o. The diffraction patterns for pure HEC film revealed a halo typical of amorphous materials at 2θ = 20° [240] and

incorporation of CNWs in the HEC matrix caused an increase in the overall crystallinity (see Figure 4.14) beyond what was expected for the CNWs alone.
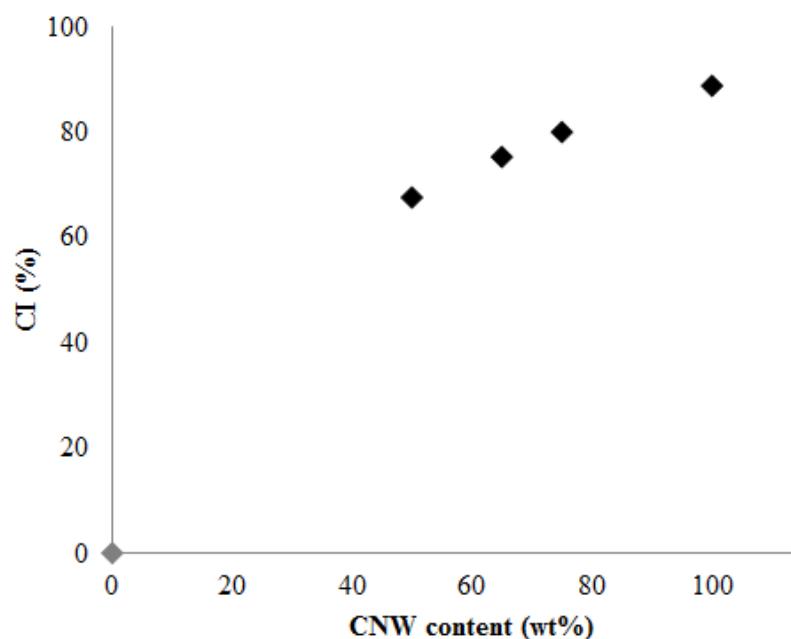
Figure 4.13: *Relationship between the crystallinity index (CI) and CNW content in the flexible films.*

4.4.7 Swelling kinetics

The swelling capacity of CNW-HEC blends in PBS media at $37^{o}C$ increased with swelling time as presented in Figure 4.15a, suggesting that the PBS fluid facilitated a decrease in the degree of physical cross-linking through weakening the hydrogen bonds in CNW-HEC and CNW-CNW interfaces.
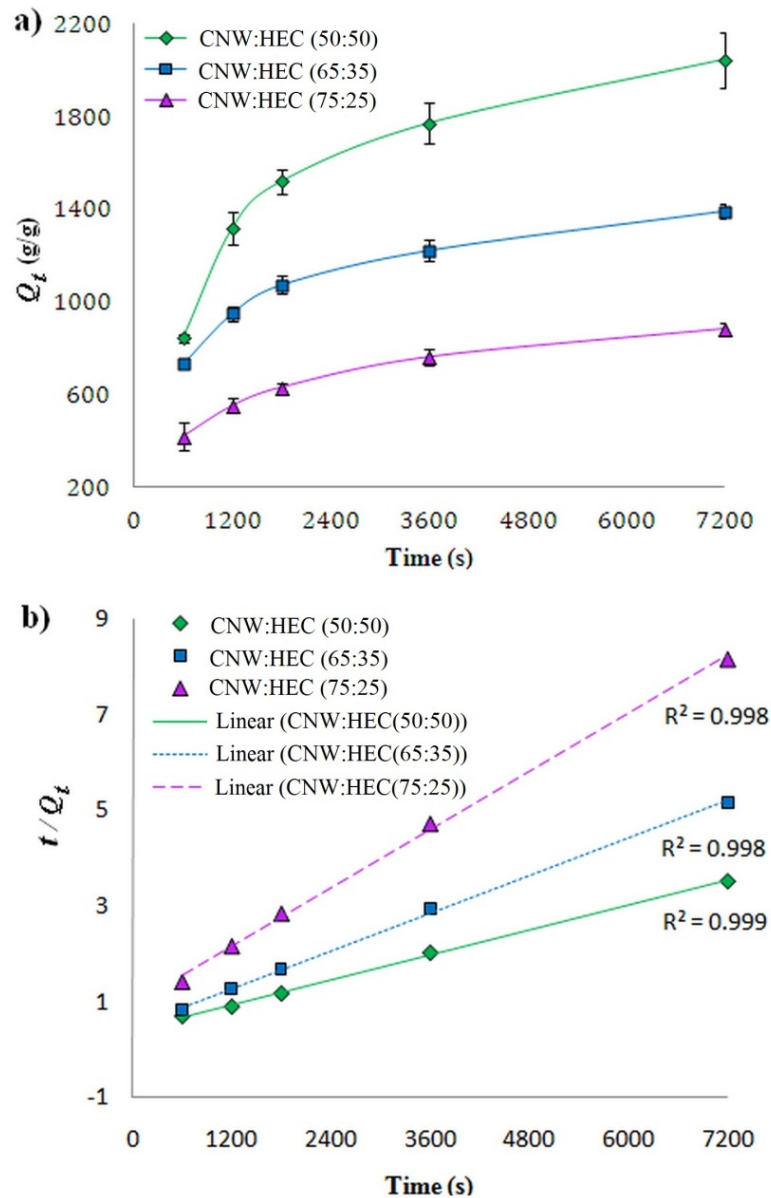
Figure 4.14: *a) Swelling kinetic curves of CNW-HEC flexible films in PBS media at 37ºC, and b) corresponding plots of t/Q_t against t of the CNW-HEC flexible films.*

The amount of CNWs in the blends also showed a significant influence on decreasing the swelling capacity of the blends. This was attributed to be due to the presence of a greater degree of CNW-CNW interaction, which decreased the hydrophilicity as well as swelling capacity of the blends by reducing the water holding capacity [239].

Schott's second order swelling kinetics model was introduced (Equation 4.5) [259] to evaluate the theoretical swelling capacity, initial swelling rate and kinetic behaviour of the CNW-HEC blends [239].

$$t/Q_t = 1/k_{is} + 1/Q_\infty t \ldots \ldots \ldots (4.5)$$

Here, Q_t (g g^{-1}) denotes the swelling capacity of the CNW-HEC blends at time t (s), Q_∞ (g g^{-1}) is the theoretical equilibrium swelling capacity and K_{is} (g g^{-1}s^{-1}) is the initial swelling rate constant. The experimental swelling data of CNW-HEC blends in PBS media at 37°C was used to plot t/Q_t against t (see Figure 4.15b) and the linear trend line obtained for these experimental values showed very good linear correlation coefficients (>0.998), which support the use of Schott's second-order swelling kinetics model to describe the swelling kinetics behaviour of CNW-HEC blends in PBS media [239].
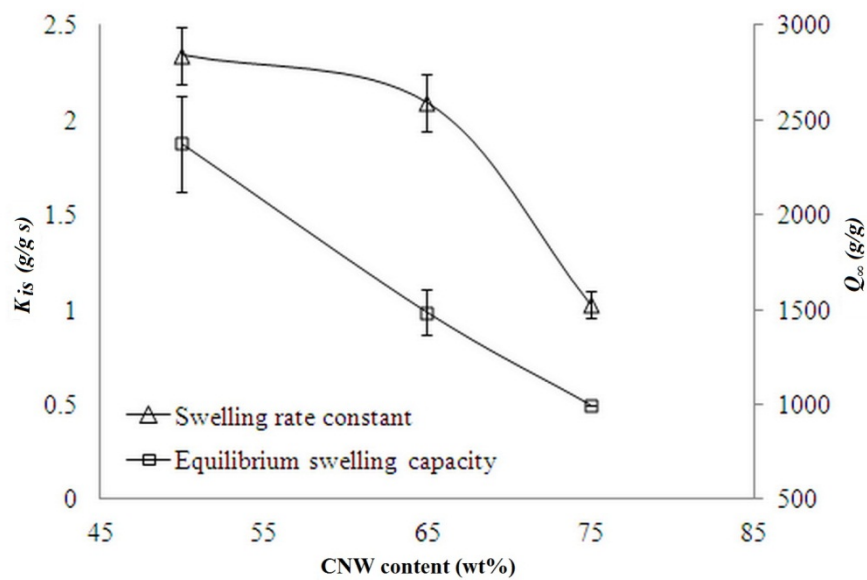
Figure 4.15: *Relationship between the swelling rate constant and equilibrium swelling capacity with CNW content in PBS media at 37°C.*

However, using the slope and intercept of the linear lines, the swelling kinetic parameters (Q_∞ and K_{is}) were calculated using the linear regression equation: *Y= a +bX,* (where, *Y=t/Q_t, a=1/K_{is}, b=1/Q_\infty and X=t*) and plotted against CNW content in the blend in Figure 4.16. The calculated theoretical swelling capacity and the initial swelling rate constant of the blends decreased with increasing CNWs also proved that the incorporation of CNWs in the blends played a significant influence on decreasing swelling rate of the CNW-HEC flexible films.

The CNW-HEC flexible films produced in this study showed that the incorporation of CNWs in a HEC matrix provide significant improvements in mechanical, thermal, thermomechanical, crystalline and swelling properties of the blends when compared to pure HEC. These modified capabilities may improve the number of potential applications for cellulose based composites in tissue engineering, drug coating and encapsulation materials.

4.5 CONCLUSIONS

Flexible films based on a range of blends incorporating CNWs and HEC were prepared in this study. CNWs within the matrix were seen to be aggregated and played an important role on the surface roughness and light transparency properties of the composite films. However, despite aggregation the CNWs still formed a percolated network and aggregates where homogeneously dispersed within the composite. The incorporation of CNWs in the HEC matrix provided a significant improvement in thermal properties by increasing the decomposition temperatures. Most significantly, the decomposition temperatures of the blends

were higher than either of the individual components. The enhanced tensile strength, modulus and storage modulus properties and the right shift of tan delta peaks of the blends compared to the HEC alone demonstrated the reinforcing effect of the CNWs. An increase in crystallinity of blends with CNW content indicated that the induced crystallisation within HEC was caused by the presence of CNWs, which acted as nucleating sites. Additionally, the presence of CNWs had a significant influence on controlling the swelling properties of CNW-HEC blends in PBS fluid at body temperature, which open up possible applications of this material within the biomedical field.

CHAPTER 5.

MECHANICAL, CRYSTALLISATION AND MOISTURE ABSORPTION

PROPERTIES OF MELT DRAWN POLYLACTIC ACID FIBRES

5.1 SUMMARY

In this chapter, polylactic acid (PLA) fibres were produced with average diameter ranging from 11 to 38 μm via a melt drawing process employing increasing take-up velocities. The PLA fibres exhibited smooth surfaces and uniformity in diameter as determined by scanning electron (SEM) and optical microscopy (OM). Fourier transform infrared spectroscopic (FTIR) analysis using the dichroic ratio demonstrated alignment of PLA chains with the draw direction, where the thinner PLA fibres exhibited a higher degree of chain orientation during the high speed melt drawing process. The crystallinity of the fibres also increased up to 34% with decreasing fibre diameter due to strain-induced crystallisation. The room temperature tensile strength and modulus of the thinner PLA fibres with an average diameter of 11 μm revealed values of 213 MPa and 4.8 GPa, respectively. These fibres revealed a significant decrease in their tensile strength (by 29%) when tested at 37$^{\text{o}}$C compared to the room temperature value. Comparatively thicker PLA fibres did not show any significant change in their tensile properties at 37$^{\text{o}}$C. The variation in diameter of PLA fibres also revealed a noticeable influence in moisture absorption at various humidity levels.

5.2 INTRODUCTION

Polylactic acid (PLA) is widely used in the field of tissue engineering for biomedical applications such as for surgical sutures, implants, scaffolds, fracture fixation devices and sustained released polymer for drug delivery systems [166, 260-264] due to its biocompatibility, biodegradability, superior transparency and suitable thermal and mechanical properties [265, 266]. PLA can be produced via ring opening polymerisation of the lactide monomer which can be derived from renewable sources such as corn and potato starch [65]. As part of its appeal, thermoplastic PLA can be formed into various architectural forms including films [166, 267], plates [268], scaffolds [269, 270], fibres [75], screws [271] and rods [272]. It can also be processed via solvent casting or by melt compounding processes (such as hot compression, injection and extrusion moulding) [65, 265] and can be produced into fibrous structures via melt spinning and/or electrospinning with distinct fibre properties [74-77].

Melt spun PLLA fibres with a 394 μm diameter was investigated by Okuzaki *et al.* [84] . They reported that further drawing (DR=10.5) of the as-spun fibre at 90°C increased the crystallinity of the PLLA fibre by 30% when compared to undrawn fibres (crystallinity 7.4%). Tensile strength of the fibre increased from 16 MPa to 275 MPa, whilst the modulus increased from 1.8 GPa to 9.1 GPa, which was due to the increased orientation factor of the polymer chains within the fibre as a direct result of drawing at 90°C.

PLA can be hydrolysed by water and as such, its degradation is accelerated in a moist environment and by the presence of water during its service life. The

moisture absorption capacity of the fibre depends on the nature of the PLA, such as hydrophilicity (ester groups), diffusion coefficient, thickness and the surrounding environment. *In vitro* degradation of PLLA fibres with varying diameter ranging from 113 to 148 μm in phosphate buffered saline (PBS) media at 37°C was investigated by Yuan *et al.* [273]. They reported that the tensile moduli and ultimate strength of the fibres was not significantly altered during 35 weeks of degradation except for PLLA fibres with the smaller diameter of 113 μm. These smaller fibres exhibited a significant decrease in ultimate strength by 20% with respect to their initial value (500 MPa). The authors suggested that formation of micro cracks on the degraded fibre surface resulted in the decrease of their mechanical properties.

The PLA fibres investigated in the literature [81-84] were produced via a melt drawn process using an extruder to feed them onto the winder drum and the fibre properties were further improved using cold and/or hot draw processes [83, 84]. The PLA fibres investigated in this study were manufactured using a gravity induced melt drawing process employing various take up velocities up to 400 m min^{-1}. The aim was to improve their crystallinity and chain orientation properties during the fibre production process with minimising the use of further cold drawing process. This would reduce required processing steps whilst still increasing mechanical properties. The morphology, chain orientation, thermal, crystallisation and moisture absorption properties of the PLA fibres produced at various take-up velocities were characterised. The effect of temperature (37°C)

and moisture absorption at various humidity levels on the mechanical properties of the PLA fibres were also investigated in this chapter.

5.3 MATERIALS AND METHODOLOGY

5.3.1 Manufacturing Process of PLA fibres

PLA fibres were produced via a melt spinning process. PLA (NatureWorks LLC, Ingeo^{TM} Grade 3251D, average M_w~90,000-120,000 g mol^{-1}, Density=1.24 g cm^3) beads dried at 50°C for 48h were melted at 180°C in air using a cylindrical steel mould attached with a band heater and polymer was allowed to exit through a base hole (2 mm) under gravity. The molten polymer was collected on a rotating drum (with a 1m circumference using a collector distance of approximately 50 cm) utilising various take-up velocities (of 100, 200, 300 and 400 m min^{-1}). The PLA fibres produced were coded as PLA 11, PLA 20, PLA 29 and PLA 38 with the number indicating the average fibre diameter in μm.

5.3.2 Scanning electron microscopic (SEM) analysis

The surface morphology of the PLA fibres was characterised using SEM (as described in section 3.3.4.1) operated at an accelerating voltage of 10 kV and a working distance of 10 mm.

5.3.3 Optical microscopic (OM) analysis

Fibre diameters were measured using a calibrated optical microscope (20x magnifications) and Image Pro Plus software was used to measure the diameter of the fibres in microns. The average fibre diameter is presented and the errors were

calculated from the measurement of at least 35 random fibres obtained utilising various take-up velocities.

5.3.4 FTIR-ATR analysis and chain orientation

Identification of the functional groups of the PLA fibres were analysed using FTIR (as previously mentioned in section 3.3.4.3) and the spectra were collected with a resolution of 4 cm^{-1} by averaging 32 scans using a standard pike ATR cell. To investigate the chain orientation of the PLA fibres with varying diameters via the dichroic ratio calculation, two different FTIR-ATR spectra for each type of PLA fibre were taken by placing the fibres in the machine both in the (parallel) and transverse (perpendicular) direction to the FTIR beam source as described elsewhere in the literature [83].

5.3.5 Differential scanning calorimetric (DSC) analysis

As described in section 3.3.4.7.

5.3.6 Mechanical properties

Single PLA fibres were glued onto a 25 mm gauge length paper tab and the tensile properties were measured at room temperature using a Hounsfield Series-S tensile testing machine (Software-QMAT) with a crosshead speed of 5 mm min^{-1} and a 1 kN load cell. An average of at least five repeat specimens for each type of fibre is reported.

5.3.7 Tensile testing at varying temperatures

Tensile strength and modulus properties of PLA fibres at two different temperatures (25°C and 37°C) were conducted using a DMA (Q800 from TA Instruments, USA) employing a controlled force method in stress/strain mode.

Single PLA fibres (using 10 mm gauge length paper tab) were conditioned at specified temperature for 10 minutes before ramping the force at a rate of 0.01N min^{-1} until break. A minimum of six repeat specimens were conducted to produce the reported average value.

5.3.8 Fibre conditioning and moisture absorption

PLA fibres (approximately 50 mm length) were conditioned at varying relative humidities (RH) of 0%, 35%, 75% and 98% at room temperature for four weeks and their moisture absorption properties were calculated by recording the weight gain of the fibres. A Bundle of PLA fibres (~1 gm) was placed in open glass vials which were kept in a sealed humidity chamber (see Figure 5.1) containing the following saturated salt solutions (P_2O_5 (0% RH), $CaCl_2. 6H_2O$ (35% RH), NaCl (75% RH), and $CuSO_4.5H_2O$ (98% RH)) [50].
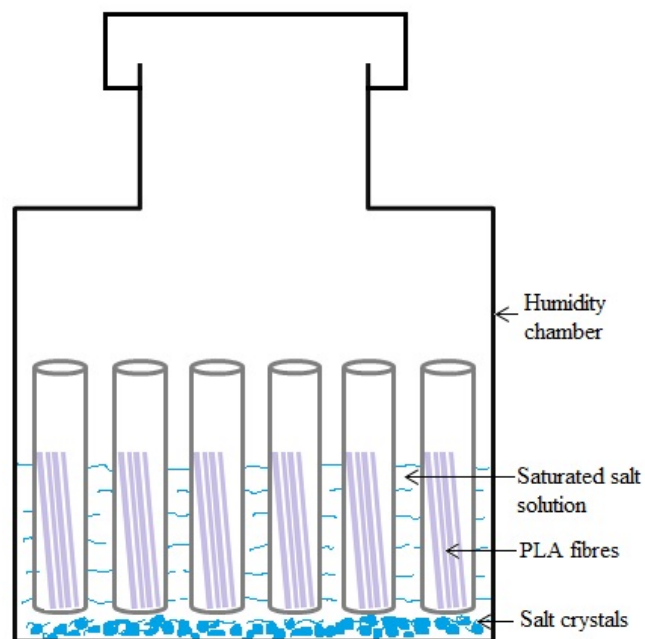
Figure 5.1: *Typical arrangement for fibres conditioned at different humidity levels.*

The weight gain due to moisture absorption can also be expressed in terms of diffusivity (*D*) and maximum moisture content (*W_m*), as shown by the following equation [274].

$$\frac{W}{W_m} = 1 - \frac{8}{\pi^2} e \; x \; p \left[- \left[\frac{D}{d^2} \right] \pi^2 t \right] \ldots \ldots \ldots \ldots \ldots . (5.1)$$

The water diffusivity in PLA fibres can be calculated by rearranging equation 5.1 as follows,

$$D = \frac{\pi \; d^2}{16 W_m^2} \times \frac{(W_2 - W_1)^2}{\left(\sqrt{t_2} - \sqrt{t_1} \right)^2} \ldots \ldots \ldots \ldots \ldots . (5.2)$$

Where, *d* is the diameter of the fibre, *W_m* is average value of several consecutive measurements that showed no significant additional moisture absorption, i.e. the water uptake at equilibrium, and $\frac{(W_2 - W_1)}{\left(\sqrt{t_2} - \sqrt{t_1} \right)}$ is the slope of the initial linear portion of the water absorption curve.

Tensile strength and modulus properties of the conditioned fibres were also measured to investigate the influence of moisture absorption on the mechanical properties of PLA fibres.

5.4 RESULTS AND DISCUSSION

5.4.1 Morphological properties

The surface morphology of the PLA fibres was observed via SEM (presented in Figure 5.2) which revealed smooth surfaces with some fibres exhibiting tiny particles on their surface which were probably formed due to partial incomplete

melting of the polymer caused by the non-uniform melt-mixing during fibre production which is common for this type of drawing process [82].
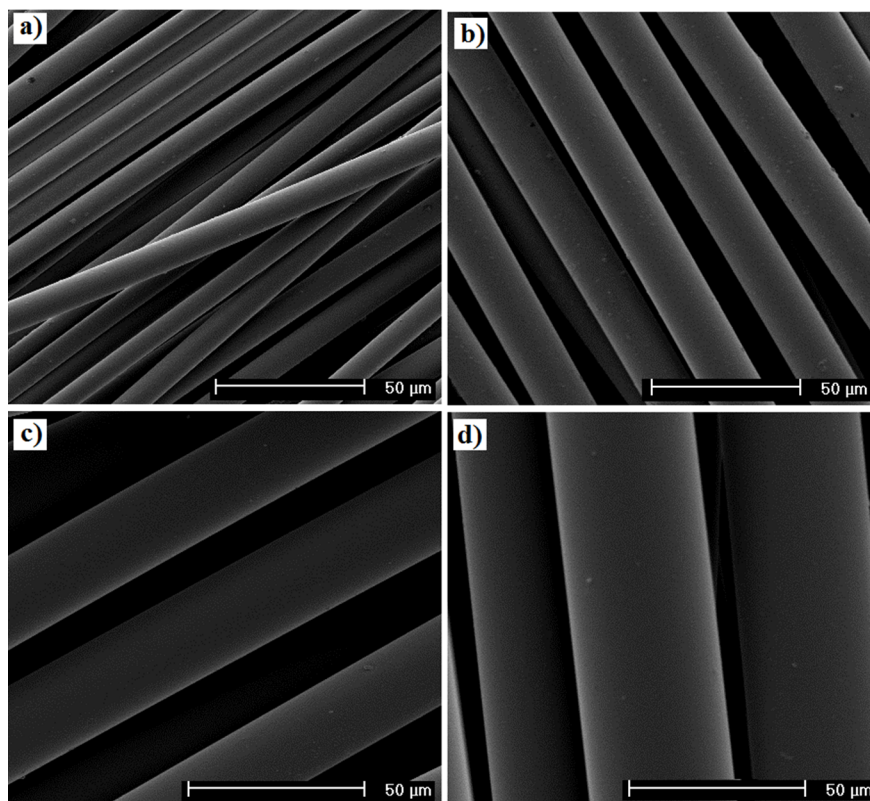
Figure 5.2: *Scanning electron microscopy images of PLA fibres: a) PLA 11, b) PLA 20, c) PLA 29, and d) PLA 38.*

The diameter of the fibres obtained at various take-up velocities was measured using an optical microscope and an average diameter of at least 35 specimens is presented in Figure 5.3. The average fibre diameter was seen to decrease linearly from 38 μm to approximately 11 μm when the take-up velocity increased from 100 m min^{-1} to 400 m min^{-1}, due to drawing at higher speed [81].
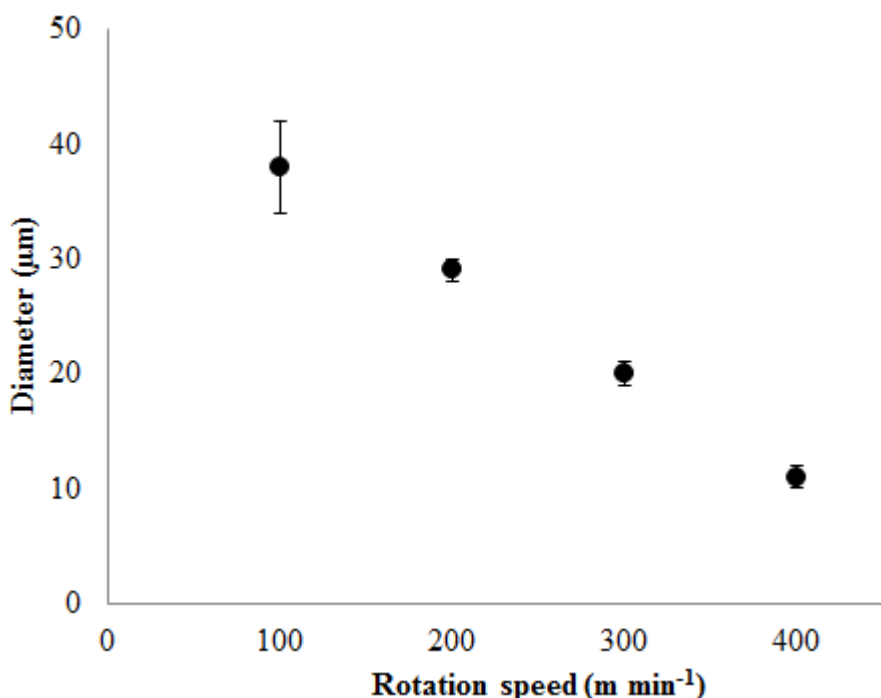
Figure 5.3: *Relationship between the rotation speed and the obtained PLA fibre*

diameter.

5.4.2 FTIR analysis and chain orientation

FTIR-ATR analysis is mainly utilised to identify functional groups and can also be used to determine chain orientation of the polymer molecules within the fibre. This process was used to investigate potential change of chain orientation with varying fibre diameter (see Figure 5.4a). From the FTIR-ATR spectra the C=O stretching groups of the PLA fibres were observed at 1751 cm^{-1}, whilst the CH$_3$ asymmetry and CH deformation bands were apparent at 1461 and 1382 cm^{-1} [83, 216]. The bands at 1178, 1132, 1080 and 862 cm^{-1} were attributed to COC asymmetric stretching, CH$_3$ in-plane bending, COC symmetric and C-COO stretching of the PLA chain, respectively [83, 216]. Changes in chain orientation of the PLA fibres with varying diameters were investigated in terms of dichroic ratio

of the C=O band at 1751 cm^{-1} where the orientation factor was seen to be influenced by the drum wind-up speed as well as the drawing effect during melt drawing of the PLA fibres [83, 275, 276].
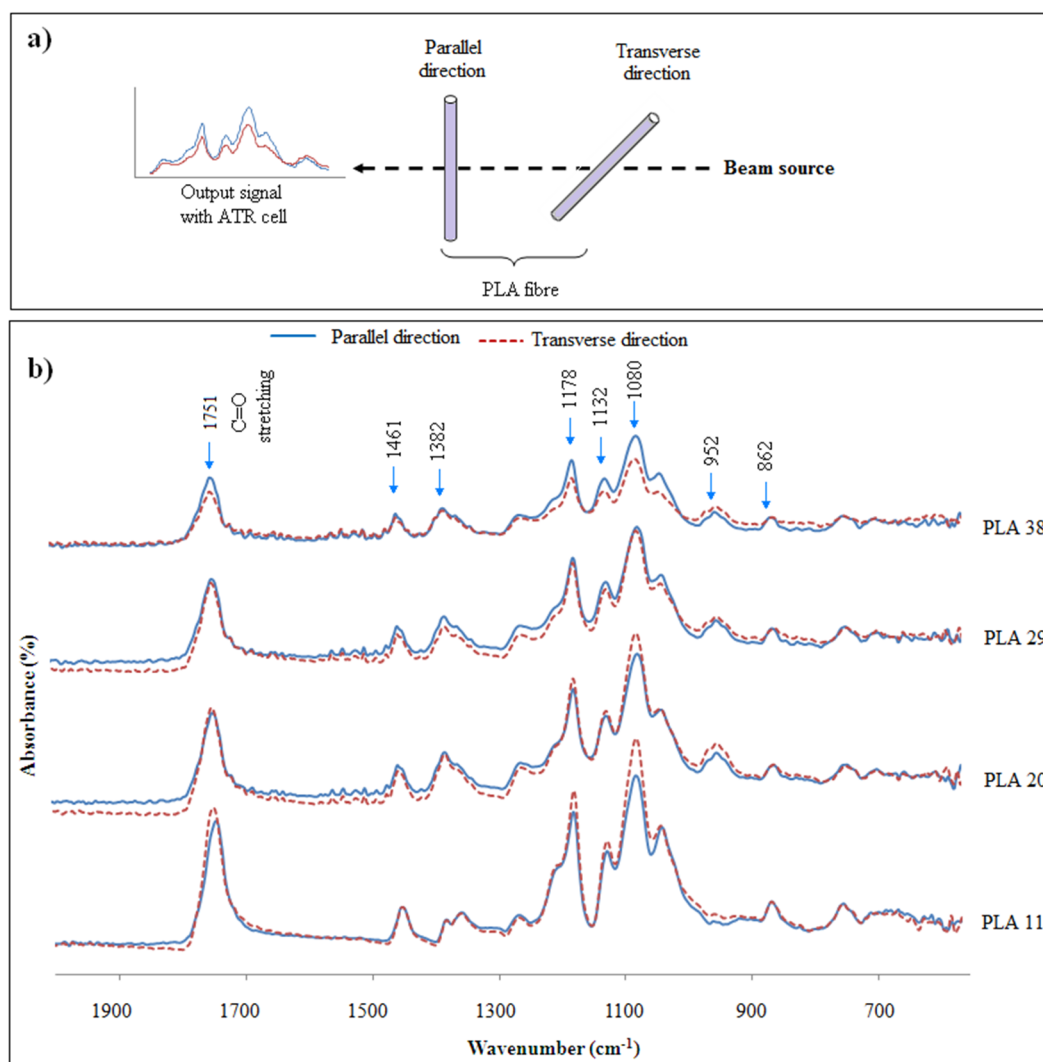
Figure 5.4: *a) Typical arrangement of PLA fibre on the FTIR-ATR instrument to measure the spectra, and b) FTIR-ATR spectra of PLA fibres with varying diameters determined in the parallel (solid line) and transverse (break line) direction.*

To calculate the dichroic ratio all the spectral intensities were normalised with the peak at 862cm^{-1} before considering the absorbance intensities of the carbonyl

group at 1751 cm^{-1} [277]. The dichroic ratio (D) of the PLA fibres was expressed using the following equation:

$$D = \frac{A_P}{A_T} \dots\dots\dots\dots\dots\dots\ (5.3)$$

where, A_P and A_T are the absorbance intensities of the C=O stretching band detected at parallel and transverse directions to the incident FTIR beam source, respectively (see Figure 5.4a). Figure 5.4b showed that the thinner PLA 11 fibre exhibited higher transverse absorbance intensity (dotted line) compared to the parallel absorbance intensity (solid line) for the same fibre, the same profile was also observed for PLA 20 with almost similar profiles seen for PLA 29. However, for the thicker PLA 38 fibre, the parallel absorbance intensity was found to be higher. The higher spectral intensity of PLA 11 fibre at 1751 cm^{-1} (associated with the C=O stretching vibration) at the transverse direction suggested a higher degree of alignment of the PLA chain backbone compared to the parallel direction of the fibre as can be seen in Figure 5.5.
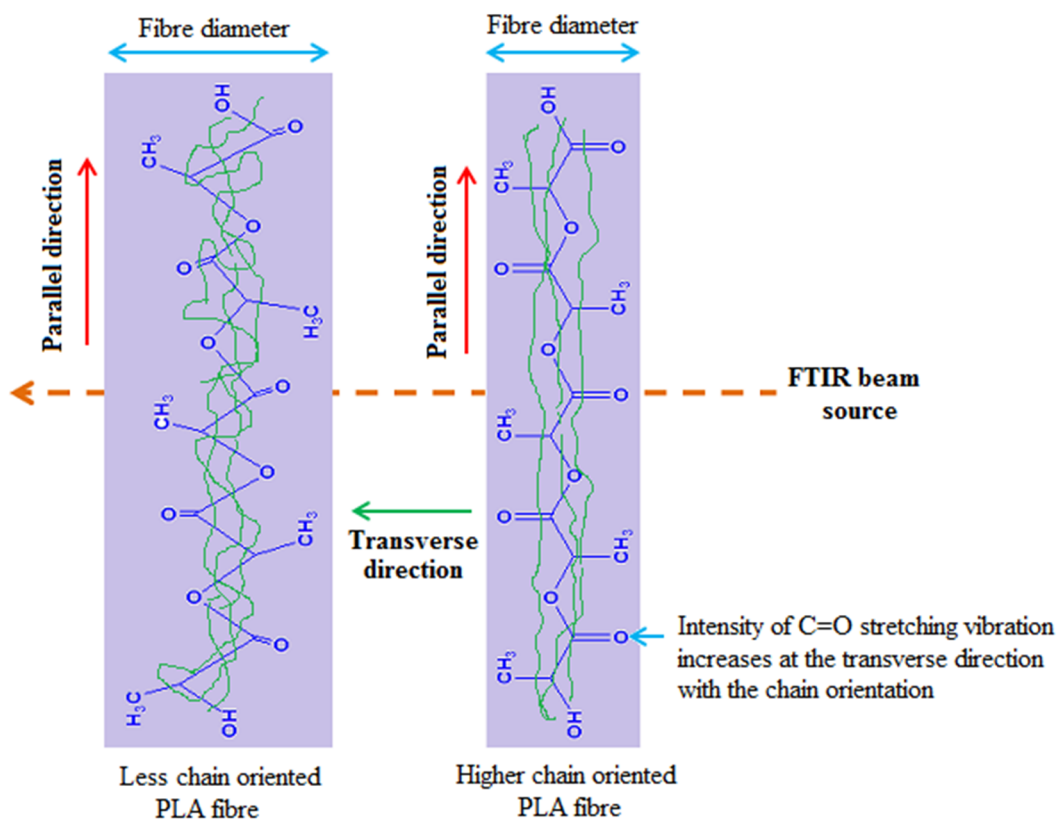
Figure 5.5: *Representative structure of PLA fibres show the chain orientation (C=O stretching vibration at the transverse direction of the fibre) due to the change in fibre diameter during melt drawing process at various take-up velocities.*

The calculated inverse dichroic ratio (1/D) of the C=O stretching vibration of the PLA fibres were seen to decrease with increasing fibre diameter (Figure 5.6). This suggested that the thicker PLA 38 fibres with lowest 1/D value exhibited less chain orientation along the transverse direction of fibre as seen by the representative drawing presented in Figure 5.4a, whilst the thinner PLA 11 fibre revealed the highest 1/D value indicated by the higher chain orientation which was probably induced during the melt-drawing process at the higher take-up velocity [83, 276]
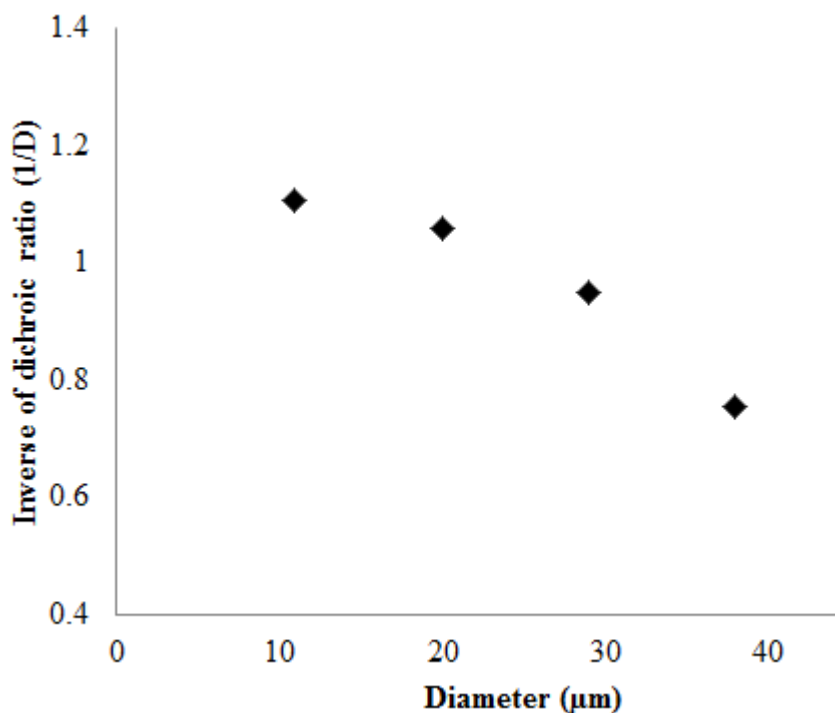
Figure 5.6: *Relationship between the inverse dichroic ratio (1/D value) of the C=O*

stretching band at 1751 cm^{-1}against PLA fibre diameter.

5.4.3 Thermal and crystallisation properties

Figure 5.7 presents the DSC thermograms of PLA fibres with varying diameters

obtained via the melt-drawing process.
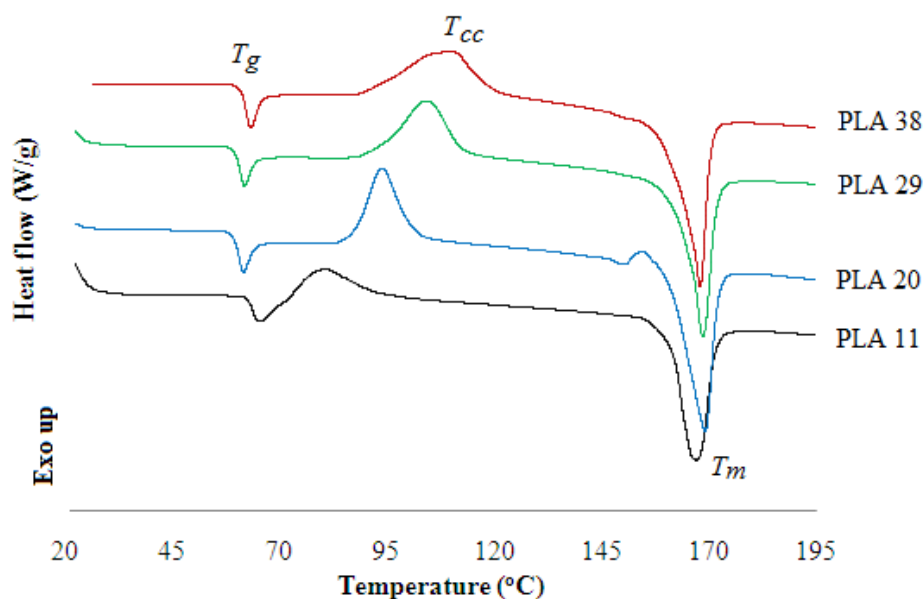
Figure 5.7: *DSC thermogram of PLA fibres with varying diameters.*

The glass transition (T_g) of the PLA fibres with varying diameters were observed to be in the range of 61 to 64°C, which correlated well with literature values [78, 79, 81, 278]. However, a higher T_g was observed for PLA 11 fibre (*P*<0.05) compared to the larger diameter fibres, with only insignificant changes in T_g (*P*>0.05) observed for PLA 20, PLA 29 and PLA 38 fibres. In addition, the cold-crystallisation exothermic peak (T_{cc}) occurred immediately above the T_g for PLA 11 fibres at 80°C, which was approximately 30°C lower than that of the thicker PLA 38 fibre. This suggested a higher degree of chain orientation in the amorphous domains of the polymer due to smaller fibre diameters obtained during the drawing process [81]. The melting temperatures of all the PLA fibres investigated were seen to be in close proximity of each other (i.e. in the region of between 166 to 169°C).
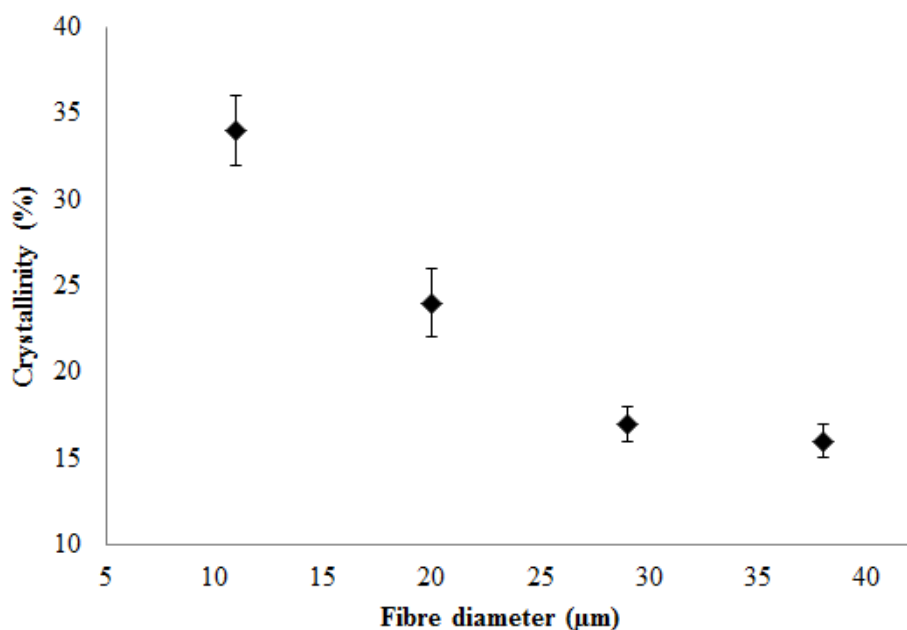
Figure 5.8: *Relationship between the crystallinity and PLA fibre diameter.*

The crystallinity of the PLA fibres was investigated from the thermograms and their relationship with varying fibre diameter is presented in Figure 5.8. An increase in the fibre diameter exhibited a significant decrease in the crystallinity index ($P<0.05$). The higher degree of crystallinity of PLA 11 (34% crystalline) when compared to PLA 38 (18% crystalline) also correlated well with the increasing chain orientation factor for the fibre with a lower diameter which was also in agreement with the dichroic ratio results discussed previously.

5.4.4 Mechanical properties

The stress–strain curves of the melt drawn PLA fibres as a function of fibre diameter are presented in Figure 5.9, where the inset Figure shows the strain region up to 5% strain and an increase in yield stress is seen with deceasing fibre diameter.
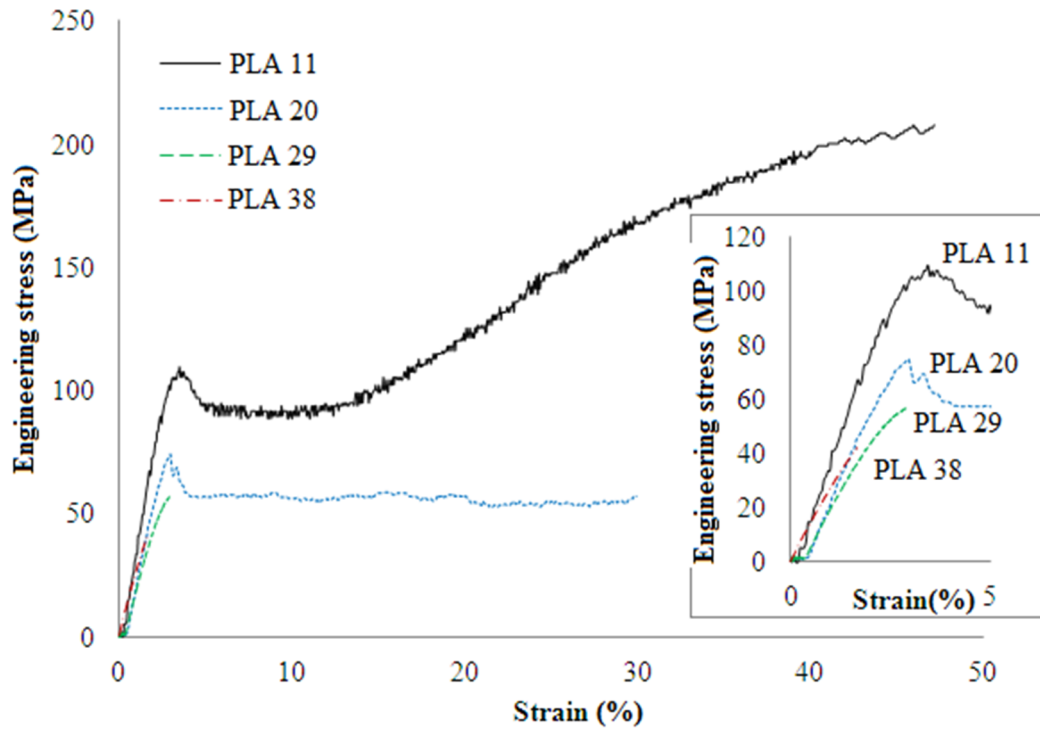
Figure 5.9: *Typical stress-strain curves for single PLA fibres with varying diameters.*

The inset figure shows the initial stage (up to 5% strain) of the stress-strain curves.

It is also evident from the stress-strain curves that the PLA 11 and PLA 20 fibres revealed ductile characteristics with sufficient flexibility compared to the larger diameter fibres which expressed a more brittle failure mechanism. However, this was unexpected, as the less oriented PLA fibres showed more brittle failure mechanism compared to highly orientated fibres. This could be due to the possibility of increasing number of defective chain created within the larger diameter fibres which promoted the immature failure during the tensile testing.

The tensile properties of PLA fibres were seen to decrease with increasing fibre diameter as presented in Figure 5.10. The tensile strength and modulus properties for PLA 11 were 213 MPa and 4.8 GPa, respectively. However, comparatively

higher tensile strength properties have been reported in the literature for PLLA fibres. For example, the tensile strength and modulus of PLLA fibre with diameter ranges from 11 to 14 µm were reported to be 320 MPa and 5.5 GPa, respectively [81].
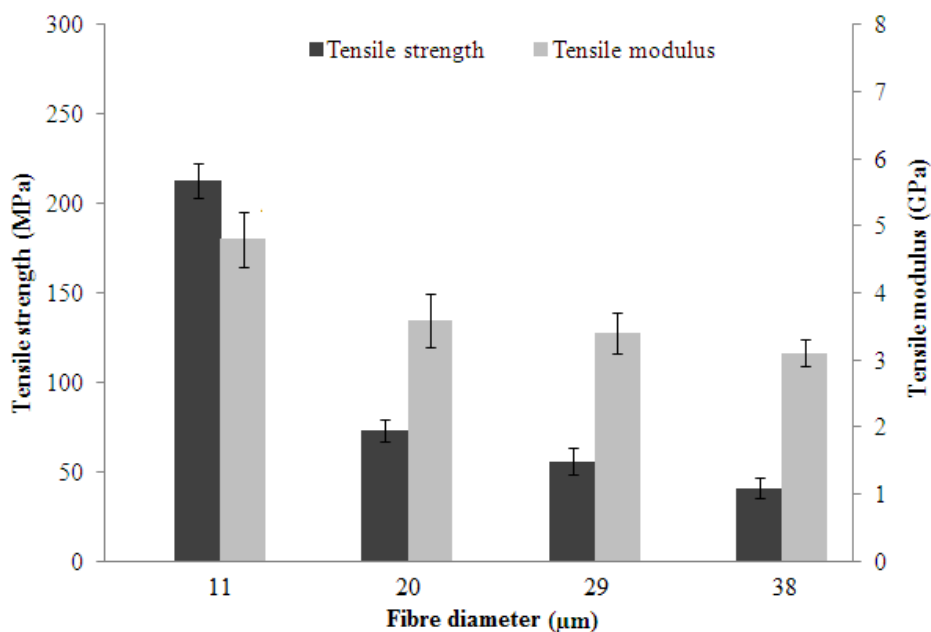
Figure 5.10: *Tensile strength and modulus properties of the single PLA fibres with varying diameters.*

PLLA is made of pure L-lactide which possesses a higher degree of crystallinity [265], which could explain the higher mechanical properties obtained for PLLA fibres compared to the PLA (Natureworks–3251D) polymer investigated in this study. As expected, PLA 11 fibre displayed a statistically significant increase (P<0.05) in tensile strength and modulus properties when compared to larger diameter PLA fibres (20 to 38 µm), since tensile properties are a function of crystallinity and molecular chain orientation of the matrix relative to the fibre axis [81]. To support this statement the tensile properties of the PLA fibres were

plotted as a function of crystallinity (see Figure 5.11) where a sharp increase in tensile strength and a steady rise in modulus properties with increasing crystallinity of the PLA fibres were observed. For instance, 34% crystallinity in PLA 11 fibre exhibited around 419% and 55% increase in tensile strength and modulus properties compared to the thicker PLA 38 fibre (18% crystalline). Similar increase in mechanical properties of nanocomposites was also observed due to the increasing crystallinity of the films, where highly crystalline cellulose nanowhiskers (~89% crystallinity) acted as a crystal nucleating agent within the matrix, which was discussed in Section 3.4.7 (Chapter 3) and Section 4.4.6 (Chapter 4).
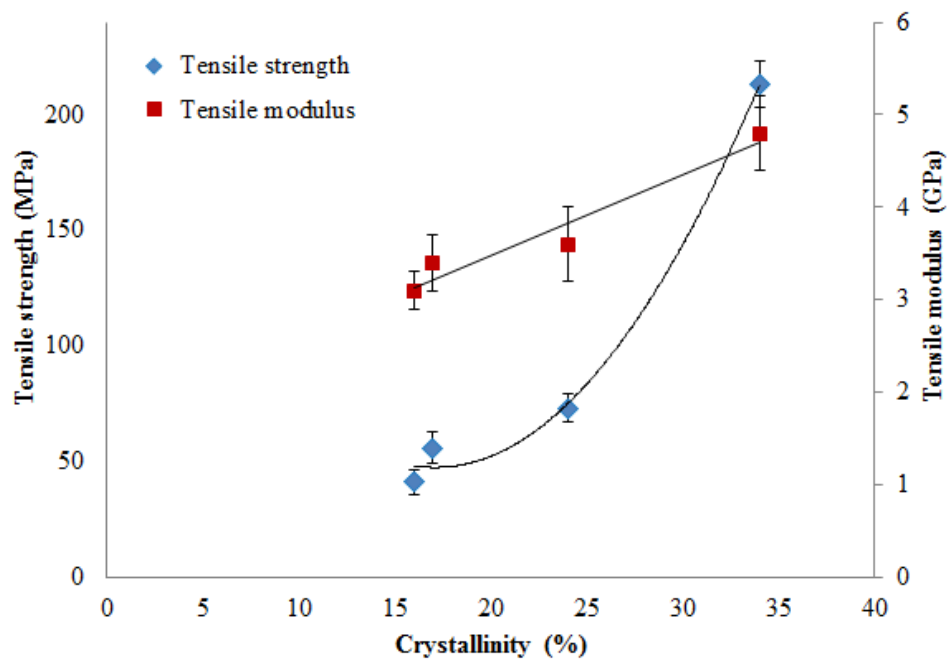
Figure 5.11: *Relationship between the tensile properties and degree of crystallinity of PLA fibres (lines were used as a guide for the eye).*

Figure 5.12 represents the elongation at break properties of the PLA fibres, where a significant reduction in elongation properties ($P<0.05$) was clearly observed upon increasing the fibre diameter when compared to the thinner PLA 11 fibre.

For example, PLA 11 fibre exhibited around 54% elongation while the larger diameter PLA 20, PLA 29 and PLA 38 fibres revealed approximately 37%, 3% and 1% elongation at break properties. The higher elongation property in PLA 11 fibre was attributed to be due to the introduction of molecular chain orientation into the thinner PLA fibre during fibre processing as highlighted above, which caused a substantial increase in the ductility of these fibres [279, 280].
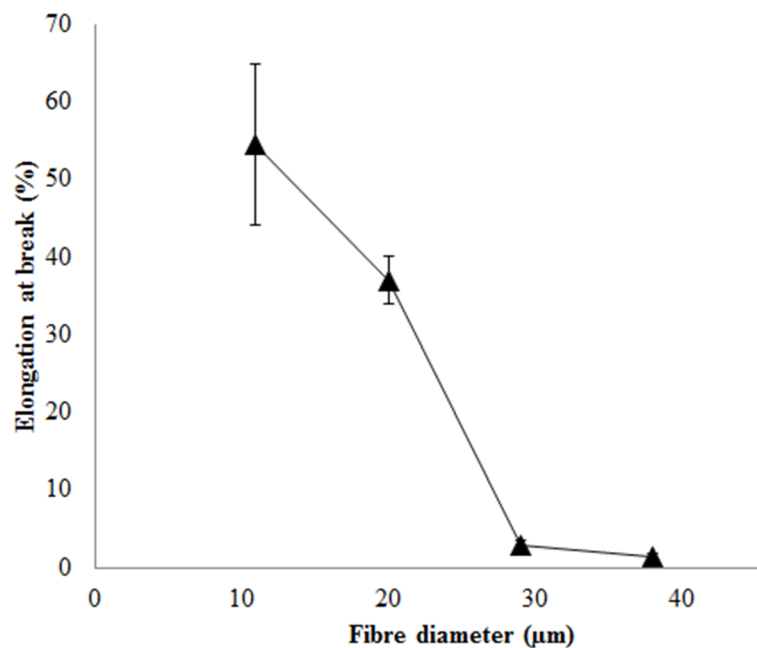
Figure 5.12: *Elongation at break properties for the single PLA fibres with varying diameters.*

Investigation into the variation of mechanical properties of the PLA fibres at body temperature (37°C) in comparison to room temperature (25°C) was also conducted, as these materials are mainly intended for use in the body as composites [86, 100, 281] and scaffolds [76, 270, 282]. Figure 5.13 shows the comparison of tensile properties of the PLA fibres at 25°C and 37°C. The values obtained revealed that the differences were not statistically significant (*P*>0.05)

for all diameter PLA fibres with the exception for the tensile strength property of PLA 11, where a significant decrease in tensile strength (29% reduction, *P<0.05*) was observed at 37°C. This was probably due to increasing chain mobility whilst approaching the flow deformation temperature of PLA (around 50°C) [84].
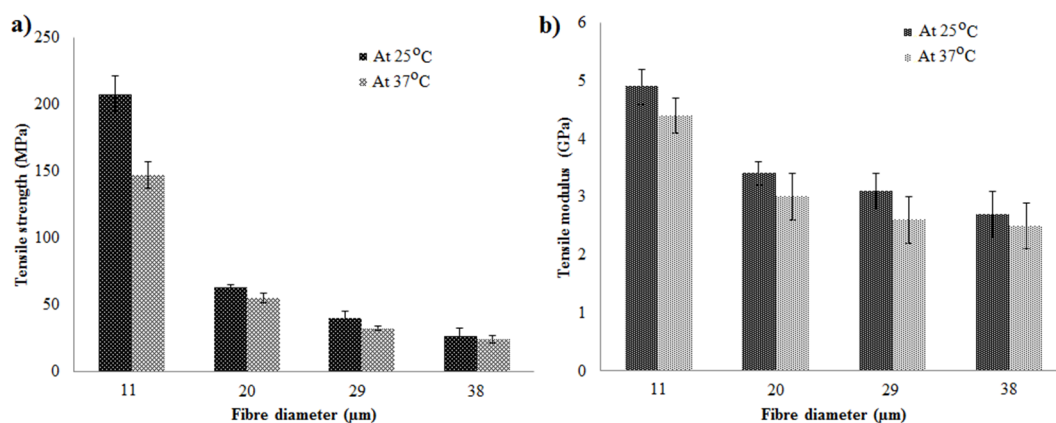
Figure 5.13: *a) Tensile strength and b) tensile modulus properties of the single PLA fibres measured at 25°C and 37°C via DMA analysis.*

5.4.5 Moisture absorption

The moisture absorption studies of the PLA fibres revealed an increasing trend when conditioned at increasing humidity levels (0, 35, 75 and 98% RH) for four weeks (as seen in Figure 5.14) [50]. During this period the PLA 38 fibres absorbed around 2.2 wt% moisture from the higher humidity atmosphere (98% RH). Pegoretti *et al.* [283] investigated the water uptake of PLLA fibre (diameter 72 and 120 microns) and reported water uptake of around 2 wt% after 3 weeks immersion in Ringer lactate solution which is in well agreement with our result for the PLA 38 fibre.
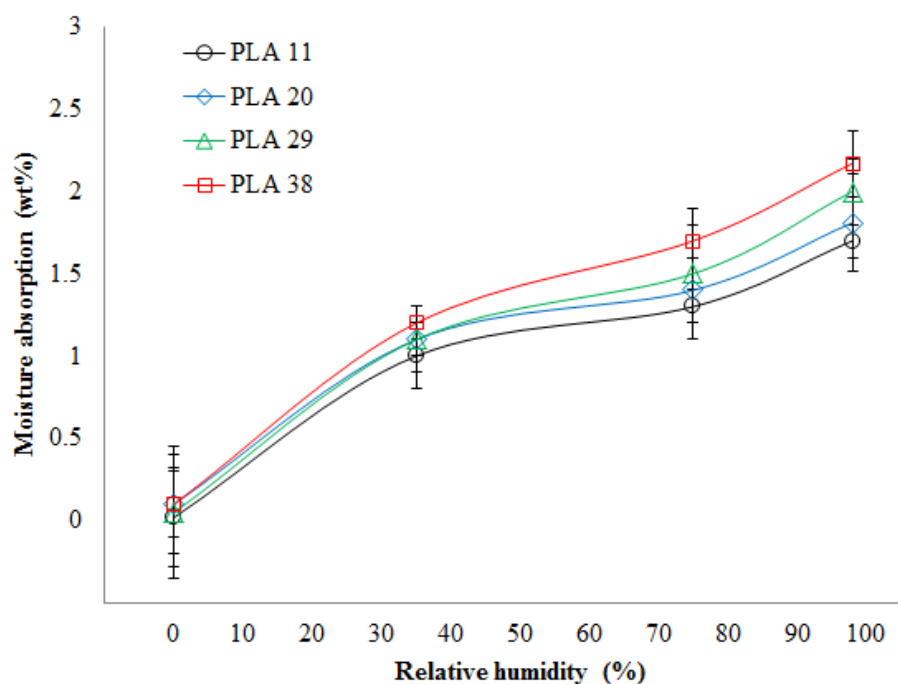
Figure 5.14: *Moisture absorption of PLA fibres with varying diameters as a*

function of relative humidity

The thicker PLA 38 fibre showed a significant increase ($P<0.05$) in their moisture absorption capacity at 98% RH compared to the thinner PLA 11 fibre (1.7 wt% moisture uptake). This moisture absorption property of the PLA fibres at varying humidity atmospheres could be attributed to the crystalline nature of the fibres. It is evident from Figure 5.15 that an increase in crystallinity of the thinner diameter PLA fibres exhibited a lower amount of moisture absorption prevalent at high humid condition, which suggested that the crystallite increased the tortuosity of the water vapour transport path within the matrix [284] and restricts the swelling capability of the PLA polymer.
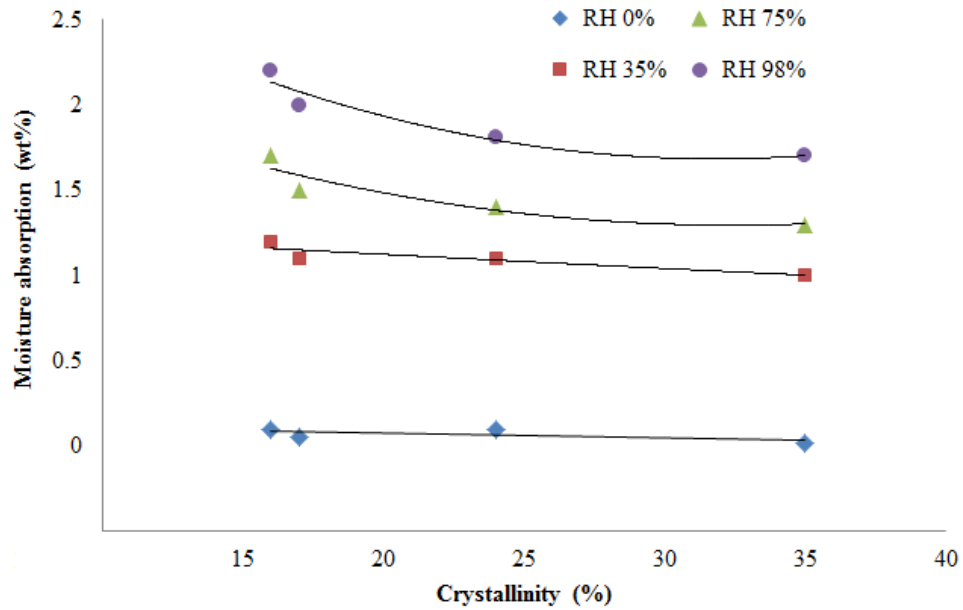
Figure 5.15: *Moisture absorption of fibres at alternate humid condition as a*

function of the crystallinity of PLA fibres.

Figure 5.16 shows the percentage moisture absorption of PLA fibres as a function

of time ($t^{\frac{1}{2}}$) at 98% relative humidity (RH). Rapid water uptake is observed for all

the fibres within the first 7 days of condition, followed by saturation.
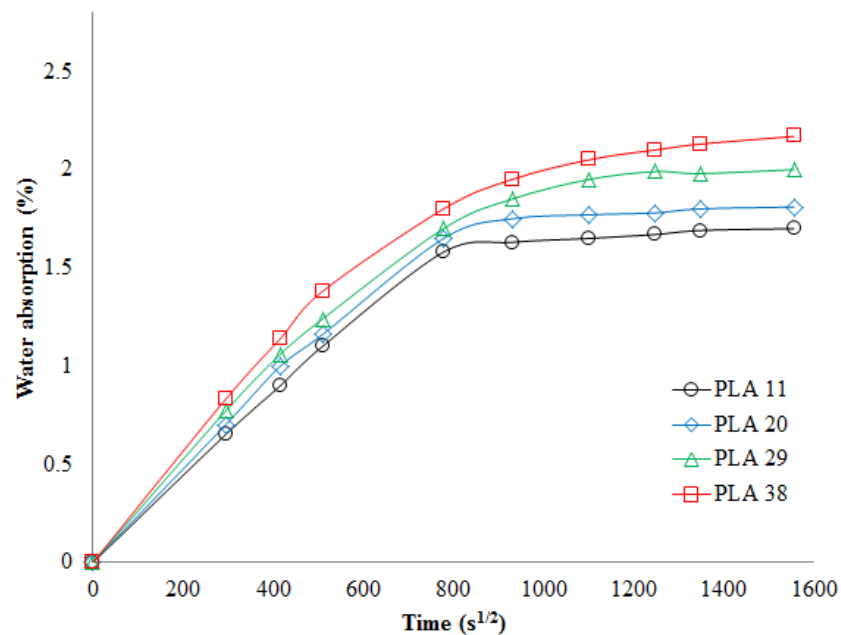
Figure 5.16: *Effect of PLA fibre diameters on moisture absorption at 98% RH.*

The water absorption of PLA fibres with varying diameters is related to the rate of diffusion. The diffusivity (*D*) of water into the fibre matrix exhibited an increasing trend with increasing fibre diameter (presented by black circles) as seen in Figure 5.17. This was also suggested to be due to the crystalline properties of the PLA fibres as the higher crystallinity in the thinner diameter fibres could provide a higher barrier to diffusion which is also presented in Figure 5.17. Drieskens *et al.* [284] investigated the effect of crystallinity of PLA on the gas and water vapour barrier properties and suggested that the vapour transport behaviour of a semi crystalline polymer were positively influenced by the presence of amorphous regions while the crystallite regions increased the tortuosity of the vapour transport path within the matrix.
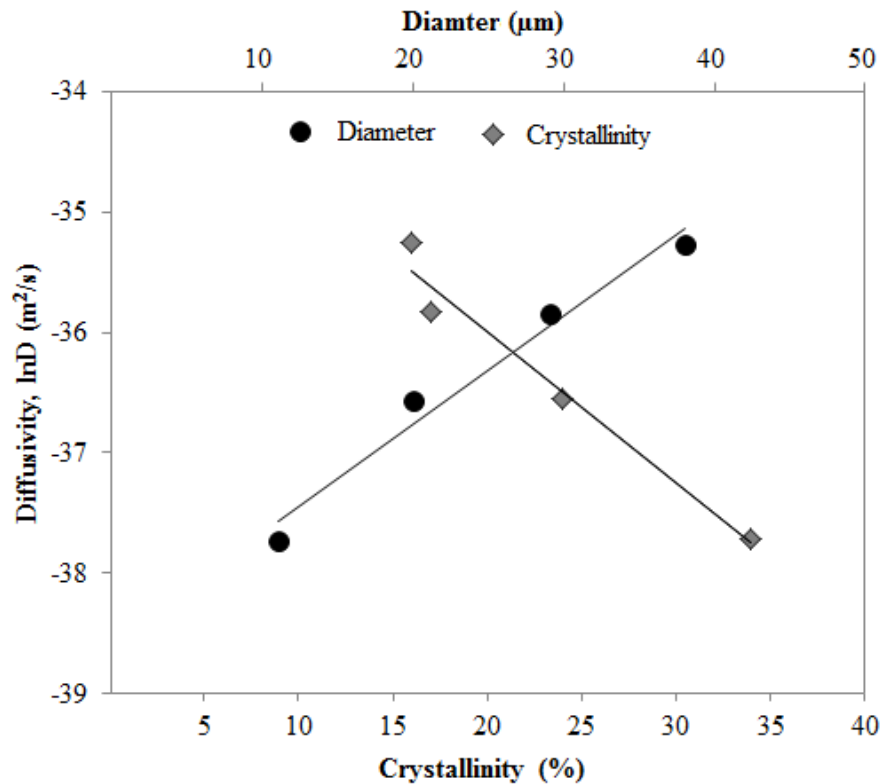
Figure 5.17: *The relationship between the diffusivity of moisture into PLA fibres*

after conditioning at 98% RH for four weeks with varying diameters and

crystallinity.

The effect of moisture absorption on fibre mechanical properties is presented in

Figure 5.18 where the thicker PLA 38 fibres did not reveal a significant change in

their tensile properties after the conditioning period at increasing humidity.

Similar to this, PLA 20 and PLA 29 fibres also exhibited an insignificant decrease in

tensile strength ($P>0.05$) when conditioned at various RH levels. However, their

tensile moduli did reveal a decrease by 17% and 12% ($P<0.05$) for PLA 20 and PLA

29 fibres when compared the 0% RH conditioned fibres.
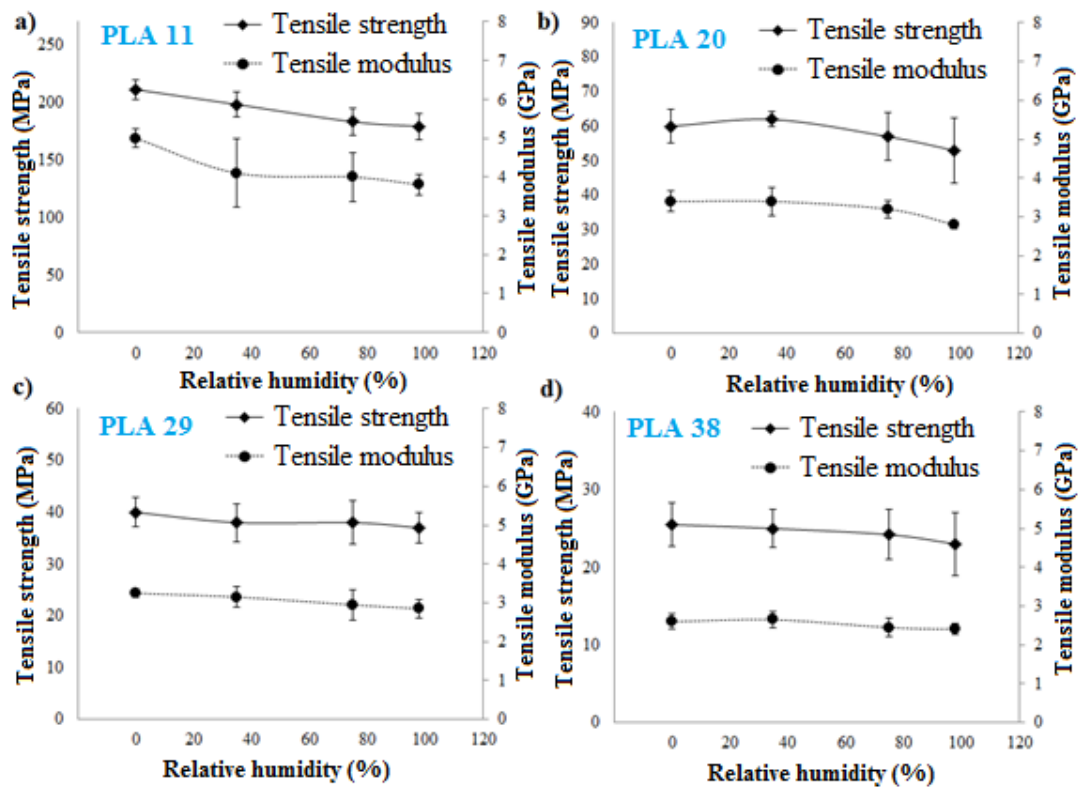
Figure 5.18: *Tensile strength and modulus properties of PLA fibres after conditioning at varying relative humidity levels: **a)** PLA 11, **b)** PLA 20, **c)** PLA 29, and **d)** PLA 38 fibres*

In addition, the moisture content in the thinner PLA fibres also induced a decrease in their mechanical properties. For instance, PLA 11 fibres showed a statistically significant decrease ($P<0.05$) in tensile strength and modulus of 15% and 24% when exposed to 98% RH compared to the fibres conditioned at 0% RH. This was attributed to the moisture effect on the thinner fibres due to their higher surface area to unit mass ratio [283]. In addition, water molecule penetrated the polymer could result plasticization and thus disrupted the some parts of crystal structure, where hydrogen bonds were not too strong and tight.

This study showed improvement of the thermal, crystallisation and mechanical properties of semi crystalline PLA fibres with average diameter ranges from 11 to

38 microns obtained via a gravity induced melt drawing process at 180°C. Conferring control over the fibre properties can be very useful depending on their end application, for example, as *in vivo* scaffolds and for use within self-reinforced composite fabrications.

5.5 CONCLUSIONS

PLA fibres with an average diameter ranging from 11 to 38 µm were successfully produced via the melt drawing process with varying take-up velocities. The higher drawing speed revealed a significant improvement on the chain orientation in the thinner PLA fibres which revealed a lower cold crystallisation temperature and a higher degree of crystallinity up to 34% resulting in higher tensile properties. The thinner PLA fibres, when tested at 37°C, showed a significant decrease in tensile strength compared to the room temperature values due to a reduction in crystallinity whilst approaching the flow deformation temperature of PLA. The moisture absorption of all the PLA fibres revealed a steady increase with increasing relative humidity. When comparing fibres with varying diameters, the thinner PLA fibres showed a gradual decrease in moisture absorption capacity at 98% humid atmosphere due to increased crystallinity reducing the fibre swelling capability. The thicker PLA fibres did not exhibit any concomitant changes on their tensile properties during the four weeks conditioning period. However, the accumulated moisture within the thinner fibres showed a significant decrease in tensile properties when exposed to 98% RH after four weeks of conditioning. Though this study demonstrated the thinnest PLA fibres revealed a significant decrease in tensile properties when they were exposed to either body

temperature or at high humidity atmosphere, the mechanical properties obtained were higher than the unconditioned larger diameter PLA fibres. This could potentially enable the use of these PLA fibres within biomedical and tissue engineering applications.

CHAPTER 6.

EFFECT OF CELLULOSE NANOWHISKERS ON SURFACE MORPHOLOGY AND MECHANICAL PROPERTIES OF MELT DRAWN POLYLACTIC ACID FIBRES

6.1 SUMMARY

Polylactic acid (PLA) fibres were produced with an average diameter of 11 (±0.9) μm by a melt-drawing process at 400 m min^{-1} rotation speed. The hydrophobic surface of the PLA fibres was coated with various blends of cotton-extracted cellulose nanowhiskers (CNWs) (65 to 95 wt%) and polyvinyl acetate (PVAc), where PVAc acted as a binder. Scanning electron microscopy (SEM) images revealed that CNWs bound to the smooth surface of PLA fibres incorporated roughness, with the degree of roughness depending on the coating blend used. This was further confirmed by fluorescence labelling of the coated fibres at the surface. The mechanical properties from tensile testing of individual fibres revealed the surface coating of PLA fibres displayed a 4% and 45% increase respectively in tensile strength and modulus at room temperature, compared to the uncoated PLA fibres believed to be due to the formation of CNW-PVAc and CNW-CNW percolating films on PLA fibre surface. The moisture absorption properties of the coated and uncoated PLA fibres were further investigated at various relative humidities (0%, 35%, 75% and 98% relative humidity) and attachment of CNWs on PLA fibre surface utilising PVAc showed a significant

influence to increase their moisture absorption properties at higher humidity conditions.

6.2 INTRODUCTION

The transformation of PLA into mono and multifilament can be achieved by melt, dry, wet, dry-jet-wet and electrospinning processes, each resulting in distinct fibre properties [74, 75, 79, 285-293]. Melt spinning provides some advantages over wet spinning techniques as it is a solvent-free process and thus more eco-friendly. The surface of PLA possesses too poor a hydrophilicity to support appropriate cell adhesion, resulting in inadequate biological activity [294, 295]. In order to improve PLA for tissue engineering and biomedical applications, its surface morphology needs modification and as a result PLA has been functionalised via graft or copolymerisation with other biopolymers [296], chemical treatment [297], plasma treatment [71], and adsorption [298] of suitable biocompatible materials, including chitosan [26], biotin [299], collagen [297, 300], gelatine [297, 301], and alginate [29].

Cellulose in the form of nanowhiskers has been extensively used with different types of biopolymers, such as, PLA [52, 63, 132, 166, 172, 199, 200, 222], PCL [19, 202, 242], PVA [244-246] and PVAc [50] due to its biodegradability [11, 12, 186], biocompatibility in composites [188] and superior mechanical properties (tensile modulus~ 105 GPa for cotton based nanocellulose) [54]. Incorporation of CNWs in PLA matrices to form composites has already shown significant improvement of their thermal and mechanical properties. John *et al.* [302] investigated PLA based

nanocomposite fibres (with diameters ranging 90-95 µm) incorporating CNWs produced via a melt spinning process using a twin screw extruder. They reported an increase in the surface roughness properties for fibres containing CNWs; however, no significant change in their mechanical properties was reported. The influence of CNWs on the thermal behaviour for electrospun PLA fibres (average diameter~ 300 nm) was investigated by Liu *et al.* [77], who showed that the CNWs reportedly acted as a heterogenous nucleating site to reduce the cold crystallisation onset temperature from $69^{o}C$ to $65^{o}C$ in nanocomposites containing 2.5 wt% CNWs when compared to the unfilled PLA nanofibre. They also suggested that the nanocomposite fibre investigated would improve the mechanical properties compared to the PLA fibre, however no mechanical test data were reported.

The PLA fibres investigated in this chapter were manufactured using a melt drawn process and CNWs were obtained from cotton via an acid hydrolysis process. The aim of this study was to improve the surface of hydrophobic PLA fibres via coating with varying blends of CNWs and PVAc in order to create a roughened and more hydrophilic surface. The morphological, thermal, mechanical and moisture absorption (at various humidity levels) properties of CNW/PVAc coated PLA fibres are reported in this chapter.

6.3 MATERIALS AND METHODOLOGY

6.3.1 PLA fibres drawing

As described in Section 5.3.1.

6.3.2 Preparation of CNWs

As described in Section 3.3.2.

6.3.3 PLA fibre coating

The coating materials were produced by blending different ratio of CNWs and polyvinyl acetate (PVAc) (formulation composition in Table 6.1) maintaining 2 w/v% suspension in deionised (DI) water.

Table 6.1: *Formulations of coating materials prepared using CNWs and PVAc for PLA fibres.*

Sample **codes** used in this study	Coating materials	
	CNWs (wt%)	PVAc (wt%)
PLA	-	-
PLA PVAc	-	100
PLA CNWs-65	65	35
PLA CNWs-75	75	25
PLA CNWs-85	85	15
PLA CNWs-95	95	5

PVAc was obtained as Kollicoat SR, a 30% dispersion of PVAc stabilised with polyvinylpyrrolidone and sodium lauryl sulphate, density 1.04 g cm^{-3}. The PLA fibres were coated using a syringe needle containing the coating suspension and running the syringe tip over the fibre 5 times followed by drying of the coated

fibres in an oven at 37°C for 24h to ensure deposition of materials on the surface of the fibre.

6.3.4 Characterisation

6.3.4.1 Electron microscopic analysis

The surface morphology of the coated and uncoated PLA fibres were characterised using SEM and the shape of the CNWs were examined using TEM according to the procedure mentioned previously in Section 3.3.4.1.

6.3.4.2 Fluorescence microscopic analysis

Coated and uncoated PLA fibres were fluorescently labelled with rhodamine B (Sigma Aldrich, UK) using a syringe needle. Drops of this aqueous dye solution (125 mg in 50 mL distilled water) were applied to the fibres 3 times and allowed to dry at room temperature. A fluorescence microscope (Leica DMLB) was employed to image the surface of the rhodamine B labelled fibres (as described in Section 4.3.4.2).

6.3.4.3 Optical microscopic analysis

Fibre diameters were measured using a calibrated optical microscope (as mentioned previously in Section 5.3.3) and an average fibre diameter was calculated from the measurement of at least 35 random fibres.

6.3.4.4 Surface roughness determination

PVAc and CNWs-PVAc blends were coated on the solvent cast (Chloroform) PLA films (Thickness around 0.3 mm) and their surface roughness was analysed according to the procedure mentioned previously in Section 4.3.4.3. The average

roughness (Ra) was determined by measuring at 35 different positions of the films.

6.3.4.5 FTIR-ATR analysis

As described in Section 3.4.3.

6.3.4.6 Differential scanning calorimetric (DSC) analysis

As described in Section 3.3.4.7. At least three tests were carried out for each material to ensure repeatability.

6.3.4.7 Tensile tests

As described in Section 5.3.7. A minimum of six repeat tests were conducted.

6.3.4.8 Fibre conditioning and moisture absorption

As described in Section 5.3.8.

6.4 RESULTS AND DISCUSSION

In this study PVAC/CNW blends with varying amounts of CNWs were used to coat the hydrophobic surface of PLA fibres. The nano-scale dimensions, hydrophilic nature and high mechanical properties of CNWs could potentially be used to improve the surface characteristics, as well as mechanical and moisture absorption properties of hydrophobic polymers through a simple post-drawing coating step as is common in reinforcing fibre manufacturing. For example, use of CNWs could create a rougher and more hydrophilic surface when compared to non-coated PLA fibres which could help to promote adequate cell attachment for tissue engineering applications and provide mechanical interlocking when used as reinforcement in composite materials.

6.4.1 Morphological properties

The surface topography of PLA fibres produced via a melt drawn process (at 180°C, 400 m min^{-1} rotation speed and 1m diameter drum roll) exhibited smooth surfaces with fairly uniform diameters as seen in Figure 6.1a. The TEM image of the CNWs produced (presented in Figure 6.1b) revealed the expected rod-like particles [303].
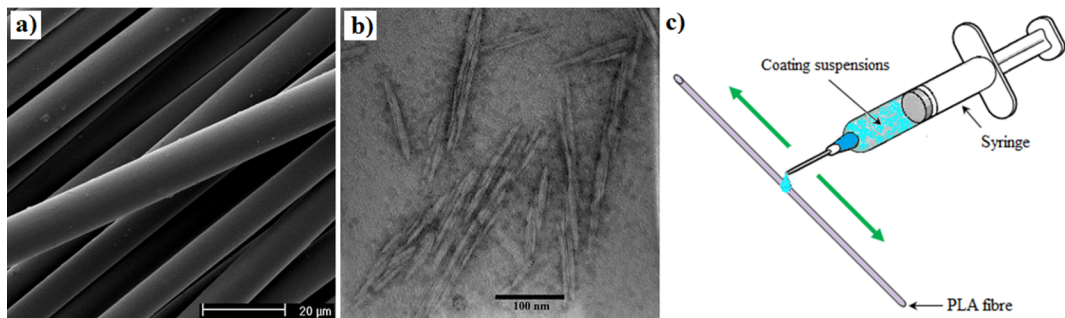
Figure 6.1: a) *Scanning electron microscopy image of PLA fibres obtained at 400 m min^{-1},* **b)** *TEM image of cellulose nanowhiskers (CNWs), and* **c)** *schematic of the coating procedure employed on the PLA fibre surface.*

Figure 6.1c represents a schematic of the coating method employed to apply the coating materials (with varying ratio of CNWs and PVAc) onto the surface of the PLA fibres using a syringe needle containing the coating suspensions.

The morphology of PVAc and CNWs-PVAc coated PLA fibres (seen in Figure 6.2) showed that the deposition process resulted in a textured surface on the fibres compared to a smooth surface for the uncoated PLA fibres. Furthermore, the increased roughness was observed for the nanowhisker coated PLA fibres with a relatively uniform distribution for PLA CNW-65, PLA CNW-75 and PLA CNW-85. The PLA CNW-95 fibres (Figure 6.2f) revealed uneven attachment of CNWs on the

fibre surface believed to be due to the insufficient amount of PVAc binder present in the coating materials to provide a homogeneous coverage, leading to CNW clustering. The control coating using only PVAc showed that good spreading of the PLA fibre surface can be achieved during application as it formed a uniform coating (Figure 6.2b).
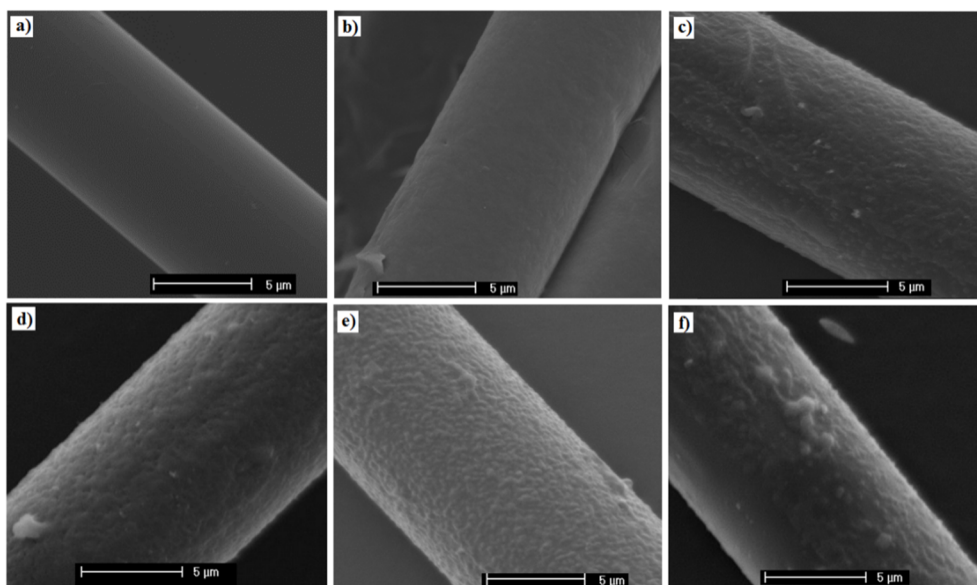
Figure 6.2: *SEM images of **a)** non coated, **b)** PLA PVAc, **c)** PLA CNW-65, **d)** PLA CNW-75, **e)** PLA CNW-85, and **f)** PLA CNW-95 fibres.*

The surface morphology of the coated and uncoated PLA fibres was further characterised via fluorescence microscopy using rhodamine B to label the fibre surfaces. Similar to the SEM images, a relatively smooth surface could be seen for the fluorescently labelled PLA fibres (Figure 6.3a), though the fluorescence intensity of the image was quite low compared to that for the coated fibres (better adsorption of rhodamine to PVAc and the PVAc/CNW blend than to PLA). The homogeneous coverage of the PVAc coating on the PLA fibre surface was also observed as can be seen in Figure 6.3b, which also indicates good binding

between the fluorescent rhodamine B probe and the PVAc coating. Figure 6.3c-f revealed that the CNW-PVAc coated fibres had a much rougher surface morphology with reduced homogeneity of the coating observed with increasing CNW content (observed via the darker areas) on the fibres which could be due to reduced wetting of the PLA fibre surface by blends with increasing CNW content. Increasing viscosity of the PVAc/CNW compared to pure PVAc and formation of inter-CNW hydrogen bonds resulting in percolated networks may well be the reason of this reduced spreading, thus leading to clusters and increased surface roughness.
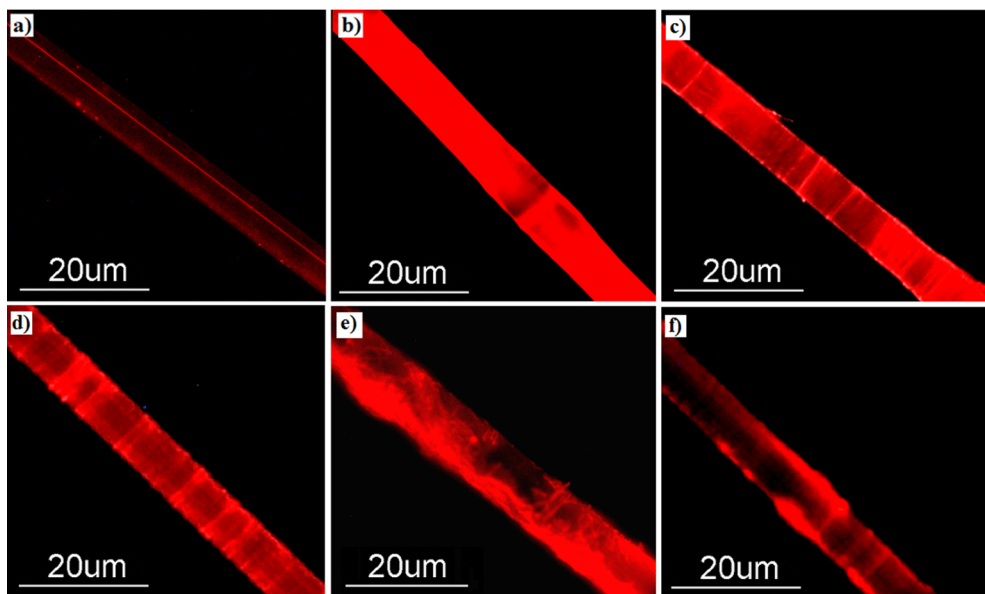
Figure 6.3: *Fluorescence images of rhodamine B labelled **a)** non coated, **b)** PLA PVAc, **c)** PLA CNW-65, **d)** PLA CNW-75, **e)** PLA CNW-85, and **f)** PLA CNW-95 fibres.*

The diameters of the coated and uncoated PLA fibres were measured via optical microscopy and an average diameter of 11 (±0.9) μm was obtained for PLA fibres (measured from at least 35 fibres, see Figure 6.4) produced in this study by melt drawing using a high speed drum [81]. The deposition of the coating materials on

the fibre surfaces resulted no significant change in average diameter compared to non-coated PLA fibres ($P > 0.05$). PLA CNWs-95 revealed an average diameter around 11.4 µm, which suggested that very little coating was retained onto the fibre surface. The low amount of PVAc thus appears to restrict the amount of CNWs that can be anchored to the PLA surface.
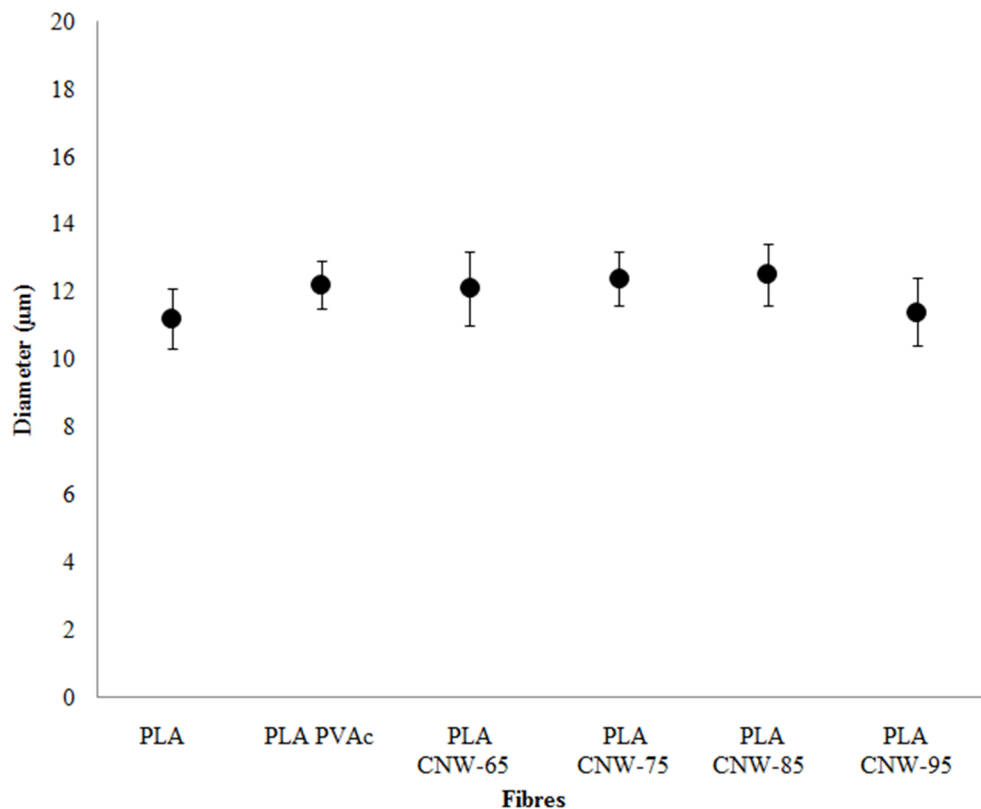
Figure 6.4: *Average diameter for coated and uncoated PLA fibres measured using optical microscope.*

6.4.2 Surface roughness

The average surface roughness (Ra) of the PLA, PLA PVAc and various ratios of CNWs-PVAc coated films are presented in Figure 6.5. The surface roughness imparted onto film produced were found to be consistent with the results obtained via SEM and fluorescence images of the single fibres, where the rod-like

nanowhiskers created increased roughness (Ra=3.0 µm and 2.8 µm for PLA CNWs-75 and PLA CNWs-85, respectively) compared to the non-coated PLA control (Ra=0.22 µm) and PVAc coated PLA films (Ra=0.19 µm).
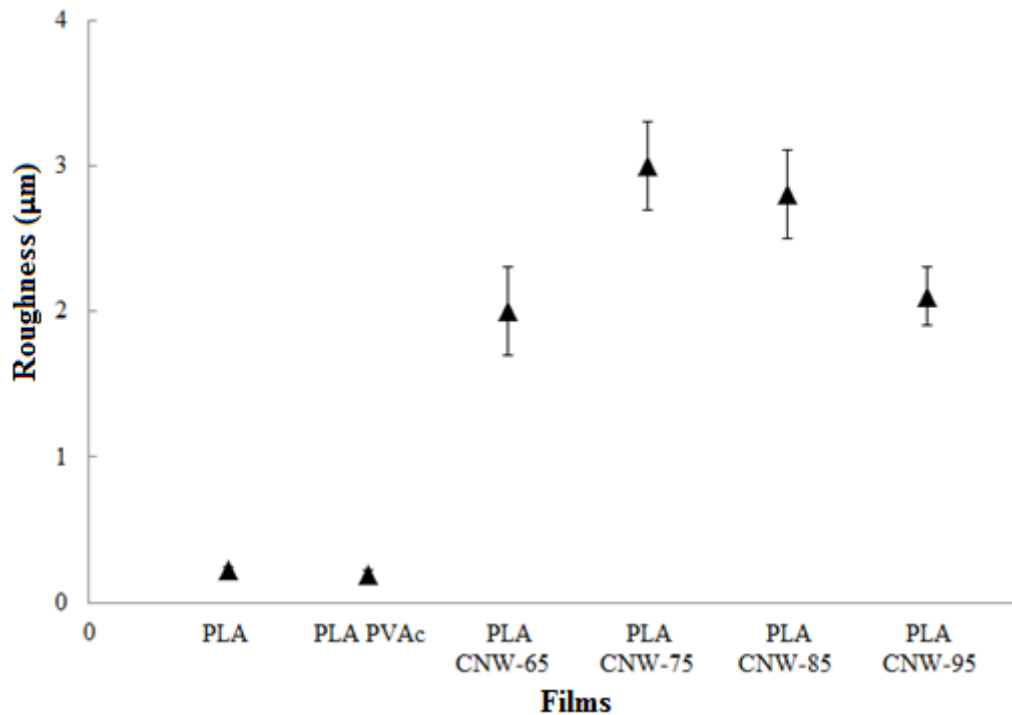
Figure 6.5: *Surface roughness of PLA films coated with PVAc and CNWs-PVAc blends.*

The greatest increase in surface roughness is observed for coating material containing 75 and 85 wt% CNWs. A similar surface roughness of approximately 3.0 µm was recently reported for high CNW content composites (75 wt% in a hydroxyethyl cellulose matrix) [303]. The roughness imparted on the surface of CNW-PVAc coated PLA may help to improve cell adhesion properties for tissue engineering applications; Khan *et al.* [304] investigated the influence of surface roughness via chemical etching on silicon based biomaterials and showed that roughness promoted cell adhesion and longevity. Similar improved cell adhesion,

growth and proliferation properties were also reported by Keshel *et al.* [305], where roughness had been created via plasma treatment on polyurethane films.

6.4.3 FTIR analysis

The deposition layer formed on the fibre surface was attributed to CNW-PVAc and CNW-CNW percolating interactions, where PVAc acts as a binding agent helping to attach the CNWs onto the surface of the fibres during the drying process. The functional groups of the PVAc and various ratios of CNW-PVAc coated and un-coated PLA fibres were identified using FTIR-ATR spectroscopy, as can be seen in Figure 6.6. The C=O groups of the non-coated and CNWs coated PLA fibres were observed at 1753 cm^{-1}, whilst the C=O of the acetate group present in the PVAc coated fibres had shifted to 1749 cm^{-1}. This was suggested to be due to the presence of the acetate group of the PVAc as it has been reported that the vibrational frequency for C=O of the acetate group of pure PVAc were observed at 1740 cm^{-1} [306]. For the PLA fibre, the bands at 1456 and 1375 cm^{-1} were attributed to CH$_3$ asymmetric stretching and CH$_3$ symmetric deformation, respectively. The bands at 1186, 1085 and 873 cm^{-1} indicated the –C-O-C asymmetric, symmetric and C-(C=O)O stretching, respectively for PLA. The bands attributed to C-H stretching and C–O vibrations of the acetate group of PVAc have a stretching mode at 1682 and 1234 cm^{-1}, respectively, however, these bands were not visible in the pure and CNWs coated PLA fibres. Moreover, the bands at 3373 and 3334 cm^{-1} observed for CNWs coated fibres were related to O-H stretching of pure CNWs [166, 252], which suggested the attachment of the cellulose nanowhiskers onto the PLA fibre surface.
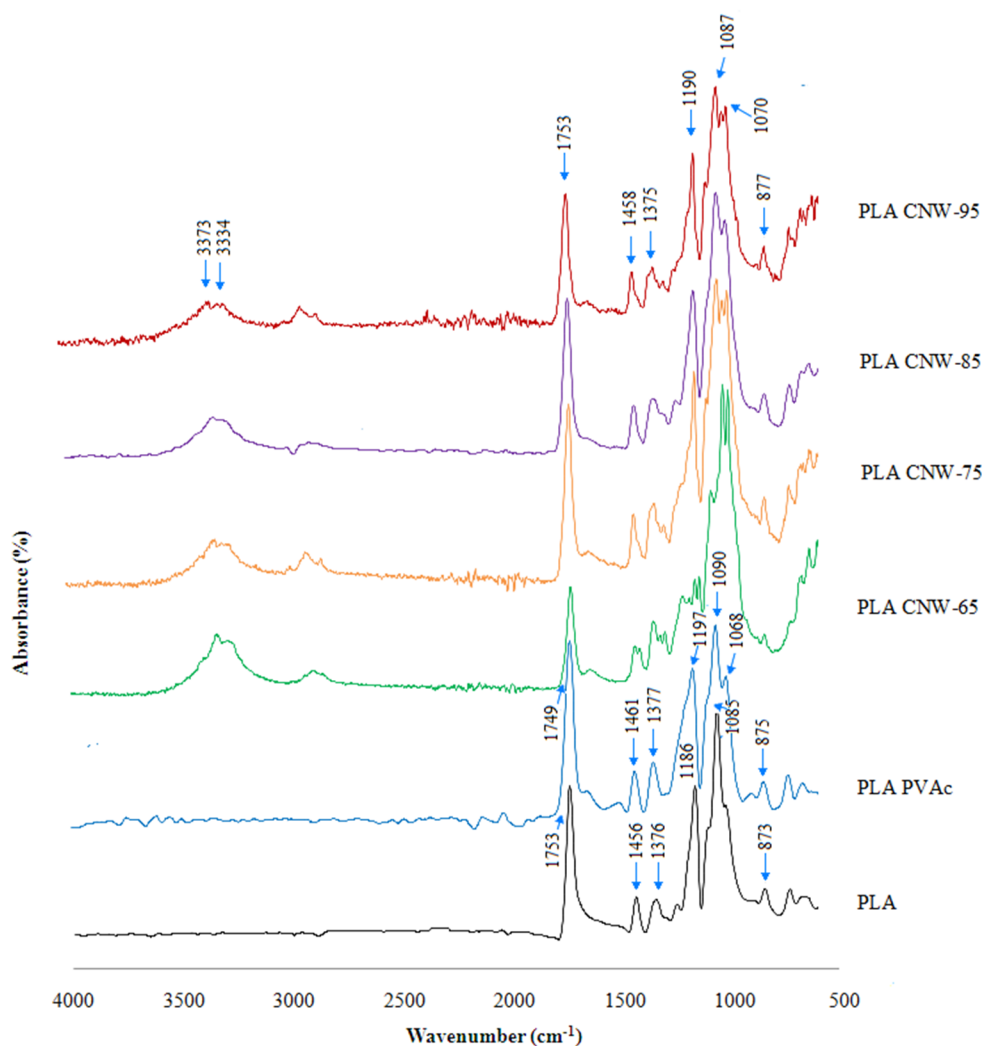
Figure 6.6: *FTIR-ATR spectrum for uncoated PLA and PVAc and CNWs-PVAc coated*

PLA fibres.

In addition the amount of coating substances on the PLA fibres were further analysed using the absorbance peak intensity of C=O group (at 1753 cm^{-1}) for the PLA and that of H-O-H group (at 3373 cm^{-1}) for the CNWs. It can be seen from the Figure 6.7 that the ratio of the peaks intensities increasing with the CNWs contents upto 85 wt%, which indicated that increasing amount of the CNWs attached on the fibre surface and further increase in CNWs reflects decreasing trend suggested the insufficient amount of coating substances on the fibre

surface. This is also well agreement with the change in fibre diameter and surface roughness results obtained for different amount of CNWs used in the coating blends.
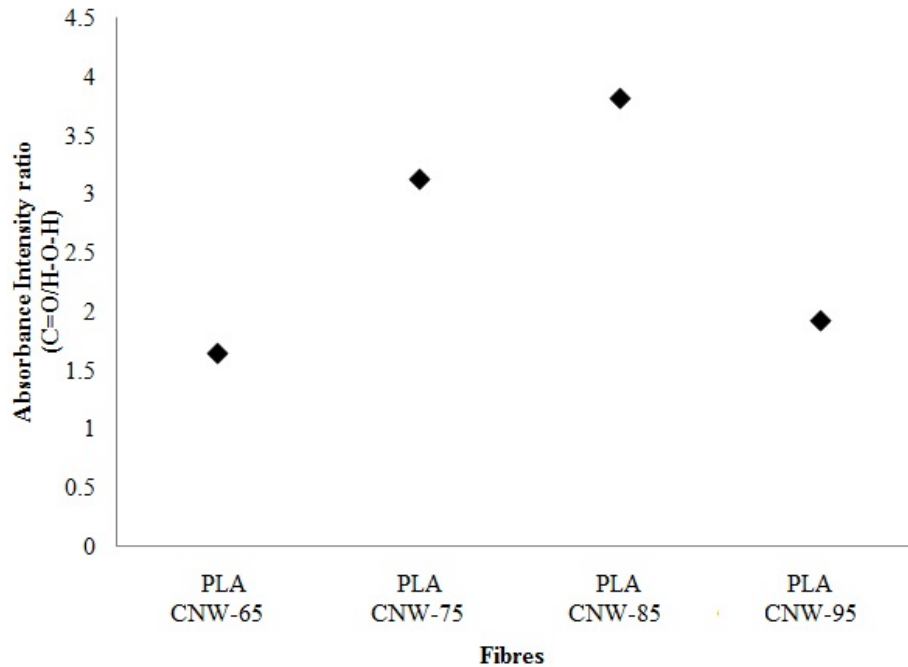
Figure 6.7: *FTIR-ATR absorbance intensity ratio of the C=O (of PLA) and H-O-H (of CNWs) of the CNWs-PVAc coated PLA fibres.*

6.4.4 Thermal properties

Figure 6.8 represents the DSC thermograms for the coated and uncoated PLA fibres. The T_g value at 63.6°C for the non-coated PLA fibres is in agreement with the literature values [78, 79, 81, 278] whereas attachment of PVAc onto the PLA surface resulted in a slight decrease of T_g to 62.6°C ($P>0.05$). On the other hand, when embedding CNWs in the coating, a significant change in the T_g values to the slightly higher values (around 65.3°C and $P<0.05$) were observed for PLA CNWs-75, PLA CNWs-85 and PLA CNWs-95. We believe this effect to be due to restriction of the polymer chain mobility along the interface caused by the hydrogen bonding

created between PLA fibre surface and the PVAC/CNW coating during the drying process similarly to findings by Keddie *et al.* [307] who reported a slight increase in the T_g of polymethyl methacrylate (PMMA) thin films covered with silicon oxide compared to the control PMMA thin film.
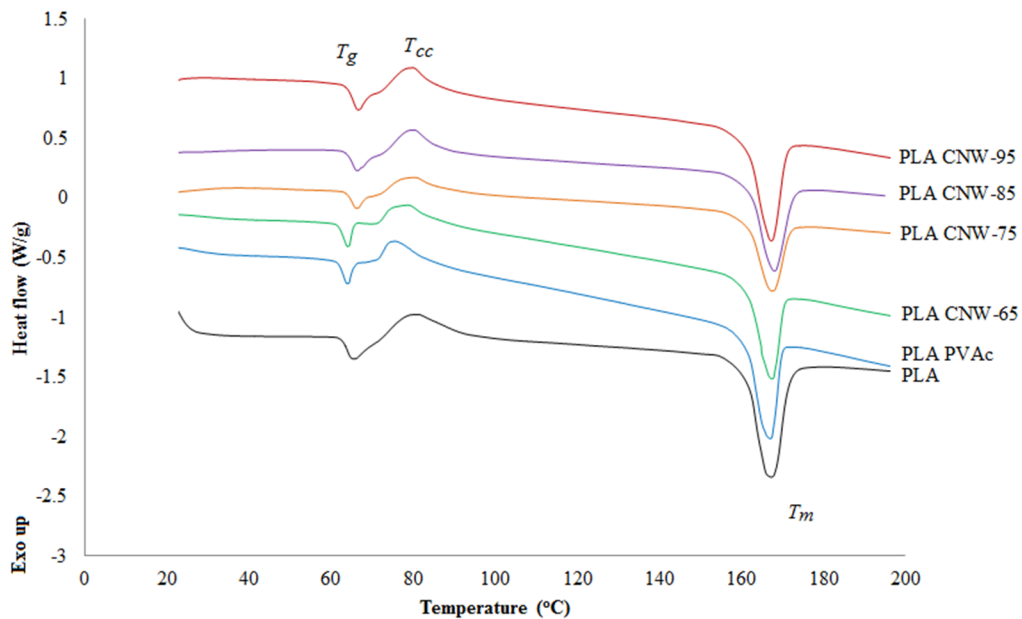
Figure 6.8: *DSC thermogram of uncoated and PVAc and CNWs-PVAc coated PLA fibres.*

The increase was only seen for coatings containing a high amount of CNWs as PLA CNWs-65 fibres revealed the glass transition temperature at around 62.8^{o}C, close to that of the PLA PVAc fibres. It does seem that the increase in T_g can be attributed to effects induced by the CNWs. The melting temperature (T_m) of all the coated and non-coated PLA fibres occurred at around 167°C. The cold crystallisation temperature (T_{cc}) of PVAc coated PLA fibres were noted to be at 75°C, approximately 5°C lower than that of the pure PLA fibre. However, T_{cc} for all the CNWs-PVAc coated PLA fibres were observed in the region of 78 to 80°C,

similar to pure PLA fibres, further indicating interactions of CNWs with PLA as the CNWs appear to offset the negative effect of PVAc on T_{cc}.

6.4.5 Mechanical properties

The tensile properties of PLA fibres (presented in Figure 6.9) coated with PVAc and CNWs-PVAc were characterised in tensile mode at 25°C. The tensile strength and modulus of the non-coated PLA fibres were 207 MPa and 4.9 GPa, respectively. While comparatively higher tensile properties have also been reported in the literature for PLLA fibres, for instance, the tensile strength and modulus of PLLA fibre with diameter ranges from 11 to 14 μm were reported to be around 320 MPa and 5.5 GPa, respectively, [81] this was due to the higher L-lactide content in PLLA as compared to the PLA (Natureworks–3251D) polymer investigated in this study.

Attachment of all the coating substances onto PLA fibres revealed a small change in tensile strength (P>0.05) compared to the non-coated PLA fibres tested at room temperature. For instance, PLA PVAc, PLA CNW-65 and PLA CNW-75 fibres revealed a 9%, 7% and 0.5% decrease and the PLA CNWs-85 and PLA CNW-95 fibres exhibited 4% and 0.5% increase in tensile strength compared to uncoated PLA fibres (tensile strength 207 MPa).
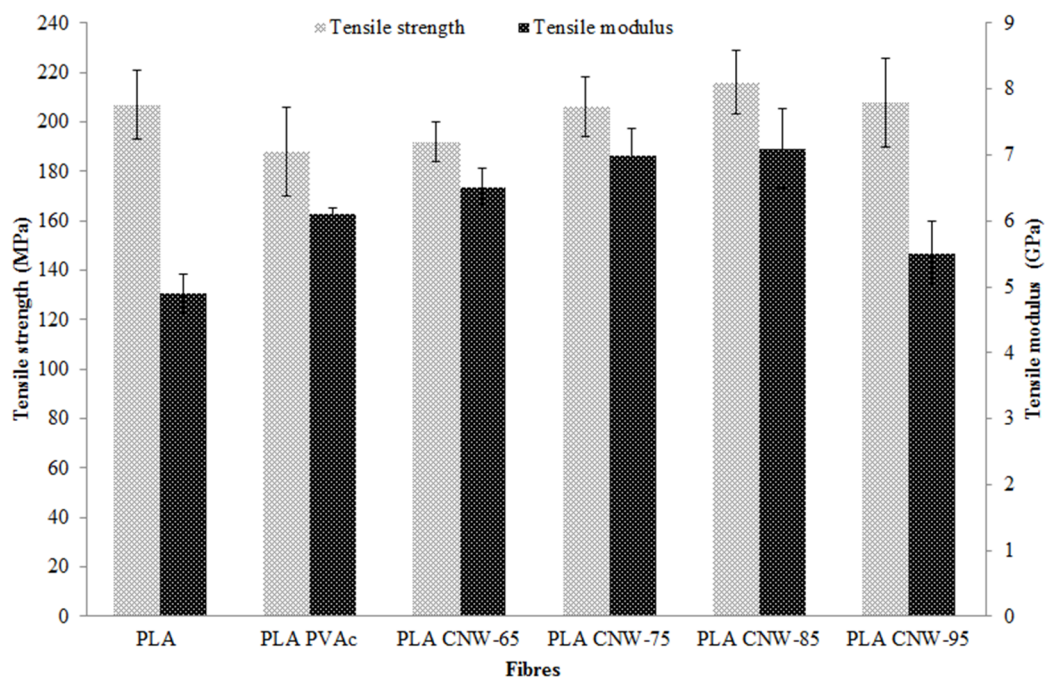
Figure 6.9: *Tensile strength and modulus properties for the single PLA fibres*

coated with PVAc and CNWs-PVAc.

However, a significant improvement in the tensile modulus ($P<0.0001$) for PLA CNWs-65, PLA CNWs-75 and PLA CNWs-85 fibres (33%, 43% and 45% increase, respectively) was observed when compared to the non-coated PLA fibres (tensile modulus 4.9 GPa), suggesting a tangible influence from the nanowhiskers (tensile modulus=105 GPa) [54] deposited on the fibre surface. This influence of the deposition layer formed on the fibre surface has been attributed to the CNW-PVAc as well as the CNW-CNW percolating interactions, where PVAc strongly attached the CNWs to the surface of the fibres during the drying process as can be seen in Figure 6.10. A similar percolation network for high cellulose nanowhisker (75 wt%) content thin film composites was also suggested when their tensile modulus increased to 8 GPa from 0.39GPa [303]. In addition, PLA CNW-95 also

exhibited a 12% increase (however, *P*>0.05) in tensile modulus compared to the uncoated PLA fibres.
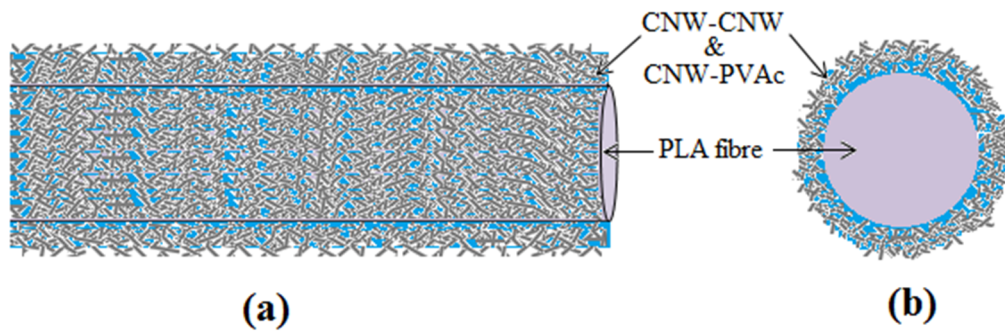
Figure 6.10: *a) Deposition pattern of CNWs-PVAc on the surface of PLA fibres, and b) cross sectional view of the deposits.*

The experimental modulus of the coated fibres could be compared using a simple two parallel system core-shell model, which predicts the tensile modulus of the coated PLA fibres. The predicted tensile modulus (*E'*) can be expressed by:

$$E' = (x \times M_1) + (y \times M_2) ....(6.1)$$

Where, *x* and *y* are the volume fraction of PLA (core) and coated materials (shell) and M_1 and M_2 are their corresponding tensile modulus, respectively. However, tensile modulus of the CNWs-PVAc blends with various CNWs contents used were calculated using Halpin-Kardos model to predict the modulus of nanocomposites containing randomly oriented nanofillers in a plane which was explained somewhere else [303]. The density of the PLA and PVAc were taken to be 1.24 and 1.04 g cm^{-3} from the supplier data sheet and CNWs was considered to be 1.59 g cm^{-3} from the literature [176]. The average tensile modulus of the PVAc was considered to be 2.4 (±0.2) GPa which was measured experimentally using PVAc films (~0.2 mm thickness) produced via a solvent casting method after dispersing

in deionised water. The aspect ratio of 20 (average length 200 nm and diameter 10 nm) [303] and tensile modulus of 57 GPa [54] of cotton based CNWs were also used to calculate the predicted modulus of the CNWs-PVAc coated PLA fibres. The experimental modulus of the PLA fibres coated with various CNWs-PVAc blends were seen to follow the same trend of the predicted modulus (please see Figure 6.11).
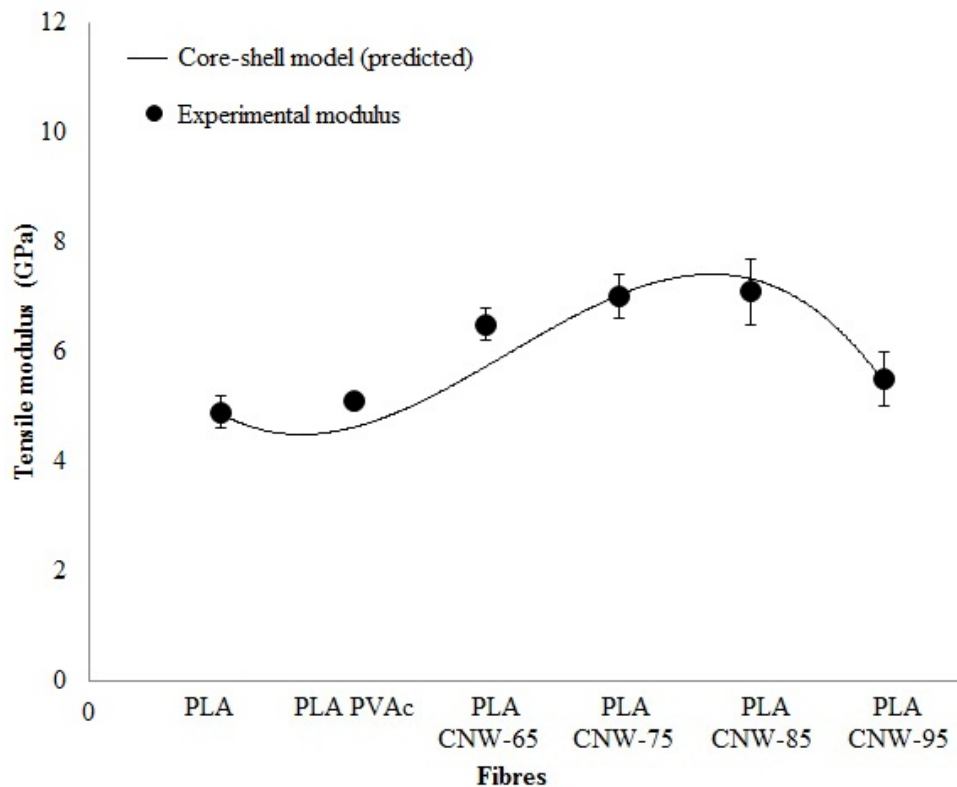
Figure 6.11: *Comparison of experimental modulus and predicted modulus using two parallel system core-shell model of the coated PLA fibres.*

However, the experimental modulus of the PLA PVAc and PLA CNW-65 fibres found higher compared to predicted modulus. This could be suggested to be due the volume fraction of the PVAc binder alone was not sufficient to reduce the modulus of the PLA PVAc fibres.

The properties for elongation at break for the coated and uncoated fibres are shown in Figure 6.12.
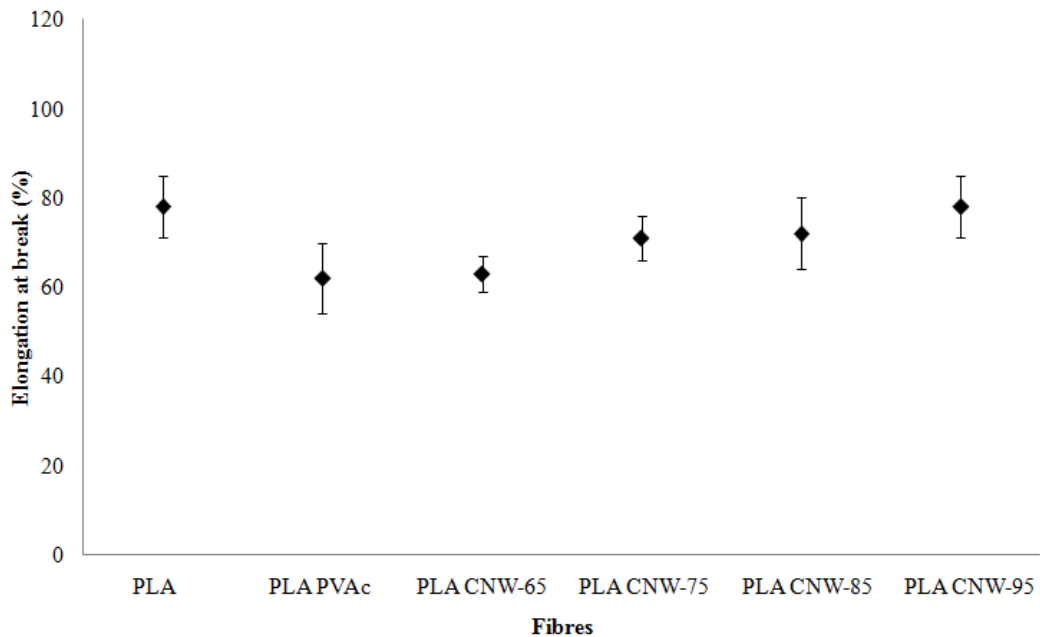
Figure 6.12: *Properties for elongation at break for single PLA fibres only and coated with PVAc and CNWs-PVAc.*

The attachment of PVAc on the PLA fibre surface exhibited a decrease ($P<0.05$) in elongation properties from 78% to 62% compared to the non-coated fibres, which was suggested to be due to the formation of a thin rigid layer of PVAc onto the PLA fibre surface. On the other hand, the CNWs-PVAc coated PLA fibres revealed their elongation at break properties increasing from 71% to 78% with the CNW contents in the coating materials indicating that CNW inclusion in the coating appears to restore the elongation at break of the coated fibres to the values for uncoated fibres with the exception for PLA CNWs-65 fibres which showed the value around 63%, closed to that of PLA PVAc fibres. The similar discrepancy was also observed for this composition of coated fibres in measuring the T_g values

using DSC compared to the others containing higher amount of CNWs and found the value close to that for the PVAc coated fibres, which could be due the presence of 65 wt% CNWs in the coating blend is not sufficient to alter neither the fibres elongation properties nor the glass transition temperature significantly compared to that of the PLA PVAc fibres.

6.4.6 Moisture absorption

The coated and uncoated PLA fibres were conditioned at various humidity levels (0, 35, 75 and 98% RH) using saturated salt solutions for two weeks to investigate their moisture absorption. The moisture absorption of the conditioned coated and uncoated PLA fibres revealed an increasing trend with increase in relative humidity, as seen in Figure in 6.13. PLA CNWs-75 fibres exhibited higher moisture absorption at 98% RH (6.0 wt%) compared to the PVAc coated (4.2 wt%) and pure PLA fibres (2 wt%). However, lower amount of moisture uptake (only 2.7 wt% at 98% RH) for PLA CNWs-95 fibres was again suggested to be due to presence of insufficient amount of PVAc binder as well as CNWs on the fibre surface which was also related to the increase in fibre diameter which didn't really occur for this composition of coating blend. Comparatively higher quantity of water accumulation was expected in the case of PLA CNWs-65, PLA CNWs-75 and PLA CNWs-85 fibres due to the hydrophilic nature of the CNWs. This has previously been shown by Garcia de Rodriguez *et al.* [50] who compared the water take-up of CNW-PVAc composite at different RH.
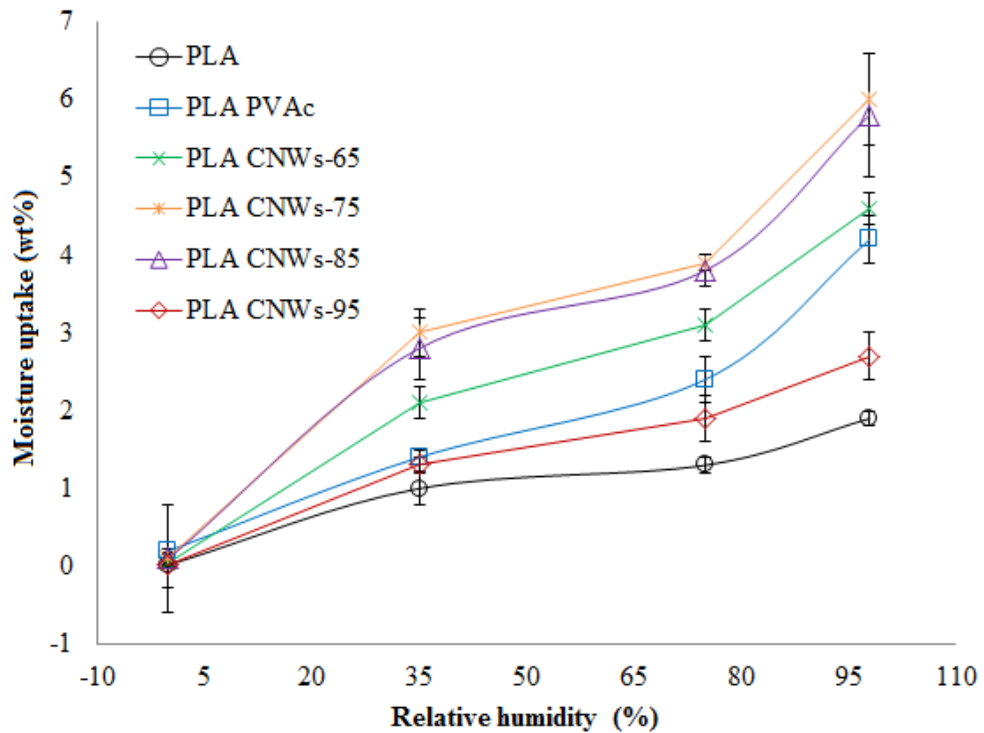
Figure 6.13: *Moisture uptake of PVAc and CNWs-PVAc coated and uncoated PLA*

fibres as a function of relative humidity.

The accumulation of water at the CNW surface was later shown by Capadona *et al.* [250] to reduce the reinforcing effect of the CNW percolated network by disrupting hydrogen bonding. In the water take-up studies of Garcia de Rodriguez *et al.* [50], they reported around 12 wt% water accumulation at 98% RH for PVAc-sisal whisker nanocomposites containing 2.5 wt% whisker content. An increase in the hydrophilic nature of CNW-PVAc coated PLA fibre could help to provide better cell attachment in cell culture media as suggested by Oh *et al.* [308] while investigating the *in vitro* cell compatibility of hydrophobic poly(lactic-coglycolic acid) (PLGA) against a hydrophilic PLGA/ PVA blend using human chondrocytes. It was reported that the PLGA/PVA blend was easily wetted in culture medium without the requirement of pre-wetting treatments and had better cell adhesion

and growth than the control hydrophobic PLGA. Apart from potential advantages associated with improvement in cell adhesion properties for the CNW-PVAc coated PLA fibre, the accumulated water content could also influence the degradation rate of the fibre. Kim *et al.* [76] suggested the improved hydrophilicity in the PLA/PLGA electrospun nanofibres enhanced their degradation rate to 65% weight loss in 7 weeks compared to hydrophobic PLA (which only revealed an approximate ~10% weight loss).

6.5 CONCLUSIONS

CNWs were successfully attached to the hydrophobic surface of melt drawn PLA fibres using PVAc as a binding agent. Addition of CNWs into the coating blend played an important role in increasing the surface roughness of PLA fibres. The attachment of CNWs-PVAc blend with 75 to 95 wt% CNWs content on the fibre surfaces revealed significant changes in their glass transition temperatures. However, no significant changes in their melting temperature and tensile strength properties were observed due to the coating substances applied on the fibres surfaces. Moreover, upto 45% increase in tensile modulus properties was obtained for the PLA fibres coated with CNWs-PVAc blend containing 85 wt% CNW, respectively demonstrated the influence of CNW-CNW and CNW-PVAc interactions onto the surface of PLA fibres. Additionally, the presence of CNWs-PVAc blend had a significant effect in increasing the moisture absorption properties by up to 6.0 wt% at 98% relative humidity, showing increased hydrophilicity of the coated PLA fibres when compared to the hydrophobic non-

coated PLA fibre. It was also suggested that the roughness and hydrophilic surface created on the PLA fibres via CNW-PVAc coating materials could impart better cell adhesion and proliferation properties and increase degradation properties.

CHAPTER 7.

ROLE OF CELLULOSE NANOWHISKERS ON THE FLEXURAL PROPERTIES

OF SELF-REINFORCED POLYLACTIC ACID (SR PLA) COMPOSITES

7.1 SUMMARY

Self-reinforced polylactic acid (SR PLA) composites incorporating cellulose nanowhiskers (CNWs) were produced by coating orientated PLA fibres with a polyvinyl acetate (PVAc)-CNW mixture as a binder prior to hot compaction at 95°C. PLA fibres were produced with an average diameter of 11 (± 0.9) μm via a melt-drawing (at 180°C) process. Scanning electron microscopy (SEM) images revealed that the CNWs imparted roughness to the PLA fibre surface. Cross-sectional examination of the SR PLA composites after hot-pressing confirmed that the PLA fibres had maintained their morphology. Incorporation of 8 wt% CNWs within the SR-PLA composites revealed an increase in their flexural strength (48%) and modulus (39%) compared to the control composite (flexural strength~82 MPa and modulus~3.9 GPa). In addition, whilst the control SR-PLA composite revealed quite brittle characteristics, the addition of CNWs and PVAc showed a more ductile behaviour.

7.2 INTRODUCTION

For self-reinforced PLA composite processing, use of highly crystalline PLA filaments also showed significantly improved interfacial bonding due to the similar chemical structure of both matrix and reinforcing elements [309]. For example, Li

and Yao [310] produced 0.5 mm thick single PLA composites using amorphous PLA sheets (5% crystallinity) and crystalline PLA yarn (40% crystallinity) via a compression moulding process at 140°C and reported that the self-reinforced PLA composite containing 25 wt% unidirectional PLA yarns (consisting of 135 continuous fibres with average diameter of around 20 μm) had improved the tensile strength by 31% and modulus by 48% compared to the control PLA sheet (tensile strength~ 44.8 MPa and modulus~ 2.5 GPa). The flexural properties of a 3.2 mm thick self-reinforced PLLA composite produced via a hot compaction process at 95°C were investigated by Wright-Charlesworth *et al.* [100] and reported that SR-PLLA had higher initial flexural properties (strength~ 139.2 MPa and modulus~ 5.4 GPa) as compared to non-reinforced PLLA (strength~ 110.8 MPa and modulus~ 3.9 GPa).

Although SRCs have shown higher strength and modulus compared to the non-reinforced polymer, recent studies have also focused on the enhancement of the material properties through modification of the processing techniques [311] as well as through the incorporation of fillers [281, 312, 313]. For instance, Foster *et al.* [314] investigated the incorporation of carbon nanofibres (CNF) into hot compacted polypropylene (PP) woven tapes and also addition of other nano and micro-sized fillers, such as talc, nanoclay, fly ash and carbon black [313]. It was reported that all of the fillers improved the interlayer adhesion properties compared to the pure PP tape/film which was confirmed via SEM images and peel testing. Natural polymers such as chitosan [26], alginate [29] and cellulose [166, 172] both in nano and microfibre form have also been investigated to

functionalise PLA for use in tissue engineering and biomedical applications. More recently, cellulose nanowhiskers (CNWs) have been utilised in nanocomposites processing due to their biodegradability [11, 12, 186], biocompatibility [188, 315] and superior mechanical properties (tensile modulus ~105 GPa for cotton based nanocellulose) [54].

In this study, PLA fibre mats were prepared using melt-spun PLA fibres coated with a blend of CNWs/PVAc. The attachment of nanowhiskers onto the fibre mats was examined via scanning electron microscopy (SEM) and confirmed via Fourier transform infrared (FTIR) spectroscopy. The self-reinforced composites investigated in this study were produced via a hot compression process by laminate stacking the PLA fibre mats and the effect of CNWs and PVAc on the structural and mechanical properties of the composites are reported in this chapter.

7.3 MATERIALS AND METHODOLOGY

7.3.1 PLA fibre drawing

As described in Section 5.3.1.

7.3.2 Preparation of cellulose nanowhiskers (CNWs)

As described in Section 3.3.2.

7.3.3 Manufacture of PLA fibre mats

CNWs suspension (2 w/v% in deionised water) were blended with poly vinylacetate (PVAc) which was obtained as Kollicoat SR, a 30% dispersion of PVAc stabilised with polyvinylpyrrolidone and sodium laurile sulphate. Aligned PLA fibre

mats were produced by gently brushing the coating blends (see Table 7.1) onto 10 layers of PLA fibres collected on the drum.

Table 7.1: *Formulations of coating materials prepared using CNWs and PVAc for PLA fibre mats.*

Sample **codes** used in this study	Coating materials	
	CNWs (wt%)	PVAc (wt%)
SR PLA	-	-
SR PLA-PVAc	-	100
SR PLA- CNWs	75	25

Preliminary testing indicated that the blend containing 75 wt% CNWs and 25 wt% PVAc was the most effective to increase the surface roughness (Figure 6.5, Section 6.4.2, Chapter 6) as well as enhancing the tensile properties (see Figure 6.9, Section 6.4.5, Chapter 6) of the individual PLA fibre. After drying at room temperature the fibre mats (with an average thickness of 0.4 mm) were removed from the drum and cut into 80 mm x 80 mm fibre mats. A final coating using the same blend was applied onto both sides of the fibre mat utilising a dip coating method. To ensure consistent deposition of the coating materials onto the individual fibre mats, after each dip coating process the coating suspension was replaced with a fresh suspension. The coating materials incorporated onto the fibre mats were calculated to be around 8 wt% after drying at $37^{o}C$ for 2 days on a polytetrafluoroethylene (PTFE) sheet.

7.3.4 Self-reinforced composite processing

To prepare SR composites, 22 layers of coated fibre mats were stacked together and preheated at 95±3°C for 15 min within a metal mould (dimension 80 mm x 80 mm x 1 mm) before pressing at the same temperature at 90 bar pressure for 10 min and cooling down to room temperature while retaining the applied pressure.

7.3.5 Electron microscopic analysis

The morphology of CNWs and the surface topography of coated and uncoated PLA fibre mats were characterised using TEM and SEM according to the procedure mentioned previously in Section 3.3.4.1.

7.3.6 Optical microscopic analysis

As described in Section 5.3.3.

In order to investigate the fibre structures within the SR PLA composites produced in this study, polished cross-sections of the composites were also analysed.

7.3.7 FTIR-ATR analysis

As described in Section 3.3.4.3.

7.3.8 Differential scanning calorimetric (DSC) analysis

As described in Section 3.3.4.7.

7.3.9 Flexural properties

The flexural strength and modulus properties were obtained via three point bending tests using a Hounsfield Series S testing machine according to the standard BS EN ISO 14125:1998 [316]. A cross head speed of 1 mm min^{-1} and a 5kN load cell was used and the average values were presented from at least five repeat specimens.

7.3.10 Statistical analysis

As described in Section 3.3.4.10.

7.4 RESULTS AND DISCUSSION

In this chapter, CNWs were incorporated as nanofiller through the use of PVAc as a binder to fix the CNWs to the PLA fibre surface. These modified fibres were then used to prepare unidirectional fibre mats in order to investigate the effect of CNWs on the mechanical properties of the SR PLA composites.

7.4.1 Morphological properties of PLA fibre mats and CNWs

SEM image presented in Figure 7.1a revealed a smooth surface morphology of the melt-spun PLA fibres with an average diameter of 11 (±0.9) μm. TEM image of the CNWs produced (seen in Figure 7.1b) exhibited rod-like shapes in line with the literature [48], which were produced from cotton via a sulphuric acid hydrolysis process and were used to coat the PLA fibre surface using PVAc as a binder to produce unidirectional fibre mats (see Figure 7.2).
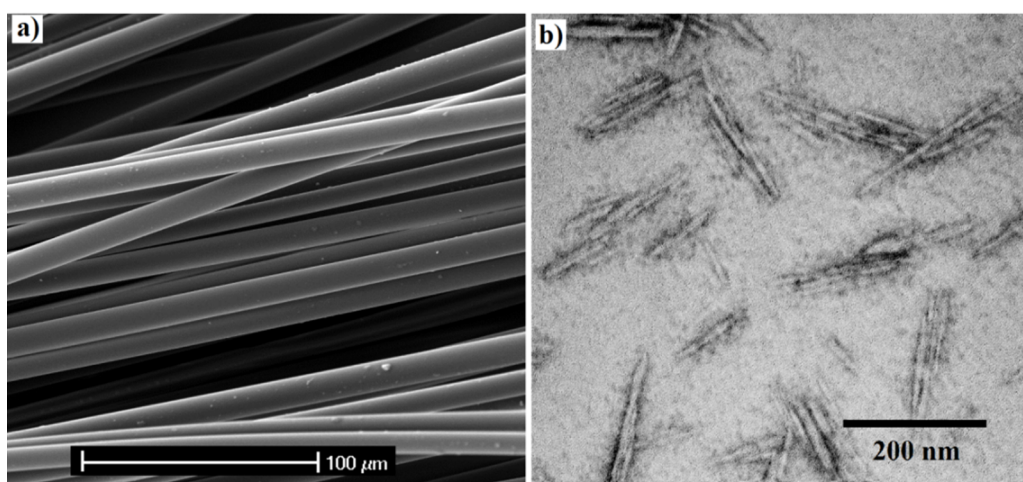
Figure 7.1: *a)* *SEM image of PLA fibres obtained at 400 m min^{-1} rotation speed, and* *b)* *TEM image of cellulose nanowhiskers (CNWs).*

Figure 7.2a shows a representative image of the coated PLA fibre mats which were collected from the winder drum. Initially, the PLA fibres were coated with approximately 1.7 wt% coating materials on one side to retain their unidirectional orientation whilst the fibres were removed from the drum. Once removed, the fibre sheets were then coated on both sides of the fibre mats utilising a dip coating method and around 8 wt% of the coating materials were incorporated onto the PLA fibre mats (shown in Figure 7.2b).
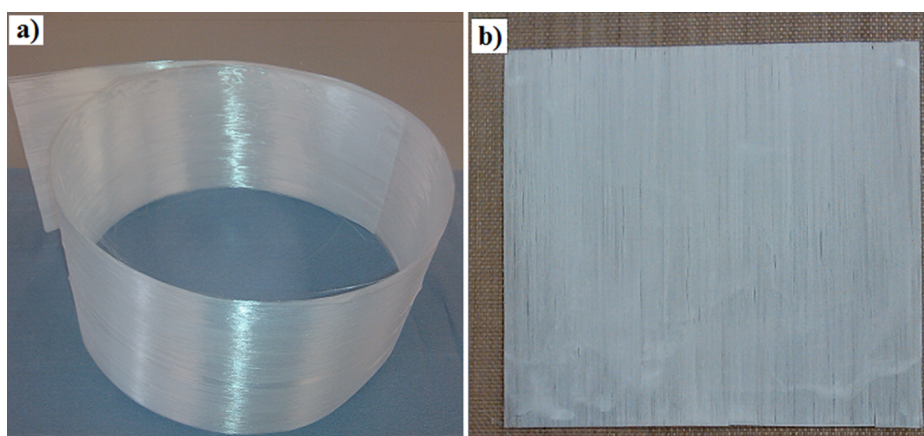
Figure 7.2: *Representative images of PLA fibre mats **a)** fibre sheet collected from the winder drum after coating (~1.7 wt% coating materials), and **b)** 80x80 mm fibre mat with both sides coated (~8 wt% coating materials).*

The surface morphology of both sides of the PLA fibre mats and single PLA fibres coated with PVAc and CNWs-PVAc are shown in Figures 7.3, where a clear deposition of coating materials can be seen on both sides of the fibre mats as well as on the single fibres when compared to the uncoated PLA fibres. The SEM images obtained for the fibre mats produced with only PVAc binder suggested homogeneous attachment of PVAc on the PLA fibre surface giving the appearance of a matt finish (see Figure 7.3a-c). The CNW-PVAc coated PLA fibre mats showed

that the CNWs were evenly distributed creating a textured surface on the PLA fibres (as seen in Figure 7.3d-f). Some flakes were also observed on the fibre mats which are believed to be due to the deposition of aggregated CNWs during the coating process. In this study, the attachment of CNW-PVAc to the PLA fibre surface was attributed to CNW-PVAc and CNW-CNW percolating interactions, where PVAc acted as a binding agent helping to attach the CNWs onto the surface of the fibres as well as to bind the unidirectional fibre mats during the drying process.
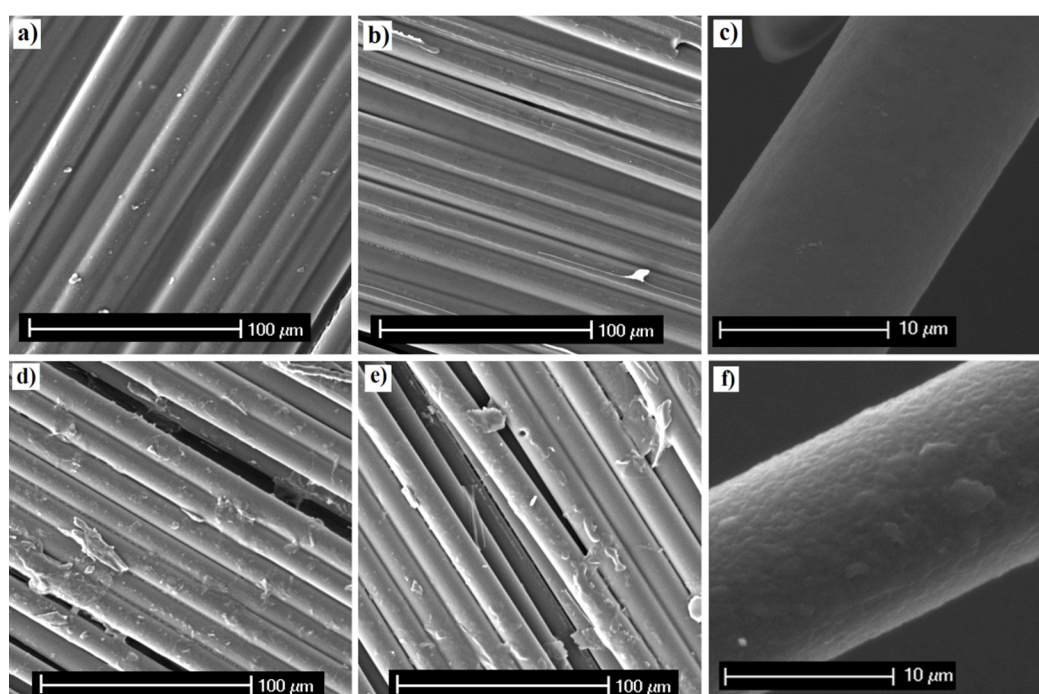
Figure 7.3: *SEM images represent **a)** PVAc coated fibre mat (top surface during drying on a PTFE sheet), **b)** PVAc coated fibre mat (bottom surface during drying), **c)** PVAc coated single PLA fibre, **d)** CNWs-PVAc coated fibre mat (top surface), **e)** CNWs-PVAc coated fibre mat (bottom surface), and **f)** CNWs-PVAc coated single PLA fibre.*

7.4.2 FTIR analysis

The attachment of coating materials (CNWs and PVAc) on the surface of PLA fibre were confirmed via their functional groups identified using FTIR-ATR spectroscopy, as can be seen in Figure 7.4. In case of the uncoated PLA fibre, the bands at 1753, 1456 and 1375 cm^{-1} were attributed to C=O stretching, CH_3 asymmetric stretching and CH_3 symmetric deformation, respectively, while the bands at 1186, 1085 and 873 cm^{-1} indicated the –C-O-C asymmetric, symmetric and C-COO stretching, respectively for PLA [83]. The addition of PVAc binder on the PLA fibre surface exhibited the vibration bands at 1682 and 1234 cm^{-1} representing the C-H and C-O stretching groups. [83]).
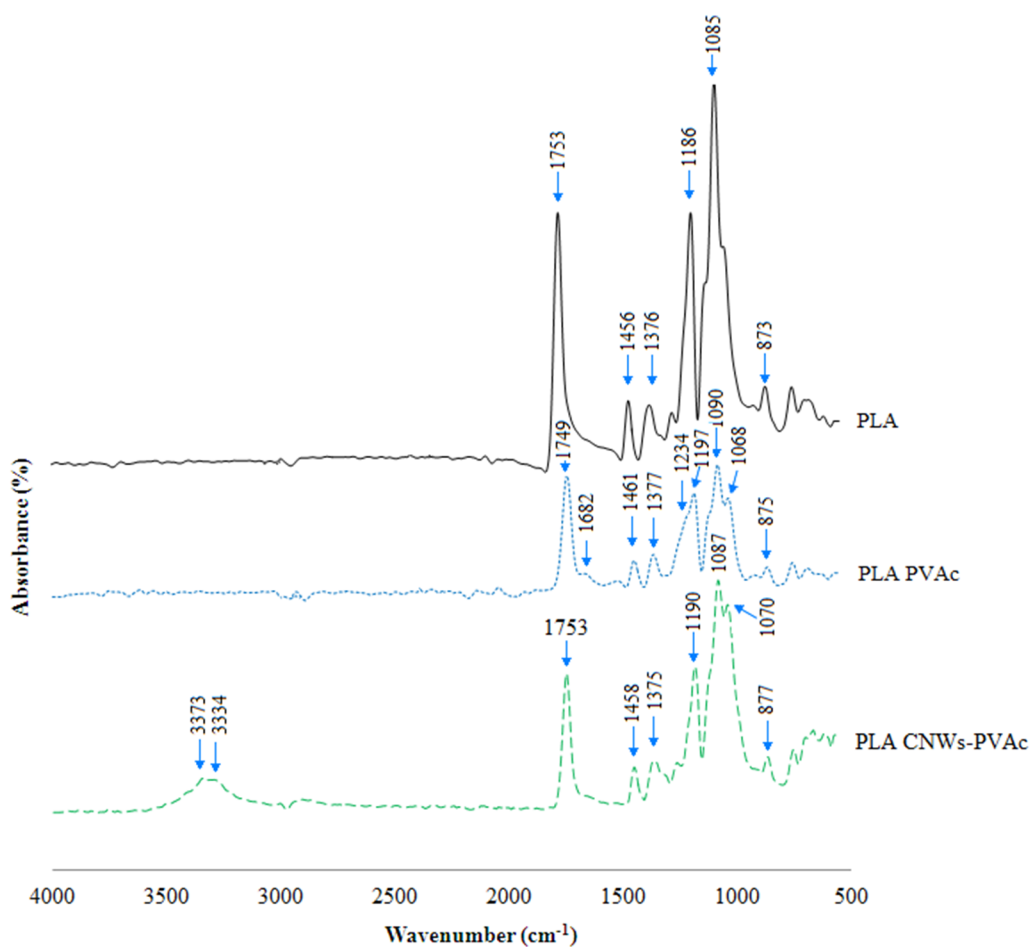
Figure 7.4: *FTIR-ATR spectra for uncoated and PVAc and CNWs-PVAc coated PLA*

fibre mats.

A shift of C=O band to 1749 cm^{-1} also observed for PVAc coated PLA fibres compared to uncoated PLA fibres was due to the presence of the acetate group as the literature reported that the vibrational frequency for C=O of the acetate group for pure PVAc was observed at 1740 cm^{-1} [306]. Likewise, the attachment of CNWs-PVAc blend on the fibre surface revealed absorbance bands at 3373 and 3334 cm^{-1} which indicated the O-H stretching vibration of cellulose structure [166, 252] and which were absent for the uncoated PLA fibre and PVAc coated fibre mats.

7.4.3 Thermal properties

Figure 7.5 represents the DSC thermograms for the uncoated PLA fibres and PVAc and CNWs-PVAc coated PLA fibre mats. The glass transition temperature (T_g) for the PVAc coated PLA fibre mat did not reveal a significant change ($P>0.05$) when compared to the PLA fibre (T_g~63.5^{o}C), while attachment of CNW-PVAc blend exhibited a slight increase ($P<0.05$) in T_g value (~65°C). This was suggested to be due to restriction of polymer chain mobility along the interface caused by the hydrogen bonding created between PLA fibre surface and the PVAC-CNW coating during the drying process [307].
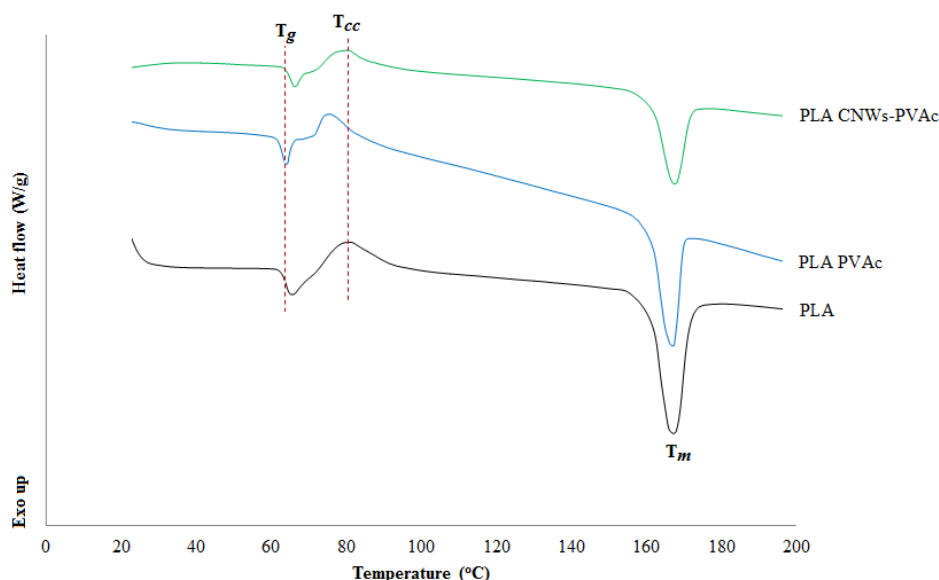
Figure 7.5: *DSC thermogram of uncoated and PVAc and CNWs-PVAc coated PLA fibre mats.*

The cold crystallisation temperature (T_{cc}) of PVAc coated PLA fibres were noted to be 75°C, which was approximately 5°C lower than that for the pure PLA fibre. However, T_{cc} for CNWs-PVAc coated PLA fibres was 79°C, which was close to that of PLA fibres, further indicating interactions of CNWs with the PLA as the CNWs

appear to offset the effect of PVAc on T_{cc}. No significant changes in melting (T_m) temperatures (P>0.05) were observed for both types of coated fibre mats (T_m=166°C) compared to the uncoated PLA fibre (T_m=167°C).

7.4.4 Structural analysis of self-reinforced PLA composites

The retention of the fibre structure within the SRCs can have a significant influence on its mechanical properties. Therefore, the polished cross-sections of the SRCs produced were investigated via a calibrated optical microscope.
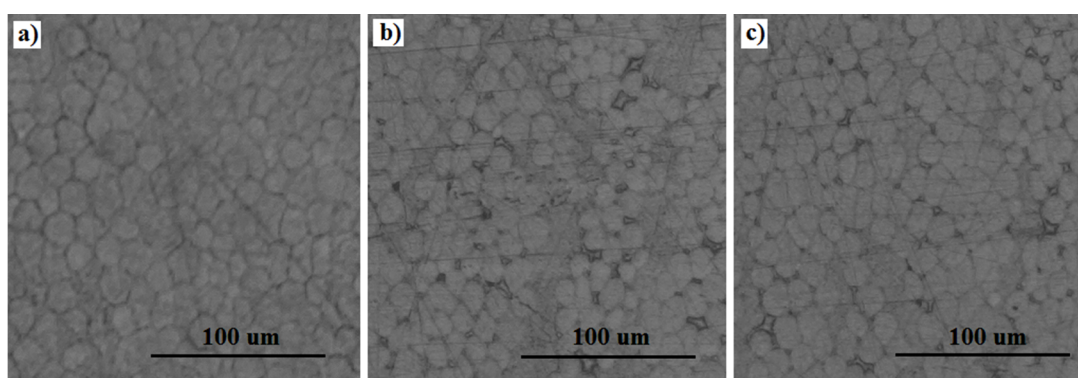
Figure 7.6: *Optical microscopy images of polished cross-section of SR PLA composites: a) control (uncoated), b) PVAc coated, and c) CNWs-PVAc coated SR PLA composites.*

From Figure 7.6a-c, it was seen that the cross-section of the SRCs revealed that the morphology of the PLA fibres had been maintained after consolidation into composites. However, the fibre morphology observed was not perfectly cylindrical for all the fibres. The temperature and pressure used in this study played an important role in preserving the fibre structure, as Wright-Charlesworth *et al.* [281] showed that for SR PLLA composites, the process parameters (95°C and 90 bar pressure) provided the best combination of flexural strength, modulus and ductility.

Furthermore, the fracture surfaces of the SRCs (Figure 7.7a-c) also showed the retention of the PLA fibrous structure as well as pull out of some fibres along the fractured cross-section within the SRCs.
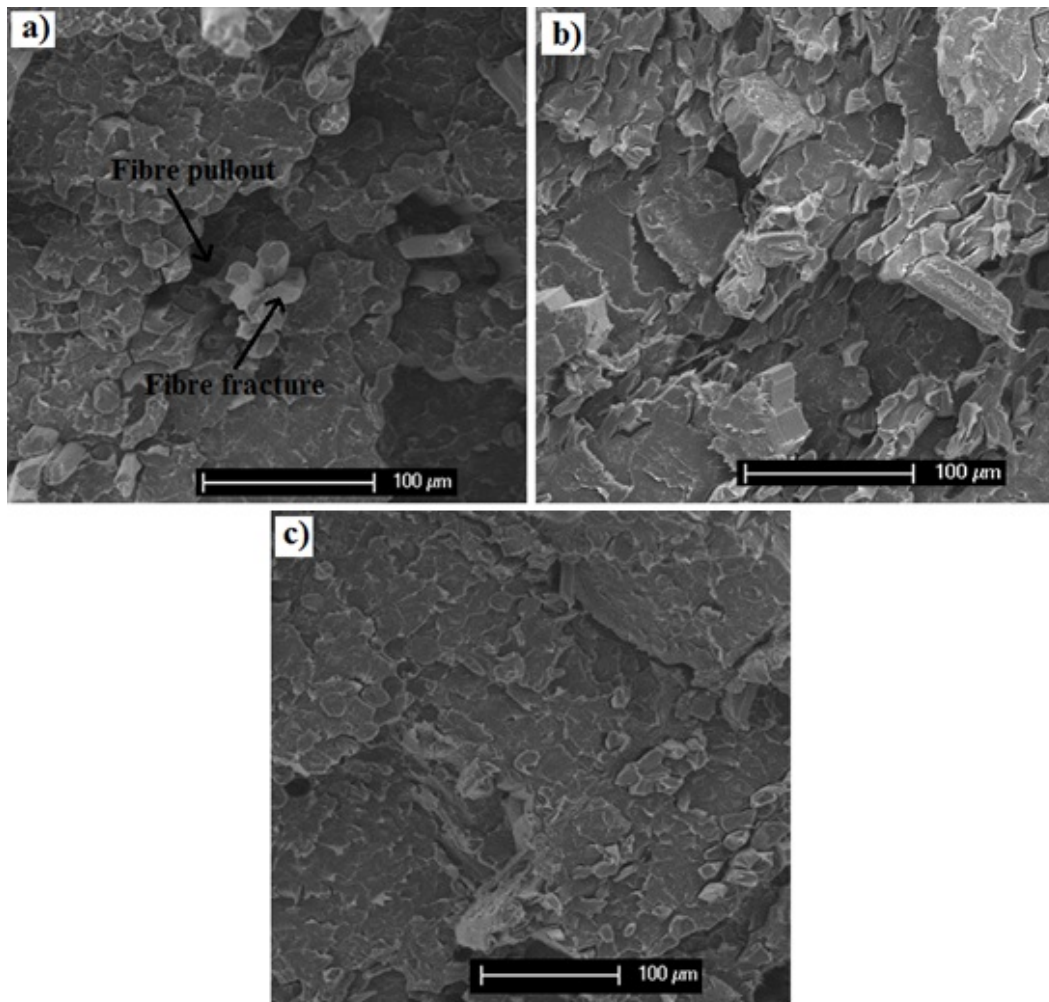
Figure 7.7: *Scanning electron microscopy (SEM) images of fracture cross-section of SR PLA composites: **a)** control (uncoated), **b)** PVAc coated, and **c)** CNWs-PVAc coated SR PLA composites.*

7.4.5 Flexural properties

The flexural properties of the SRCs are presented in Figure 7.8, where the flexural strength and modulus of the SR PLA-PVAc and SR PLA-CNWs composites were seen to increase compared to the SR PLA composite. The control SR PLA

composite had a flexural strength and modulus of 82 MPa and 3.9 GPa respectively, which was lower than that found by Wright-Charlesworth *et al.* [281] for SR-PLLA composites (139 MPa flexural strength and 5.4 GPa modulus). However, in this study PLA (Natureworks–3251D) resin was investigated which contained a lower amount of L-lactide compared to the PLLA resin.
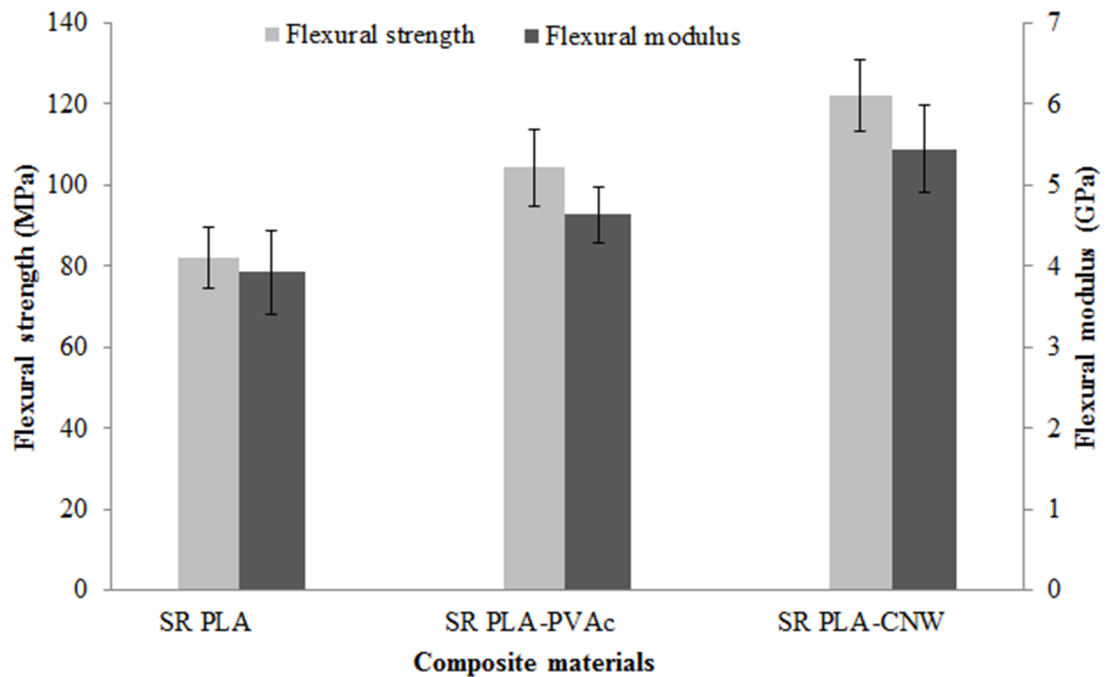
Figure 7.8: *Flexural strength and modulus properties of self-reinforced PLA, PLA-PVAc and PLA-CNW composites produced in this study.*

In addition, the fibre processing conditions and further improvement of their initial strength could improve the flexural properties of SRCs. For SR PLA-CNW composites the flexural strength and modulus increased to 122 MPa (~48% increase) and 5.5 GPa (~39% increase), which was comparable with other studies on SR PLLA composites [281]. This was attributed to the mechanical interlocking of nanofiller (CNWs) within the SR PLA-CNW composite which improved the interfacial properties between the fibre and matrix. Foster *et al.* [313] investigated

nano and micron-size particles (nanoclay, talc, carbon black) to enhance the interlayer adhesion in SRCs, which was believed to increase the mechanical properties of the composites. Though the SR PLA-PVAc composite exhibited an increase in flexural properties (flexural strength~102 MPa and modulus~4.6 GPa) compared to the control SR PLA composite, these values were significantly lower (P<0.05) compared to SR PLA-CNW, which demonstrated the influence of CNW in the coating blends to enhance the mechanical properties of SR PLA composites.

The flexural stress-strain curve presented in Figure 7.9 shows the brittle and/or ductile behaviour of the SRCs produced in this study, where SR PLA revealed a sudden break during testing which highlighted their brittleness. However, the SR PLA-CNW composite revealed less brittle properties and the SR PLA-PVAc composites exhibited quite ductile properties during the flexural test.
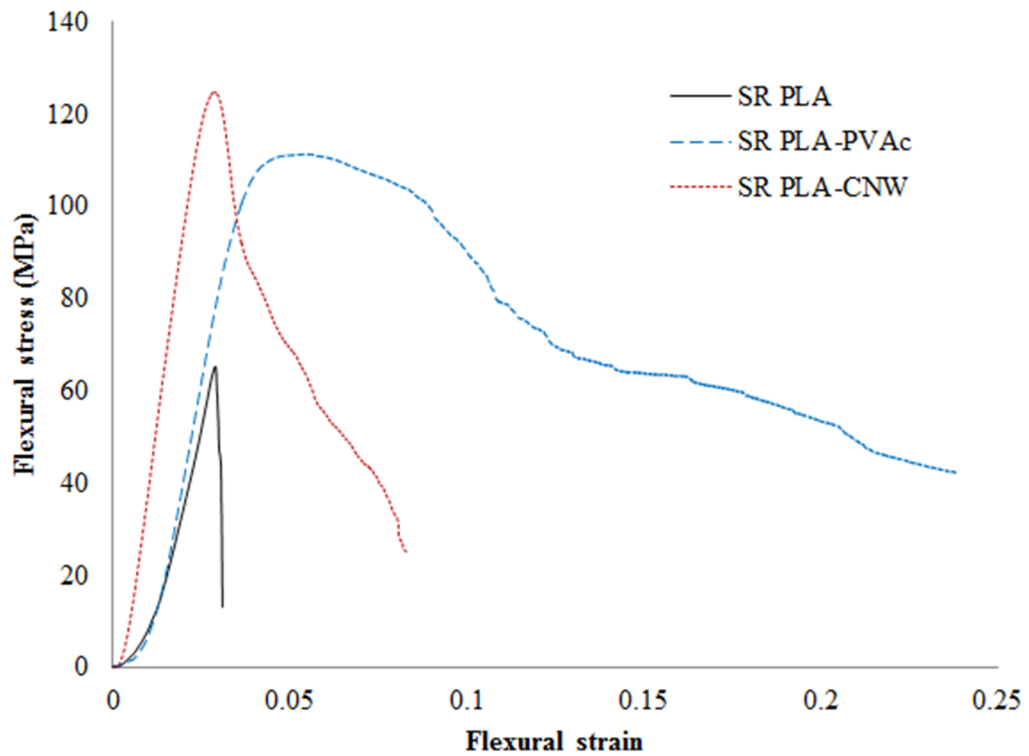
Figure 7.9: *Typical flexural stress-strain curves for self-reinforced PLA, PLA-PVAc*

and PLA-CNW composites produced.

The SR PLA composite exhibited brittle failure mode during flexural testing, whilst the highest ductile properties were observed for the SR PLA-PVAc composite, which was suggested to be due to the presence of plasticized PVAc matrix within the SRCs. The SR PLA-CNW composite exhibited less ductile behaviour compared to SR PLA-PVAc composites which was also expected due to the presence of stiff CNWs.
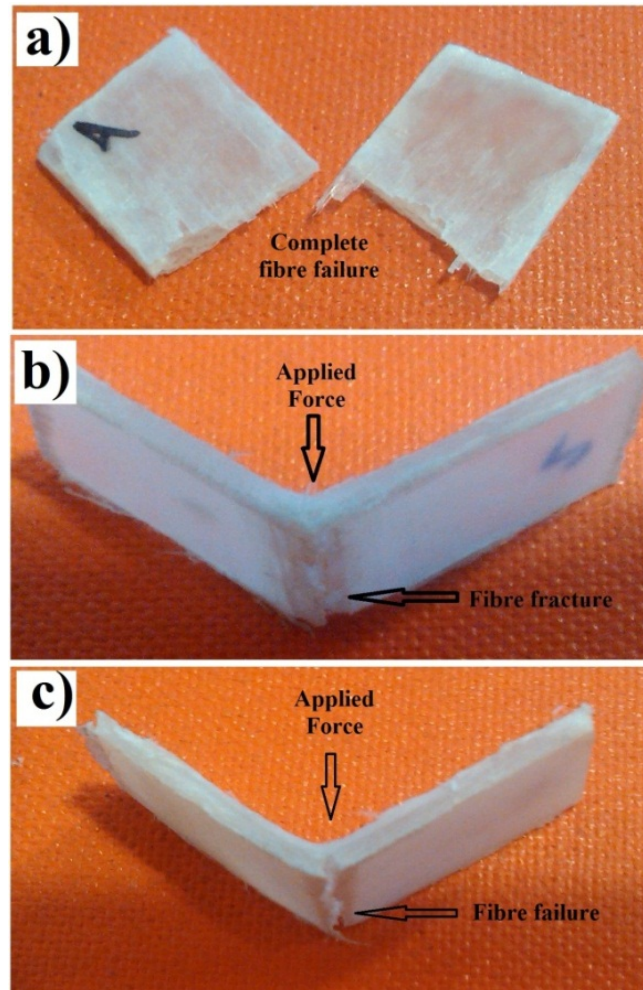
Figure 7.10: *Image representing the fracture mode of SR composites: **a)** SR PLA, **b)** SR PLA-PVAc, and **c)** SR PLA-CNW composites.*

The control SR PLA showed complete breakdown of the fibres within the composites during the flexural test (see Figure 7.10a). The brittleness of the SR PLA was suggested to be associated with the failure of the fibre, deboning along the matrix and pull out of fibres from the matrix (please see Figure 7.7a and Figure 7.11a) due to the misalignment of fibres as well as poor interfacial adhesion between the fibre and matrix. While the fracture surfaces of the SR PLA-PVAc and SR PLA-CNW composites revealed that a significant portion of the aligned fibres had been preserved even after fully bending the composites as presented in

Figure 7.10b-c and 7.11b-c. It is to be noted from the fracture images of SR PLA-PVAc and SR PLA-CNW (Figures 7.10b-c) that the initial crack within the SRCs started to appear at the bottom portion of the composites, which was suggested to be due to the failure of fibers along their longitudinal axis under the flexural stress condition [105]. In addition, retention of a significant portion of aligned fibres during the flexural test could also have been due to the improved interlayer adhesion of PLA fibres and PVAc matrix formed during the SR composite production.
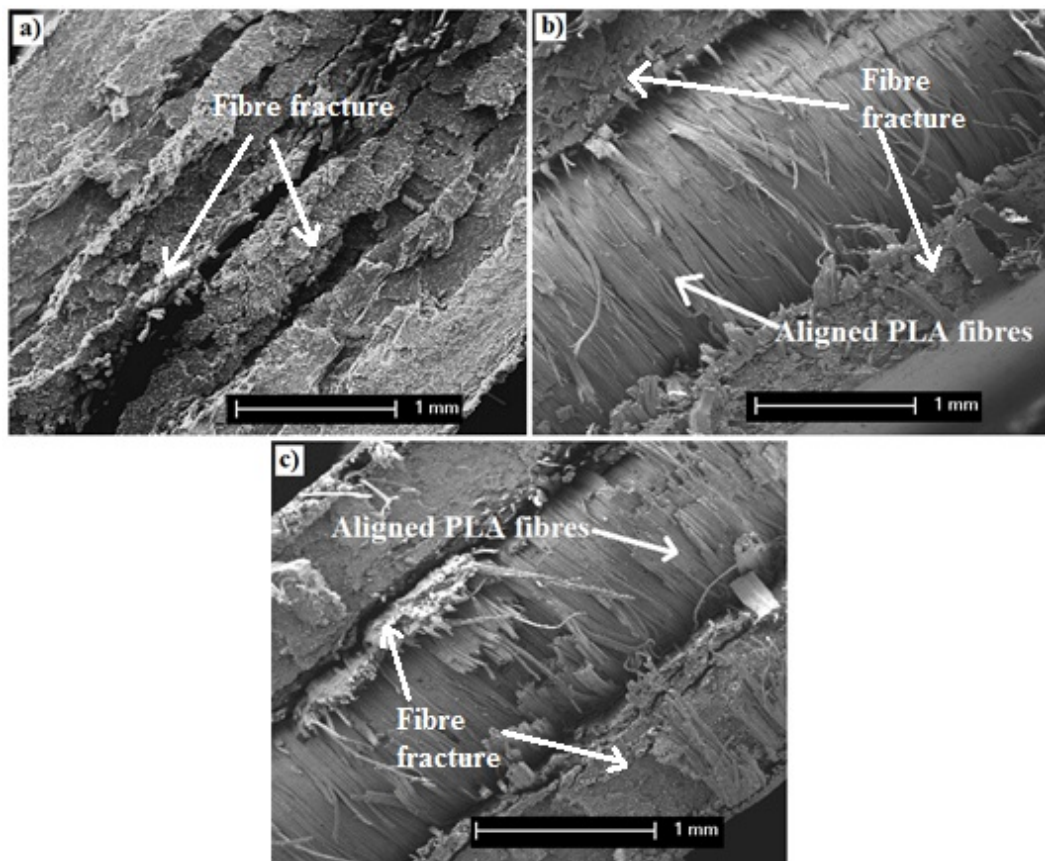
Figure 7.11: *SEM images of the fracture surface of SRCs obtained after flexural test: **a)** control SR PLA (complete fracture of fibres), **b)** SR PLA-PVAc (partial fracture of fibres), and **c)** SR PLA-CNW composites (partial fracture of fibres).*

This study showed that utilising CNWs and PVAc in SR PLA composites improved their flexural properties and imparted ductility. The enhanced mechanical properties enable the potential use of these SR PLA composite materials within packaging and biomedical fields.

7.5 CONCLUSIONS

The influence of CNWs and PVAc on the improvement of the flexural properties of self-reinforced PLA composites was investigated in this study. CNWs and PVAc coated highly oriented PLA fibre mats were used to produce SR composite via a hot compaction process maintaining the integrity of fibre within the composites. Incorporation of CNWs and PVAc within the SR composites a significant improvement in flexural properties was achieved. For example, CNWs (8 wt%) within the SR PLA composites exhibited 48% and 39% increase in flexural strength and modulus properties, respectively compared to the control SR PLA composite (flexural strength~82 MPa and modulus~3.9 GPa), whereas, the PVAc binder alone used within the SR composites revealed around 27% and 18% increase, respectively. The control SR PLA showed complete breakdown of fibres consolidated within the composites, whilst, the presence of CNWs and PVAc had a significant influence on ductile behaviour of the SR composites by retaining a portion of aligned fibres even after fully bending the composites, which reduced the chances of sudden failure during flexural test.

CHAPTER 8.

CONCLUSIONS AND FUTURE WORK

8.1 CONCLUSIONS

The aim of this project was to manufacture composite materials utilising cotton extracted cellulose nanowhiskers (CNWs) and characterise their mechanical, thermal and degradation properties.

The following conclusion can be made from the work carried out in this thesis:

- Cotton extracted cellulose nanowhiskers (CNWs) can be produced via sulphuric acid hydrolysis process and can be blended with polylactic acid (PLA) to produce thin and flexible bio-based nanocomposite films. By adding 1-5 wt% CNWs into the PLA matrix significant improvement of the mechanical and thermomechanical properties can be achieved. However, the tensile modulus was seen to be well below the expected modulus (predicted using Rule of Mixture), which was suggested to be due to the presence of voids and the aggregated morphology of the CNWs within the nanocomposites. CNWs induced crystallisation within the nanocomposites can also be achieved, which was also believed to have influenced improvement seen in the mechanical properties. Incorporation of hydrophilic CNW within the hydrophobic PLA matrix and the voids created within the nanocomposites can be suggested for accelerating the degradation properties at varying temperatures (25°C, 37°C and 50°C).

- Flexible thin films (~60 micron) with high CNW content can be produced by blending CNWs and hydrophilic hydroxyethyl cellulose (HEC) matrix. The aggregation nature of freeze dried CNWs within the matrix was a major contributor to the surface roughness and light transparency properties of the composite films. The incorporation of CNWs in the HEC matrix provided a significant improvement in their thermal properties by increasing the decomposition temperatures from $261^{o}C$ to $361^{o}C$. The enhanced storage modulus properties and the shift of the tan delta peaks of the nanocomposites compared to the HEC alone demonstrated the reinforcing effect of CNWs. An increase in crystallinity of blends with CNW content indicated that the induced crystallisation within HEC was caused by the presence of highly crystalline CNWs (crystallinity~89.1%). In addition, the presence of CNWs had a positive influence on controlling the swelling properties of CNW-HEC blends in phosphate buffer saline (PBS) media at body temperature ($37^{o}C$).

- PLA fibres (with diameters ranging from 11 µm to 38 µm) can be produced via the melt drawing process with varying take-up velocities. The higher drawing speed revealed a significant improvement on the chain orientation (via dichroic ratio measurement) in the thinner PLA fibres which revealed a higher degree of crystallinity (up to 34%) resulting in higher tensile properties. The tensile strength and modulus of the thinner PLA fibre (11±0.9 µm) revealed values of 213 MPa and 4.8 GPa, respectively and exhibited a significant decrease in tensile strength when tested at $37^{o}C$ compared to the room

temperature values due to a reduction in crystallinity whilst approaching the flow deformation temperature of PLA. The moisture uptake of all the PLA fibres revealed a steady increase with increasing relative humidity (RH). The accumulated moisture within the thinner fibres had a significant influence to decrease the tensile properties when exposed to 98% RH after four weeks of conditioning. Though the thinnest PLA fibres revealed a significant decrease in tensile properties when they were exposed to either body temperature or at high humidity atmosphere, the mechanical properties obtained were higher than the unconditioned larger diameter PLA fibres.

- CNWs can be successfully attached to the surface of melt drawn PLA fibres using polyvinyl acetate (PVAc) as a binding agent. The attachment of CNWs-PVAc blend with 75 to 95 wt% CNWs content on the fibre surfaces revealed significant changes in their surface roughness and glass transition temperatures. Moreover, upto 45% increase in tensile modulus properties can be obtained for the PLA fibres coated with CNWs-PVAc blend containing 85 wt% CNW (tensile modulus of PLA fibre~4.8 GPa), which suggested the positive influence of CNW-CNW and CNW-PVAc interactions on the surface of PLA fibres. The moisture absorption properties could be improved up to 6.0 wt% at 98% RH by incorporating CNWs-PVAc blend on the surface of hydrophobic PLA fibres.

- Finally, highly oriented PLA fibre mats can be produced using CNW-PVAc blends and can be used for the production of self-reinforced (SR) composite.

Incorporation of stiff CNWs and plasticized PVAc within the SR PLA composites can reveal a significant improvement in their flexural and ductile properties compared to the control SR PLA composite.

8.2 RECOMMENDATION FOR FUTURE WORK

Based on the overall summary of this project, the following points are suggested to extend the usability of CNWs based composite materials in various applications:

1. Use of coupling agent or surface modified CNWs to increase their dispersion in order to improve the interfacial properties with PLA matrix. However, coupling agent and/or surface active agent should not be cytotoxic if biomedical and food packaging applications are targeted.

2. Better dispersion of CNWs within the matrix can also be achieved using non-dried CNWs. Thus, aggregated morphology of CNWs through the formation of hydrogen bonds during the drying process could be minimised. Homogeneous dispersion of CNWs within the matrix believed to achieve maximum percolation of the network of cellulose crystals to acquire the optimum mechanical properties.

3. Use of CNWs to impart roughness on the surface of phosphate based glass (PBG) fibres with intentions to improve their interfacial properties of PBG reinforced PLA composites (please see Figure 8.1).
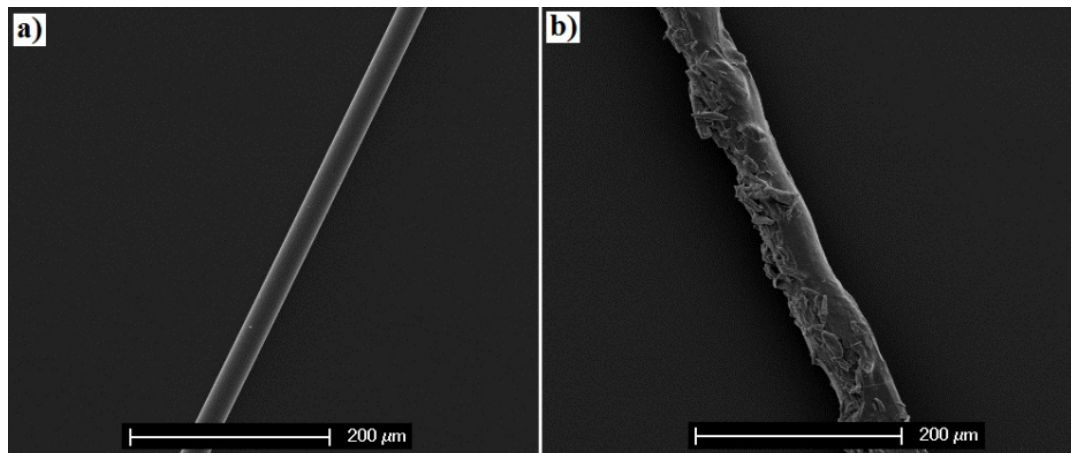
Figure 8.1: *a) SEM image showing the smooth surface morphology of PBG fibres (P40; Composition: 40P$_2$O$_5$-24MgO-16CaO-16Na$_2$O-4Fe$_2$O$_3$), and **b)** CNWs coated PBG fibre representing surface roughness.*

4. Manufacture of commingled composites using PLA fibre and PBG fibre and investigate their mechanical properties.

5. Use of CNW coated oriented PLA fibre mats to manufacture scaffolds and cell guide tubes for tissue engineering applications. The roughness and hydrophillicity imparted by CNWs on the surface of PLA fibres suggests the improvement in cell attachment and spreading properties.
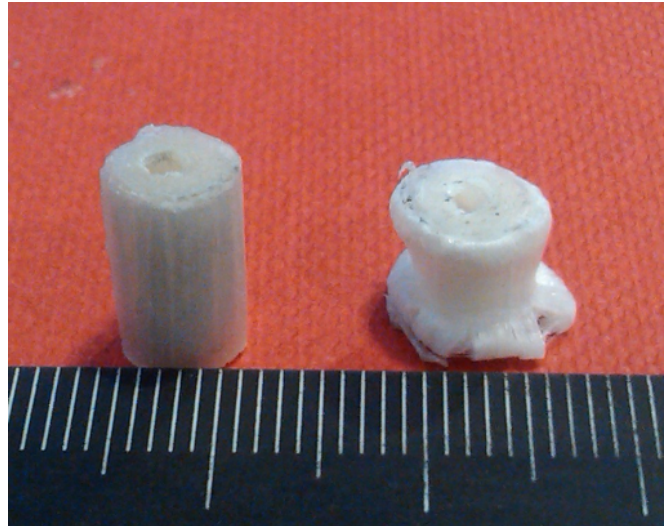
Figure 8.2: *Highly oriented PLA fibre tubes (left image) for soft tissue repair*

applications. The right image is representing the tube deformation after

compression test.

6. Investigate the retention of and cyclic mechanical properties after *in vitro*

degradation of SR PLA composites.

REFERENCES

1. FAOSTAT(2009). *Food and Agricultural Organisation of the United Nations-data collected from 245 countries and 35 regional areas*. [Accessed 6 April,2009]; Available from: http://faostat.fao.org/.

2. Powel, P.C. (1983), *Engineering with polymers*. New York: Chapman and Hall.

3. Hull, D. and Clyne, T.W. (1996), *An Introduction to Composite Materials*. 2nd ed: Cambridge University Press.

4. Agarwal, B.D., Broutman, L.J.and Shekhara, C. (1980), *Analysis and performance of fiber composites*. 3rd ed: John Wiley & Sons.

5. Holbery, J. and Houston, D. (2006), *Natural-fiber-reinforced polymer composites in automotive applications.* Journal of the Minerals, Metals and Materials Society, 58(11): p. 80-86.

6. Labet, M., Hossain, K.M.Z., Ahmed, I.and Thielemans, W. (2012), *Biomass in Composite Materials*, in *Materials for a Sustainable Future*, T.M. Letcher and J.L. Scott, Editors. Royal Scoety of Chemistry: UK. p. 698-739.

7. Satyanarayana, K.G., Arizaga, G.G.C.and Wypych, F. (2009), *Biodegradable composites based on lignocellulosic fibers—An overview.* Progress in Polymer Science, 34(9): p. 982-1021.

8. Pickering, K.L. (2008), *Properties and Performance of Natural-fibre Composites*. England: Woodhead Publishing Limited.

9. McCrum, N.G., Buckley, C.P.and Bucknall, C.B. (1997), *Principles of Polymer Engineering*. 2nd ed: Oxford Science Publications.

10. de Souza Lima, M.M. and Borsali, R. (2004), *Rodlike Cellulose Microcrystals: Structure, Properties, and Applications.* Macromolecular Rapid Communications, 25(7): p. 771-787.

11. Glasser, W.G., McCartney, B.K.and Samaranayake, G. (1994), *Cellulose derivatives with a low degree of substitution. 3. The biodegradability of cellulose esters using a simple enzyme assay.* Biotechnology Progress, 10(2): p. 214-219.

12. Park, C.H., Kang, Y.K.and Im, S.S. (2004), *Biodegradability of cellulose fabrics.* Journal of Applied Polymer Science, 94(1): p. 248-253.

13. Suh, H., Duckett, K.and Bhat, G. (1996), *Biodegradable and Tensile Properties of Cotton/Cellulose Acetate Nonwovens.* Textile Research Journal, 66(4): p. 230-237.

14. McCrum, N.G., Buckley, C.P. and Bucknall, C.B. (2nd edition, 1997), *Principles of Polymer Engineering.* Oxford Science Publications: p. 254.

15. Favier, V., Chanzy, H.and Cavaille, J.Y. (1995), *Polymer Nanocomposites Reinforced by Cellulose Whiskers.* Macromolecules, 28(18): p. 6365-6367.

16. Eichhorn, S.J., Dufresne, A., Aranguren, M., Marcovich, N.E., Capadona, J.R., Rowan, S.J., Weder, C., Thielemans, W., Roman, M., Renneckar, S., Gindl, W., Veigel, S., Keckes, J., Yano, H., Abe, K., Nogi, M., Nakagaito, A.N., Mangalam, A., Simonsen, J., Benight, A.S., Bismarck, A., Berglund, L.A.and

Peijs, T. (2010), *Review: current international research into cellulose nanofibres and nanocomposites.* Journal of Materials Science, 45(1): p. 1-33.

17. Herrick, F.W., Casebier, R.L., Hamilton, J.K.and Sandberg, K.R. (1983), *Microfibrillated cellulose: morphology and accessibility*. Medium: X; Size: Pages: 797-813.

18. Arinstein, A., Burman, M., Gendelman, O.and Zussman, E. (2007), *Effect of supramolecular structure on polymer nanofibre elasticity.* Nat Nano, 2(1): p. 59-62.

19. Siqueira, G., Bras, J.and Dufresne, A. (2009), *Cellulose Whiskers versus Microfibrils: Influence of the Nature of the Nanoparticle and its Surface Functionalization on the Thermal and Mechanical Properties of Nanocomposites.* Biomacromolecules, 10(2): p. 425-432.

20. Park, J.B. and Lakes, R.S. (2007), *Biomaterials : an introduction*. New York: Springer.

21. Mahapatro, A., Kulshrestha, A.S., American Chemical Society, M., American Chemical Society. Division of Polymeric Materials, S.and Engineering.(*Polymers for biomedical applications*. Washington, DC: American Chemical Society : Distributed by Oxford University Press.

22. Pietrzak, W.S., Sarver, D.R.and Verstynen, M.L. (1997), *Bioabsorbable Polymer Science for the Practicing Surgeon.* Journal of Craniofacial Surgery, 8(2): p. 87-91.

23. Grande, C.J., Torres, F.G., Gomez, C.M.and Carmen Bañó, M. (2009), *Nanocomposites of bacterial cellulose/hydroxyapatite for biomedical applications.* Acta Biomaterialia, 5(5): p. 1605-1615.

24. Helenius, G., Bäckdahl, H., Bodin, A., Nannmark, U., Gatenholm, P.and Risberg, B. (2006), *In vivo biocompatibility of bacterial cellulose.* Journal of Biomedical Materials Research Part A, 76A(2): p. 431-438.

25. Jia, H., Jia, Y., Wang, J., Hu, Y., Zhang, Y.and Jia, S.(2009), *Potentiality of Bacterial Cellulose as the Scaffold of Tissue Engineering of Cornea*. in *Biomedical Engineering and Informatics, 2009. BMEI '09. 2nd International Conference on*.

26. Cai, K., Yao, K., Cui, Y., Lin, S., Yang, Z., Li, X., Xie, H., Qing, T.and Luo, J. (2002), *Surface modification of poly (D,L-lactic acid) with chitosan and its effects on the culture of osteoblasts in vitro.* Journal of Biomedical Materials Research, 60(3): p. 398-404.

27. Sarasam, A. and Madihally, S.V. (2005), *Characterization of chitosan-polycaprolactone blends for tissue engineering applications.* Biomaterials, 26(27): p. 5500-5508.

28. Ko, H.-F., Sfeir, C.and Kumta, P.N. (2010), *Novel synthesis strategies for natural polymer and composite biomaterials as potential scaffolds for tissue engineering.* Philosophical Transactions of the Royal Society A: Mathematical, Physical and Engineering Sciences, 368(1917): p. 1981-1997.

29. Zhu, H., Ji, J., Lin, R., Gao, C., Feng, L.and Shen, J. (2002), *Surface engineering of poly(dl-lactic acid) by entrapment of alginate-amino acid*

derivatives for promotion of chondrogenesis. Biomaterials, 23(15): p. 3141-3148.

30. Pachence, J.M. (1996), *Collagen-based devices for soft tissue repair.* J Biomed Mater Res, 33(1): p. 35-40.

31. Dunn, M.G., Bellincampi, L.D., Tria, A.J.and Zawadsky, J.P. (1997), *Preliminary development of a collagen-PLA composite for ACL reconstruction.* Journal of Applied Polymer Science, 63(11): p. 1423-1428.

32. Ma, L., Gao, C., Mao, Z., Zhou, J., Shen, J., Hu, X.and Han, C. (2003), *Collagen/chitosan porous scaffolds with improved biostability for skin tissue engineering.* Biomaterials, 24(26): p. 4833-4841.

33. Meinel, L., Betz, O., Fajardo, R., Hofmann, S., Nazarian, A., Cory, E., Hilbe, M., McCool, J., Langer, R., Vunjak-Novakovic, G., Merkle, H.P., Rechenberg, B., Kaplan, D.L.and Kirker-Head, C. (2006), *Silk based biomaterials to heal critical sized femur defects.* Bone, 39(4): p. 922-31.

34. Altman, G.H., Diaz, F., Jakuba, C., Calabro, T., Horan, R.L., Chen, J., Lu, H., Richmond, J.and Kaplan, D.L. (2003), *Silk-based biomaterials.* Biomaterials, 24(3): p. 401-16.

35. Mauck, R.L., Soltz, M.A., Wang, C.C.B., Wong, D.D., Chao, P.-H.G., Valhmu, W.B., Hung, C.T.and Ateshian, G.A. (2000), *Functional Tissue Engineering of Articular Cartilage Through Dynamic Loading of Chondrocyte-Seeded Agarose Gels.* Journal of Biomechanical Engineering, 122(3): p. 252-260.

36. Hendrickson, D.A., Nixon, A.J., Grande, D.A., Todhunter, R.J., Minor, R.M., Erb, H.and Lust, G. (1994), *Chondrocyte-fibrin matrix transplants for resurfacing extensive articular cartilage defects.* Journal of Orthopaedic Research, 12(4): p. 485-497.

37. Tang, X.Z., Kumar, P., Alavi, S.and Sandeep, K.P. (2011), *Recent Advances in Biopolymers and Biopolymer-Based Nanocomposites for Food Packaging Materials.* Critical Reviews in Food Science and Nutrition, 52(5): p. 426-442.

38. Navarro, M., Michiardi, A., Castaño, O.and Planell, J.A. (2008), *Biomaterials in orthopaedics.* Journal of The Royal Society Interface, 5(27): p. 1137-1158.

39. Ramakrishna, S., Mayer, J., Wintermantel, E.and Leong, K.W. (2001), *Biomedical applications of polymer-composite materials: a review.* Composites Science and Technology, 61(9): p. 1189-1224.

40. d'Ayala, G.G., Malinconico, M.and Laurienzo, P. (2008), *Marine derived polysaccharides for biomedical applications: chemical modification approaches.* Molecules (Basel, Switzerland), 13(9): p. 2069-2106.

41. Updegraff, D.M. (1969), *Semimicro determination of cellulose inbiological materials.* Analytical Biochemistry, 32(3): p. 420-424.

42. Luo, K., Yin, J., Khutoryanskaya, O.V.and Khutoryanskiy, V.V. (2008), *Mucoadhesive and Elastic Films Based on Blends of Chitosan and Hydroxyethylcellulose.* Macromolecular Bioscience, 8(2): p. 184-192.

43. Baldwin, A.D. and Kiick, K.L. (2010), *Polysaccharide-Modified Synthetic Polymeric Biomaterials.* Biopolymers, 94(1): p. 128-140.

44.   Blaine, M.G. (1947), *Experimental Observations on Absorbable Alginate Products in Surgery*.* Annals of Surgery, 125(1): p. 102-114.

45.   Moon, R.J., Martini, A., Nairn, J., Simonsen, J.and Youngblood, J. (2011), *Cellulose nanomaterials review: structure, properties and nanocomposites.* Chemical Society Reviews, 40(7): p. 3941-3994.

46.   Krässig, H.A. (1993), *Cellulose: Structure, Accessibility and Reactivity*. Gordon and Breach Science Publishers.

47.   Revol, J.F., Bradford, H., Giasson, J., Marchessault, R.H.and Gray, D.G. (1992), *Helicoidal self-ordering of cellulose microfibrils in aqueous suspension.* Int J Biol Macromol, 14(3): p. 170-2.

48.   Eichhorn, S., Dufresne, A., Aranguren, M., Marcovich, N., Capadona, J., Rowan, S., Weder, C., Thielemans, W., Roman, M., Renneckar, S., Gindl, W., Veigel, S., Keckes, J., Yano, H., Abe, K., Nogi, M., Nakagaito, A., Mangalam, A., Simonsen, J., Benight, A., Bismarck, A., Berglund, L.and Peijs, T. (2010), *Review: current international research into cellulose nanofibres and nanocomposites.* Journal of Materials Science, 45(1): p. 1-33.

49.   Shanmuganathan, K., Capadona, J.R., Rowan, S.J.and Weder, C. (2010), *Bio-inspired mechanically-adaptive nanocomposites derived from cotton cellulose whiskers.* Journal of Materials Chemistry, 20(1): p. 180-186.

50.   Garcia de Rodriguez, N.L., Thielemans, W.and Dufresne, A. (2006), *Sisal cellulose whiskers reinforced polyvinyl acetate nanocomposites.* Cellulose, 13(3): p. 261-270.

51.   Habibi, Y., Goffin, A.-L., Schiltz, N., Duquesne, E., Dubois, P.and Dufresne, A. (2008), *Bionanocomposites based on poly([varepsilon]-caprolactone)-grafted cellulose nanocrystals by ring-opening polymerization.* Journal of Materials Chemistry, 18(41): p. 5002-5010.

52.   Petersson, L., Kvien, I.and Oksman, K. (2007), *Structure and thermal properties of poly(lactic acid)/cellulose whiskers nanocomposite materials.* Composites Science and Technology, 67(11-12): p. 2535-2544.

53.   Tashiro, K. and Kobayashi, M. (1991), *Theoretical evaluation of 3-dimensional elastic-constants of native and regenerated celluloses-Role of hydrogen bonds.* Polymer, 32(8): p. 1516-1530.

54.   Rusli, R. and Eichhorn, S.J. (2008), *Determination of the stiffness of cellulose nanowhiskers and the fiber-matrix interface in a nanocomposite using Raman spectroscopy.* Applied Physics Letters, 93(3): p. 033111-3.

55.   David E. Henton, P.G., Jim Lunt, and Jed Randall (2005), *Polylactic Acid Technology.* Natural Fibers, Biopolymers, and Biocomposites , CRC Press, USA, Edition-1: p. Chapter 16, 524-577.

56.   Dorgan, J.R., Lehermeier, H.and Mang, M. (2000), *Thermal and Rheological Properties of Commercial-Grade Poly(Lactic Acid)s.* Journal of Polymers and the Environment, 8(1): p. 1-9.

57.   Drumright, R.E., P. R. Gruber, et al. (2000), *Polylactic Acid Technology.* Advanced Materials 12(23): p. 1841-1846.

58.   Gupta, B., Revagade, N.and Hilborn, J. (2007), *Poly(lactic acid) fiber: An overview.* Progress in Polymer Science, 32(4): p. 455-482.

59. Auras, R., Harte, B.and Selke, S. (2004), *An Overview of Polylactides as Packaging Materials.* Macromolecular Bioscience, 4(9): p. 835-864.

60. Avinc, O. and Khoddami, A. (2009), *Overview of Poly(lactic acid) (PLA) Fibre.* Fibre Chemistry, 41(6): p. 391-401.

61. Ahmed, I., Cronin, P.S., Abou Neel, E.A., Parsons, A.J., Knowles, J.C.and Rudd, C.D. (2009), *Retention of mechanical properties and cytocompatibility of a phosphate-based glass fiber/polylactic acid composite.* J Biomed Mater Res B Appl Biomater, 89(1): p. 18-27.

62. Ahmed, I., Jones, I., Parsons, A., Bernard, J., Farmer, J., Scotchford, C., Walker, G.and Rudd, C. (2011), *Composites for bone repair: phosphate glass fibre reinforced PLA with varying fibre architecture.* Journal of Materials Science: Materials in Medicine, 22(8): p. 1825-1834.

63. Oksman, K., Skrifvars, M.and Selin, J.F. (2003), *Natural fibres as reinforcement in polylactic acid (PLA) composites.* Composites Science and Technology, 63(9): p. 1317-1324.

64. Wollerdorfer, M. and Bader, H. (1998), *Influence of natural fibres on the mechanical properties of biodegradable polymers.* Industrial Crops and Products, 8(2): p. 105-112.

65. Garlotta, D. (2001), *A Literature Review of Poly(Lactic Acid).* Journal of Polymers and the Environment, 9(2): p. 63-84.

66. Athanasiou, K.A., Agrawal, C.M., Barber, F.A.and Burkhart, S.S. (1998), *Orthopaedic applications for PLA-PGA biodegradable polymers.* Arthroscopy: The Journal of Arthroscopic & Related Surgery, 14(7): p. 726-737.

67. Waris, E., Ashammakhi, N., Kaarela, O., Raatikainen, T.and Vasenius, J. (2004), *Use of Bioabsorbable Osteofixation Devices in the Hand.* Journal of Hand Surgery (British and European Volume), 29(6): p. 590-598.

68. Maurus, P.B. and Kaeding, C.C. (2004), *Bioabsorbable implant material review.* Operative Techniques in Sports Medicine, 12(3): p. 158-160.

69. An, Y.H., Woolf, S.K.and Friedman, R.J. (2000), *Pre-clinical in vivo evaluation of orthopaedic bioabsorbable devices.* Biomaterials, 21(24): p. 2635-2652.

70. Woodruff, M.A. and Hutmacher, D.W. (2010), *The return of a forgotten polymer - Polycaprolactone in the 21st century.* Progress in Polymer Science, 35(10): p. 1217–1256.

71. Khorasani, M.T., Mirzadeh, H.and Irani, S. (2008), *Plasma surface modification of poly (l-lactic acid) and poly (lactic-co-glycolic acid) films for improvement of nerve cells adhesion.* Radiation Physics and Chemistry, 77(3): p. 280-287.

72. Morrow, F.A., Kogan, S.J., Freed, S.Z.and Laufman, H. (1974), *In vivo comparison of polyglycolic acid, chromic catgut and silk in tissue of the genitourinary tract: an experimental study of tissue retrieval and calculogenesis.* J Urol, 112(5): p. 655-8.

73. Kohane, D.S., Tse, J.Y., Yeo, Y., Padera, R., Shubina, M.and Langer, R. (2006), *Biodegradable polymeric microspheres and nanospheres for drug delivery in the peritoneum.* J Biomed Mater Res A, 77(2): p. 351-61.

74. Eling, B., Gogolewski, S.and Pennings, A.J. (1982), *Biodegradable materials of poly(l-lactic acid): 1. Melt-spun and solution-spun fibres.* Polymer, 23(11): p. 1587-1593.

75. Leenslag, J.W. and Pennings, A.J. (1987), *High-strength poly(l-lactide) fibres by a dry-spinning/hot-drawing process.* Polymer, 28(10): p. 1695-1702.

76. Kim, K., Yu, M., Zong, X., Chiu, J., Fang, D., Seo, Y.-S., Hsiao, B.S., Chu, B.and Hadjiargyrou, M. (2003), *Control of degradation rate and hydrophilicity in electrospun non-woven poly(d,l-lactide) nanofiber scaffolds for biomedical applications.* Biomaterials, 24(27): p. 4977-4985.

77. Liu, D., Yuan, X.and Bhattacharyya, D. (2012), *The effects of cellulose nanowhiskers on electrospun poly (lactic acid) nanofibres.* Journal of Materials Science, 47(7): p. 3159-3165.

78. Fambri, L., Pegoretti, A., Fenner, R., Incardona, S.D.and Migliaresi, C. (1997), *Biodegradable fibres of poly(l-lactic acid) produced by melt spinning.* Polymer, 38(1): p. 79-85.

79. Penning, J.P., Dijkstra, H.and Pennings, A.J. (1993), *Preparation and properties of absorbable fibres from l-lactide copolymers.* Polymer, 34(5): p. 942-951.

80. Incardona, S.D., Fambri, L.and Migliaresi, C. (1996), *Poly-L-lactic acid braided fibres produced by melt spinning: characterization and in vitro degradation.* Journal of Materials Science: Materials in Medicine, 7(7): p. 387-391.

81. Mezghani, K. and Spruiell, J.E. (1998), *High speed melt spinning of poly(L-lactic acid) filaments.* Journal of Polymer Science Part B: Polymer Physics, 36(6): p. 1005-1012.

82. Yuan, X., Mak, A.F.T., Kwok, K.W., Yung, B.K.O.and Yao, K. (2001), *Characterization of poly(L-lactic acid) fibers produced by melt spinning.* Journal of Applied Polymer Science, 81(1): p. 251-260.

83. Kim, I.-H., Lee, S.and Jeong, Y. (2009), *Tensile behavior and structural evolution of poly(lactic acid) monofilaments in glass transition region.* Fibers and Polymers, 10(5): p. 687-693.

84. Okuzaki, H., Kubota, I.and Kunugi, T. (1999), *Mechanical properties and structure of the zone-drawn poly(L-lactic acid) fibers.* Journal of Polymer Science Part B: Polymer Physics, 37(10): p. 991-996.

85. Gao, C., Yu, L., Liu, H.and Chen, L. (2012), *Development of self-reinforced polymer composites.* Progress in Polymer Science, 37(6): p. 767-780.

86. Kmetty, Á., Bárány, T.and Karger-Kocsis, J. (2010), *Self-reinforced polymeric materials: A review.* Progress in Polymer Science, 35(10): p. 1288-1310.

87. Capiati, N. and Porter, R. (1975), *The concept of one polymer composites modelled with high density polyethylene.* Journal of Materials Science, 10(10): p. 1671-1677.

88. Törmälä, P., Pohjonen, T.and Rokkanen, P. (1997), *Ultrahigh-strength self-reinforced polylactide composites and their surgical applications.* Macromolecular Symposia, 123(1): p. 123-131.

89. Ashammakhi, N., Peltoniemi, H., Waris, E., Suuronen, R., Serlo, W., Kellomaki, M., Tormala, P.and Waris, T. (2001), *Developments in*

craniomaxillofacial surgery: use of self-reinforced bioabsorbable osteofixation devices. Plast Reconstr Surg, 108(1): p. 167-80.

90. Hine, P.J., Ward, I.M., Olley, R.H.and Bassett, D.C. (1993), *The hot compaction of high modulus melt-spun polyethylene fibres.* Journal of Materials Science, 28(2): p. 316-324.

91. Da Silva Perez, D., Tapin-Lingua, S., Lavalette, A., Barbosa, T., Gonzalez, I., Siqueira, G., Bras, J.and Dufresne, A. (2010), *Impact of micro/nano-fibrillated cellulose preparation on the reinforcement properties of paper and composites.* International Conference on Nanotechnology for the forest product industry, Finland.

92. Deng, M. and Shalaby, S.W. (1997), *Properties of self-reinforced ultra-high-molecular-weight polyethylene composites.* Biomaterials, 18(9): p. 645-655.

93. Devaux, E. and Cazé, C. (1999), *Composites of ultra-high-molecular-weight polyethylene fibres in a low-density polyethylene matrix: II. Fibre/matrix adhesion.* Composites Science and Technology, 59(6): p. 879-882.

94. Hine, P.J., Unwin, A.P.and Ward, I.M. (2011), *The use of an interleaved film for optimising the properties of hot compacted polyethylene single polymer composites.* Polymer, 52(13): p. 2891-2898.

95. Hine, P.J., Ward, I.M., Jordan, N.D., Olley, R.and Bassett, D.C. (2003), *The hot compaction behaviour of woven oriented polypropylene fibres and tapes. I. Mechanical properties.* Polymer, 44(4): p. 1117-1131.

96. Ward, I.M. and Hine, P.J. (2004), *The science and technology of hot compaction.* Polymer, 45(5): p. 1413-1427.

97. Hine, P.J. and Ward, I.M. (2004), *Hot compaction of woven poly(ethylene terephthalate) multifilaments.* Journal of Applied Polymer Science, 91(4): p. 2223-2233.

98. Hine, P.J. and Ward, I.M. (2006), *Hot compaction of woven nylon 6,6 multifilaments.* Journal of Applied Polymer Science, 101(2): p. 991-997.

99. Barkoula, N.-M., Peijs, T., Schimanski, T.and Loos, J. (2005), *Processing of single polymer composites using the concept of constrained fibers.* Polymer Composites, 26(1): p. 114-120.

100. Wright-Charlesworth, D.D., Miller, D.M., Miskioglu, I.and King, J.A. (2005), *Nanoindentation of injection molded PLA and self-reinforced composite PLA after in vitro conditioning for three months.* Journal of Biomedical Materials Research Part A, 74A(3): p. 388-396.

101. Majola, A., Vainionpää, S., Rokkanen, P., Mikkola, H.M.and Törmälä, P. (1992), *Absorbable self-reinforced polylactide (SR-PLA) composite rods for fracture fixation: strength and strength retention in the bone and subcutaneous tissue of rabbits.* Journal of Materials Science: Materials in Medicine, 3(1): p. 43-47.

102. Törmälä, P., Vasenius, J., Vainionpää, S., Laiho, J., Pohjonen, T.and Rokkanen, P. (1991), *Ultra-high-strength absorbable self-reinforced polyglycolide (SR-PGA) composite rods for internal fixation of bone fractures: In vitro and in vivo study.* Journal of Biomedical Materials Research, 25(1): p. 1-22.

103. Vainionpää, S., Kilpikari, J., Laiho, J., Helevirta, P., Rokkanen, P.and Törmälä, P. (1987), *Strength and strength retention vitro, of absorbable, self-reinforced polyglycolide (PGA) rods for fracture fixation.* Biomaterials, 8(1): p. 46-48.

104. Wright, D.D., Gilbert, J.L.and Lautenschlager, E.P. (1999), *The effect of processing temperature and time on the structure and fracture characteristics of self-reinforced composite poly(methyl methacrylate).* Journal of Materials Science: Materials in Medicine, 10(8): p. 503-512.

105. Wright, D.D., Lautenschlager, E.P.and Gilbert, J.L. (1997), *Bending and fracture toughness of woven self-reinforced composite poly(methyl methacrylate).* Journal of Biomedical Materials Research, 36(4): p. 441-453.

106. Ward, I.M. and Hine, P.J. (1997), *Novel composites by hot compaction of fibers.* Polymer Engineering & Science, 37(11): p. 1809-1814.

107. Törmälä, P., Pohjonen, T.and Rokkanen, P. (1998), *Bioabsorbable polymers: materials technology and surgical applications.* Proceedings of the Institution of Mechanical Engineers - H, 212(2): p. 101 - 111.

108. Kmetty, Ã.k., BÃ¡rÃ¡ny, T.s.and Karger-Kocsis, J.z. (2010), *Self-reinforced polymeric materials: A review.* Progress in Polymer Science, 35(10): p. 1288-1310.

109. Wang, H.P., Chum, S.P., Hiltner, A.and Baer, E. (2009), *Deformation of elastomeric polyolefin spherulites.* Journal of Polymer Science Part B: Polymer Physics, 47(13): p. 1313-1330.

110. Niemelä, T., Niiranen, H., Kellomäki, M.and Törmälä, P. (2005), *Self-reinforced composites of bioabsorbable polymer and bioactive glass with different bioactive glass contents. Part I: Initial mechanical properties and bioactivity.* Acta Biomaterialia, 1(2): p. 235-242.

111. Niiranen, H., Pyhältö, T., Rokkanen, P., Kellomäki, M.and Törmälä, P. (2004), *In vitro and in vivo behavior of self-reinforced bioabsorbable polymer and self-reinforced bioabsorbable polymer/bioactive glass composites.* Journal of Biomedical Materials Research Part A, 69A(4): p. 699-708.

112. Hu, Y.S., Zhang, P.Z., Song, D., Wang, Y.M.and Bai, D.R. (2000), *Preparation and Properties of Self-reinforced L- and D,L-lactide Copolymer Rods.* Chinese Chemical Letters 11(11): p. 1023–1026.

113. Niemela, T. (2005), *Effect of Î²-tricalcium phosphate addition on the in vitro degradation of self-reinforced poly-l,d-lactide.* Polymer Degradation and Stability, 89(3): p. 492-500.

114. Waris, T., Pohjonen, T.and Törmälä, P. (1994), *Self-reinforced absorbable polylactide (SR-PLLA) plates in craniofacial surgery.* European Journal of Plastic Surgery, 17(5): p. 236-238.

115. Karen, C. (2010), *Natural Fiber Composites in Biomedical and Bioengineering Applications*, in *Multifunctional Polymer Nanocomposites*CRC Press. p. 283-308.

116. Kalia, S., Dufresne, A., Cherian, B.M., Kaith, B.S., Averous, L., Njuguna, J.and Nassiopoulos, E. (2011), *Cellulose-Based Bio- and Nanocomposites: A Review.* International Journal of Polymer Science.

117. Siqueira, G., Bras, J.and Dufresne, A. (2010), *Cellulosic Bionanocomposites: A Review of Preparation, Properties and Applications.* Polymers, 2(4): p. 728-765.

118. Dweib, M.A., Hu, B., Shenton Iii, H.W.and Wool, R.P. (2006), *Bio-based composite roof structure: Manufacturing and processing issues.* Composite Structures, 74(4): p. 379-388.

119. Burgueño, R., Quagliata, M., Mehta, G., Mohanty, A., Misra, M.and Drzal, L. (2005), *Sustainable Cellular Biocomposites from Natural Fibers and Unsaturated Polyester Resin for Housing Panel Applications.* Journal of Polymers and the Environment, 13(2): p. 139-149.

120. Shah, J. and Malcolm Brown, R., Jr. (2005), *Towards electronic paper displays made from microbial cellulose.* Applied Microbiology and Biotechnology, 66(4): p. 352-355.

121. Evans, B.R., O'Neill, H.M., Malyvanh, V.P., Lee, I.and Woodward, J. (2003), *Palladium-bacterial cellulose membranes for fuel cells.* Biosensors and Bioelectronics, 18(7): p. 917-923.

122. Barud, H.S., Souza, J.L., Santos, D.B., Crespi, M.S., Ribeiro, C.A., Messaddeq, Y.and Ribeiro, S.J.L. (2011), *Bacterial cellulose/poly(3-hydroxybutyrate) composite membranes.* Carbohydrate Polymers, 83(3): p. 1279-1284.

123. Eichhorn, S.J. (2011), *Cellulose nanowhiskers: promising materials for advanced applications.* Soft Matter, 7(2): p. 303-315.

124. Woodhams, R.T., Thomas, G.and Rodgers, D.K. (1984), *Wood fibers as reinforcing fillers for polyolefins.* Polymer Engineering & Science, 24(15): p. 1166-1171.

125. Belgacem, M.N. and Gandini, A. (2008), *Surface modification of cellulose fibres*. Monomers, polymers and composites from renewable resources, ed. M.N. Belgacem and A. GandiniAmsterdam: Elsevier.

126. Belgacem, M.N. and Gandini, A. (2009), *Natural fibre-surface modificaiton and characterisation*. Cellulose Fibre Reinforced Polymer Composites, ed. T. Sabu and L.A. PothanPhiladelphia: Old City Publishing.

127. Thielemans, W. and Wool, R.P. (2004), *Butyrated kraft lignin as compatibilizing agent for natural fiber reinforced thermoset composites.* Composites, Part A, 35A(3): p. 327-338.

128. Thielemans, W. and Wool, R.P. (2005), *Kraft lignin as fiber treatment for natural fiber-reinforced composites.* Polymer Composites, 26(5): p. 695-705.

129. Binder, W.H. and Sachsenhofer, R. (2007), *'Click' Chemistry in Polymer and Materials Science.* Macromolecular Rapid Communications, 28(1): p. 15-54.

130. Ly, E.H.B., Bras, J., Sadocco, P., Belgacem, M.N., Dufresne, A.and Thielemans, W. (2010), *Surface functionalization of cellulose by grafting oligoether chains.* Materials Chemistry and Physics, 120(2-3): p. 438-445.

131. Paquet, O., Krouit, M., Bras, J., Thielemans, W.and Belgacem, M.N. (2010), *Surface modification of cellulose by PCL grafts.* Acta Materialia, 58(3): p. 792-801.

132. Frone, A.N., Berlioz, S., Chailan, J.F., Panaitescu, D.M.and Donescu, D. (2011), *Cellulose Fiber-Reinforced Polylactic Acid.* Polymer Composites, 32(6): p. 976-985.

133. Kim, J.T. and Netravali, A.N. (2010), *Mercerization of sisal fibers: Effect of tension on mechanical properties of sisal fiber and fiber-reinforced composites.* Composites Part a-Applied Science and Manufacturing, 41(9): p. 1245-1252.

134. Li, Y., Mai, Y.W.and Ye, L. (2000), *Sisal fibre and its composites: a review of recent developments.* Composites Science and Technology, 60(11): p. 2037-2055.

135. Beshay, A.D., Kokta, B.V.and Daneault, C. (1985), *Use of wood fibers in thermoplastic composites II: Polyethylene.* Polymer Composites, 6(4): p. 261-271.

136. Maldas, D., Kokta, B.V.and Daneault, C. (1989), *Composites of polyvinyl chloride—wood fibers: IV. Effect of the nature of fibers.* Journal of Vinyl Technology, 11(2): p. 90-99.

137. Kokta, B.V., Maldas, D., Daneault, C.and Béland, P. (1990), *Composites of poly(vinyl chloride) and wood fibers. Part II: Effect of chemical treatment.* Polymer Composites, 11(2): p. 84-89.

138. Maldas, D. and Kokta, B.V. (1993), *Performance of hybrid reinforcements in PVC composites. II: Use of surface-modified mica and different cellulosic materials as reinforcements.* Journal of Vinyl Technology, 15(1): p. 38-44.

139. Raj, R.G., Kokta, B.V., Maldas, D.and Daneault, C. (1988), *Use of wood fibers in thermoplastic composites: VI. Isocyanate as a bonding agent for polyethylene–wood fiber composites.* Polymer Composites, 9(6): p. 404-411.

140. Arbelaiz, A., Fernández, B., Cantero, G., Llano-Ponte, R., Valea, A.and Mondragon, I. (2005), *Mechanical properties of flax fibre/polypropylene composites. Influence of fibre/matrix modification and glass fibre hybridization.* Composites Part A: Applied Science and Manufacturing, 36(12): p. 1637-1644.

141. Blaker, J.J., Lee, K.Y.and Bismarck, A. (2011), *Hierarchical Composites Made Entirely from Renewable Resources.* Journal of Biobased Materials and Bioenergy, 5(1): p. 1-16.

142. Williams, G.I. and Wool, R.P. (2000), *Composites from natural fibers and soy oil resins.* Applied Composite Materials, 7(5-6): p. 421-432.

143. Wool, R.P., Khot, S.N., LaScala, J.J., Bunker, S.P., Lu, J., Thielemans, W., Can, E., Morye, S.S.and Williams, G.I. (2002), *Affordable composites and plastics from renewable resources: part II: manufacture of composites.* ACS Symp. Ser., 823(Advancing Sustainability through Green Chemistry and Engineering): p. 205-224.

144. Espinoza-Perez, J.D., Ulven, C.A.and Wiesenborn, D.P. (2010), *EPOXIDIZED HIGH-OLEIC VEGETABLE OILS APPLIED TO COMPOSITES.* Transactions of the Asabe, 53(4): p. 1167-1174.

145. Adekunle, K., Akesson, D.and Skrifvars, M. (2010), *Biobased Composites Prepared by Compression Molding with a Novel Thermoset Resin from Soybean Oil and a Natural-Fiber Reinforcement.* Journal of Applied Polymer Science, 116(3): p. 1759-1765.

146. Akesson, D., Skrifvars, M.and Walkenstrom, P. (2009), *Preparation of Thermoset Composites from Natural Fibres and Acrylate Modified Soybean Oil Resins.* Journal of Applied Polymer Science, 114(4): p. 2502-2508.

147. Graupner, N., Herrmann, A.S.and Mussig, J. (2009), *Natural and man-made cellulose fibre-reinforced poly(lactic acid) (PLA) composites: An overview about mechanical characteristics and application areas.* Composites Part a-Applied Science and Manufacturing, 40(6-7): p. 810-821.

148. Mukherjee, T. and Kao, N. (2011), *PLA Based Biopolymer Reinforced with Natural Fibre: A Review.* Journal of Polymers and the Environment, 19(3): p. 714-725.

149. Wu, C.S. (2009), *Renewable resource-based composites of recycled natural fibers and maleated polylactide bioplastic: Characterization and biodegradability.* Polymer Degradation and Stability, 94(7): p. 1076-1084.

150. Reddy, N. and Yang, Y.Q. (2011), *Completely biodegradable soyprotein-jute biocomposites developed using water without any chemicals as plasticizer.* Industrial Crops and Products, 33(1): p. 35-41.

151. Batista, K.C., Silva, D.A.K., Coelho, L.A.F., Pezzin, S.H.and Pezzin, A.P.T. (2010), *Soil Biodegradation of PHBV/Peach Palm Particles Biocomposites.* Journal of Polymers and the Environment, 18(3): p. 346-354.

152. Macedo, J.D., Costa, M.F., Tavares, M.I.B.and Thire, R. (2010), *Preparation and Characterization of Composites Based on Polyhydroxybutyrate and Waste Powder From Coconut Fibers Processing.* Polymer Engineering and Science, 50(7): p. 1466-1475.

153. Jiang, L., Chen, F., Qian, J., Huang, J.J., Wolcott, M., Liu, L.S.and Zhang, J.W. (2010), *Reinforcing and Toughening Effects of Bamboo Pulp Fiber on Poly(3-hydroxybutyrate-co-3-hydroxyvalerate) Fiber Composites.* Industrial & Engineering Chemistry Research, 49(2): p. 572-577.

154. Reddy, N. and Yang, Y.Q. (2011), *Biocomposites developed using water-plasticized wheat gluten as matrix and jute fibers as reinforcement.* Polymer International, 60(4): p. 711-716.

155. Bax, B. and Müssig, J. (2008), *Impact and tensile properties of PLA/Cordenka and PLA/flax composites.* Composites Science and Technology, 68(7-8): p. 1601-1607.

156. Plackett, D., Løgstrup Andersen, T., Batsberg Pedersen, W.and Nielsen, L. (2003), *Biodegradable composites based on l-polylactide and jute fibres.* Composites Science and Technology, 63(9): p. 1287-1296.

157. Turbak, A.F.S., F. W.; Sandberg, K. R., (1983), *Microfibrilated cellulose, a new cellulose product: properties, uses, and commercial potential.* Journal of Applied Polymer Science: Applied Polymer Symposium, 37(815-827).

158. Nickerson, R.F. and Habrle, J.A. (1947), *Cellulose intercrystalline structures-study by hydrolytic methods.* J. Ind. Eng. Chem. (Washington, D. C.), 39: p. 1507-12.

159. Favier, V., Canova, G.R., Cavaille, J.Y., Chanzy, H., Dufresne, A.and Gauthier, C. (1995), *Nanocomposite materials from latex and cellulose whiskers.* Polymers for Advanced Technologies, 6(5): p. 351-355.

160. Mathew, A.P., Thielemans, W.and Dufresne, A. (2008), *Mechanical properties of nanocomposites from sorbitol plasticized starch and tunicin whiskers.* Journal of Applied Polymer Science, 109(6): p. 4065-4074.

161. Orts, W.J., Shey, J., Imam, S.H., Glenn, G.M., Guttman, M.E.and Revol, J.-F. (2005), *Application of Cellulose Microfibrils in Polymer Nanocomposites.* Journal of Polymers and the Environment, 13(4): p. 301-306.

162. Kohler, R. and Nebel, K. (2006), *Cellulose-Nanocomposites: Towards High Performance Composite Materials.* Macromolecular Symposia, 244(1): p. 97-106.

163. de Rodriguez, N.L.G., Thielemans, W.and Dufresne, A. (2006), *Sisal cellulose whiskers reinforced polyvinyl acetate nanocomposites.* Cellulose, 13(3): p. 261-270.

164. Brown, E.E. and Laborie, M.-P.G. (2007), *Bioengineering Bacterial Cellulose/Poly(ethylene oxide) Nanocomposites.* Biomacromolecules, 8(10): p. 3074-3081.

165. Leitner, J., Hinterstoisser, B., Wastyn, M., Keckes, J.and Gindl, W. (2007), *Sugar beet cellulose nanofibril-reinforced composites.* Cellulose, 14(5): p. 419-425.

166. Hossain, K.M.Z., Ahmed, I., Parsons, A., Scotchford, C., Walker, G., Thielemans, W.and Rudd, C. (2012), *Physico-chemical and mechanical properties of nanocomposites prepared using cellulose nanowhiskers and poly(lactic acid).* Journal of Materials Science, 47(6): p. 2675-2686.

167. de Mesquita, J.o.P., Donnici, C.L.and Pereira, F.V. (2010), *Biobased Nanocomposites from Layer-by-Layer Assembly of Cellulose Nanowhiskers with Chitosan.* Biomacromolecules, 11(2): p. 473-480.

168. Bonne, M.J., Edler, K.J., Buchanan, J.G., Wolverson, D., Psillakis, E., Helton, M., Thielemans, W.and Marken, F. (2008), *Thin-film modified electrodes with reconstituted cellulose-PDDAC films for the accumulation and detection of triclosan.* Journal of Physical Chemistry C, 112(7): p. 2660-2666.

169. Bonne, M.J., Galbraith, E., James, T.D., Wasbrough, M.J., Edler, K.J., Jenkins, A.T.A., Helton, M., McKee, A., Thielemans, W., Psillakis, E.and Marken, F. (2010), *Boronic acid dendrimer receptor modified nanofibrillar cellulose membranes.* Journal of Materials Chemistry, 20(3): p. 588-594.

170. Tsourounaki, K., Bonne, M.J., Thielemans, W., Psillakis, E., Helton, M., McKee, A.and Marken, F. (2008), *Nanofibrillar Cellulose-Chitosan Composite Film Electrodes: Competitive Binding of Triclosan, Fe(CN)(6)(3-/4-), and SDS Surfactant.* Electroanalysis, 20(22): p. 2395-2402.

171. Sanchez-Garcia, M. and Lagaron, J. (2010), *On the use of plant cellulose nanowhiskers to enhance the barrier properties of polylactic acid.* Cellulose, 17(5): p. 987-1004.

172. Oksman, K., Mathew, A.P., Bondeson, D.and Kvien, I. (2006), *Manufacturing process of cellulose whiskers/polylactic acid nanocomposites.* Composites Science and Technology, 66(15): p. 2776-2784.

173. Jonoobi, M., Harun, J., Mathew, A.P.and Oksman, K. (2010), *Mechanical properties of cellulose nanofiber (CNF) reinforced polylactic acid (PLA) prepared by twin screw extrusion.* Composites Science and Technology, 70(12): p. 1742-1747.

174. Li, Q., Zhou, J.and Zhang, L. (2009), *Structure and properties of the nanocomposite films of chitosan reinforced with cellulose whiskers.* Journal of Polymer Science Part B: Polymer Physics, 47(11): p. 1069-1077.

175. Zhou, C., Wu, Q., Yue, Y.and Zhang, Q. (2011), *Application of rod-shaped cellulose nanocrystals in polyacrylamide hydrogels.* Journal of Colloid and Interface Science, 353(1): p. 116-123.

176. Heath, L. and Thielemans, W. (2010), *Cellulose nanowhisker aerogels.* Green Chemistry, 12(8): p. 1448-1453.

177. Yano, H., Sugiyama, J., Nakagaito, A.N., Nogi, M., Matsuura, T., Hikita, M.and Handa, K. (2005), *Optically Transparent Composites Reinforced with Networks of Bacterial Nanofibers.* Advanced Materials, 17(2): p. 153-155.

178. Watanabe, Y., Mukai, B., Kawamura, K.I., Ishikawa, T., Namiki, M., Utoguchi, N.and Fujii, M. (2002), *Preparation and evaluation of press-coated aminophylline tablet using crystalline cellulose and polyethylene glycol in the outer shell for timed-release dosage forms.* Yakugaku Zasshi, 122(2): p. 157-162.

179. Ni, H., Zeng, S., Wu, J., Cheng, X., Luo, T., Wang, W., Zeng, W.and Chen, Y. (2012), *Cellulose nanowhiskers: Preparation, characterization and cytotoxicity evaluation.* Bio-Medical Materials and Engineering, 22(1): p. 121-127.

180. Clift, M.J.D., Foster, E.J., Vanhecke, D., Studer, D., Wick, P., Gehr, P., Rothen-Rutishauser, B.and Weder, C. (2011), *Investigating the Interaction of Cellulose Nanofibers Derived from Cotton with a Sophisticated 3D Human Lung Cell Coculture.* Biomacromolecules, 12(10): p. 3666-3673.

181. Mahmoud, K.A., Mena, J.A., Male, K.B., Hrapovic, S., Kamen, A.and Luong, J.H.T. (2010), *Effect of Surface Charge on the Cellular Uptake and Cytotoxicity of Fluorescent Labeled Cellulose Nanocrystals.* ACS Applied Materials & Interfaces, 2(10): p. 2924-2932.

182. Petersson, L. and Oksman, K. (2006), *Biopolymer based nanocomposites: Comparing layered silicates and microcrystalline cellulose as nanoreinforcement.* Composites Science and Technology, 66(13): p. 2187-2196.

183. Azami, M., Orang, F.and Moztarzadeh, F.(2006), *Nanocomposite bone tissue-engineering scaffolds prepared from gelatin and hydroxyapatite*

using layer solvent casting and freeze-drying technique. in *International Conference on Biomedical and Pharmaceutical Engineering*. Singapore

184. Ma, Z.W., Kotaki, M., Inai, R.and Ramakrishna, S. (2005), *Potential of nanofiber matrix as tissue-engineering scaffolds.* TISSUE ENGINEERING, 11(1-2): p. 101-109.

185. McCullen, S.D., Ramaswamy, S., Clarke, L.I.and Gorga, R.E. (2009), *Nanofibrous composites for tissue engineering applications.* Wiley Interdisciplinary Reviews: Nanomedicine and Nanobiotechnology, 1(4): p. 369-390.

186. Kümmerer, K., Menz, J., Schubert, T.and Thielemans, W. (2011), *Biodegradability of organic nanoparticles in the aqueous environment.* Chemosphere, 82(10): p. 1387-1392.

187. Miyamoto, T., Takahashi, S., Ito, H., Inagaki, H.and Noishiki, Y. (1989), *Tissue biocompatibility of cellulose and its derivatives.* J Biomed Mater Res, 23(1): p. 125-33.

188. Luo, L.H., Wang, X.M., Zhang, Y.F., Liu, Y.M., Chang, P.R., Wang, Y.and Chen, Y. (2008), *Physical properties and biocompatibility of cellulose/soy protein isolate membranes coagulated from acetic aqueous solution.* J Biomater Sci Polym Ed, 19(4): p. 479-96.

189. Dufresne, A., Kellerhals, M.B.and Witholt, B. (1999), *Transcrystallization in Mcl-PHAs/Cellulose Whiskers Composites.* Macromolecules, 32(22): p. 7396-7401.

190. Habibi, Y., Chanzy, H.and Vignon, M. (2006), *TEMPO-mediated surface oxidation of cellulose whiskers.* Cellulose, 13(6): p. 679-687.

191. Morin, A. and Dufresne, A. (2002), *Nanocomposites of Chitin Whiskers from Riftia Tubes and Poly(caprolactone).* Macromolecules, 35(6): p. 2190-2199.

192. Zuluaga, R., Putaux, J.-L., Restrepo, A., Mondragon, I.and Gañán, P. (2007), *Cellulose microfibrils from banana farming residues: isolation and characterization.* Cellulose, 14(6): p. 585-592.

193. Felfel, R.M., Ahmed, I., Parsons, A.J., Haque, P., Walker, G.S.and Rudd, C.D. (2012), *Investigation of Crystallinity, Molecular Weight Change, and Mechanical Properties of PLA/PBG Bioresorbable Composites as Bone Fracture Fixation Plates.* Journal of Biomaterials Applications, 26(7): p. 765-789.

194. Parsons, A.J., Ahmed, I., Haque, P., Fitzpatrick, B., Niazi, M.I.K., Walker, G.S.and Rudd, C.D. (2009), *Phosphate Glass Fibre Composites for Bone Repair.* Journal of Bionic Engineering, 6(4): p. 318-323.

195. Gattin, R., Copinet, A., Bertrand, C.and Couturier, Y. (2002), *Biodegradation study of a starch and poly(lactic acid) co-extruded material in liquid, composting and inert mineral media.* International Biodeterioration & Biodegradation, 50(1): p. 25-31.

196. Martin, O. and Avérous, L. (2001), *Poly(lactic acid): plasticization and properties of biodegradable multiphase systems.* Polymer, 42(14): p. 6209-6219.

197. Sriupayo, J., Supaphol, P., Blackwell, J.and Rujiravanit, R. (2005), *Preparation and characterization of [alpha]-chitin whisker-reinforced chitosan nanocomposite films with or without heat treatment.* Carbohydrate Polymers, 62(2): p. 130-136.

198. Bleach, N.C., Nazhat, S.N., Tanner, K.E., Kellomäki, M.and Törmälä, P. (2002), *Effect of filler content on mechanical and dynamic mechanical properties of particulate biphasic calcium phosphate--polylactide composites.* Biomaterials, 23(7): p. 1579-1585.

199. Bondeson, D. and Oksman, K. (2007), *Polylactic acid/cellulose whisker nanocomposites modified by polyvinyl alcohol.* Composites Part A: Applied Science and Manufacturing, 38(12): p. 2486-2492.

200. Liu, D.Y., Yuan, X.W., Bhattacharyya, D.and Easteal, A.J. (2010), *Characterisation of solution cast cellulose nanofibre - Reinforced poly(lactic acid).* Express Polymer Letters 4(1): p. 26-31.

201. Revol, J.F.B., H.; Giasson, J.; Marchessault, R. H.; Gray, D. G. (1992), *Helicoidal self-ordering of cellulose microfibrils in aqueous suspension.* International Journal of Biological Macromolecules, 14: p. 170-172.

202. Labet, M. and Thielemans, W. (2011), *Improving the reproducibility of chemical reactions on the surface of cellulose nanocrystals: ROP of ε-caprolactone as a case study.* Cellulose, 18(3): p. 607-617.

203. Anon (1994), *Standard test methods for void content of reinforced plastics.* ASTM D 2734-94, New York.

204. Fischer, E.W., Sterzel, H.J.and Wegner, G. (1973), *Investigation of the structure of solution grown crystals of lactide copolymers by means of chemical reactions.* Colloid & Polymer Science, 51(11): p. 980-990.

205. Khurma, J.R., Rohindra, D. R. and Devi, R. (2005), *Miscibility study of solution cast blends of poly(lactic acid) and poly(vinyl butyral).* The South Pacific Journal of Natural Science, 23: p. 22-25.

206. Segal S., C.J.J., Martin A.E., Conrad C.M. (1959), *An empirical method of estimating the degree of crystallinity of native cellulose using the X-ray diffractometer.* Textile Research Journal, 29: p. 786-794.

207. Weimer, P.J., Hackney, J.M.and French, A.D. (1995), *Effects of chemical treatments and heating on the crystallinity of celluloses and their implications for evaluating the effect of crystallinity on cellulose biodegradation.* Biotechnology and Bioengineering, 48(2): p. 169-178.

208. Elazzouzi-Hafraoui, S., Nishiyama, Y., Putaux, J.L., Heux, L., Dubreuil, F.and Rochas, C. (2008), *The shape and size distribution of crystalline nanoparticles prepared by acid hydrolysis of native cellulose.* Biomacromolecules, 9(1): p. 57-65.

209. Thielemans, W., Warbey, C.R.and Walsh, D.A. (2009), *Permselective nanostructured membranes based on cellulose nanowhiskers.* Green Chemistry, 11(4): p. 531-537.

210. Azizi Samir, M.A.S., Alloin, F.and Dufresne, A. (2005), *Review of Recent Research into Cellulosic Whiskers, Their Properties and Their Application in Nanocomposite Field.* Biomacromolecules, 6(2): p. 612-626.

211. Han, J., Zhou, C., Wu, Y., Liu, F.and Wu, Q. (2013), *Self-Assembling Behavior of Cellulose Nanoparticles during Freeze-Drying: Effect of Suspension Concentration, Particle Size, Crystal Structure, and Surface Charge.* Biomacromolecules, 14(5): p. 1529-1540.

212. Eyley, S. and Thielemans, W. (2011), *Imidazolium grafted cellulose nanocrystals for ion exchange applications.* Chemical Communications, 47(14): p. 4177-4179.

213. Chua, P., Dai, S.and Piggott, M. (1992), *Mechanical properties of the glass fibre-polyester interphase.* Journal of Materials Science, 27(4): p. 919-924.

214. Jawaid, M., Khalil, H.P.S.A., Bakar, A.A.and Khanam, P.N. (2011), *Chemical resistance, void content and tensile properties of oil palm/jute fibre reinforced polymer hybrid composites.* Materials & Design, 32(2): p. 1014-1019.

215. Mohan, R. and Kishore (1985), *Jute-Glass Sandwich Composites.* Journal of Reinforced Plastics and Composites, 4(2): p. 186-194.

216. Ndazi, B.S., Karlsson, S. (2011), *Characterization of hydrolytic degradation of polylactic acid/rice hulls composites in water at different temperatures.* Express Polymer Letters, 5(2): p. 119-131.

217. Asgari, M. and Masoomi, M. (2013), *Tensile and flexural properties of polypropylene/short poly(ethylene terephthalate) fibre composites compatibilized with glycidyl methacrylate and maleic anhydride.* Journal of Thermoplastic Composite Materials: p. 1-15.

218. Pan, N. (1996) *The Elastic Constants of Randomly Oriented Fiber Composites: A New Approach to Prediction*, in *Science and Engineering of Composite Materials*1996. p. 63.

219. Luo, J.-J. and Daniel, I.M. (2003), *Characterization and modeling of mechanical behavior of polymer/clay nanocomposites.* Composites Science and Technology, 63(11): p. 1607-1616.

220. Zhu, H., Wu, B., Li, D., Zhang, D.and Chen, Y. (2011), *Influence of Voids on the Tensile Performance of Carbon/epoxy Fabric Laminates.* Journal of Materials Science & Technology, 27(1): p. 69-73.

221. Huang, H. and Talreja, R. (2005), *Effects of void geometry on elastic properties of unidirectional fiber reinforced composites.* Composites Science and Technology, 65(13): p. 1964-1981.

222. Shumigin, D., Tarasova, E., Krumme, A.and Meier, P. (2011), *Rheological and Mechanical Properties of Poly(lactic) Acid/Cellulose and LDPE/Cellulose Composites.* Materials Science (MEDŽIAGOTYRA), 17(1): p. 32-37.

223. Menard, K.P. (2008), *Dynamic Mechanical Analysis: A Practical Introduction*. 2nd ed: CRC Press, Taylor & Francis Group.

224. Oksman, K., Etang, J.A., Mathew, A.P.and Jonoobi, M. (2011), *Cellulose nanowhiskers separated from a bio-residue from wood bioethanol production.* Biomass and Bioenergy, 35(1): p. 146-152.

225. Roman, M. and Winter, W.T. (2004), *Effect of sulphate groups from sulphuric acid hydrolysis on the thermal degradation behaviour of bacterial cellulose.* Biomacromolecules, 5: p. 1048-1054.

226. Abou-Sekkina, M.M., Sakran, M.A. and Saafan, A.A. (1986), Industrial & Engineering Chemistry Product Research and Development 25: p. 676.

227. Yasuniwa, M., Tsubakihara, S., Iura, K., Ono, Y., Dan, Y.and Takahashi, K. (2006), *Crystallization behavior of poly(l-lactic acid).* Polymer, 47(21): p. 7554-7563.

228. Shen, L., Yang, H., Ying, J., Qiao, F.and Peng, M. (2009), *Preparation and mechanical properties of carbon fiber reinforced hydroxyapatite/polylactide biocomposites.* Journal of Materials Science: Materials in Medicine, 20(11): p. 2259-2265.

229. Nurkeeva, Z.S., Mun, G.A.and Khutoryanskiy, V.V. (2003), *Interpolymer Complexes of Water-Soluble Nonionic Polysaccharides with Polycarboxylic Acids and Their Applications.* Macromolecular Bioscience, 3(6): p. 283-295.

230. Cascone, M.G., Sim, B.and Sandra, D. (1995), *Blends of synthetic and natural polymers as drug delivery systems for growth hormone.* Biomaterials, 16(7): p. 569-574.

231. Nguyen, M.K. and Lee, D.S. (2010), *Injectable Biodegradable Hydrogels.* Macromolecular Bioscience, 10(6): p. 563-579.

232. Nguyen, K.T. and West, J.L. (2002), *Photopolymerizable hydrogels for tissue engineering applications.* Biomaterials, 23(22): p. 4307-4314.

233. Chiellini, E., Cinelli, P., Fernandes, E.G., Kenawy, E.-R.S.and Lazzeri, A. (2001), *Gelatin-Based Blends and Composites. Morphological and Thermal Mechanical Characterization.* Biomacromolecules, 2(3): p. 806-811.

234. Serrero, A.l., Trombotto, S.p., Bayon, Y., Gravagna, P., Montanari, S.and David, L. (2011), *Polysaccharide-Based Adhesive for Biomedical Applications: Correlation between Rheological Behavior and Adhesion.* Biomacromolecules, 12(5): p. 1556-1566.

235. Nikolaeva, O., Budtova, T., Brestkin, Y., Zoolshoev, Z.and Frenkel, S. (1999), *Rheological properties of an interpolymer complex formed between poly(acrylic acid) and methyl cellulose.* Journal of Applied Polymer Science, 72(12): p. 1523-1528.

236. Khutoryanskiy, V.V., Cascone, M.G., Lazzeri, L., Barbani, N., Nurkeeva, Z.S., Mun, G.A.and Dubolazov, A.V. (2004), *Morphological and thermal characterization of interpolymer complexes and blends based on poly(acrylic acid) and hydroxypropylcellulose.* Polymer International, 53(3): p. 307-311.

237. Nikolaeva, O., Budtova, T., Alexeev, V.and Frenkel, S. (2000), *Interpolymer complexation between polyacrylic acid and cellulose ethers: Formation and properties.* Journal of Polymer Science Part B: Polymer Physics, 38(10): p. 1323-1330.

238. Khutoryanskaya, O.V., Khutoryanskiy, V.V.and Pethrick, R.A. (2005), *Characterisation of Blends Based on Hydroxyethylcellulose and Maleic Acid-alt-Methyl Vinyl Ether.* Macromolecular Chemistry and Physics, 206(15): p. 1497-1510.

239. Wang, W., Wang, J., Kang, Y.and Wang, A. (2011), *Synthesis, swelling and responsive properties of a new composite hydrogel based on hydroxyethyl*

cellulose and medicinal stone. Composites Part B: Engineering, 42(4): p. 809-818.

240. Chen, R., Yi, C., Wu, H.and Guo, S. (2010), *Degradation kinetics and molecular structure development of hydroxyethyl cellulose under the solid state mechanochemical treatment.* Carbohydrate Polymers, 81(2): p. 188-195.

241. Li, X.-G., Huang, M.-R.and Bai, H. (1999), *Thermal decomposition of cellulose ethers.* Journal of Applied Polymer Science, 73(14): p. 2927-2936.

242. Lönnberg, H., Zhou, Q., Brumer, H., Teeri, T.T., Malmström, E.and Hult, A. (2006), *Grafting of Cellulose Fibers with Poly(ε-caprolactone) and Poly(l-lactic acid) via Ring-Opening Polymerization.* Biomacromolecules, 7(7): p. 2178-2185.

243. Anglès, M.N. and Dufresne, A. (2000), *Plasticized Starch/Tunicin Whiskers Nanocomposites. 1. Structural Analysis.* Macromolecules, 33(22): p. 8344-8353.

244. Chakraborty, A., Sain, M.and Kortschot, M. (2006) *Reinforcing potential of wood pulp-derived microfibres in a PVA matrix*, in *Holzforschung*2006. p. 53.

245. Lu, J., Wang, T.and Drzal, L.T. (2008), *Preparation and properties of microfibrillated cellulose polyvinyl alcohol composite materials.* Composites Part A: Applied Science and Manufacturing, 39(5): p. 738-746.

246. Roohani, M., Habibi, Y., Belgacem, N.M., Ebrahim, G., Karimi, A.N.and Dufresne, A. (2008), *Cellulose whiskers reinforced polyvinyl alcohol copolymers nanocomposites.* European Polymer Journal, 44(8): p. 2489-2498.

247. Ma, H., Zhou, B., Li, H.-S., Li, Y.-Q.and Ou, S.-Y. (2011), *Green composite films composed of nanocrystalline cellulose and a cellulose matrix regenerated from functionalized ionic liquid solution.* Carbohydrate Polymers, 84(1): p. 383-389.

248. Gindl, W. and Keckes, J. (2005), *All-cellulose nanocomposite.* Polymer, 46(23): p. 10221-10225.

249. Nogi, M., Iwamoto, S., Nakagaito, A.N.and Yano, H. (2009), *Optically Transparent Nanofiber Paper.* Advanced Materials, 21(16): p. 1595-1598.

250. Capadona, J.R., Shanmuganathan, K., Tyler, D.J., Rowan, S.J.and Weder, C. (2008), *Stimuli-Responsive Polymer Nanocomposites Inspired by the Sea Cucumber Dermis.* Science, 319(5868): p. 1370-1374.

251. Goff, H.D., Ferdinando, D.and Schorsch, C. (1999), *Fluorescence microscopy to study galactomannan structure in frozen sucrose and milk protein solutions.* Food Hydrocolloids, 13(4): p. 353-362.

252. Qua, E., Hornsby, P., Sharma, H.and Lyons, G. (2011), *Preparation and characterisation of cellulose nanofibres.* Journal of Materials Science, 46(18): p. 6029-6045.

253. McNeill, I.C., Ahmed, S.and Rendall, S. (1998), *Thermal degradation studies of alternating copolymers--V. Degradation of the alternating copolymer of isopropenyl acetate and maleic anhydride.* Polymer Degradation and Stability, 62(1): p. 85-95.

254. Rusli, R., Shanmuganathan, K., Rowan, S.J., Weder, C.and Eichhorn, S.J. (2011), *Stress Transfer in Cellulose Nanowhisker Composites—Influence of Whisker Aspect Ratio and Surface Charge.* Biomacromolecules, 12(4): p. 1363-1369.

255. Lahiji, R.R., Xu, X., Reifenberger, R., Raman, A., Rudie, A.and Moon, R.J. (2010), *Atomic Force Microscopy Characterization of Cellulose Nanocrystals.* Langmuir, 26(6): p. 4480-4488.

256. Capadona, J.R., Van Den Berg, O., Capadona, L.A., Schroeter, M., Rowan, S.J., Tyler, D.J.and Weder, C. (2007), *A versatile approach for the processing of polymer nanocomposites with self-assembled nanofibre templates.* Nat Nano, 2(12): p. 765-769.

257. Halpin, J.C. and Kardos, J.L. (1972), *Moduli of Crystalline Polymers Employing Composite Theory.* Journal of Applied Physics, 43(5): p. 2235-2241.

258. Elazzouzi-Hafraoui, S., Nishiyama, Y., Putaux, J.-L., Heux, L., Dubreuil, F.and Rochas, C. (2007), *The Shape and Size Distribution of Crystalline Nanoparticles Prepared by Acid Hydrolysis of Native Cellulose.* Biomacromolecules, 9(1): p. 57-65.

259. Schott, H. (1992), *Swelling kinetics of polymers.* Journal of Macromolecular Science, Part B, 31(1): p. 1-9.

260. Mikos, A.G., Thorsen, A.J., Czerwonka, L.A., Bao, Y., Langer, R., Winslow, D.N.and Vacanti, J.P. (1994), *Preparation and characterization of poly(l-lactic acid) foams.* Polymer, 35(5): p. 1068-1077.

261. Heino, A., Naukkarinen, A., Kulju, T., Törmälä, P., Pohjonen, T.and Mäkelä, E.A. (1996), *Characteristics of poly(L-)lactic acid suture applied to fascial closure in rats.* Journal of Biomedical Materials Research, 30(2): p. 187-192.

262. Lam, K.H., Nijenhuis, A.J., Bartels, H., Postema, A.R., Jonkman, M.F., Pennings, A.J.and Nieuwenhuis, P. (1995), *Reinforced poly(L-lactic acid) fibres as suture material.* Journal of applied biomaterials : an official journal of the Society for Biomaterials, 6(3): p. 191-197.

263. Ahmed, I., Jones, I., Parsons, A., Bernard, J., Farmer, J., Scotchford, C., Walker, G.and Rudd, C. (2011), *Composites for bone repair: phosphate glass fibre reinforced PLA with varying fibre architecture.* Journal of Materials Science: Materials in Medicine: p. 1-10.

264. Cont, L., Grant, D., Scotchford, C., Todea, M.and Popa, C. (2011), *Composite PLA scaffolds reinforced with PDO fibers for tissue engineering.* Journal of Biomaterials Applications: p. 1-10.

265. Drumright, R.E., Gruber, P.R.and Henton, D.E. (2000), *Polylactic Acid Technology.* Advanced Materials, 12(23): p. 1841-1846.

266. Henton, D.E., Gruber, P.R., Lunt, J.and Randall, J. (2005), *Polylactic Acid Technology.* Natural Fibers, Biopolymers, and Biocomposites , CRC Press, USA, Edition-1: p. Chapter 16, 524-577.

267. Auras, R.A., Harte, B., Selke, S.and Hernandez, R. (2003), *Mechanical, Physical, and Barrier Properties of Poly(Lactide) Films.* Journal of Plastic Film and Sheeting, 19(2): p. 123-135.

268. Wittenberg, J.M., Wittenberg, R.H.and Hipp, J.A. (1991), *Biomechanical properties of resorbable poly-L-lactide plates and screws: A comparison with traditional systems.* Journal of Oral and Maxillofacial Surgery, 49(5): p. 512-516.

269. Montjovent, M.O., Mathieu, L., Hinz, B., Applegate, L.L., Bourban, P.E., Zambelli, P.Y., Manson, J.A.and Pioletti, D.P. (2005), *Biocompatibility of bioresorbable poly(L-lactic acid) composite scaffolds obtained by supercritical gas foaming with human fetal bone cells.* Tissue Engineering, 11(11-12): p. 1640-9.

270. Chung, S., Gamcsik, M.P.and King, M.W. (2011), *Novel scaffold design with multi-grooved PLA fibers.* Biomed Mater, 6(4): p. 045001.

271. Felfel, R.M., Ahmed, I., Parsons, A.J.and Rudd, C.D. (2013), *Bioresorbable screws reinforced with phosphate glass fibre: Manufacturing and mechanical property characterisation.* Journal of the Mechanical Behavior of Biomedical Materials, 17: p. 76-88.

272. Felfel, R.M., Ahmed, I., Parsons, A.J., Walker, G.S.and Rudd, C.D. (2011), *In vitro degradation, flexural, compressive and shear properties of fully bioresorbable composite rods.* J Mech Behav Biomed Mater, 4(7): p. 1462-72.

273. Yuan, X., Mak, A.F.T.and Yao, K. (2002), *In vitro degradation of poly(L- lactic acid) fibers in phosphate buffered saline.* Journal of Applied Polymer Science, 85(5): p. 936-943.

274. Leu, Y.Y. and Chow, W.S. (2011), *Kinetics of water absorption and thermal properties of poly(lactic acid)/organomontmorillonite/poly(ethylene glycol) nanocomposites.* Journal of Vinyl and Additive Technology, 17(1): p. 40-47.

275. Carter, R.O., Carduner, K.R., Paputa Peck, M.C.and Motry, D.H. (1989), *The Infrared Analysis of Polyethylene Terephthalate Fibers and of Their Strength as Related to Sample Preparation and to Particle Size.* Appl. Spectrosc., 43(5): p. 791-794.

276. Fujimoto, K., Iohara, K., Ohwaki, S.and Murase, Y. (1991), *Superstructure in ultrahigh speed spun fibers of poly(ethylene terephthalate).* Journal of Applied Polymer Science, 42(6): p. 1509-1517.

277. Smith, P.B., Leugers, A., Kang, S., Yang, X.and Ling Hsu, S. (2001), *Raman characterization of orientation in poly(lactic acid) films.* Macromolecular Symposia, 175(1): p. 81-94.

278. Vasanthakumari, R. and Pennings, A.J. (1983), *Crystallization kinetics of poly(l-lactic acid).* Polymer, 24(2): p. 175-178.

279. Choi, K.-J., Spruiell, J.E.and White, J.L. (1989), *Structure development in biaxially stretched polystyrene film: Part I. Property-orientation correlation.* Polymer Engineering & Science, 29(21): p. 1516-1523.

280. Matsumoto, K., Fellers, J.F.and White, J.L. (1981), *Uniaxial and biaxial orientation development and mechanical properties of polystyrene films.* Journal of Applied Polymer Science, 26(1): p. 85-96.

281. Wright-Charlesworth, D.D., King, J.A., Miller, D.M.and Lim, C.H. (2006), *In vitro flexural properties of hydroxyapatite and self-reinforced poly(L-lactic acid).* Journal of Biomedical Materials Research Part A, 78A(3): p. 541-549.

282. McCullen, S.D., Stano, K.L., Stevens, D.R., Roberts, W.A., Monteiro-Riviere, N.A., Clarke, L.I.and Gorga, R.E. (2007), *Development, optimization, and characterization of electrospun poly(lactic acid) nanofibers containing multi-walled carbon nanotubes.* Journal of Applied Polymer Science, 105(3): p. 1668-1678.

283. Pegoretti, A., Fambri, L.and Migliaresi, C. (1997), *In vitro degradation of poly(L-lactic acid) fibers produced by melt spinning.* Journal of Applied Polymer Science, 64(2): p. 213-223.

284. Drieskens, M., Peeters, R., Mullens, J., Franco, D., Lemstra, P.J.and Hristova-Bogaerds, D.G. (2009), *Structure versus properties relationship of poly(lactic acid). I. Effect of crystallinity on barrier properties.* Journal of Polymer Science Part B: Polymer Physics, 47(22): p. 2247-2258.

285. Gogolewski, S. and Pennings, A.J. (1983), *Resorbable materials of poly(L-lactide). II. Fibers spun from solutions of poly(L-lactide) in good solvents.* Journal of Applied Polymer Science, 28(3): p. 1045-1061.

286. Horáček, I. and Kalíšek (1994), *Polylactide. II. Discontinuous dry spinning– hot drawing preparation of fibers.* Journal of Applied Polymer Science, 54(11): p. 1759-1765.

287. Horáček, I. and Kalíšek, V. (1994), *Polylactide. I. Continuous dry spinning– hot drawing preparation of fibers.* Journal of Applied Polymer Science, 54(11): p. 1751-1757.

288. Horáček, I. and Kalíšek, V. (1994), *Polylactide. III. Fiber preparation by spinning in precipitant vapor.* Journal of Applied Polymer Science, 54(11): p. 1767-1771.

289. Horáček, I. and Kudláček, L. (1993), *Influence of molecular weight on the resistance of polylactide fibers by radiation sterilization.* Journal of Applied Polymer Science, 50(1): p. 1-5.

290. Postema, A.R., Luiten, A.H., Oostra, H.and Pennings, A.J. (1990), *High-strength poly(L-lactide) fibers by a dry-spinning/hot-drawing process. II. Influence of the extrusion speed and winding speed on the dry-spinning process.* Journal of Applied Polymer Science, 39(6): p. 1275-1288.

291. Tsuji, H., Ikada, Y., Hyon, S.-H., Kimura, Y.and Kitao, T. (1994), *Stereocomplex formation between enantiomeric poly(lactic acid). VIII. Complex fibers spun from mixed solution of poly(D-lactic acid) and poly(L-lactic acid).* Journal of Applied Polymer Science, 51(2): p. 337-344.

292. Xu, X., Yang, Q., Wang, Y., Yu, H., Chen, X.and Jing, X. (2006), *Biodegradable electrospun poly(l-lactide) fibers containing antibacterial silver nanoparticles.* European Polymer Journal, 42(9): p. 2081-2087.

293. Liao, C.-C., Wang, C.-C.and Chen, C.-Y. (2011), *Stretching-induced crystallinity and orientation of polylactic acid nanofibers with improved mechanical properties using an electrically charged rotating viscoelastic jet.* Polymer, 52(19): p. 4303-4318.

294. Kakinoki, S., Uchida, S., Ehashi, T., Murakami, A.and Yamaoka, T. (2011), *Surface Modification of Poly(L-lactic acid) Nanofiber with Oligo(D-lactic acid) Bioactive-Peptide Conjugates for Peripheral Nerve Regeneration.* Polymers, 3(2): p. 820-832.

295. Ma, Z., Gao, C., Gong, Y., Ji, J.and Shen, J. (2002), *Immobilization of natural macromolecules on poly-L-lactic acid membrane surface in order to improve its cytocompatibility.* Journal of Biomedical Materials Research, 63(6): p. 838-847.

296. Jiao, Y.P. and Cui, F.Z. (2007), *Surface modification of polyester biomaterials for tissue engineering.* Biomedical materials (Bristol, England), 2(4): p. R24-37.

297. Ma, Z., Gao, C., Ji, J.and Shen, J. (2002), *Protein immobilization on the surface of poly-L-lactic acid films for improvement of cellular interactions.* European Polymer Journal, 38(11): p. 2279-2284.

298. Kakinoki, S. and Yamaoka, T. (2010), *Stable modification of poly(lactic acid) surface with neurite outgrowth-promoting peptides via hydrophobic collagen-like sequence.* Acta Biomaterialia, 6(6): p. 1925-1930.

299. Black, F.E., Hartshorne, M., Davies, M.C., Roberts, C.J., Tendler, S.J.B., Williams, P.M., Shakesheff, K.M., Cannizzaro, S.M., Kim, I.and Langer, R. (1999), *Surface Engineering and Surface Analysis of a Biodegradable Polymer with Biotinylated End Groups.* Langmuir, 15(9): p. 3157-3161.

300. Shu, D. (2004), Biomaterials and tissue engineering. Germany: Springer: p. 195-243.

301. Lin, Y., Wang, L., Zhang, P., Wang, X., Chen, X., Jing, X.and Su, Z. (2006), *Surface modification of poly(l-lactic acid) to improve its cytocompatibility via assembly of polyelectrolytes and gelatin.* Acta Biomaterialia, 2(2): p. 155-164.

302. John, M.J., Anandjiwala, R., Oksman, K.and Mathew, A.P. (2013), *Melt-spun polylactic acid fibers: Effect of cellulose nanowhiskers on processing and properties.* Journal of Applied Polymer Science, 127(1): p. 274-281.

303. Hossain, K.M.Z., Jasmani, L., Ahmed, I., Parsons, A.J., Scotchford, C.A., Thielemans, W.and Rudd, C.D. (2012), *High cellulose nanowhisker content composites through cellosize bonding.* Soft Matter, 8(48): p. 12099-12110.

304. Khan, S.P., Auner, G.G.and Newaz, G.M. (2005), *Influence of nanoscale surface roughness on neural cell attachment on silicon.* Nanomedicine: Nanotechnology, Biology and Medicine, 1(2): p. 125-129.

305. Keshel, S.H., Azhdadi, S.N., Asefnejad, A., Asefnezhad, A., Sadraeian, M., Montazeri, M.and Biazar, E. (2011), *The relationship between cellular adhesion and surface roughness for polyurethane modified by microwave plasma radiation.* International journal of nanomedicine, 6: p. 641-647.

306. Toja, F., Saviello, D., Nevin, A., Comelli, D., Lazzari, M., Levi, M.and Toniolo, L. (2012), *The degradation of poly(vinyl acetate) as a material for design objects: A multi-analytical study of the effect of dibutyl phthalate plasticizer. Part 1.* Polymer Degradation and Stability, 97(11): p. 2441-2448.

307. Keddie, J.L., Jones, R.A.L.and Cory, R.A. (1994), *Interface and surface effects on the glass-transition temperature in thin polymer films.* Faraday Discussions, 98(0): p. 219-230.

308. Oh, S.H., Kang, S.G., Kim, E.S., Cho, S.H.and Lee, J.H. (2003), *Fabrication and characterization of hydrophilic poly(lactic-co-glycolic acid)/poly(vinyl*

alcohol) blend cell scaffolds by melt-molding particulate-leaching method. Biomaterials, 24(22): p. 4011-4021.

309. Törmälä, P. (1992), *Biodegradable self-reinforced composite materials; Manufacturing structure and mechanical properties.* Clinical Materials, 10(1–2): p. 29-34.

310. Li, R. and Yao, D. (2008), *Preparation of single poly(lactic acid) composites.* Journal of Applied Polymer Science, 107(5): p. 2909-2916.

311. Hine, J., P., Olley, H., R., Wardand M., I. (2008), *The use of interleaved films for optimising the production and properties of hot compacted, self reinforced polymer composites.* Composites science and technology, 68(6).

312. Foster, R.J., Hine, P.J.and Ward, I.M. (2009), *Characterisation and modelling of polypropylene/carbon nanofibre nanocomposites.* Polymer, 50(16): p. 4018-4027.

313. Foster, R.J., Bonner, M.J.and Ward, I.M. (2011), *The use of nano and micron-sized particles to enhance the interlayer adhesion in self-reinforced, single-polymer composites.* Composites Science and Technology, 71(4): p. 461-465.

314. Hine, P., Broome, V.and Ward, I. (2005), *The incorporation of carbon nanofibres to enhance the properties of self reinforced, single polymer composites.* Polymer, 46(24): p. 10936-10944.

315. Dugan, J.M., Gough, J.E.and Eichhorn, S.J. (2013), *Bacterial cellulose scaffolds and cellulose nanowhiskers for tissue engineering.* Nanomedicine, 8(2): p. 287-298.

316. BS_EN_ISO_14125 (1998), Fiber Reinforced Plastic Composites-Determination of Flexural Properties, Geneva, Switzerland.